

TOWARDS DEVELOPING SPECIFIC INHIBITORS OF THE ATP-DEPENDENT
LON PROTEASE

Hilary Frase

Submitted in partial fulfillment of the requirements
for the degree of Doctor of Philosophy

Department of Chemistry
Case Western Reserve University

May 2007

CASE WESTERN RESERVE UNIVERSITY
SCHOOL OF GRADUATE STUDIES

We hereby approve the dissertation of

candidate for the Ph.D. degree *.

(signed) _____

(chair of the committee)

(date) _____

*We also certify that written approval has been obtained for any proprietary material contained therein.

Copyright © 2007 by Hilary Frase

All rights reserved

Table of Contents

	Page
List of Tables	5
List of Figures	6
List of Schemes	10
Acknowledgements	11
List of Abbreviations	13
Abstract	16
Chapter 1 Function and Structure of the ATP-Dependent Protease Lon	18
Introduction	18
Importance of Lon in Bacterial Pathogenicity	19
Importance of Lon in Maintaining Mitochondrial Function	19
Structure of Lon Protease	20
Domain Organization	20
Three-Dimensional Structure	21
HslUV: A Structural Model for Lon Protease	22
AAA ⁺ Superfamily	22
Three-Dimensional Structure	23
Conformational Changes	23
Substrate Specificity of Lon Protease	24
Inhibition of the Proteolytic Activity of Lon Protease	25
Enzymatic Activity of Lon Protease	25
General Mechanism	25
Monitoring Peptide Bond Hydrolysis	26
Monitoring ATP Hydrolysis	27
Kinetic Mechanism for Peptide and ATP Hydrolysis During Catalysis	28
Specific Aims	28
Chapter 2 Purification and Steady-State Kinetic Characterization of the Human and <i>Salmonella enterica</i> serovar Typhimurium Lon Protease	45
Abstract	45
Introduction	46
Materials and Methods	49
Materials	49
Plasmid Construction	49
<i>S. Typhimurium</i> Lon	49
Human Lon	50
Purification of Recombinant Lon	50
<i>S. Typhimurium</i> Lon	50
Human Lon	51

Peptide Synthesis	52
Steady-State Peptide Hydrolysis Assay	52
Continuous Assay	52
Discontinuous Assay	53
Inhibition Assays for Determination of K_{ij} and K_{is} Values	54
Steady-State ATP Hydrolysis Assay	54
Mass Spectrometry of Peptide Cleavage Products	55
Data Analysis	55
Determination of k_{obs} Values	55
Determination of k_{cat} and K_m Values for Peptide Hydrolysis	56
Determination of k_{cat} and K_m Values for ATP Hydrolysis	56
Determination of K_{ij} and K_{is} Values	57
Results	58
Cloning and Purification of Recombinant Lon	58
Peptide Hydrolysis Activity of Lon	59
ATP Hydrolysis Activity of Lon	60
Alternate Peptides (2 , 5 , 6) as Substrates for Lon	61
Inhibition of Lon Peptide Cleavage by Peptide Hydrolysis Products	62
Stimulation of ATP Hydrolysis Activity in Lon by Peptide Hydrolysis Products	63
Discussion	64
Chapter 3 Identification of Peptidyl Boronates as Potent Inhibitors of the Peptide Hydrolysis Activity of Lon Protease	85
Abstract	85
Introduction	87
Materials and Methods	90
Materials	90
Purification of Recombinant Lon	90
<i>S. Typhimurium</i> Lon	90
Human Lon	91
Peptide Synthesis	91
Steady-State Peptide Hydrolysis Activity	91
Inhibition Assays for Determination of IC_{50} Values of Peptide Hydrolysis Products	91
Inhibition Assay for Determination of IC_{50} Values of Proteasome Inhibitors	92
Data Analysis	93
Determination of k_{obs} Values	93
Determination of IC_{50} Values	93
Estimation of K_i from IC_{50} Values	94
Results	95
Inhibition of Lon Peptide Cleavage by Peptide Hydrolysis Products	95
Inhibition of Lon Peptide Hydrolysis by Common Proteasome Inhibitors	96
Evaluating the Importance of the Peptidyl and Boronic Acid Moieties of	97

MG262	
Inhibition of Human Lon by MG262	98
Discussion	99
Chapter 4 Insight into the Mechanism for Time-Dependent Inhibition of the Peptide Hydrolysis Activity of Lon Protease by Peptidyl Boronates	124
Abstract	124
Introduction	125
Materials and Methods	128
Materials	128
Plasmid Construction	128
S680A <i>S. Typhimurium</i> Lon	128
Purification of Recombinant Lon	129
<i>S. Typhimurium</i> Lon	129
Human Lon	129
Peptide Synthesis	129
Steady-State Peptide Hydrolysis Assay	130
ZL ₃ AMC Hydrolysis Assay	130
Substrate Assays	131
Inhibition Assays for the Determination of <i>IC</i> ₅₀ Values	131
Inhibition Assays for the Determination of <i>K</i> _i and <i>K</i> _i [*] Values	131
Steady-State ATP Hydrolysis Assay	132
ATP-Dependence of Time-Dependent Inhibition	133
Detecting the Interaction of 4 with Lon by Fluorescence Spectroscopy	133
Nucleotide Assays	133
Reversibility Assays	134
Assay to Detect Covalent Adduct Using Separation by SDS-PAGE	134
Assay to Detect Covalent Adduct Using Separation by Gel Filtration	134
Data Analysis	135
Experimental Time Courses	135
Determination of <i>k</i> _{obs} Values	135
Determination of <i>k</i> _{cat} and <i>K</i> _m Values	136
Determination of <i>IC</i> ₅₀ Values	136
Mode of Inhibition	137
Estimation of Inhibition Constants from Initial and Steady-State Rate Data	137
Determination of <i>K</i> _i and <i>K</i> _i [*] Values	138
Global Nonlinear Fitting of Experimental Time Courses	139
Determination of the Half-Life for Reversal of Inhibition	140
Results	141
Lon Inhibition Assays	141
Detection of ZL ₃ AMC Hydrolysis by Lon	142
The Peptidyl Boronate Dansyl-YRGIT-Abu-B(OH) ₂ (4)	143
Time-Dependent Inhibition of <i>S. Typhimurium</i> Lon Peptide Hydrolysis	143

ATP-Dependence of Peptidyl Boronate Inhibition of <i>S. Typhimurium</i> Lon	145
Fluorescent Detection of the Interaction of <i>S. Typhimurium</i> Lon with 4	147
Detection of the Putative Covalent Adduct	149
Time-Dependent Inhibition of Human Lon Peptide Hydrolysis	150
Discussion	152
Chapter 5 Towards Developing a Peptide Substrate for the Human Lon Protease: The Steroidogenic Acute Regulatory (StAR) Protein	190
Abstract	190
Introduction	191
Materials and Methods	193
Materials	193
Plasmid Construction	193
D203A, F206L StAR	193
Wild Type StAR	194
Purification of Recombinant Proteins	194
StAR	194
Human Lon	196
NBD-Cholesterol Binding Assay	195
Immunoblot Analysis	196
Phosphorylation of StAR with ³² P	196
Degradation of StAR by Human Lon	197
Data Analysis	197
Determination of StAR Extinction Coefficient	197
Determination of K_d Values	198
Results	199
Cloning and Purification of Recombinant StAR	199
Fluorescent Detection of the Cholesterol Binding Activity of StAR	200
Phosphorylation of StAR	200
Degradation of Human StAR by Human Lon	201
Discussion	202
Appendix	216
Appendix A: Oligonucleotides	216
Appendix B: Plasmids	217
Appendix C: Peptide Substrates, Hydrolysis Products, and Inhibitors	218
Appendix D: HPLC Data for Synthetic Peptides	223
Appendix E: Mass Spectrometry Data for Synthetic Peptides	238
Appendix F: Mass Spectrometry Data for Peptide Degradation by Lon	252
Appendix G: TNBSA Assay	260
Appendix H: Limited Tryptic Digest of Human Lon	261
References	264

List of Tables

Table		Page
2.1	Summary of Peptide-Based Substrates and Products	70
2.2	Steady-State Kinetic Parameters for Peptide Hydrolysis – Continuous Assay	75
2.3	Steady-State Kinetic Parameters for Peptide Hydrolysis – Discontinuous Assay	77
2.4	Steady-State Kinetic Parameters for ATP Hydrolysis	79
2.5	Mass Spectrometry Data for Peptide Hydrolysis Products	81
3.1	Summary of Peptide-Based Substrates and Products	107
3.2	Summary of IC_{50} Values for Peptide Product Inhibitors	109
3.3	Summary of IC_{50} Values for Proteasome Inhibitors	112
3.4	Summary of IC_{50} Values for Peptidyl and Boronic Acid Moieties	114
4.1	Summary of Peptide-Based Substrates and Inhibitors	159
4.2	Parameters for Peptidyl Boronate Inhibition of <i>S. Typhimurium</i> Lon	172
4.3	Parameters for Inhibition of <i>S. Typhimurium</i> Lon Derived from Global Fitting	174
4.4	Parameters for Inhibition of Human Lon by 4	185
A.1	Oligonucleotides Used for Cloning and Site-Directed Mutagenesis	216
B.1	Plasmids Generated for the Expression of Recombinant Proteins	217
C.1	Structures of Non-Natural Amino Acids Used in Synthetic Peptides	218
C.2	Structures of N-terminal Protecting Groups Used in Synthetic Peptides	219
C.3	Peptide Substrates	220
C.4	Peptide Hydrolysis Products	221
C.5	Peptide Inhibitors	222

List of Figures

Figure		Page
1.1	Domain organization of a single subunit of Lon protease	30
1.2	Partial sequence alignment of the <i>E. coli</i> and human Lon proteases	31
1.3	X-ray crystal structure of the proteolytic domain of <i>E. coli</i> Lon	32
1.4	Proposed orientation of proteolytic and SSD domains of <i>E. coli</i> Lon	33
1.5	Structure of HslUV complex from <i>E. coli</i>	34
1.6	Nucleotide-dependent conformational changes within HslU	35
1.7	Conformational change resulting in productive alignment of the proteolytic active site of HslV	36
1.8	Degradation profile of the bacteriophage λ N protein by <i>E. coli</i> Lon	37
1.9	Proposed mechanism for peptide bond cleavage in Lon	38
1.10	Hydrolysis of ATP to ADP and inorganic phosphate by Lon	39
1.11	Model peptide for continuous monitoring of peptide cleavage by Lon	40
1.12	Hydrolysis of the model peptide 1 by Lon.	41
1.13	Non-fluorescent analog of the model peptide 1	42
1.14	Separation of radiolabeled ATP and ADP by thin layer chromatography	43
1.15	Minimal kinetic mechanism describing the hydrolysis activities of Lon	44
2.1	Dependence of the observed rate constant on the concentration of substrate	68
2.2	Double reciprocal plots for classical enzyme inhibition	69
2.3	Fluorescence-based steady-state peptide hydrolysis assay	71
2.4	Coomassie stain of purified recombinant <i>S. Typhimurium</i> and human Lon	72
2.5	Peptide hydrolysis by <i>S. Typhimurium</i> and human Lon requires ATP	73
2.6	Steady-state peptide hydrolysis by <i>S. Typhimurium</i> and human Lon using a continuous assay	74
2.7	Steady-state peptide hydrolysis by <i>S. Typhimurium</i> and human Lon using a discontinuous assay	76
2.8	Steady-state ATP hydrolysis by <i>S. Typhimurium</i> and human Lon	78
2.9	ATP-dependent peptide hydrolysis of 2 , 5 , and 6 by <i>S. Typhimurium</i> Lon	80
2.10	Inhibition of <i>S. Typhimurium</i> Lon peptide hydrolysis by 6	82
2.11	ATP hydrolysis by <i>S. Typhimurium</i> Lon in the presence of peptide hydrolysis products	83
2.12	Proposed mechanism for peptide bond cleavage in Lon	84
3.1	Determination of the IC_{50} value of an inhibitor	106
3.2	Inhibition of <i>S. Typhimurium</i> Lon peptide cleavage by peptide hydrolysis products	108
3.3	Inhibition of human Lon peptide hydrolysis by 7	110
3.4	Inhibition of <i>S. Typhimurium</i> Lon peptide hydrolysis by proteasome inhibitors	111
3.5	Time-dependent inhibition by MG262 and <i>clasto</i> -lactacystin β -lactone	113
3.6	Inhibition of <i>S. Typhimurium</i> Lon peptide hydrolysis by isopropylboronic acid	115
3.7	Inhibition of <i>S. Typhimurium</i> Lon peptide hydrolysis by ZL ₃ OH	116

3.8	Inhibition of human Lon peptide hydrolysis by MG262	117
3.9	General mechanism for inhibition by vinyl sulfones	118
3.10	General mechanism for inhibition of the proteasome by epoxomicin	119
3.11	General mechanism for inhibition by peptidyl aldehydes and boronates	120
3.12	Spontaneous formation of <i>clasto</i> -lactacystin β -lactone from lactacystin at neutral pH	121
3.13	General mechanism for inhibition by <i>clasto</i> -lactacystin β -lactone	122
3.14	Proposed mechanism for inhibition of Lon by MG262	123
4.1	Representative time course for time-dependent inhibition	160
4.2	One-step time-dependent inhibition	161
4.3	Two-step time-dependent inhibition	162
4.4	Uninhibited enzymatic reaction	162
4.5	Experimental setup for measuring time-dependent inhibition of Lon peptide hydrolysis	164
4.6	Representative emission spectra of ZL ₃ OH and AMC	165
4.7	Hydrolysis of ZL ₃ OH by <i>S. Typhimurium</i> Lon	166
4.8	Inhibition of <i>S. Typhimurium</i> Lon peptide hydrolysis by 3	167
4.9	Time-dependent inhibition of <i>S. Typhimurium</i> Lon peptide hydrolysis by peptidyl boronates in the presence of varying concentrations of peptide substrate	168
4.10	Time-dependent inhibition of <i>S. Typhimurium</i> Lon peptide hydrolysis by peptidyl boronates in the presence of varying concentrations of inhibitor	169
4.11	Peptidyl boronates are competitive inhibitors of <i>S. Typhimurium</i> Lon peptide hydrolysis	170
4.12	The initial and final steady-state rates for <i>S. Typhimurium</i> Lon peptide hydrolysis vary during inhibition by peptidyl boronates	171
4.13	Peptidyl boronates inhibit <i>S. Typhimurium</i> Lon peptide hydrolysis via a two-step mechanism	173
4.14	Global nonlinear fitting on inhibition of <i>S. Typhimurium</i> Lon peptide hydrolysis by 4	175
4.15	Inhibition of <i>S. Typhimurium</i> Lon by 4 requires the binding of ATP	176
4.16	The presence of DMSO during the preincubation period does not affect peptide hydrolysis by <i>S. Typhimurium</i> Lon	177
4.17	Fluorescent detection of the interaction between <i>S. Typhimurium</i> Lon and 4	178
4.18	Steady-state kinetic characterization of the S680A <i>S. Typhimurium</i> Lon mutant	179
4.19	4 is a reversible inhibitor of <i>S. Typhimurium</i> Lon	180
4.20	Detection of the putative covalent adduct	181
4.21	Time-dependent inhibition of human Lon peptide hydrolysis by the peptidyl boronate 4 in the presence of varying concentrations of inhibitor	182
4.22	The peptidyl boronate 4 is a competitive inhibitor of human Lon peptide hydrolysis	183

4.23	The initial and final steady-state rates for human Lon peptide hydrolysis vary during inhibition by 4	184
4.24	The peptidyl boronate 4 inhibits human Lon peptide hydrolysis via a two-step mechanism	186
4.25	Proposed mechanism for peptidyl boronate inhibition of serine and threonine proteases	187
4.26	Reaction pathway for inhibition of Lon by peptidyl boronates	188
5.1	Amino acid sequence of human StAR	205
5.2	Summary of the majority of known StAR mutations found in patients with lipoid CAH	206
5.3	N-terminal of recombinant StAR	207
5.4	Coomassie stain of purified recombinant human StAR	208
5.5	Structure of NBD-cholesterol	209
5.6	Fluorescent detection of StAR binding to NBD-cholesterol	210
5.7	Increased fluorescent signal from StAR binding to NBD-cholesterol is concentration dependent	211
5.8	Representative binding isotherm for StAR binding to NBD-cholesterol	212
5.9	<i>In vitro</i> phosphorylation of human StAR by protein kinase A	213
5.10	Immunoblot analysis of human Lon degradation of human StAR	214
5.11	Structure of MLN64	215
D.1	HPLC trace of the fluorescent analog of compound 1	223
D.2	HPLC trace of the non-fluorescent analog of compound 1	224
D.3	HPLC trace of the fluorescent analog of compound 2	225
D.4	HPLC trace of the non-fluorescent analog of compound 2	226
D.5	HPLC trace of compound 3	227
D.6	HPLC trace of compound 4	228
D.7	HPLC trace of compound 5	229
D.8	HPLC trace of compound 6	230
D.9	HPLC trace of compound 7	231
D.10	HPLC trace of compound 8	232
D.11	HPLC trace of compound 9	233
D.12	HPLC trace of compound 10	234
D.13	HPLC trace of compound 11	235
D.14	HPLC trace of compound 12	236
D.15	HPLC trace of ZL ₃ OH	237
E.1	MALDI mass spectrum of the fluorescent analog of compound 1	238
E.2	Positive mode electrospray ionization mass spectrum of the fluorescent analog of compound 2	239
E.3	Positive mode electrospray ionization mass spectrum of the non-fluorescent analog of compound 2	240
E.4	Positive mode electrospray ionization mass spectrum of compound 3	241
E.5	Positive mode electrospray ionization mass spectrum of compound 4	242
E.6	Positive mode electrospray ionization mass spectrum of compound 5	243
E.7	Positive mode electrospray ionization mass spectrum of compound 6	244
E.8	Positive mode electrospray ionization mass spectrum of compound 7	245
E.9	Positive mode electrospray ionization mass spectrum of compound 8	246

E.10	Positive mode electrospray ionization mass spectrum of compound 9	247
E.11	Positive mode electrospray ionization mass spectrum of compound 10	248
E.12	Positive mode electrospray ionization mass spectrum of compound 11	249
E.13	Positive mode electrospray ionization mass spectrum of compound 12	250
E.14	Positive mode electrospray ionization mass spectrum of ZL ₃ OH	251
F.1	<i>S. Typhimurium</i> Lon degradation of the fluorescent analog of 1	252
F.2	<i>S. Typhimurium</i> Lon degradation of the non-fluorescent analog of 1	253
F.3	<i>S. Typhimurium</i> Lon degradation of the fluorescent analog of 2	254
F.4	<i>S. Typhimurium</i> Lon degradation of the non-fluorescent analog of 2	255
F.5	Human Lon degradation of the fluorescent analog of 1	256
F.6	Human Lon degradation of the non-fluorescent analog of 1	257
F.7	Human Lon degradation of the fluorescent analog of 2	258
F.8	Human Lon degradation of the non-fluorescent analog of 2	259
H.1	Limited tryptic digest of human Lon	262
H.2	Protein sequencing of trypsin protected protein fragments	263

List of Schemes

Scheme	Page
4.1 Proposed mechanism for peptidyl boronate inhibition of Lon protease	189

Acknowledgements

I would first like to thank Warren Kroll, my boyfriend and best friend, whose unconditional love and support has helped me through every obstacle of my graduate career. I love you and could not have done this without you. Thank you for being the funny, carefree, and ever happy man of my dreams. I would like to thank my sister, Heather Frase. Thank you for being there for me and understanding me as no one else can. And remember, “Come to the Potato”. I would also like to thank my parents, Ken and Ruth Ann Frase, for encouraging and supporting me in all my endeavors. I love you both. And yes, I am finally done with school.

I would also like to thank my teachers who have inspired me to pursue my desire to understand why things happen and not just accept that they do. My undergraduate research advisor at The University of Akron, Dr. Gerald F. Koser, was the best professor I have ever had the pleasure of learning from. You made me love chemistry, even organic, and convinced me that my true calling was as a research chemist. My mentor as an undergraduate in the Koser lab was Mike Justik. Thank you for making it fun to be in the lab, even on a Friday night. I would like to thank my graduate research advisor at Purdue University, Dr. Christine Hrycyna. You taught me how to be a biochemist, how to read science critically, and how to give a seminar. Thank you for taking me into your lab...and letting me go. I would also like to thank my committee members, Dr. Tony Berdis, Dr. Tony Pearson, Dr. Larry Sayre, and Dr. Witold Surewicz. And finally, I would like to thank my graduate research advisor at Case Western Reserve University,

Dr. Irene Lee. Thanks for taking a chance on me and being so understanding. You taught me to trust myself and for that I will always be grateful.

Finally, I would like to thank all of my friends, who have listened when life was not so fabulous, distracted me from the stress of graduate school, and most importantly made me laugh. Jessica Anderson: you're an amazing woman, please never change. Thanks for being my best bud both in and out of the lab. The rest of my lab mates in the Hrycyna lab, Aarti, Kaisa and Ney: you made me feel right at home in West Lafayette. I wish you all the best. My lab mates in the Lee lab, Jessica, Diana, and Jen: thanks for always making it "A Great Day in the Lee Lab". I will miss you all.

List of Abbreviations

$\lambda_{\text{excitation}}$	excitation wavelength
λ_{max}	wavelength at which the maximal optical signal is observed
AAA ⁺	ATPases associated with different cellular activities
Abz	anthranilamide
Abu	2-aminobutyric
ADP	adenosine diphosphate
Aloc	allyloxycarbonyl
AMC	7-amino-4-methylcoumarin
AMPPNP	adenosine 5'-(β,γ -imino)triphosphate
ATP	adenosine triphosphate
BCIP	5-bromo-4-chloro-3-indolyl phosphate
Boc	butoxycarbonyl
BSA	bovine serum albumin
CAH	congenital adrenal hyperplasia
Cam	chloramphenicol
CAPS	<i>N</i> -cyclohexyl-3-aminopropanesulfonic acid
CTP	cytidine triphosphate
Da	daltons or g/mol
dansyl	5-dimethylamino-1-naphthalenesulfonyl
DE52	diethylaminoethylcellulose anion exchange resin
DIFP	diisopropyl fluorophosphate
dlu	density light unit
DMSO	dimethylsulfoxide
DNA	deoxyribonucleic acid
DTT	dithiothreitol
<i>E</i>	Lon monomer
<i>E. coli</i>	<i>Escherichia coli</i>
EDTA	ethylenediaminetetraacetic acid
eq	equation
Fmoc	9-fluorenylmethoxycarbonyl
GTP	guanosine triphosphate
HBTU	O-Benzotriazole- <i>N,N,N',N'</i> -tetramethyl-uronium-hexafluoro-phosphate
HEPES	4-(2-hydroxyethyl)-1-piperazineethanesulfonic acid
HOAc	acetic acid
HPLC	high performance liquid chromatography
<i>I</i>	inhibitor
IC_{50}	concentration of inhibitor required to reduce the measured enzymatic activity by 50%
IPTG	isopropyl β - <i>D</i> -1-thiogalactopyranoside
K(Abz)	lysine anthranilamide
Kan	kanamycin
K(Bz)	lysine benzoic acid
k_{cat}	turnover number, maximal value for k_{obs}

k_{cat}/K_m	specificity constant
K_d	dissociation constant for enzyme-ligand complex
kDa	kilodaltons
K_i	dissociation constant for the initial enzyme-inhibitor (EI) complex
K_i^{app}	apparent value for K_i
K_i^*	overall dissociation constant for the final enzyme-inhibitor (EI*) complex
$K_i^{*\text{app}}$	apparent value for K_i^*
K_{ii}	dissociation constant for the enzyme-inhibitor complex at high concentrations of the analogous substrate
k_{inter}	rate constant for the interconversion of v_i and v_{ss}
$k_{\text{inter,max}}$	maximal value for k_{inter}
K_{is}	dissociation constant for the enzyme-inhibitor complex at low concentrations of the analogous substrate
K_m	Michaelis-Menton constant, concentration of substrate under which $k_{\text{obs}} = \frac{1}{2} k_{\text{cat}}$
k_{obs}	observed rate constant
$k_{\text{obs,i}}$	observed rate constant in the presence of inhibitor
MALDI	matrix assisted laser desorption ionization
MeOH	methanol
MLN64	metastatic lymph node 64
MOPS	3-(<i>N</i> -morpholino)propanesulfonic acid
mw	molecular weight
n	Hill coefficient
NBD-cholesterol	22-(<i>N</i> -(7-nitrobenz-2-oxa-1,3-diazol-4-yl)amino)-23,24-bisnor-5-cholen-3 β -ol
NBT	nitro blue tetrazolium
NEM	<i>N</i> -ethylmaleimide
NTA	nitrilotriacetic acid
OD	optical density
OSu	<i>N</i> -hydroxysuccinimide ester
P	peptide cleaved or fluorescent signal
P11	phosphocellulose cation exchange resin
PAGE	polyacrylamide gel electrophoresis
PCR	polymerase chain reaction
PEI	polyethyleneimine
P_i	inorganic phosphate
PKA	protein kinase A
PMSF	phenylmethanesulfonyl fluoride
PVDF	polyvinylidene fluoride
S	peptide substrate
SB	superbroth
SBTI	soybean trypsin inhibitor
SD	standard deviation
SDS	sodium dodecyl sulfate
SSD	sensor and substrate discrimination

StAR	steroidogenic acute regulatory protein
<i>S. cerevisiae</i>	<i>Saccharomyces cerevisiae</i>
<i>S. Typhi</i>	<i>Salmonella enterica</i> serovar Typhi
<i>S. Typhimurium</i>	<i>Salmonella enterica</i> serovar Typhimurium
TBST	Tris buffered saline with Tween 20
TCA	trichloroacetic acid
TFA	trifluoroacetic acid
TLC	thin layer chromatography
TNBSA	2,4,6-trinitrobenzene sulfonic acid
Tris	2-amino-2-(hydroxymethyl)-1,3-propanediol
UTP	uridine triphosphate
UV	ultraviolet
v	steady-state velocity
v_i	initial rate
v_o	steady-state rate in the absence of inhibitor
v_{ss}	steady-state rate
Y(3-NO ₂)	3-nitrotyrosine
Z	benzyloxycarbonyl
ZL ₃ AMC	<i>N</i> ^α -benzyloxycarbonyl-L-leucyl-L-leucyl-L-leucinyl 7-amino-4-methylcoumarin
ZL ₃ OH	<i>N</i> ^α -benzyloxycarbonyl-L-leucyl-L-leucyl-L-leucine
ZL ₃ VS	<i>N</i> ^α -benzyloxycarbonyl-L-leucyl-L-leucyl-L-leucinyl vinyl sulfone

Towards Developing Specific Inhibitors of the ATP-Dependent Lon Protease

Abstract

by

HILARY FRASE

The ATP-dependent serine protease Lon is responsible for degrading damaged and certain regulatory proteins *in vivo*. The importance of Lon activity in bacterial pathogenicity has led to its emergence as a target in the development of novel antibiotics however no potent or specific inhibitors had been reported. This study focused on identifying a lead compound(s) for the development of potent inhibitors of the proteolytic activity of Lon.

Steady-state kinetic characterization of the ATP and peptide hydrolysis activities of human and *Salmonella enterica* serovar Typhimurium (*S. Typhimurium*) Lon revealed no kinetic differences in ATP hydrolysis, but marked differences in substrate specificity. This suggests a peptide-based inhibitor may be developed which exploits these differences to target an inhibitor to a single homolog, minimizing cross-reactivity. Screening of commercially available peptide-based inhibitors highlight the utility of transition state analogs in inhibiting peptide hydrolysis. The peptidyl boronate, MG262, was the most potent inhibitor tested and was effective against both human and *S. Typhimurium* homologs ($IC_{50} = 160 \pm 10$ nM and 122 ± 9 nM, respectively). Peptidyl boronates inhibit peptide hydrolysis through a two-step time-dependent mechanism with

an overall K_i of ~ 20 nM. The first step is rapid and involves binding of the inhibitor and formation of a covalent adduct with the active site serine. A second slow step occurs in which the protease undergoes a conformational change or isomerization to enhance the interaction of the inhibitor with the proteolytic active site. Although inhibition of serine and threonine proteases by peptidyl boronates has been detected previously, Lon is the first protease which requires the binding of ATP to observe inhibition.

Finally, the purification of the human homolog of the steroidogenic acute regulatory protein (StAR) is described. It is shown to be a substrate of human Lon and provides a starting point for the development of a physiologically relevant peptide substrate(s) for the human enzyme. This peptide(s) will be useful in studying the kinetic mechanism of human Lon and for understanding the effect of mutations on the turnover of StAR in patients suffering from congenital lipoid adrenal hyperplasia.

CHAPTER 1

Function and Structure of the ATP-Dependent Protease Lon

Introduction

Lon, also known as the protease La, is an ATP-dependent serine protease which functions in the degradation of damaged and certain short-lived regulatory proteins (1-10). Homologs are found throughout nature however they have different localizations within the cell. In prokaryotes, the enzyme exists as a cytosolic protease, whereas in eukaryotes, the nuclear-encoded enzyme localizes to the mitochondrial matrix (4, 11, 12). The bacterial proteases from *Escherichia coli* (*E. coli*) and *Salmonella enterica* serovar Typhimurium (*S. Typhimurium*) share greater than 99% sequence identity (13). In fact, they differ in only 3 amino acids, none of which occur within the functional domains of the enzyme; thus the two may function comparably. This is supported by the fact that Lon-deficient *E. coli* and *S. Typhimurium* are indistinguishable in their increased sensitivity to UV light and other DNA damaging agents, as well as their decreased ability to degrade abnormal proteins (7, 14-19). Comparison of the bacterial and human enzymes show only 42% sequence identity (13) and complementation studies have revealed the *E. coli* enzyme can only partially complement the function of the eukaryotic protease (20). However no detailed kinetic studies had been performed which examined the basis for these differences.

Importance of Lon in Bacterial Pathogenicity

Lon has emerged as a novel target in the development of antibiotics as it has been shown to confer virulence to many bacteria (21, 22). Pathogenic *Salmonella enterica* are responsible for causing a range of human diseases from mild gastroenteritis (serovar Typhimurium and serovar Enteritidis) to typhoid fever (serovar Typhi). It has previously been shown that *S. Typhimurium* Lon protease activity is required for systemic infection in mice, a common study model for *S. Typhi* infection in humans (23). It plays a dual role in pathogenicity, both preventing rampant bacterial penetration of the intestinal lining and facilitating proliferation of the bacteria within macrophages (22, 23). Lon-deficient *S. Typhimurium*, when administered as an oral vaccine to mice, has been shown to confer protection against subsequent infection by virulent *S. Typhimurium* (24). Taken together, these studies highlight Lon as an important target in the development of novel therapeutic agents.

Importance of Lon in Maintaining Mitochondrial Function

Mitochondrial dysfunction is involved in a wide range of diseases from ischaemia-reperfusion to neurodegenerative diseases (25). In part, this is due to oxidative damage from free radicals generated during oxidative phosphorylation. Accumulation of oxidatively modified proteins is avoided through the action of ATP-dependent proteases within the mitochondria, such as Lon (26). In fact, the human homolog prefers the

oxidized form of aconitase to the native form, as a substrate (27). In the absence of *Saccharomyces cerevisiae* (*S. cerevisiae*) Lon, the mitochondrial genome accumulates large deletions and the cells become respiratory deficient (28). Furthermore, the mitochondria within these cells have an abnormal morphology and contain electron-dense inclusion bodies which are believed to be aggregated proteins (29). Downregulation of the human enzyme has also been shown to lead to apoptotic cell death (30), and increased expression of Lon in rats is associated with enhanced mitochondrial biogenesis (31). Taken together, these studies highlight the role of Lon in mitochondrial maintenance.

Structure of Lon Protease

Domain Organization

The bacterial *lon* gene encodes a protein with a predicted molecular mass of ~89 kDa (4). Eukaryotic *lon* genes encode a protein with a predicted molecular mass of ~110 kDa; however upon import into the mitochondria the mature protein has a molecular mass of ~100 kDa (12, 32, 33). The resultant enzymes are comprised of 4 domains (Figure 1.1). The function of the N-terminal domain is unknown, but has been proposed to be involved in oligomerization and stimulation of ATP hydrolysis (34). The discrepancy in size between the bacterial and eukaryotic homologs is due to a larger N-terminal domain in the eukaryotic proteases. The ATP hydrolysis domain, also referred to as the α/β domain, contains the Walker A and B nucleotide binding motifs (35) as well

as the “sensor-1” motif and “arginine finger” (Figure 1.2). The “sensor-1” motif is responsible for positioning the water molecule which acts as a nucleophile during ATP hydrolysis (36, 37), and the “arginine finger” functions to stabilize the developing negative charge of the transition state (38). The sensor and substrate discrimination (SSD) domain, also referred to as the α domain, contains the “sensor-2” motif (Figure 1.2) which participates in the binding and hydrolysis of ATP (39). The SSD has been shown to interact with proteolytic substrates (40). In some cases, the ATP hydrolysis and SSD domains are collectively referred to as the AAA⁺ domain. Finally, the proteolytic domain contains the active site serine-lysine dyad (Figure 1.2) used to catalyze peptide bond hydrolysis (41).

Three-Dimensional Structure

Lon has been shown to exist as a homo-oligomer; however there is no consensus on the number of subunits in the oligomer. The *E. coli* enzyme has been suggested to exist as either a tetramer, hexamer, or octamer (4, 42), whereas the *Mycobacterium smegmatis* homolog has been shown to be a hexamer (43). Cryoelectron microscopy indicates *S. cerevisiae* Lon exists as a ring-shaped heptamer (44).

The structure of an entire Lon monomer has not been determined, however x-ray crystal structures of the SSD or α domain, the proteolytic domain, and a portion of the N-terminal domain have been elucidated (41, 45, 46). The structure of the proteolytic domain, containing an alanine residue in place of the active site serine, crystallized as a ring-shaped hexamer (Figure 1.3) (41). Based upon the residue adjacent to the active site

serine, it was proposed the enzyme utilized a serine-lysine dyad in catalysis (41). The two structures were modeled onto the known structure of a related protein, HslUV (see below), to create a putative structure of the intact protease (Figure 1.4).

HslUV: A Structural Model for Lon Protease

AAA⁺ Superfamily

Lon belongs to the AAA⁺ superfamily (ATPases Associated with a variety of cellular Activities) along with other ATP-dependent proteases such as ClpXP, HslUV, and the proteasome. In addition to proteolysis, proteins in this family are involved in cellular processes such as regulating transcription and cell division, in organisms throughout nature (47). Thus, members of this superfamily are vital to maintaining proper cellular function. These enzymes all share a common ATP hydrolysis domain consisting of the Walker A and B motifs (35), and their activity is often modulated by small adaptor proteins (47). To date, no such adaptor protein as been identified which associates with Lon.

Three-Dimensional Structure

Due to the lack of an intact three-dimensional structure of Lon, the AAA⁺ protein HslUV, a bacterial homolog of the proteasome, is often used as a model to understand how the various domains interact during enzymatic catalysis. HslUV is a hetero-oligomer consisting of 2 subunits, HslU and HslV. The HslU subunit contains the ATP hydrolysis domain whereas the HslV subunit contains the proteolytic domain and active site threonine (48). The HslV subunits spontaneously associate to form a dodecamer in which two hexameric rings stack on top of one another (49). The HslU subunits exist as monomers in the absence of any nucleotide, but the binding of ATP or ADP results in the formation of hexameric rings (50). Only in the presence of ATP will the HslU hexamers associate with both ends of the HslV dodecamer to yield a stack of 4 hexameric rings and an active HslUV complex (Figure 1.5) (50-52).

Conformational Changes

Multiple structures of HslUV have been determined and comparison of these structures has confirmed the importance of conformational changes in enzymatic catalysis. In the absence of any nucleotide, the ATP hydrolysis domain, HslU, exists in an open conformation (Figure 1.6) (53). During ATP binding and hydrolysis, the enzyme clamps down on the nucleotide resulting in a closed conformation. This conformational change is proposed to facilitate unfolding of the substrate and its translocation to the proteolytic active site of the HslV subunits (53). Limited tryptic digests of *E. coli* Lon

have revealed the presence of a similar conformational change in the presence of an adenine nucleotide (54).

Conformational changes are also important in aligning a protein or peptide substrate for peptide bond cleavage. In the absence of the HslU subunit, the proteolytic active site of HslV would bind the substrate nearly 4 Å away from the active site threonine (Figure 1.7) (55). The presence of HslU causes residues of HslV that bind the substrate to move, and results in the productive alignment of the substrate for nucleophilic attack (55).

Substrate Specificity of Lon Protease

Lon catalyzes the hydrolysis of proteins into small peptides of 5 – 15 amino acids in length (4). No consensus sequence has been determined which allows the prediction of cleavage sites *a priori*, but some preference has been seen for cleavage after hydrophobic residues (56-59). The degradation profile of the λN protein by the *E. coli* enzyme highlights the importance of residues distal to the scissile bond in cleavage site selection, as sites with identical amino acid sequences are not both cleaved (Figure 1.8) (56). The lack of a consensus sequence has also hindered the identification of physiological substrates of the protease, which would facilitate an understanding of the role of Lon in maintaining cellular function.

Inhibition of the Proteolytic Activity of Lon Protease

Although Lon is a serine protease, it is relatively unreactive towards most serine protease inhibitors. Both phenylmethylsulfonyl fluoride (PMSF) and diisopropyl fluorophosphate (DIFP) required concentrations in the low millimolar range to achieve even 50% inhibition of the proteolytic activity (2, 60, 61). Interestingly, the enzyme is also susceptible to deactivation by certain cysteine protease inhibitors, such as *N*-ethylmaleimide (NEM), iodoacetamide, and dansyl fluoride, although these are equally as poor at inhibiting proteolysis (2, 27, 61, 62). When the studies described in Chapters 1 – 5 were undertaken, no potent inhibitors of Lon had been described.

Enzymatic Activity of Lon Protease

General Mechanism

Lon possesses two enzymatic activities, ATP and peptide bond hydrolysis. In the presence of ATP, the enzyme is proposed to catalyze peptide bond hydrolysis using a serine-lysine dyad (Figure 1.9). Maximal peptide hydrolysis activity requires ATP, however other nucleotide triphosphates (GTP, UTP, and CTP) and nonhydrolyzable ATP analogs, such as AMPPNP, also support this activity (54, 63, 64). ATP is hydrolyzed to ADP and inorganic phosphate (P_i) (Figure 1.10) and occurs in the absence of a substrate

(intrinsic ATP hydrolysis) and is enhanced in the presence of a peptide (65) or protein substrate (4, 66) (peptide- or protein-stimulated ATP hydrolysis, respectively).

Monitoring Peptide Bond Hydrolysis

Although both fluorogenic and radiochemical assays have been developed to monitor protein degradation by Lon (4, 34), these do not allow the evaluation of a single peptide bond. Fluorogenic tetrapeptides containing a single cleavage site were developed, however they were unable to mimic the enhanced ATP hydrolysis observed in the presence of protein substrates (5, 60). The lack of peptide substrate, containing a single cleavage site and which truly mimicked a protein substrate, hindered kinetic characterization of the enzyme.

A synthetic peptide substrate based on the cleavage profile of the λ N protein by *E. coli* Lon was recently developed (Figure 1.11) (65). This peptide (**1**) contains a C-terminal lysine anthranilamide fluorophore whose fluorescence is internally quenched by the N-terminal 3-nitrotyrosine in the intact peptide (67). In the presence of ATP, Lon cleaves the peptide, between the cysteine and serine. Peptide cleavage can be continuously monitored at 420 nm ($\lambda_{\text{excitation}} = 320$ nm) as an increase in fluorescence over time, as the fluorophore and quencher dissociate (Figure 1.12). The amount of peptide cleaved can be calibrated by determining the change in fluorescence/ μ M peptide cleaved after complete trypsin digestion under identical reaction conditions. The specificity of *E. coli* Lon for **1** is similar to that obtained with the full length λ N protein

(65). Furthermore, **1** was able to stimulate ATP hydrolysis to the same extent as other protein substrates (65). Thus, it is a true mimic of a protein substrate.

A limitation of this assay is the limited linear range (0 – 100 μ M) due to a phenomenon known as the inner filter effect. The fluorescence of the lysine anthranilamide is quenched not only in the intact peptide, but also in the hydrolysis product because of its closer proximity to the 3-nitrotyrosine quencher at higher concentrations. To avoid the inner filter effect and extend the linear range of the assay up to 4 mM, mixtures of both the fluorescent peptide and a non-fluorescent analog (Figure 1.13) are used (64). This is possible because both peptides are cleaved identically by Lon (64).

Monitoring ATP Hydrolysis

The most sensitive method for detecting ATP hydrolysis in Lon is a discontinuous radiolabeled ATP assay described by Gilbert and Mackey (68). The enzyme hydrolyzes ATP to ADP and P_i (Figure 1.10) which can be resolved from one another by thin layer chromatography (TLC). The reaction mixture can be spotted directly onto the TLC plate if formic acid, which is highly volatile, is used to quench the reaction. Either [α - 32 P] ATP or [γ - 32 P] ATP can be used as the substrate and the amount of product, [α - 32 P] ADP or [γ - 32 P] P_i , quantified by Phosphor imaging (Figure 1.14). This assay can also be extended to other nucleotides, such as CTP or GTP, if necessary.

Kinetic Mechanism for Peptide and ATP Hydrolysis During Catalysis

The full kinetic mechanism describing the enzymatic activity of Lon is still being determined. Kinetic characterization of the *E. coli* homolog, using the assays described above, has resulted in the construction of the minimal kinetic mechanism shown in Figure 1.15 (64). In the absence of a peptide substrate, Lon hydrolyzes ATP to yield ADP, which has a higher affinity for the enzyme than ATP (64) and is a potent inhibitor of both ATP and peptide bond hydrolysis (5, 60). This is the intrinsic ATP hydrolysis activity of the enzyme and is represented by the red arrows. In the presence of a peptide substrate, the protease binds both ATP and the peptide substrate. The binding of ATP causes a conformational change resulting in a closed conformation and correct orientation of the active site residues (54). Next, ATP is hydrolyzed to ADP and P_i , which is proposed to facilitate translocation of the peptide to the proteolytic active site (69). Peptide hydrolysis occurs and generates a post-catalytic form (green) which binds the peptide products, but not the peptide substrate (64). Finally, the products are released from the enzyme and the post-catalytic form converts back to the pre-catalytic form to complete the catalytic cycle.

Specific Aims

The goal of the following studies is to understand the similarities and differences in the enzymatic activities of Lon homologs from human and *S. Typhimurium*. This

knowledge will then be used to identify potent inhibitors of this protease, an important target in the development of novel therapeutic agents. Towards this goal, the following specific aims are proposed.

- (1) Clone and express the *S. Typhimurium* and human Lon proteases and characterize their steady-state ATP and peptide hydrolysis activities.
- (2) Screen a series of commercially available inhibitors to identify a lead target for the development of novel Lon inhibitors.
- (3) Elucidate the mechanism by which the most potent inhibitors inactivate the enzymatic activity of Lon.
- (4) Develop methodology to study the enzymatic activity of the human Lon protease with a physiologically relevant substrate.

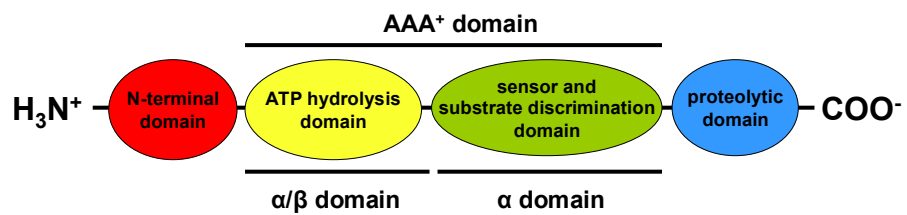


Figure 1.1 Domain organization of a single subunit of Lon protease.

<i>E. coli</i>	354	LVGPPGVGKTSLGQSI	AKATGRKYVRMALGGVRDEAEIRGHRRTY
Human	407	FYGPPGVGKTSIARSI	ARALNREYFRFSVGGMTDVAEIKGHRRTY
<i>E. coli</i>	399	IGSMPGKLIQKMAK	KVGVKNPFLFLLEIDKMSSDMRGDPASALLEV
Human	452	VGAMPGKIIQCLK	KTKTENPLILIDEVDKIGRGYQGDPSALLEL
<i>E. coli</i>	444	LDPEQNVAFSDHYLEVDYDLS	DVMFVATSNSMN-IPAPLLDRMEV
Human	497	LDPEQANANFLDHYLDVPVDLS	KVLFICTANVTDTIPEPLDRMEM
<i>E. coli</i>	488	IRLSGYTEDEKLNIAKRHLLPKQI	ERNALKKGELTVDDSAIIGII
Human	542	INVSGYVAQEKLAI	AERYLVPQARALCGLDESKAKLSSDVLTLII
<i>E. coli</i>	533	RYYTREAGVR	GLEREISKLCRKAVKQLLLDKSLKHIEINGDNLHD
Human	587	KQYCRESGVR	NLQKQVEKVLKRSAYKIVSG-EAESVEVTPENLQD
<i>E. coli</i>	578	YLGVQRFDYGRADNENRVGQVT	GLAWTEVGGDLLTIETAC-VP--
Human	631	FVGKPVFTVERMYDVT	PPGVVMGLAWTAMGGSTLFFVETSLRRPQD
<i>E. coli</i>	620	----GK--GKLT	YTGSLGEVMQESIQAALTVVRARA
Human	676	KDAKGDKDGSLEVT	GQLGEVMKESARIAYTFARAFLMQHAPANDY
<i>E. coli</i>	659	YEKRDIHVHVPEGATPKDGP	SAGIAMCTALVSCLTGNPVRADVAM
Human	721	LVTSHIHLHVPEGATPKDGP	SAGCTIVTALLSLAMGRPVRQNLAM
<i>E. coli</i>	704	TGEITLRGQVLP	IGGLKEKLLAAHRGGIKTVLIPFENKRDLEEIP
Human	766	TGEVSLTGKILPVGGI	KEKTTIAAKRAGVTCIVLPAENKKDFYDLA

Figure 1.2 **Partial sequence alignment of the *E. coli* and human Lon proteases.** The Walker A (yellow) and B (blue) motifs, “sensor-1” motif (grey and underlined), “arginine finger” (pink), “sensor-2 motif (red), and active site serine-lysine dyad (green) are indicated. The numbering of the human sequence is based on the predicted mature protein after import into the mitochondria. Alignment was obtained using ClustalW (70).



Figure 1.3 **X-ray crystal structure of the proteolytic domain of *E. coli* Lon.** The proteolytic domains associate in a ring comprising six monomers. The central opening is 18 Å in diameter and 32 Å long. Reproduced with permission from (41). Copyright 2004, American Society for Biochemistry and Molecular Biology.

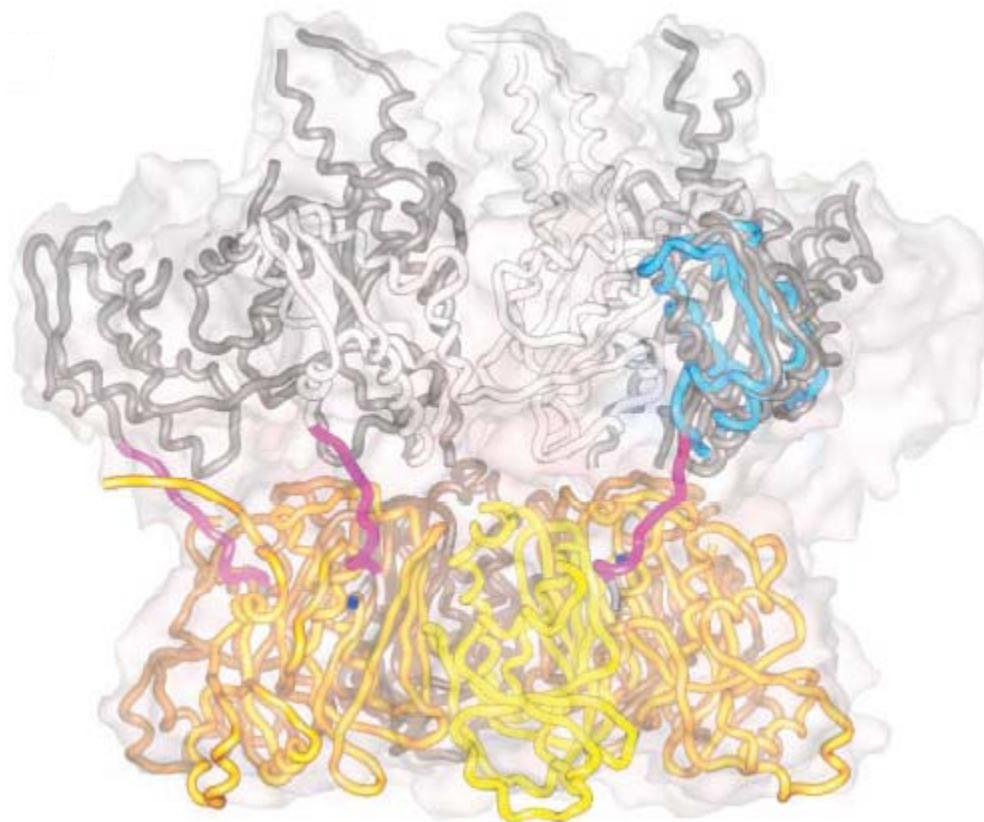


Figure 1.4 **Proposed orientation of proteolytic and SSD domains of *E. coli* Lon.** The x-ray crystal structures of the proteolytic (yellow) and SSD (blue) domains of *E. coli* Lon superimposed on the structure of the related AAA⁺ protein HslUV (grey). The putative linker between the two domains is shown in pink. Reproduced with permission from (41). Copyright 2004, American Society for Biochemistry and Molecular Biology.

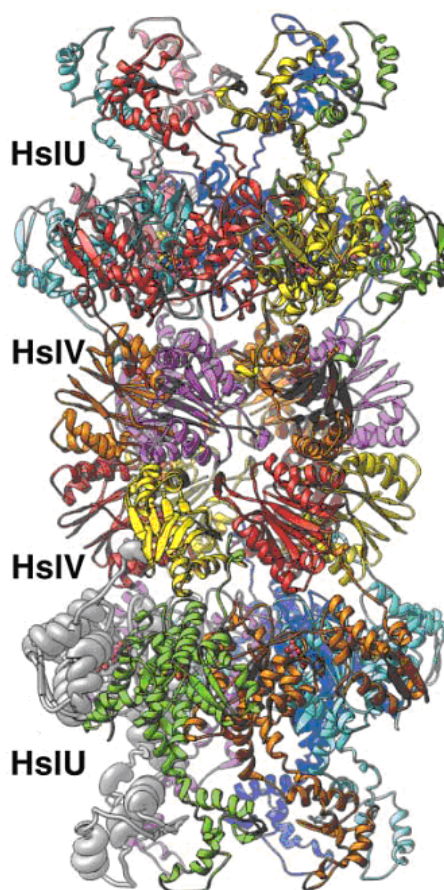


Figure 1.5 **Structure of HslIUV complex from *E. coli*.** View of HslIUV complex along the central axis. The hetero-oligomer contains two hexameric rings containing HslV subunits capped by hexameric rings of HslU subunits.[†]

[†] Reprinted from *Structure (Cambridge)*, **9**, Wang, J. *et al.*, Nucleotide-Dependent Conformational Changes in a Protease-Associated ATPase HslU, 1107-1116, Copyright (2001), with permission from Elsevier.

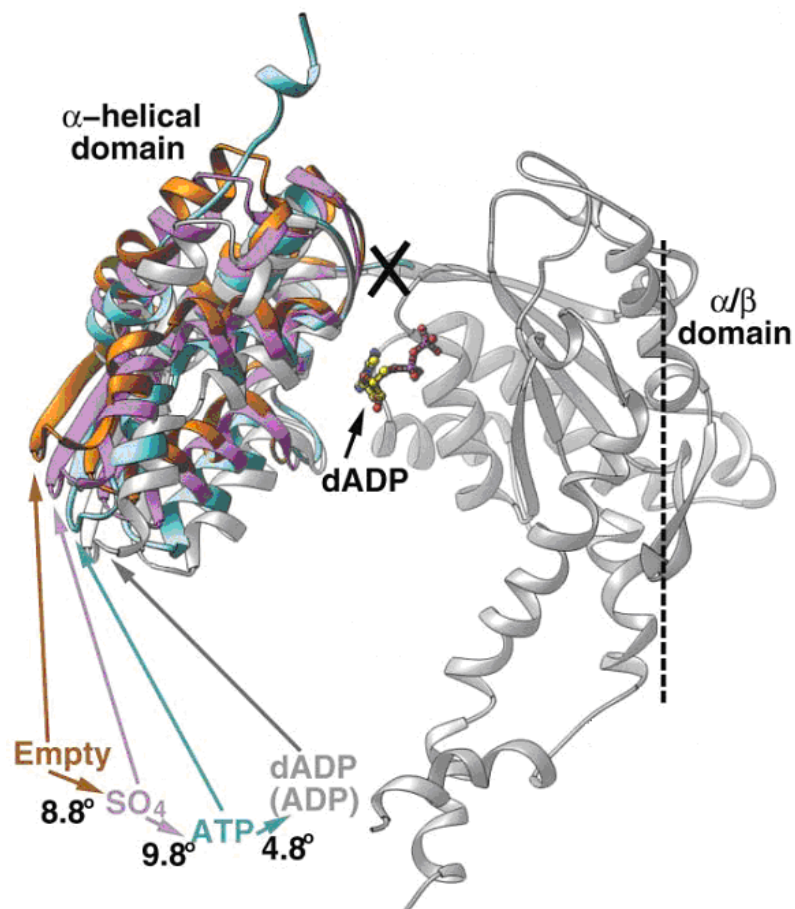


Figure 1.6 **Nucleotide-dependent conformational changes within HslU.** The HslU subunit of HslUV undergoes a series of conformational changes upon binding and hydrolyzing ATP. In the absence of nucleotide the enzyme exists in an open conformation (orange). The α -domain progressively moves towards the α/β domain as ATP binds (blue) and is hydrolyzed to ADP (grey) resulting in a closed conformation.[‡]

[‡] Reprinted from *Structure (Cambridge)*, **9**, Wang, J. *et al.*, Nucleotide-Dependent Conformational Changes in a Protease-Associated ATPase HslU, 1107-1116, Copyright (2001), with permission from Elsevier.

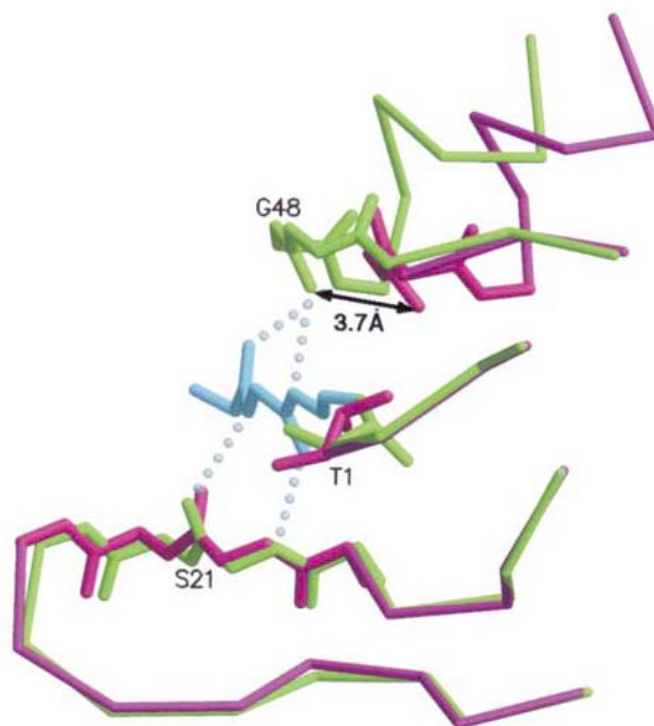


Figure 1.7 **Conformational change resulting in productive alignment of the proteolytic active site of HslV.** The active site of HslV (pink), containing the catalytic threonine (T1), undergoes a conformational change in the presence of ATP (green) which aligns the peptide (blue) for nucleophilic attack.[§]

[§] Reprinted from *Journal of Molecular Biology*, **318**, Sousa, M.C. *et al.*, Crystal Structure of HslUV Complexed with a Vinyl Sulfone Inhibitor: Corroboration of a Proposed Mechanism of Allosteric Activation of HslV by HslU, 779-785, Copyright (2002), with permission from Elsevier.

1 MDAQTRRRERRAEKQA↓QWKAANPLLVGVSA↓KPVNLPILSL↓NRKPKSRVES
50 ALNPIDLTVL↓A↓EYHKQIESNLQRIERKNQRTWYS↓KPGERGITC↓SGRQKIK
100 GKSIPLI

Figure 1.8 **Degradation profile of the bacteriophage λ N protein by *E. coli* Lon.** The amino acid sequence of the bacteriophage λ N protein. *E. coli* Lon cleavage sites are indicated by green arrows. The amino acids flanking a potential cleavage site do not determine whether it will be cleaved by Lon, as only the second AQ site (red) is cleaved.

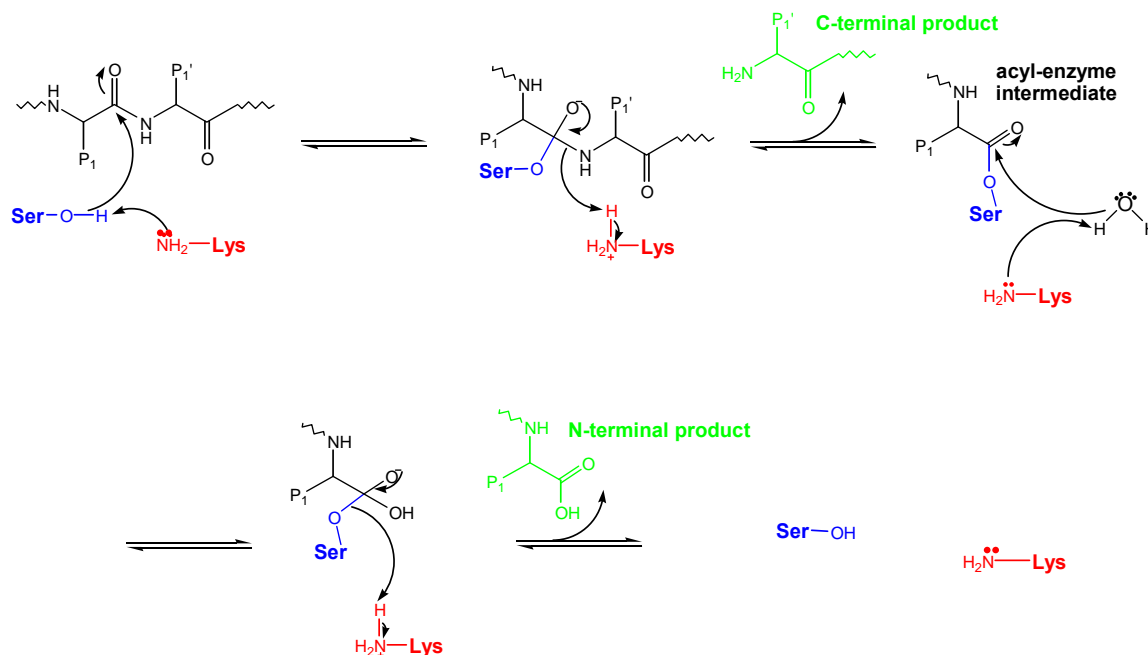


Figure 1.9 **Proposed mechanism for peptide bond cleavage in Lon.** Upon binding the substrate, the active site serine acts as a nucleophile and attacks the carbonyl carbon of the scissile bond, resulting in the first tetrahedral intermediate. This intermediate collapses and the C-terminal product is released, yielding the acyl-enzyme intermediate. An activated water molecule attacks the carbonyl carbon, resulting in the second tetrahedral intermediate. This intermediate again collapses, the N-terminal product is released, and the active site is regenerated.

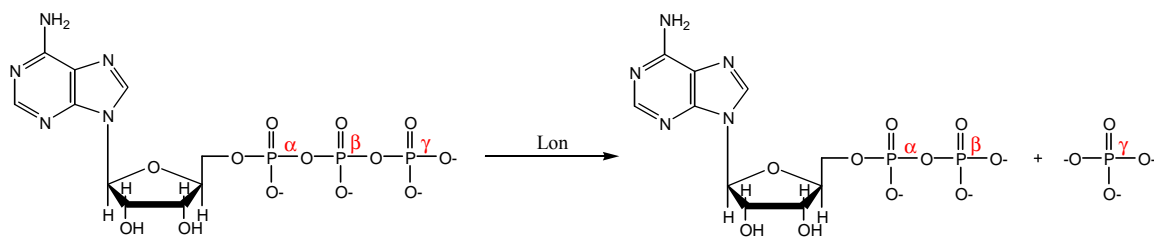


Figure 1.10 **Hydrolysis of ATP to ADP and inorganic phosphate by Lon.** The α , β , and γ phosphates are indicated in red.

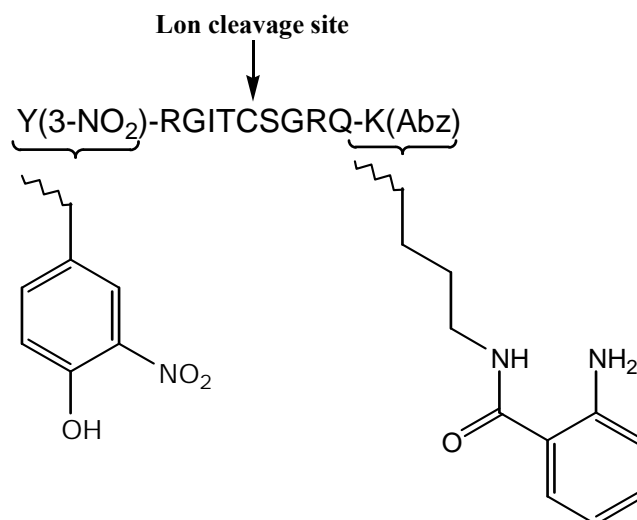


Figure 1.11 **Model peptide (1) for continuous monitoring of peptide cleavage by Lon.** In the presence of ATP, Lon hydrolyzes the peptide bond between the cysteine and serine and an increase in fluorescence is observed as the fluorophore, K(Abz) (lysine anthranilamide), and quencher, Y(3-NO₂) (3-nitrotyrosine) separate.

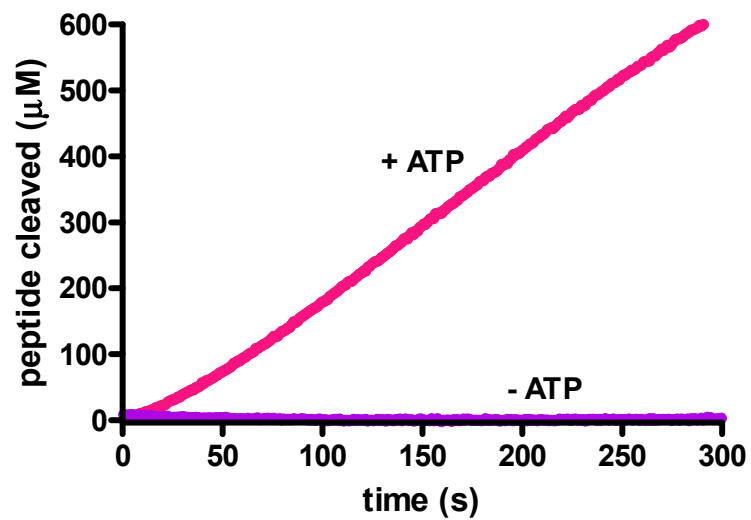


Figure 1.12 **Hydrolysis of the model peptide 1 by Lon.** Representative time course for Lon degradation of 1 in the presence and absence of ATP.

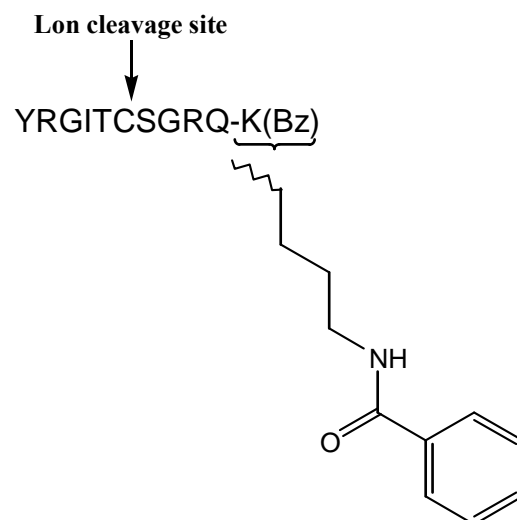


Figure 1.13 **Non-fluorescent analog of the model peptide 1.** In the non-fluorescent analog of **1**, the anthranilamide is replaced by a benzoic acid group and the 3-nitrotyrosine is replaced by tyrosine.

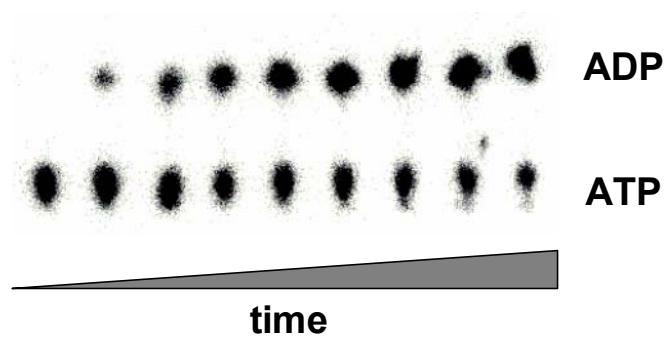


Figure 1.14 **Separation of radiolabeled ATP and ADP by thin layer chromatography.** Lon protease hydrolyzes [α - 32 P] ATP to [α - 32 P] ADP and inorganic phosphate. The substrate and products can be separated by TLC and the concentrations of the radiolabeled species determined by Phosphor imaging.

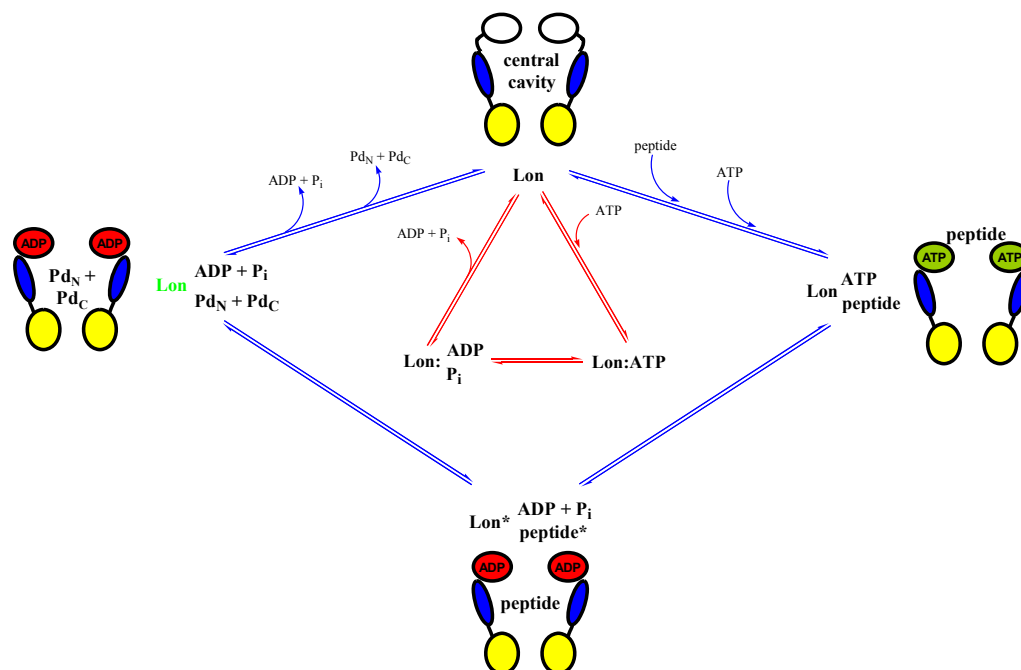


Figure 1.15 Minimal kinetic mechanism describing the hydrolysis activities of Lon. A cross-section of Lon, showing two subunits, is shown. The ATP hydrolysis (white, green, and red), SSD (blue), and proteolytic (yellow) domains are depicted. The intrinsic ATP hydrolysis activity of Lon is represented by the red arrows whereas the blue arrows represent peptide hydrolysis which is facilitated by ATP hydrolysis. The free enzyme (top) binds ATP, resulting in a closed conformation, and the peptide substrate (right). ATP hydrolysis results in translocation of the peptide to the proteolytic active sites (bottom). Lon hydrolyzes the peptide substrate yielding the post-catalytic form (green) and the products, Pd_N and Pd_C (left). Finally, the products are released and the pre-catalytic form (top) is regenerated to complete enzyme turnover.

CHAPTER 2

Purification and Steady-State Kinetic Characterization of the Human and *Salmonella*
enterica serovar Typhimurium Lon Protease**

Abstract

This study describes the cloning and purification of the human and *Salmonella enterica* serovar Typhimurium Lon proteases in their mature form, free of any exogenous tags. It also explores the similarities and differences in the peptide and ATP hydrolysis activities of the bacterial and human homologs. A radioactive ATP hydrolysis assay demonstrates that the steady-state kinetic parameters for ATP hydrolysis by both enzymes are kinetically indistinguishable from one another or *Escherichia coli* Lon. A continuous, fluorescence-based peptide hydrolysis assay is used to highlight the marked difference in substrate specificity between the human and bacterial enzymes. A novel peptide substrate is also described, which is free of any cysteine residues, greatly simplifying the synthesis of the peptide substrate. Finally, a series of peptides are used to investigate how Lon interacts with peptide substrates and/or products.

** The bulk of this work was published in *Biochemistry* on July 11, 2006 (*Biochemistry* **2006**, *45*, 8264-8274).

Introduction

Lon, also known as the protease La, is a homo-oligomeric ATP-dependent serine protease, which functions in the degradation of damaged and certain short-lived regulatory proteins (1-10). Homologs exist ubiquitously in nature, however they localize to the cytosol in prokaryotes and to the mitochondrial matrix in eukaryotes (4, 11, 12). Sequence alignment of the human, *Escherichia coli* (*E. coli*), and *Salmonella enterica* serovar Typhimurium (*S. Typhimurium*) Lon proteases reveals the bacterial enzymes share greater than 99% sequence identity, but only 42% identity with their human homolog (13). In fact the *E. coli* and *S. Typhimurium* enzymes differ in only 3 amino acids, none of which occur within the functional domains of the enzyme, indicating the two may function comparably. This is supported by the fact that Lon-deficient *E. coli* and *S. Typhimurium* are indistinguishable in their increased sensitivity to UV light and other DNA damaging agents as well as their decreased ability to degrade abnormal proteins (7, 14-19).

No detailed kinetic studies of the peptide and ATP hydrolysis activities of human or *S. Typhimurium* Lon have been completed. This study sought to define the steady-state kinetic parameters for both of these activities. Under pseudo-first order conditions, in which the concentration of one substrate (peptide or ATP) is held constant while the other is varied, the observed rate constants (k_{obs}) for the enzymatic reaction will vary either hyperbolically or sigmoidally with the varied substrate (Figure 2.1). A sigmoidal dependence implies the binding of the substrate is cooperative; meaning the binding of the first substrate molecule to the oligomer influences the binding of subsequent substrate

molecules. The degree of cooperativity is described by the Hill coefficient, n . The parameter k_{cat} is the maximal value for k_{obs} and is the turnover number for enzymatic catalysis. The Michaelis-Menton constant, K_m , is the apparent dissociation constant for the enzyme-substrate (ES) complex and is defined as the concentration of substrate required to achieve a value for k_{obs} equal to half k_{cat} . Finally, the parameter k_{cat}/K_m , also called the specificity constant, sets the lower limit for the second order rate constant describing formation of the ES complex and is the best measure of the catalytic efficiency of the enzyme with respect to a particular substrate.

Inhibition studies are often used to gain insight into the interaction between the enzyme, substrate, and inhibitor. Evaluation of the values for k_{obs} at varying concentrations of the substrate and several fixed concentrations of the inhibitor allow deduction of the mode of inhibition and true inhibition constants. The modality is deduced from the pattern of lines created by a double reciprocal plot of the steady-state rates against concentration of the substrate, at several fixed concentrations of inhibitor (Figure 2.2). Global nonlinear fitting of the raw data, using the appropriate equation, will allow the elucidation of the corresponding inhibition constants.

In this study, the steady-state kinetic parameters associated with ATP and peptide hydrolysis by human and *S. Typhimurium* Lon are evaluated. Although the ATP hydrolysis activities of both homologs are kinetically indistinguishable, they display differences in their substrate specificity. Modifications to the amino acid in the P1 position of the peptide substrate (Figure 2.3) highlight the importance of this residue in substrate recognition. Peptide product inhibition studies reconfirm the existence of an enzyme isomerization step. And finally, evidence that the enhanced ATP hydrolysis

activity is due to interaction of the enzyme with the N-terminal of the peptide substrate is presented.

Materials and Methods

Materials

All oligonucleotide primers were purchased from Integrated DNA Technologies, Inc. (Coralville, IA). All cloning reagents were purchased from Promega (Madison, WI), New England BioLabs, Inc. (Ipswich, MA), Invitrogen (Carlsbad, CA) and USB Corporation (Cleveland, OH). Fmoc-protected amino acids, Boc-2-Abz-OH, Fmoc-Lys(Aloc)-Wang resin, and HBTU were purchased from Advanced ChemTech and NovaBiochem. Tris buffer, cell culture media, IPTG, chromatography media, DTT, NaCl, Mg(OAc)₂, trypsin, kanamycin, EDTA, SDS, ATP, and all other reagents were purchased from Fisher, Sigma and Amresco (Solon, OH).

Plasmid Construction

S. Typhimurium Lon

The *S. Typhimurium* Lon gene was amplified from *S. Typhimurium* genomic DNA (a gift from D. Kehres in M. Maguire's lab at Case Western Reserve University School of Medicine) using the oligonucleotides oHF018 and oHF019 (Appendix A). The resultant PCR product was cloned into the NcoI and HindIII sites of pET24d(+) (Novagen) to create the plasmid pHF020 (Appendix B). The plasmid sequence was verified by DNA sequencing using the oligonucleotides oHF005, oHF006, oHF029, oHF030, and oHF031. Our *S. Typhimurium* Lon gene harbors a naturally occurring

conservative mutation, V378I, which does not occur within the functional domains of the enzyme.

Human Lon

The NdeI-BamHI fragment from proEx-1/hLon (72), containing the human Lon gene, was cloned into pET24c(+) (Novagen) to create the plasmid pHF002. The plasmid sequence was verified by DNA sequencing using the oligonucleotides oHF005, oHF006, oHF037, oHF038, oHF045, oHF046, oHF049, and oHF050.

Purification of Recombinant Lon

S. Typhimurium Lon

Recombinant *S. Typhimurium* Lon was overexpressed in BL21 (DE3) (Novagen), using the plasmid pHF020. The cells were grown in superbroth (SB, per L: 5 g MOPS, 30 g tryptone, 20 g yeast extract, pH 7.5), containing 30 µg/mL kanamycin (Kan), at 37°C and induced with 1 mM IPTG at OD₆₀₀ = 1.0 for 1 h. The cells were harvested at 2700 x g and resuspended in Buffer A (5 mM β-mercaptoethanol, 20% (v/v) glycerol, and 0.01% (v/v) Tween 20) containing 50 mM KP_i, pH 7. The cell paste was homogenized followed by sonication (5 min at 200 W in 5 s pulses) on ice. The homogenate was centrifuged at 28000 x g, 4°C for 2 h, to remove cell debris, and the supernatant loaded onto a P11 (phosphocellulose cation exchange resin) column equilibrated in Buffer A containing 50 mM KP_i, pH 7. The column was eluted at 4°C using a linear gradient from 100 mM - 500 mM KP_i, pH 7 in Buffer A. The fractions containing *S. Typhimurium* Lon

were pooled and dialyzed into Buffer A containing 85 mM KPi , pH 7. The dialyzed fractions were loaded onto a DE52 column (diethylaminoethylcellulose anion exchange column) equilibrated in same buffer. The column was eluted at 4°C using a linear gradient from 85 mM - 300 mM KPi , pH 7 in Buffer A. The fractions containing *S. Typhimurium* Lon were again pooled and precipitated using saturated ammonium sulfate. The precipitate was recovered by centrifugation at 28000 x g, 4°C for 2 h and resuspended in Buffer B (50 mM HEPES, 75 mM KPi , 75 mM KOAc, 2 mM DTT, 20% (v/v) glycerol, 0.01% (v/v) Tween 20, pH 7). The protein was fractionated on a Sephacryl S-300 (Amersham Biosciences) gel filtration column equilibrated in Buffer B. The concentration of purified *S. Typhimurium* Lon monomer was determined by Bradford assay (73) using BSA as a standard, and the protein stored at -80°C.

Human Lon

Recombinant human Lon was overexpressed in Rosetta (DE3) (Novagen), using the plasmid pHF002. The cells were grown in superbrotth containing 30 $\mu\text{g/mL}$ Kan and 34 $\mu\text{g/mL}$ chloramphenicol (Cam), at 37°C and induced with 1 mM IPTG at $\text{OD}_{600} = 0.8$ for 1 h. The cells were harvested at 2700 x g and resuspended in Buffer C (25 mM Tris, pH 7.5, 2 mM β -mercaptoethanol, 20% (v/v) glycerol, 0.01% (v/v) Tween 20) containing 0.5 M EDTA and 0.2 M NaCl. The cell paste was homogenized followed by sonication (5 min at 200 W in 5 s pulses) on ice. The homogenate was centrifuged at 28000 x g, 4°C for 2 h, to remove cell debris, and the supernatant loaded onto a P11 (phosphocellulose cation exchange resin) column equilibrated in Buffer C containing 0.2 M NaCl. The column was eluted at 4°C using a linear gradient from 0.2 M - 2 M NaCl in

Buffer C. The fractions containing human Lon were pooled and precipitated using saturated ammonium sulfate. The precipitate was recovered by centrifugation at 28000 x g, 4°C for 2 h and resuspended in Buffer D (50 mM Tris, pH 7.5, 0.5 M NaCl, 2 mM DTT, 20% (v/v) glycerol, 0.01% (v/v) Tween 20). The protein was fractionated on a Sephacryl S-300 (Amersham Biosciences) gel filtration column equilibrated in Buffer D. The concentration of purified human Lon monomer was determined by Bradford assay (73) using BSA as a standard, and the protein stored at -80°C.

Peptide Synthesis

The peptide substrates and peptide hydrolysis products shown in Table 2.1 were synthesized using standard Fmoc solid-phase synthesis techniques (74). All peptides were purified by reverse phase HPLC (Appendix D) and their identities verified by mass spectrometry (Appendix E).

Steady-State Peptide Hydrolysis Assay

Continuous Assay

Reactions contained 50 mM Tris (pH 8.1), 10 mM Mg(OAc)₂, 2 mM DTT, 150 mM NaCl (human Lon reactions only), 125 - 200 nM *S. Typhimurium* Lon monomer or 900 nM human Lon monomer, and varying concentrations of the peptide substrate. At peptide concentrations between 100 μM and 1 mM, a mixture containing 10% fluorescent peptide and 90% of the corresponding non-fluorescent analog were used to avoid the

inner filter effect. Likewise, at peptide concentrations greater than 1 mM, a mixture containing 1% fluorescent peptide and 99% of the corresponding non-fluorescent analog were used to avoid the inner filter effect. After equilibration at 37°C for 1 min, the reaction was initiated by the addition of 1 mM ATP. The fluorescent signal resulting from excitation at 320 nm (slit 2) was monitored at 420 nm (slit 1) using a Fluoromax 3 spectrophotometer (Horiba Group). The amount of peptide cleaved was calibrated by determining the change in fluorescence/ μM peptide cleaved after complete trypsin digestion under identical reaction conditions. All experiments were performed at least in triplicate.

Discontinuous Assay

Reactions containing 50 mM Tris (pH 8.1), 10 mM $\text{Mg}(\text{OAc})_2$, 2 mM DTT, 150 mM NaCl (human Lon reactions only), 100 - 200 nM *S. Typhimurium* Lon monomer or 900 nM human Lon monomer, and varying concentrations of the peptide substrate (100% fluorescent) were initiated by the addition of 1 mM ATP and incubated at 37°C. At different time points (from 0 - 10 min), aliquots were quenched in Buffer E (100 mM EDTA, pH 8, 1% SDS, and 700 mM Tris, pH 8.1). The quenched reaction time points were then further diluted in Buffer E such that the final peptide concentration did not exceed 100 μM . The fluorescent signal at each time point was determined by excitation at 320 nm (slit 2) and monitoring at 420 nm (slit 2) using a Fluoromax 3 spectrophotometer (Horiba Group). The amount of peptide cleaved was calibrated by determining the change in fluorescence/ μM peptide cleaved after complete trypsin

digestion under identical reaction conditions. All experiments were performed at least in triplicate.

Inhibition Assays for Determination of K_{ii} and K_{is} Values

Experiments were performed as described under Continuous Assay with the following modifications. All reactions contained 50 mM Tris (pH 8.1), 10 mM $\text{Mg}(\text{OAc})_2$, 2 mM DTT, 150 nM *S. Typhimurium* Lon monomer, varying concentrations of **2** (10% fluorescent, 90% non-fluorescent), and varying concentrations of **7**. All reactions were performed in triplicate.

Steady-State ATP Hydrolysis Assay

Steady-state velocity data was collected using a modification of the method described by Gilbert and Mackey (68). Reactions containing 50 mM Tris (pH 8.1), 10 mM $\text{Mg}(\text{OAc})_2$, 2 mM DTT, 150 mM NaCl (human Lon reactions only), and 200 nM Lon monomer in the presence and absence of a peptide substrate or product, were initiated by the addition of varying concentrations of $[\alpha\text{-}^{32}\text{P}]$ ATP (0-1 mM) and incubated at 37°C. At different time points (from 0 - 20 min), aliquots were quenched in 0.5 N formic acid. A 3 μL aliquot of each quenched reaction time point was spotted onto a PEI-cellulose TLC plate (10 cm x 20 cm) and the plate developed in 0.3 M KPi (pH 3.4). The amount of $[\alpha\text{-}^{32}\text{P}]$ ATP (ICN or Perkin-Elmer) and $[\alpha\text{-}^{32}\text{P}]$ ADP was quantified using a Packard Cyclone storage phosphor screen Phosphor imager (Perkin-Elmer Life Science). All experiments were performed at least in triplicate unless otherwise noted.

Mass Spectrometry of Peptide Cleavage Products

Reactions containing 50 mM Tris (pH 8.1), 10 mM Mg(OAc)₂, 150 mM NaCl (human Lon reactions only), 2 mM DTT, 200 nM *S. Typhimurium* or 900 nM human Lon monomer, and 100 μM of the peptide substrate were initiated by the addition of 1 mM ATP and incubated at 37°C. After 10 minutes, the reaction mixture was quenched in 0.15% TFA final and submitted for MALDI mass spectrometry analysis at the University of Cincinnati Mass Spectrometry Facility (Appendix F).

Data Analysis

Determination of k_{obs} Values

The steady-state velocities were determined from the linear phase of the reaction time courses using KaleidaGraph (Synergy, Inc.). These were converted to k_{obs} using eq 1, with the following exception: the k_{obs} values resulting from data using the Discontinuous Assay must be multiplied by the dilution factor used to reduce the peptide concentration to less than 100 μM.

$$k_{obs} = \frac{v}{[E]} \quad (1)$$

In eq 1, k_{obs} is the observed rate constant, v is the steady-state velocity, and E is Lon monomer.

Determination of k_{cat} and K_m Values for Peptide Hydrolysis

The steady-state kinetic parameters associated with peptide hydrolysis were determined by fitting the k_{obs} data with eq 2 using the nonlinear regression program Prism 4 (GraphPad Software, Inc.).

$$k_{obs} = \frac{k_{cat}[S]^n}{K_m^n + [S]^n} \quad (2)$$

In eq 2, k_{obs} is as defined in eq 1, k_{cat} is the maximal k_{obs} , S is the peptide substrate, n is the Hill coefficient, and K_m is the Michaelis-Menton constant.

Determination of k_{cat} and K_m Values for ATP Hydrolysis

The concentration of ADP generated was calculated from the phosphor imaging signal, in density light units (dlu), using eq 3. The steady-state velocities were then determined from the linear phase of a plot of the amount of ADP generated versus time using KaleidaGraph (Synergy, Inc.). The steady-state kinetic parameters associated with ATP hydrolysis were determined by fitting the k_{obs} data with eq 4 using the nonlinear regression program Prism 4 (GraphPad Software, Inc.).

$$[ADP] = \left(\frac{ADP_{dlu}}{ATP_{dlu} + ADP_{dlu}} \right) [ATP] \quad (3)$$

$$k_{obs} = \frac{k_{cat}[ATP]}{K_m + [ATP]} \quad (4)$$

In eq 4, k_{obs} is the observed rate constant, k_{cat} is the maximal k_{obs} , and K_m is the Michaelis-Menton constant.

Determination of K_{ii} and K_{is} Values

The k_{obs} data in the presence of 1 mM ATP, varying concentrations of **2**, and varying concentrations of **7** were globally fit with eq 5, describing noncompetitive inhibition, using the nonlinear regression program Prism 4 (GraphPad Software, Inc.).

$$k_{obs} = \frac{k_{cat}[S]^n}{[S]^n \left(1 + \frac{[I]}{K_{ii}}\right) + K_m^n \left(1 + \frac{[I]}{K_{is}}\right)} \quad (5)$$

In eq 5, k_{obs} , k_{cat} , S , n , and K_m , are as defined in eq 2, I is the inhibitor, and K_{ii} and K_{is} are the inhibition constants at high and low concentrations of S , respectively.

Results

Cloning and Purification of Recombinant Lon

The *S. Typhimurium* Lon gene was PCR amplified from *S. Typhimurium* genomic DNA. The resultant PCR product was cloned into the pET24d(+) vector (Novagen), containing both a kanamycin resistance gene and the *T7/lac* promoter, creating the plasmid pHF020. The enzyme was overexpressed in BL21 (DE3) after induction with 1 mM IPTG. After lysing the cells, the cellular debris was removed by centrifugation and the protease recovered from the cell lysate by fractionation on a series of three chromatography columns: affinity, ion exchange, and gel filtration. As much as 11 mg of purified *S. Typhimurium* Lon can be recovered from each liter of culture (Figure 2.4), free of any exogenous tags.

Previous characterization of human Lon was performed using an N-terminal 6x His-tagged enzyme. To eliminate the possibility the His tag was affecting the activity of the enzyme, the mature human Lon gene was cloned into the pET24c(+) vector (Novagen), containing both a kanamycin resistance gene and the *T7/lac* promoter, creating the plasmid pHF002. The enzyme was overexpressed in Rosetta (DE3) after induction with 1 mM IPTG. The Rosetta strain harbors a plasmid expressing tRNAs for codons not commonly used in the bacterial host, enhancing expression of eukaryotic enzymes. This strain is also deficient in the endogenous Lon protease, therefore only the human homolog will be recovered. The protein was purified in a manner similar to the *S.*

Typhimurium homolog, resulting in 1.2 mg of purified human Lon from each liter of culture (Figure 2.4), free of any exogenous tags.

Peptide Hydrolysis Activity of Lon

A continuous assay was previously developed to monitor Lon peptide cleavage using fluorescence spectroscopy, as described in detail in Chapter 1 (65). Upon cleavage of **1** (Table 2.1), an increase in fluorescence is observed as the N-terminal 3-nitrotyrosine quencher separates from the C-terminal lysine anthranilamide fluorophore (Figure 2.3). In the absence of ATP, no peptide cleavage is observed, but in the presence of 1 mM ATP, *S. Typhimurium* and human Lon degrade **1** (Figure 2.5). As with their *E. coli* homolog, a lag is observed in the time course for peptide cleavage prior to reaching steady-state turnover (64).

The steady-state kinetic parameters associated with ATP-dependent degradation of **1** by both *S. Typhimurium* and human Lon were evaluated. The observed rate constant (k_{obs}) was determined at varying concentrations of **1** and saturating ATP using the continuous assay described in Materials and Methods. The value for k_{obs} displays a sigmoidal dependence on **1** for both homologs (Figure 2.6) however the kinetic parameters are quite different (Table 2.2). The *S. Typhimurium* protease degrades **1** in a manner comparable to *E. coli* Lon (54, 64). The human protease has a similar degree of cooperativity (n), but the value for k_{cat} is 2.5-fold lower and the value for K_m is 5-fold greater than the *S. Typhimurium* homolog (Table 2.2). This results in a k_{cat}/K_m for human Lon which is 10-fold lower than the *S. Typhimurium* enzyme (Table 2.2).

At high concentrations of the fluorescent peptide, the change in fluorescence due to peptide hydrolysis becomes nonlinear. This is caused by a phenomenon known as the inner filter effect. The fluorescence of the lysine anthranilamide is quenched not only in the intact peptide, but also the hydrolysis product because of its closer proximity to the 3-nitrotyrosine quencher at higher concentrations. To avoid the inner filter effect when determining the kinetic constants for peptide hydrolysis using the continuous assay, mixtures of both the fluorescent peptide and its non-fluorescent analog were used. To rule out the possibility the fluorescent and non-fluorescent analogs of **1** are degraded differently, the steady-state kinetic parameters for peptide hydrolysis were also determined by a discontinuous assay using only the fluorescent analog. Similar results were obtained using either method (Figure 2.7, Table 2.3).

ATP Hydrolysis Activity of Lon

ATP hydrolysis by Lon protease occurs in the absence of a substrate (intrinsic ATP hydrolysis) and is enhanced or stimulated in the presence of a peptide (65) or protein (4, 66) substrate (peptide- or protein-stimulated ATP hydrolysis, respectively). The steady-state kinetic parameters associated with ATP hydrolysis by both the *S. Typhimurium* and human enzymes were evaluated using a radiolabeled ATP hydrolysis assay, described in detail in Chapter 1 (68). The values for k_{obs} varied hyperbolically with the concentration of ATP both in the presence and absence of saturating **1** (Figure 2.8). As expected, the intrinsic ATP hydrolysis activity of both enzymes is stimulated by the presence of the peptide substrate. Furthermore, similar kinetic constants for intrinsic

and peptide-stimulated ATP hydrolysis are obtained irrespective of the homolog used (Table 2.4) and are comparable to those obtained previously with *E. coli* Lon (54).

Alternate Peptides (**2**, **5**, **6**) as Substrates for Lon

The model peptide, **1**, contains a cysteine residue at the P1 position (Figure 2.3), making its synthesis problematic, due to the resulting low yield. To simplify the synthetic procedure, conservative substitutions were made at the P1 position. These peptides were evaluated by monitoring the degradation of 100 μ M peptide substrate in the absence and presence of saturating ATP. No peptide hydrolysis by *S. Typhimurium* Lon was observed in the absence of ATP for any of the peptides. In the presence of ATP, substitution of serine (**5**) or glycine (**6**) at the P1 position abolishes degradation of the peptide (Figure 2.9). However, substitution of the P1 position with the non-natural amino acid 2-aminobutyric (Abu, **2**) still results in peptide hydrolysis (Figure 2.9).

The steady-state kinetic parameters for peptide and ATP hydrolysis in the presence of **2** by *S. Typhimurium* Lon were further evaluated. The value for k_{obs} associated with peptide hydrolysis displays a sigmoidal dependence on **2** (Figure 2.6 and 2.7) and the kinetic parameters are nearly identical to **1** using both the continuous and discontinuous assay (Table 2.2 and 2.3). The values for k_{obs} associated with ATP hydrolysis in the presence of saturating **2** varied hyperbolically with the concentration of ATP (Figure 2.8) and the kinetic parameters are similar to those obtained with **1** (Table 2.4). Mass spectral analysis of the *S. Typhimurium* Lon cleavage products of **1** and **2** verify that both peptides are cleaved at the same position (Table 2.5), as indicated in

Figure 2.3. As the N-terminal product of the fluorescent analogs contain 3-nitrotyrosine, not only is the parent ion, $[M+H]^+$, observed by MALDI, but also $[M+H-16]^+$ and $[M+H-32]^+$. This is due to photodecomposition of the 3-nitrotyrosine, resulting in the loss of one or two oxygen atoms from the nitro group (75). The cleavage sites of **1** and **2** are identical with the human enzyme (Appendix F).

Inhibition of Lon Peptide Cleavage by Peptide Hydrolysis Products

Earlier steady-state kinetic studies of the *E. coli* Lon protease revealed the C-terminal product from hydrolysis of **1** (**8**) is a noncompetitive inhibitor with respect to the peptide substrate (64). This led to the hypothesis that the enzyme undergoes an isomerization step after peptide cleavage, resulting in a post-catalytic form which does not bind to the peptide substrate. The effect of the N-terminal product was not investigated at this time. Using the *S. Typhimurium* homolog, the values for k_{obs} in the presence of saturating ATP and varying concentrations of **2** and the N-terminal peptide product of **2** (**7**) were determined. A double reciprocal plot, of the steady-state velocity data against the concentration of **2** (Figure 2.10), shows a set of lines intersecting to the left of the y-axis, indicative of noncompetitive inhibition with respect to the peptide substrate. Global fitting of the k_{obs} data with the equation for noncompetitive inhibition (eq 5) yields values for K_{ii} and K_{is} , the inhibition constants for **7** in the presence of high and low concentrations of **2**, respectively (Figure 2.10). These values are greater than 10-fold higher than those obtained for the C-terminal peptide with *E. coli* Lon (64).

Stimulation of ATP Hydrolysis Activity in Lon by Peptide Hydrolysis Products

The presence of the peptide substrate **2** enhanced the ATP hydrolysis activity of *S. Typhimurium* Lon by 8-fold (Figure 2.8, Table 2.4). The effect of peptide hydrolysis products on ATP hydrolysis is yet unknown. The values for k_{obs} associated with hydrolysis of 1 mM ATP in the presence and absence of 100 μM **2** or the peptide hydrolysis products of **2** (**7** and **8**) were determined. The enhanced rate of peptide hydrolysis is observed only in the presence of the intact peptide (**2**) or the N-terminal product (**7**) (Figure 2.11).

Discussion

Lon is an ATP-dependent serine protease found ubiquitously in nature. Homologs can be found in organisms from the archaea to mammalia, however their localization changes from the cytosol in prokaryotes to the mitochondrial matrix of eukaryotes (4, 11, 12). Although the bacterial Lon proteases from *E. coli* and *S. Typhimurium* share >99% identity, they share only 42% with the human enzyme (76). Lon activity is known to be important for cellular functions as diverse as bacterial virulence and maintenance of the mitochondrial genome (21, 23, 28, 29), however little is known about how substrates are selected for degradation. Furthermore, it was unknown whether the human and bacterial enzymes catalyzed peptide hydrolysis via the same mechanism. In this study, steady-state kinetic techniques are used to evaluate the peptide and ATP hydrolysis activities of the human and *S. Typhimurium* enzymes to gain mechanistic insight into the similarities and differences in catalysis.

It has previously been shown that both the *E. coli* and human enzymes cleave the model peptide substrate **1**, however the rate of peptide cleavage is much slower with human Lon (65). To investigate the basis for this difference, the steady-state kinetic parameters for peptide and ATP hydrolysis were evaluated for both the *S. Typhimurium* and human enzymes. Both homologs possess intrinsic ATP hydrolysis activity which is stimulated in the presence of a peptide substrate (Figure 2.8). The steady-state kinetic parameters associated with this activity are similar for both (Table 2.4), thus at the steady-state level there are no detectable kinetic differences in their mechanism for ATP

hydrolysis. Studies on the pre-steady-state timescale will be required to confirm the similarities of microscopic rate constants associated with ATP hydrolysis.

S. Typhimurium and human Lon both require ATP in the degradation of **1** (Figure 2.5) and degradation is cooperative, as evident from the sigmoidal nature of a plot of k_{obs} versus the concentration of **1** (Figure 2.6). The Hill coefficient is comparable between both the *S. Typhimurium* and human enzymes (Table 2.2), however the catalytic efficiency ($k_{\text{cat}}/K_{\text{m}}$) of peptide degradation by human Lon is 10-fold lower (Table 2.2). Assuming the general mechanism for peptide bond hydrolysis is the same in both, this difference arises not only from a lower turnover in human (k_{cat} 2.5-fold lower), but also a 5-fold increase in relative affinity (K_{m}) for **1** (Table 2.2). This suggests there is a difference in the substrate specificity between the two homologs. This is not unexpected as the two localize differently (*S. Typhimurium* in the cytosol and human in the mitochondria) and would degrade a vastly different protein pool (4, 12). The steady-state kinetic parameters for degradation of **1** are similar in *S. Typhimurium* and *E. coli* (Table 2.2 and (54, 64)), indicating the substrate specificity of the bacterial enzymes is similar.

Conservative substitutions at the P1 position (Figure 2.3) of **1** were made in an effort to improve the overall yield during peptide synthesis, without affecting recognition by Lon. Neither serine (**5**) nor glycine (**6**) allowed for recognition of the peptide for hydrolysis (Figure 2.9). However, the non-natural amino acid 2-aminobutyric (Abu, **2**) resulted in a peptide with steady-state kinetic parameters for ATP and peptide hydrolysis comparable to **1** (Figure 2.6 and 2.8). Both serine and 2-aminobutyric are isosteric with cysteine, thus the size of the side chain at the P1 position does not control recognition. The hydrophobicity of the four amino increases in the following order: serine (-4.3) <

glycine (-2.4) \approx cysteine (-2.3) < 2-aminobutyric (1.7) (77). Therefore, the hydrophobicity of the side chain at the P1 position also does not control recognition. It has previously been shown that the residues at the P1 and P1' positions are not the sole determinant of a Lon cleavage site and that residues upstream and/or downstream of these residues must also play a role (56). This study provides the first evidence that the P1 position is important in cleavage site selection, as serine or glycine at the P1 position abolished recognition of the peptide as a substrate (Figure 2.9). Future studies will be required to further examine the importance of this position in substrate recognition.

Previous steady-state kinetic characterization of the *E. coli* Lon protease revealed the C-terminal product of hydrolysis of **1** (**8**) is a noncompetitive inhibitor with respect to the peptide substrate (64). Noncompetitive inhibition cannot be overcome, even at high concentrations of the substrate. To explain this observation, it was proposed that the enzyme undergoes an isomerization step following peptide cleavage, resulting in a post-catalytic form which does not bind the peptide substrate. It was unclear from these studies how and when the post-catalytic form underwent a second isomerization step to regenerate the pre-catalytic form, completing the cycle for enzyme turnover. As shown in Figure 2.10, the N-terminal product of hydrolysis of **2** (**7**) is also a noncompetitive inhibitor with respect to the peptide substrate. Thus the post-catalytic form cannot relax back to the pre-catalytic form until after release of both peptide hydrolysis products (Figure 2.12). Both the acyl-enzyme and second tetrahedral intermediate must be associated with the post-catalytic form. The values for K_{ii} and K_{is} are comparable, thus the affinity of **7** for Lon is not dependent on the concentration of peptide substrate (Figure 2.10). Interestingly, the values for K_{ii} and K_{is} for **7** are 10-fold higher than those

obtained for **8** (64). The lower affinity for the N-terminal product would therefore facilitate enzyme turnover by promoting the release the second product (Figure 2.12).

The enhancement of ATP hydrolysis by Lon in the presence of peptide (65) and protein (4, 66) substrates has been previously observed. However, the affect of peptide hydrolysis products on ATP hydrolysis have yet to be evaluated. The presence of the C-terminal product (**8**) alone has no effect on the value for k_{obs} (Figure 2.11). However, the N-terminal product (**7**) stimulated to the same extent as the intact peptide substrate (**2**) (Figure 2.11). The combination of both the N- and C-terminal products does result in an increased enhancement, thus interaction of the N-terminal of the peptide substrate is responsible for the stimulated ATP hydrolysis activity.

This study explores the similarities and differences in the peptide and ATP hydrolysis activities of the bacterial and human homologs. The steady-state kinetic parameters associated with ATP and peptide hydrolysis by human and *S. Typhimurium* Lon reveal the ATP hydrolysis activities of both homologs are kinetically indistinguishable for one another or *E. coli* Lon however the bacterial and human proteases display differences in their substrate specificity. Modifications to the amino acid in the P1 position of the peptide substrate (Figure 2.4) highlight the importance of this residue in substrate recognition. The enhanced ATP hydrolysis activity is due to the interaction of the enzyme with the N-terminal of the peptide substrate. These studies provide the basis for the development of Lon protease inhibitors which are described in Chapters 3 and 4.

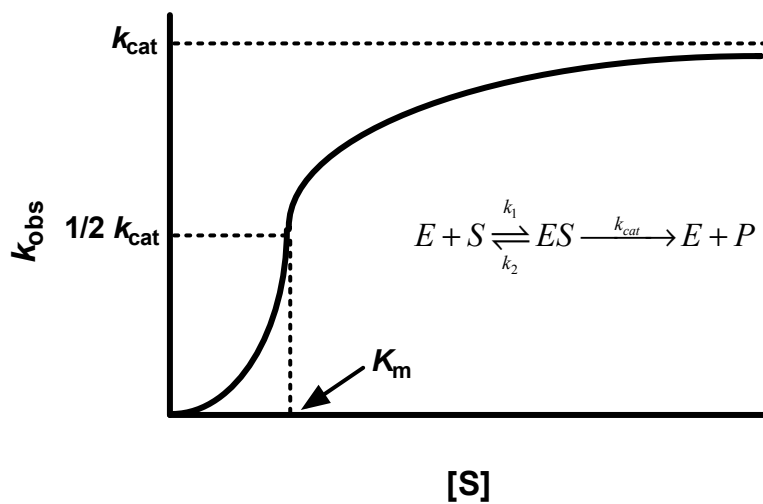
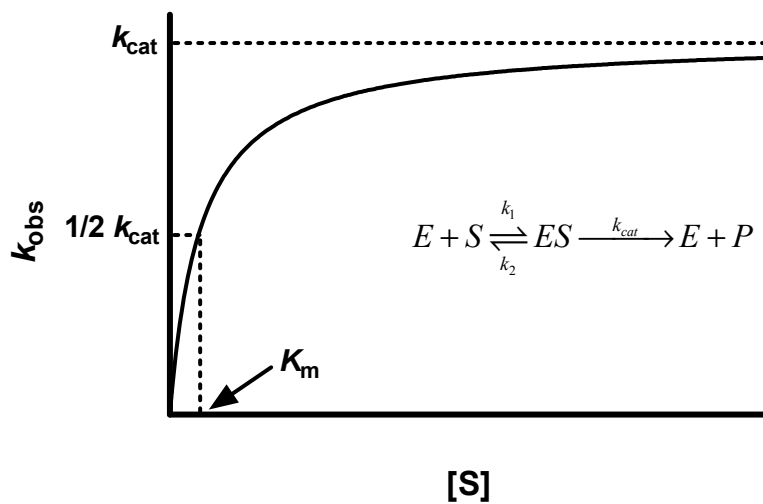


Figure 2.1 **Dependence of the observed rate constant on the concentration of substrate.** Representative plots of k_{obs} against the concentration of substrate for a noncooperative (top) and cooperative (bottom) enzymatic reaction. The maximal value for k_{obs} approaches k_{cat} and K_m is equal to the $[S]$ in which $k_{\text{obs}} = \frac{1}{2} k_{\text{cat}}$.

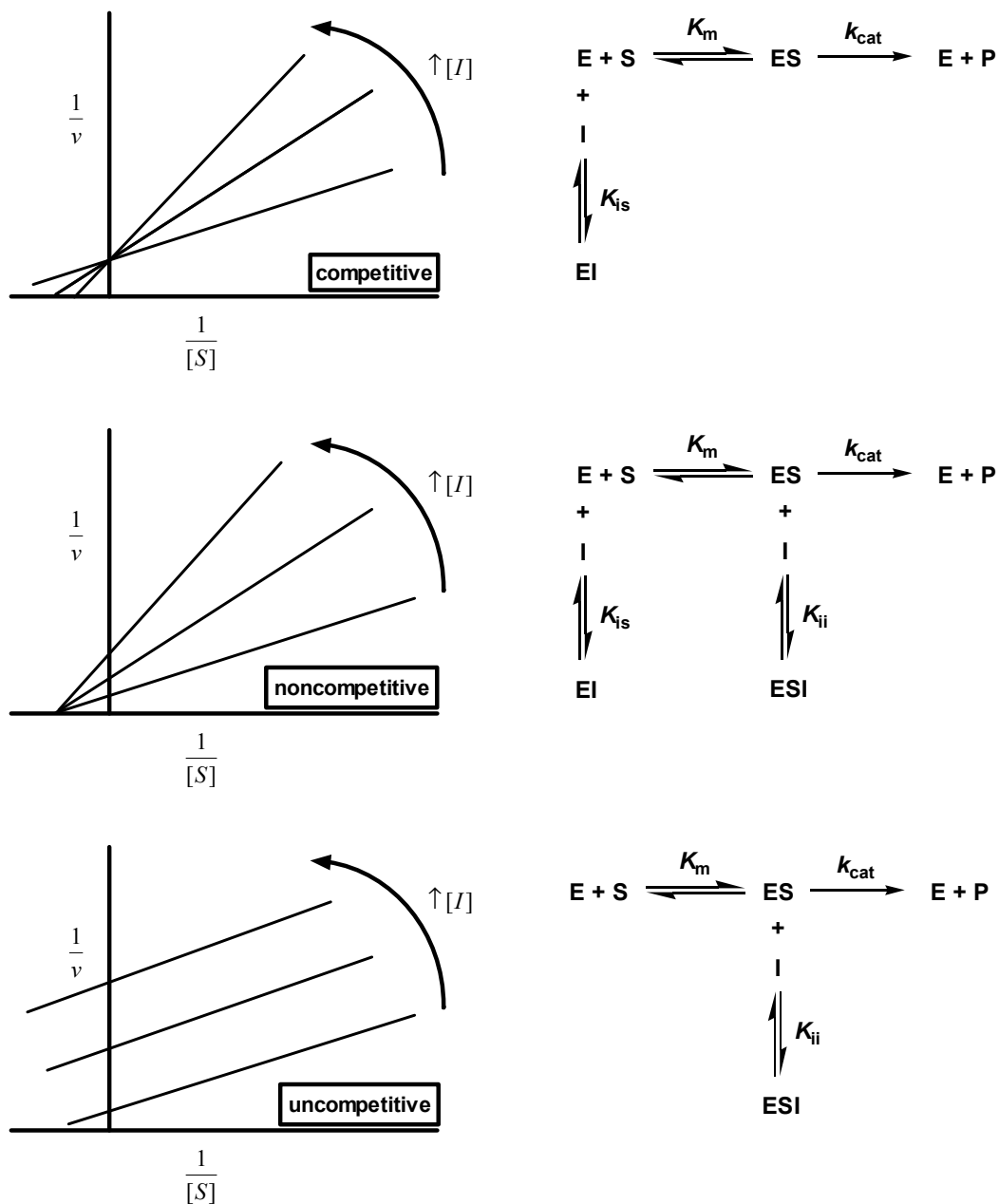
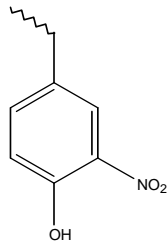
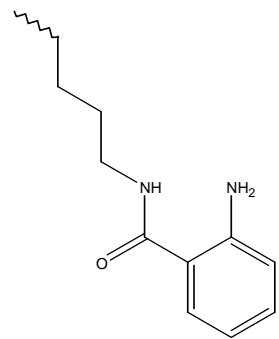
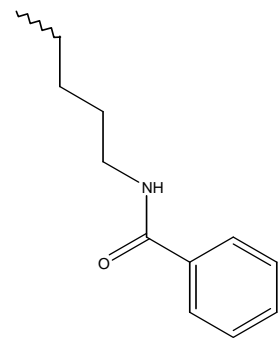


Figure 2.2 **Double reciprocal plots for classical enzyme inhibition.** Representative pattern of lines for inhibition by competitive (top), noncompetitive (middle), and uncompetitive (bottom) enzyme inhibitors. The enzyme species with which each type of inhibitor interacts is indicated on the left. The inhibition constants K_{is} and K_{ii} represent the inhibition constants at low and high concentrations of substrate, respectively.

Table 2.1 Summary of Peptide-Based Substrates and Products

1	fluorescent non-fluorescent	Y(3-NO ₂)RGITCSGRQK(Abz) YRGITCSGRQK(Bz)	
2	fluorescent non-fluorescent	Y(3-NO ₂)RGIT-Abu-SGRQK(Abz) YRGIT-Abu-SGRQK(Bz)	
5	fluorescent	Y(3-NO ₂)RGITSSGRQK(Abz)	
6	fluorescent	Y(3-NO ₂)RGITGSGRQK(Abz)	
7	non-fluorescent	YRGIT-Abu	
8	non-fluorescent	SGRQK(Bz)	
Y(3-NO ₂)	K(Abz)	K(Bz)	Abu
			

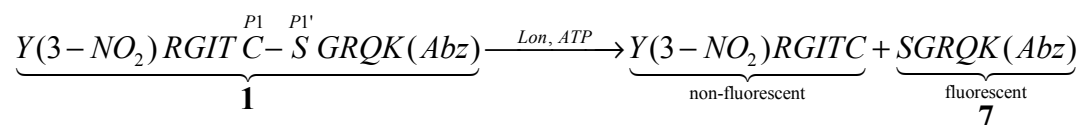


Figure 2.3 **Fluorescence-based steady-state peptide hydrolysis assay.** In the presence of ATP, Lon hydrolyzes **1** between cysteine and serine. An increase in fluorescence is observed as the C-terminal product (**7**), containing a lysine anthranilamide fluorophore (K(Abz)), separates from the N-terminal product, containing a 3-nitrotyrosine quencher (Y(3-NO₂)). The amino acids which flank the scissile bond, P1 and P1', are labeled.

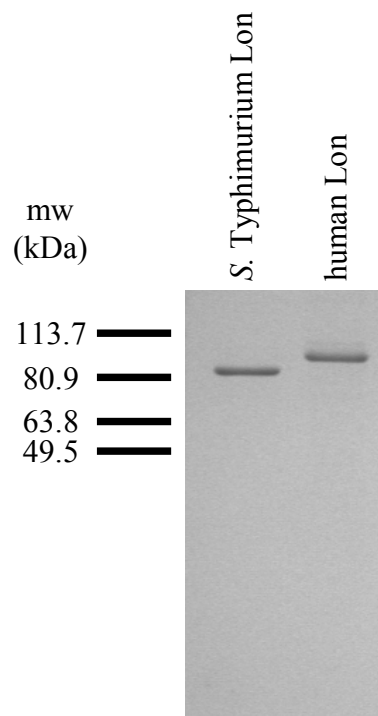


Figure 2.4 **Coomassie stain of purified recombinant *S. Typhimurium* and human Lon.** SDS-PAGE of ~365 ng purified recombinant *S. Typhimurium* (87 kDa) and human Lon (95 kDa) visualized by coomassie.

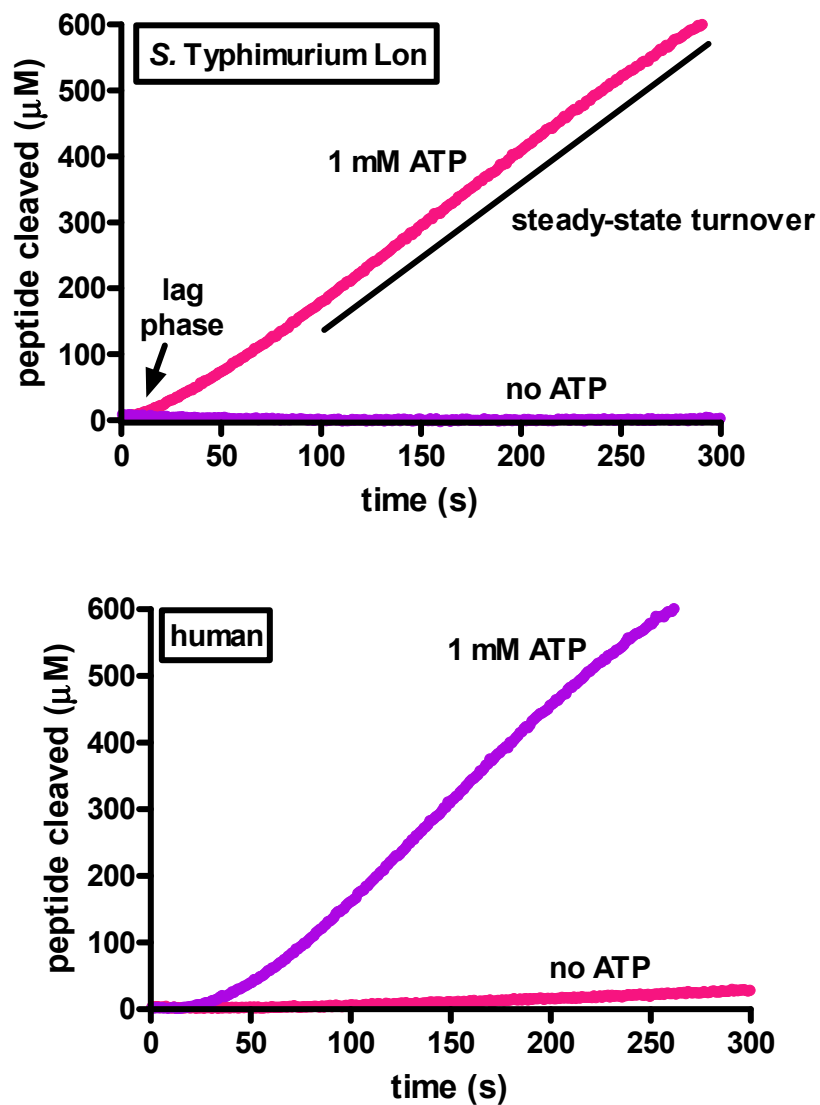


Figure 2.5 Peptide hydrolysis by *S. Typhimurium* and human Lon requires ATP. Representative time courses for 125 nM *S. Typhimurium* (top) and 900 nM human (bottom) Lon degradation of 1 (1 mM) in the presence and absence of ATP. The regions corresponding to the lag phase and steady-state turnover are indicated.

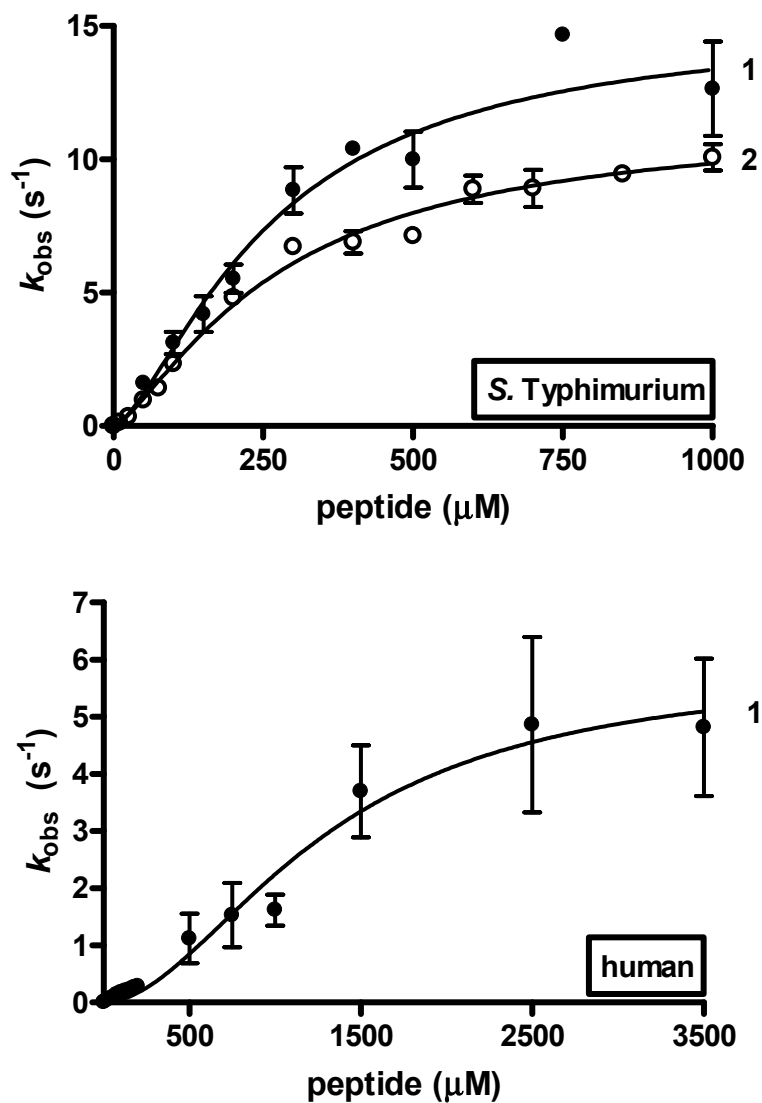


Figure 2.6 **Steady-state peptide hydrolysis by *S. Typhimurium* and human Lon using a continuous assay.** Reactions containing *S. Typhimurium* (top) or human (bottom) Lon were preincubated with varying concentrations of **1** (●) or **2** (○) prior to the addition of 1 mM ATP. All experiments were performed at least in triplicate and the averaged k_{obs} values (± 1 SD) were plotted against the corresponding peptide concentration. The data were best fit with the Hill equation (eq 2) as described in Materials and Methods.

Table 2.2 Steady-State Kinetic Parameters for Peptide Hydrolysis - Continuous Assay

	S. Typhimurium Lon		human Lon
	1	2	1
k_{cat} (s ⁻¹)	15 ± 2	11 ± 1	5.9 ± 0.7
K_m (μM)	262 ± 61	276 ± 38	1300 ± 200
k_{cat}/K_m (x 10 ³ M ⁻¹ s ⁻¹)	57	40	4.5
n	1.5 ± 0.3	1.4 ± 0.2	1.9 ± 0.3

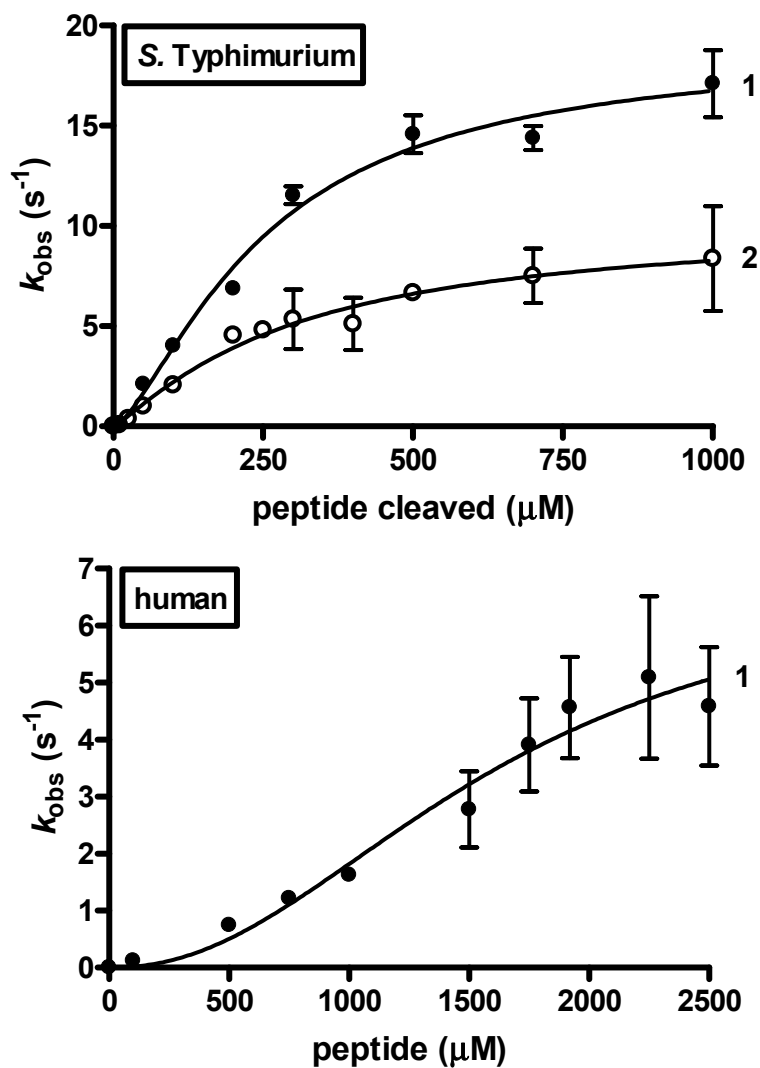


Figure 2.7 **Steady-state peptide hydrolysis by *S. Typhimurium* and human Lon using a discontinuous assay.** Reactions containing *S. Typhimurium* (top) or human (bottom) Lon were preincubated with varying concentrations of **1** (●) or **2** (○) prior to the addition of 1 mM ATP. All experiments were performed at least in triplicate and the averaged k_{obs} values (± 1 SD) were plotted against the corresponding peptide concentration. The data were best fit with the Hill equation (eq 2) as described in Materials and Methods.

Table 2.3 Steady-State Kinetic Parameters for Peptide Hydrolysis - Discontinuous Assay

	S. Typhimurium Lon		human Lon
	1	2	1
k_{cat} (s^{-1})	19 ± 2	10 ± 2	7 ± 2
K_m (μM)	251 ± 46	287 ± 70	1600 ± 500
k_{cat}/K_m ($\times 10^3 \text{ M}^{-1} \text{ s}^{-1}$)	75	35	4.4
n	1.4 ± 0.3	1.2 ± 0.2	2.2 ± 0.6

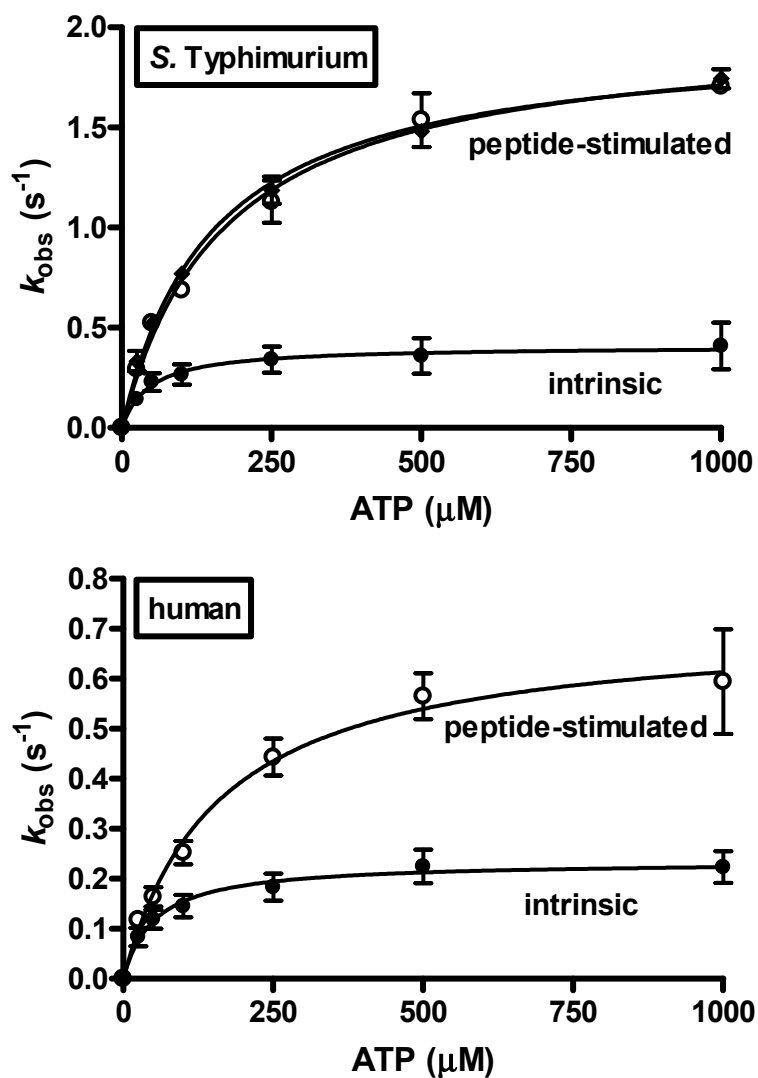


Figure 2.8 **Steady-state ATP hydrolysis by *S. Typhimurium* and human Lon.** Reactions containing *S. Typhimurium* (top) or human Lon (bottom) were preincubated in the absence (●) and presence of saturating ($5x K_m$) **1** (○) or **2** (◆) prior to the addition of varying concentrations of ATP. All experiments were performed at least in triplicate and the averaged k_{obs} values (± 1 SD) were plotted against the corresponding ATP concentration. The data were best fit with the Michaelis-Menton equation (eq 4) as described in Materials and Methods.

Table 2.4 Steady-State Kinetic Parameters for ATP Hydrolysis

	<i>S. Typhimurium</i> Lon			human Lon	
	intrinsic	1 stimulated	2 stimulated	intrinsic	1 stimulated
k_{cat} (s^{-1})	0.41 ± 0.05	2.0 ± 0.1	2.0 ± 0.1	0.23 ± 0.02	0.71 ± 0.06
K_m (μM)	46 ± 24	172 ± 24	150 ± 12	52 ± 17	158 ± 39

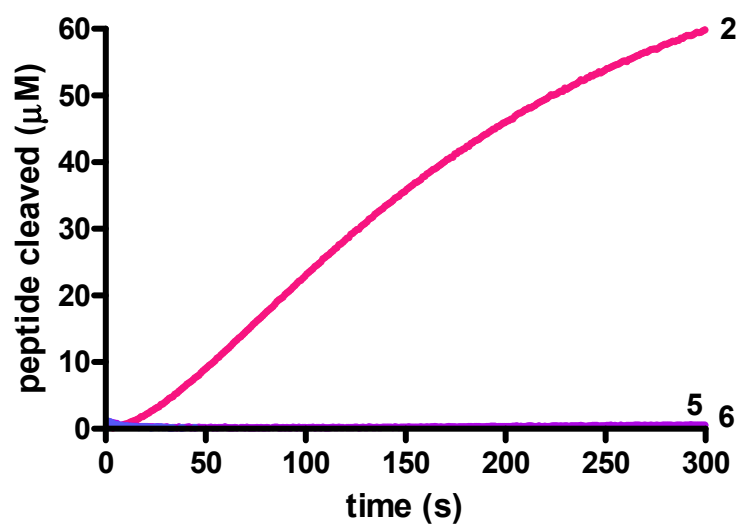


Figure 2.9 ATP-dependent peptide hydrolysis of 2, 5, and 6 by *S. Typhimurium* Lon. Representative time courses for 200 nM *S. Typhimurium* Lon degradation of 100 μM 2, 5, and 6 in the presence of 1 mM ATP.

Table 2.5 Mass Spectrometry Data for Peptide Hydrolysis Products

	1 (fluorescent)		2 (fluorescent)	
	N-terminal product	C-terminal product	N-terminal product	C-terminal product
sequence	Y(3-NO ₂)-RGITC	SGRQ-K(Abz)	Y(3-NO ₂)-RGIT-Abu	SGRQ-K(Abz)
predicted	757 Da	694 Da	739 Da	694 Da
[M+H] ⁺	757.6 Da	694.6 Da	739.6 Da	694.6 Da
[M+H-16] ⁺	741.6 Da		723.6 Da	
[M+H-32] ⁺	725.6 Da		708.1 Da	
	1 (non-fluorescent)		2 (non-fluorescent)	
	N-terminal product	C-terminal product	N-terminal product	C-terminal product
sequence	YRGITC	SGRQ-K(Bz)	YRGIT-Abu	SGRQ-K(Bz)
predicted	712 Da	679 Da	694 Da	679 Da
[M+H] ⁺	712.5 Da	679.5 Da	694.6 Da	679.6 Da

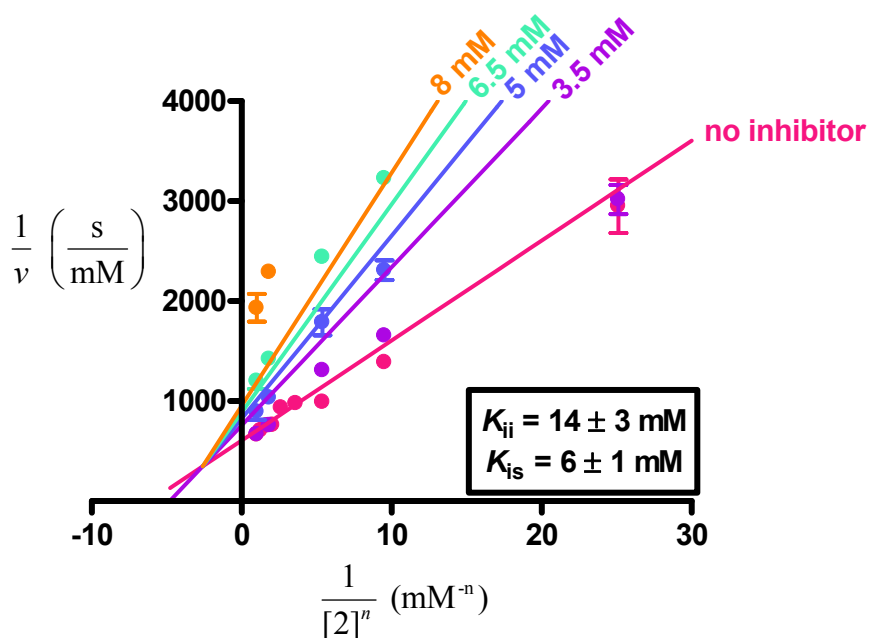


Figure 2.10 **Inhibition of *S. Typhimurium* Lon peptide hydrolysis by 6.** Reactions containing 150 nM *S. Typhimurium* Lon and varying concentration of 2 were preincubated in the presence and absence of varying concentrations of 7 prior to the addition of 1 mM ATP. All experiments were performed in triplicate and the steady-state velocity (v) determined as described in Materials and Methods. The averaged reciprocal v data (± 1 SD) was plotted against the corresponding reciprocal $[2]^n$, where n is the Hill coefficient for peptide hydrolysis of 2 by *S. Typhimurium* Lon (Table 2.2). The solid lines represent the best fit of the data at each concentration of 7 with eq 5. The averaged k_{obs} data was fit with eq 5 for noncompetitive inhibition to yield values for the inhibition constants at low and high concentrations of 2, K_{is} and K_{ii} respectively (Figure 2.2).

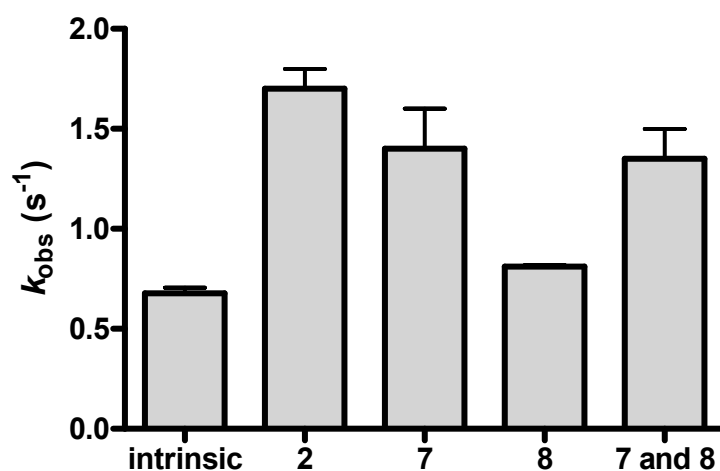


Figure 2.11 **ATP hydrolysis by *S. Typhimurium* Lon in the presence of peptide hydrolysis products.** Reactions containing *S. Typhimurium* Lon were preincubated in the absence (intrinsic) and presence of 100 μM of the indicated peptide substrate or hydrolysis product(s) prior to the addition of 1 mM ATP. All experiments were performed in duplicate and the averaged k_{obs} values (± 1 SD) were are shown.

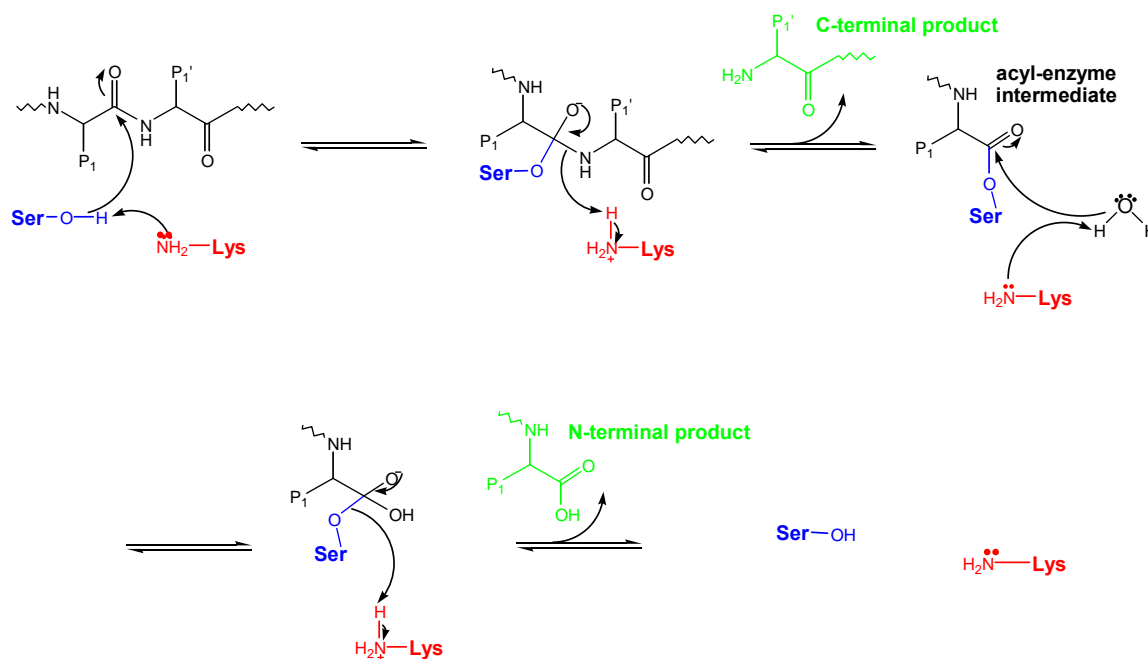


Figure 2.12 **Proposed mechanism for peptide bond cleavage in Lon.** Upon binding of the substrate, the active site serine nucleophilically attacks the carbonyl carbon of the scissile bond, resulting in the first tetrahedral intermediate. This intermediate collapses and the C-terminal product is released, yielding the acyl-enzyme intermediate. An activated water molecule attacks the carbonyl carbon, resulting in the second tetrahedral intermediate. This intermediate again collapses, the N-terminal product is released, and the active site regenerated.

CHAPTER 3

Identification of Peptidyl Boronates as Potent Inhibitors of the Peptide Hydrolysis

Activity of Lon Protease^{††}Abstract

The importance of Lon activity in bacterial pathogenicity has led to its emergence as a target in the development of novel antibiotics. This study focuses on identifying a lead compound(s) for the development of potent inhibitors. The IC_{50} values were evaluated for a series of peptide hydrolysis products to gain insight into the effect various modifications had on inhibition. The IC_{50} values for a series of peptide-based inhibitors were also evaluated to identify functional groups useful in inhibiting peptide hydrolysis activity. Those inhibitors which are proposed to behave as transition state analogs were the most useful in inhibiting Lon activity. The peptidyl boronate, MG262, was the most potent inhibitor tested and was effective against both the human and *Salmonella enterica* serovar Typhimurium homologs ($IC_{50} = 160 \pm 10$ nM and 122 ± 9 nM, respectively). As the bacterial and human enzymes display differences in peptide substrate specificity, as discussed in Chapter 2, modifications to the peptidyl moiety should allow discrimination between them and reduce side-effects due to cross-reactivity. MG262 will be used as a

^{††} The bulk of this work was published in *Biochemistry* on July 11, 2006 (*Biochemistry* **2006**, *45*, 8264-8274).

lead compound for the generation of alternative peptidyl boronate inhibitors, as described in Chapter 4.

Introduction

The number of pathogenic, antibiotic resistant bacteria increases each year, however the development of new antibiotics to treat them lags behind (78). Recent studies aimed at identifying proteins necessary for virulence have implicated the importance of Lon protease (21, 23). Pathogenic *Salmonella enterica* are responsible for causing a range of human diseases from mild gastroenteritis (serovar Typhimurium and serovar Enteritidis) to typhoid fever (serovar Typhi). It has been demonstrated that *Salmonella enterica* serovar Typhimurium (*S. Typhimurium*) Lon protease activity is required for systemic infection in mice, a common study model for *S. Typhi* infection in humans (23). In fact, Lon-deficient *S. Typhimurium*, when administered as an oral vaccine to mice, conferred subsequent protection against infection by virulent *S. Typhimurium* (24). In spite of its importance in pathogenicity, no potent inhibitors of Lon activity have been identified.

Lon is a homo-oligomeric ATP-dependent serine protease, which functions in the degradation of damaged and certain short-lived regulatory proteins (1-10). This enzyme is a member of the AAA⁺ superfamily (ATPases Associated with different cellular Activities) along with other ATP-dependent proteases such as ClpXP, HslUV, and the proteasome (47, 79). The proteasome also functions to degrade damaged proteins and is the responsible for the majority of protein degradation in the cytosol and nucleus of eukaryotes (80). As a result, it is an important target in the development of novel therapeutic agents. These proteins all share a common ATPase domain consisting of the Walker A and B motifs. Both Lon and HslUV, the bacterial homolog of the proteasome,

undergo a conformational change upon ATP binding (54, 71). Crystallographic studies of a truncated *Escherichia coli* (*E. coli*) Lon mutant have suggested the protease utilizes a serine-lysine dyad to catalyze peptide bond hydrolysis, similar to the threonine-N-terminal amino group dyad used by the proteasome (45, 81). Furthermore, both Lon and the proteasome are susceptible to serine, as well as, cysteine protease inhibitors (27, 60, 62, 80). Taken together, this suggests that approaches useful in developing inhibitors against the proteasome may also be useful in developing inhibitors of the peptide hydrolysis activity of Lon.

Inhibition studies are often used to gain insight into the interaction between the enzyme, substrate, and inhibitor. The IC_{50} value for an inhibitor is defined as the concentration of inhibitor required to reduce the observed rate constant (k_{obs}) for the measured activity by 2-fold (Figure 3.1). If determined under identical reaction conditions, these values can be used as a measure of the affinity of the inhibitor for the enzyme, allowing quantitative comparison of an entire series of inhibitors.

In this study, *S. Typhimurium* Lon was used as a model to quantitatively evaluate a series of peptide product inhibitors and commercially available proteasome inhibitors. The studies will show that protection of the amino terminal with a dansyl moiety will increase the affinity for the bacterial enzyme by 30-fold. Inhibitors containing an aldehyde, boronate, or β -lactone moiety will be shown to be potent inhibitors of the peptide hydrolysis activity of Lon, however the peptidyl boronate, MG262, is the best inhibitor to be identified ($IC_{50} = 122 \pm 9$ nM). Both the peptidyl and boronic acid moieties of MG262 are essential to obtain this degree of inhibition. Furthermore, MG262

is also effective against the human enzyme ($IC_{50} = 160 \pm 10$ nM). Thus, MG262 will serve as a lead compound in the development of future Lon inhibitors.

Materials and Methods

Materials

Fmoc-protected amino acids, Boc-2-Abz-OH, Fmoc-Lys(Aloc)-Wang resin, Fmoc-Leu-Wang resin, Z-Leu-OSu and HBTU were purchased from Advanced ChemTech and NovaBiochem. MG262, epoxomicin and ZL₃VS were purchased from Biomol International, LP. MG132 and *clasto*-lactacystin β -lactone were purchased from BostonBiochem. Tris buffer, cell culture media, IPTG, chromatography media, DTT, Mg(OAc)₂, trypsin, kanamycin, ATP, ethylboronic acid, isopropylboronic acid, DMSO, and all other reagents were purchased from Fisher, Sigma and Amresco (Solon, OH).

Purification of Recombinant Lon

S. Typhimurium Lon

Recombinant *S. Typhimurium* Lon was overexpressed in BL21 (DE3) (Novagen), using the plasmid pHF020 (Appendix B). Cells were grown and the purified protein isolated as described in Chapter 2 (82). The concentration of purified Lon monomer was determined by Bradford assay (73) using BSA as a standard, and the protein stored at -80°C.

Human Lon

Recombinant human Lon was overexpressed in Rosetta (DE3) (Novagen), using the plasmid pHF002, described in Chapter 2 (82). Cells were grown and the purified protein isolated as described in Chapter 2 (82). The concentration of purified human Lon monomer was determined by Bradford assay (73) using BSA as a standard, and the protein stored at -80°C.

Peptide Synthesis

The peptide substrates and peptide hydrolysis products shown in Table 3.1 and ZL₃OH (Table 3.4) were synthesized using standard Fmoc solid-phase synthesis techniques (74), with the exception of **9** and **11** which were purchased from Sigma. All peptides were purified by reverse phase HPLC (Appendix D) and their identities verified by mass spectrometry (Appendix E).

Steady-State Peptide Hydrolysis Assay

Inhibition Assays for Determination of IC_{50} Values of Peptide Hydrolysis Products

Steady-state velocity data were collected on a Fluoromax 3 spectrophotometer (Horiba Group) as described in Chapter 2 with minor modifications (64). Reactions contained 50 mM Tris (pH 8.1), 10 mM Mg(OAc)₂, 150 mM NaCl (human Lon reactions only), 2 mM DTT, 300 nM *S. Typhimurium* Lon monomer or 1 μM human Lon monomer, K_m level of the peptide substrate (10% fluorescent, 90% non-fluorescent), and

varying concentrations of the inhibitor. After equilibration at 37°C for 1 min, the reaction was initiated by the addition of 1 mM ATP. Due to the fluorescence of the dansyl moiety of **3** (Table 3.1), the amount of peptide cleaved was calibrated by determining the change in fluorescence/ μM peptide cleaved in the presence of each concentration of **3** evaluated. All experiments were performed at least in triplicate unless otherwise noted.

Inhibition Assays for Determination of IC_{50} Values of Proteasome Inhibitors

Steady-state velocity data were collected on a Fluoromax 3 spectrophotometer (Horiba Group) as described in Chapter 2 with minor modifications (64). Reactions contained 50 mM Tris (pH 8.1), 10 mM $\text{Mg}(\text{OAc})_2$, 150 mM NaCl (human Lon reactions only), 2 mM DTT, 300 nM *S. Typhimurium* or 0.3 - 1 μM human Lon monomer, and K_m level of the peptide substrate (10% fluorescent, 90% non-fluorescent). After equilibration at 37°C for 1 min, the reaction was initiated by the addition of 1 mM ATP. Varying concentrations of the inhibitor (in DMSO) were added once the enzyme reached steady-state turnover (50 s for *S. Typhimurium* Lon reactions or 90 s for human Lon reactions) and was considered time zero for the inhibition reaction. All experiments were performed in triplicate.

Data Analysis

Determination of k_{obs} Values

The steady-state velocities were determined from the final linear phase of the reaction time courses using KaleidaGraph (Synergy, Inc.). These values were converted to k_{obs} using eq 1.

$$k_{obs} = \frac{v}{[E]} \quad (1)$$

In eq 1, k_{obs} is the observed rate constant, v is the steady-state velocity, and E is Lon monomer.

Determination of IC_{50} Values

The k_{obs} data in the presence of 1 mM ATP, K_m level of the peptide substrate, and varying concentrations of inhibitor were fit with eq 2 to obtain an IC_{50} value for the inhibitor (83).

$$\frac{k_{obs,i}}{k_{obs}} = \frac{1}{1 + \frac{[I]}{IC_{50}}} \quad (2)$$

In eq 2, $k_{obs,i}$ is the observed rate constant in the presence of inhibitor, k_{obs} is the observed rate constant in the absence of inhibitor, and IC_{50} is the $[I]$ under which $k_{obs,i}/k_{obs} = 0.5$.

Estimation of K_i from IC_{50} Values

To approximate the K_i values for MG132, MG262, ethylboronic acid and ZL₃OH, it was assumed they were all competitive inhibitors with respect to **2** (Table 3.1). The IC_{50} values determined were used to estimate K_i using eq 3.

$$IC_{50} = K_i \left(1 + \frac{[S]}{K_m} \right) \quad (3)$$

In eq 3, IC_{50} is as defined as in eq 2, K_i is the inhibition constant, S is the peptide substrate, and K_m is the Michaelis-Menton constant. To estimate the expected K_i for MG262 if it were simply a competitive, bivalent inhibitor made up of a peptidly moiety (ZL₃OH) and a boronate moiety (ethylbornic acid), we used eqs 4-6 (84).

$$\Delta G_{binding,ZL_3OH} = RT \ln(K_{i,ZL_3OH}) \quad (4)$$

$$\Delta G_{binding,ethyl} = RT \ln(K_{i,ethyl}) \quad (5)$$

$$\Delta G_{binding,MG262} = \Delta G_{binding,ZL_3OH} + \Delta G_{binding,ethyl} = RT \ln(K_{i,MG262}) \quad (6)$$

In eqs 4 - 6, $\Delta G_{binding,ZL_3OH}$ is the free energy of binding for ZL₃OH, K_{i,ZL_3OH} is the inhibition constant for ZL₃OH, $\Delta G_{binding,ethyl}$ is the free energy of binding for ethylboronic acid, $K_{i,ethyl}$ is the inhibition constant for ethylbornic acid, $\Delta G_{binding,MG262}$ is the estimated free energy of binding for MG262, and $K_{i,MG262}$ is the estimated inhibition constant for MG262.

Results

Inhibition of Lon Peptide Cleavage by Peptide Hydrolysis Products

Although Lon is known to be important in cellular protein turnover, little is known about how it selects substrates for degradation. A series of peptides based on the amino acid sequence of the N-terminal product from hydrolysis of **1** (**3**, **7**, **9** - **12** in Table 3.1) were evaluated for their ability to inhibit *S. Typhimurium* Lon peptide hydrolysis of **2**. The observed rate constant (k_{obs}) at varying concentrations of the peptide product inhibitor were determined in the presence of K_m level of **2** and saturating ATP (Figure 3.2). The IC_{50} value for each peptide is summarized in Table 3.2. Compared to the unaltered product (**9**), substitution of 2-aminobutyric (**7**) or leucine (**10**) for the cysteine residue does not alter the inhibitory effect of the product. Neutralization of the negative charge at the C-terminal by substitution of an amide (**11**) for the carboxyl group results in a 4-fold decrease in inhibition. Conversely, comparison of **7** and **12** demonstrate that neutralization of the positive charge at the N-terminal with a benzyloxycarbonyl group has no significant effect on inhibition.

Interestingly, modification of the N-terminal with a dansyl group (**3**) results in a 30-fold increase in inhibition. To investigate whether this dramatic increase in potency could also be achieved in the human enzyme, preliminary IC_{50} values for **7** and **3** were determined in the presence of K_m level of **1** and saturating ATP (Figure 3.3). Due to solubility limitations, the effect of concentrations of **3** greater than 600 μM could not be

evaluated. At best, the N-terminal dansyl group confers a 6-fold increase in potency for the human homolog (Table 3.2).

Inhibition of Lon Peptide Hydrolysis by Common Proteasome Inhibitors

No potent or specific inhibitors of Lon protease activity were previously known. Due to mechanistic and structural similarities between Lon and HslUV (41, 45, 54), the bacterial homolog of the proteasome, a series of commercially available proteasome inhibitors were screened to identify a lead compound suitable for inhibiting the peptide hydrolysis activity of Lon. Using the *S. Typhimurium* enzyme as a model, the values for k_{obs} in the presence and absence of varying concentrations of the inhibitors were evaluated with respect to peptide hydrolysis activity, at K_m level of **2** and saturating ATP (Figure 3.4). The IC_{50} value for each inhibitor is summarized in Table 3.3. MG132, a peptidyl aldehyde, inhibited *S. Typhimurium* Lon with an IC_{50} of $4.1 \pm 0.3 \mu\text{M}$. Epoxomicin, a peptidyl epoxyketone, and ZL₃VS, a peptidyl vinyl sulfone, were ineffective at inhibiting peptide hydrolysis activity at micromolar concentrations. All proteasome inhibitors were dissolved in DMSO which did not affect peptide hydrolysis when it was less than 4% of the reaction volume. At concentrations greater than 4%, DMSO itself inhibited the peptide hydrolysis activity of Lon. Due to this limitation, the effect of higher concentrations of epoxomicin and ZL₃VS could not be evaluated.

Most of the proteasome inhibitors acted as classical inhibitors, with inhibition occurring instantaneously upon addition. However, inhibition by MG262, a peptidyl boronate, and *clasto*-lactacystin β -lactone were time dependent or biphasic (Figure 3.5).

This type of inhibition will be discussed in more detail in Chapter 4. When calculating the IC_{50} for MG262 and *clasto*-lactacystin β -lactone (Table 3.3), the final steady-state rate was used, as this was the final effect of inhibition. This resulted in an IC_{50} of $1.6 \pm 0.2 \mu\text{M}$ for *clasto*-lactacystin β -lactone and $122 \pm 9 \text{ nM}$ for MG262. Thus, MG262 is by far the most potent of all inhibitors tested. Peptidyl boronate inhibitors are also the most potent inhibitors of the proteasome (80).

Evaluating the Importance of the Peptidyl and Boronic Acid Moieties of MG262

MG262 has both a peptidyl and boronic acid moiety, both of which are important in inhibiting the proteasome (85). To explore the contribution of each of these moieties towards inhibition of the peptide hydrolysis activity of *S. Typhimurium* Lon, the IC_{50} values for related compounds which resemble each moiety alone were evaluated. Ethylboronic acid and isopropylboronic acid were chosen as models for the boronic acid moiety of MG262 (Table 3.4). The IC_{50} of ethylboronic acid could not be determined accurately due to solubility limitations, but was greater than 10 mM. Isopropylboronic acid, on the other hand, had an IC_{50} of $810 \pm 50 \mu\text{M}$ (Figure 3.6). The peptide ZL₃OH (Table 3.4) was synthesized as a model of the peptidyl moiety of MG262. The IC_{50} of ZL₃OH was $740 \pm 29 \mu\text{M}$ (Figure 3.7).

Inhibition of Human Lon by MG262

To investigate whether MG262, the most potent inhibitor identified in these studies, would be a potent inhibitor of human Lon, the values for k_{obs} in the presence and absence of varying concentrations of MG262 were evaluated with respect to peptide hydrolysis activity, at K_m level of **1** and saturating ATP (Figure 3.8). Not only is MG262 a potent inhibitor ($IC_{50} = 0.16 \pm 0.01 \mu\text{M}$), the inhibition is time-dependent as well.

Discussion

Lon is an ATP-dependent serine protease which has emerged as a target in the development of novel antibiotics due to its importance in bacterial pathogenicity (21, 23). Although x-ray crystallographic studies have suggested the enzyme utilizes a serine-lysine dyad to catalyze peptide bond hydrolysis, it is relatively unreactive towards small serine protease inhibitors (27, 45, 60, 62). Furthermore, of the inhibitors tested, both cysteine and serine protease inhibitors have displayed some inhibitory effect on peptide hydrolysis (27, 60, 62). This study focuses on identifying a lead compound(s) for the development of potent Lon inhibitors by evaluating the IC_{50} values of a series of peptide hydrolysis products and peptide-based inhibitors.

Lon catalyzes the hydrolysis of both ATP and proteins within different domains, presenting two possible approaches in developing inhibitors. As demonstrated in Chapter 2, the ATP hydrolysis activities of the bacterial and human homologs are kinetically indistinguishable, whereas they display differences in their substrate specificity (82). This suggests that a peptide-based approach would be more useful, as the differences in substrate specificity could potentially be exploited to target an inhibitor specifically to the bacterial enzyme, thereby decreasing the chance for side-effects resulting from cross-reactivity with the human homolog.

To gain insight into how various modifications to the peptide affect the strength of inhibition, a series of peptides based on the amino acid sequence of the N-terminal product from hydrolysis of **1** (**9**) were evaluated for their ability to inhibit *S. Typhimurium* Lon peptide hydrolysis of **2**. The cysteine residue presents both synthetic

difficulties as well as the potential for undesired side reactions, such as disulfide bond formation. As substitution of the cysteine with either leucine (**10**) or 2-aminobutyric (**7**) does not affect the potency of inhibition, either amino acid will be suitable for replacing cysteine in future inhibitors (Table 3.2). Under physiological conditions, peptides exist as a zwitterion. The charges at the N- and C-terminal impair cellular uptake across the hydrophobic plasma membrane, thus they are often masked by protecting groups. Replacement of the negative C-terminal carboxyl group with a neutral amide group (**11**) reduces inhibition by 4-fold (Table 3.2). This may indicate Lon has a preference for a negative charge at the C-terminal and a protecting group with a partial negative charge will have a smaller effect on inhibition. Protection of the N-terminal amino group with a benzyloxycarbonyl (**12**) had no adverse affect on inhibition. In fact protection with a dansyl group (**3**) increases the potency by 30-fold (Table 3.2). Interestingly, the dansyl group confers only a maximum 6-fold increase in potency in the human homolog (Table 3.2), presenting another approach to discriminate between the bacterial and human enzymes. An N-terminal dansyl moiety itself may be able to discriminate between the two proteases.

Lon is unique in that while classified as a serine protease, it is susceptible to both serine and cysteine protease inhibitors (27, 60, 62). Of the soluble ATP-dependent proteases within the AAA⁺ superfamily, Lon more closely resembles proteases within the proteasome family (41, 54, 71, 81). As such, the search for a potent Lon inhibitor began by screening a series of commercially available proteasome inhibitors. It should be noted that understanding the cross-reactivity of these inhibitors with Lon will also benefit the development of future proteasome inhibitors, as both enzymes are important targets for

creating novel therapeutic agents. Peptide-based inhibitors were chosen which contained similar peptide sequences, with only the reactive functional group varying. Thus, the potency of different functional groups could be compared directly. Using a standard set of conditions, 300 μM **2** (K_m level), 300 nM *S. Typhimurium* Lon, and saturating ATP, the IC_{50} value was determined for each inhibitor in the series (Table 3.3).

Peptidyl vinyl sulfones were designed to inhibit cysteine proteases via Michael addition (86), however they were later shown to react with both serine and threonine proteases (Figure 3.9) (55, 87-89). The peptidyl vinyl sulfone ZL₃VS was tested as an inhibitor of the peptide hydrolysis activity of *S. Typhimurium* Lon, but it did not appear to have any inhibitory effect (Table 3.3). The reason for the lack of inhibition is unclear, although it may suggest that the orientation of the active site residues, with respect to the peptide binding pocket, are different between the proteasome and Lon, thereby misaligning the vinyl sulfone for nucleophilic attack.

The natural product epoxomicin, a peptidyl epoxyketone, is the most selective proteasome inhibitor known due to its unique mechanism of inhibition (Figure 3.10) (90, 91). The final covalent adduct is a morpholino ring which contains not only the active site threonine (residue 1) hydroxyl, but also the N-terminal amino group (92). The crystal structure of the proteolytic domain of *E. coli* Lon was determined with a proteolytically inactive mutant, thus the orientation of the nucleophilic hydroxyl group is unknown, as well as how this hydroxyl affects the orientation of the ϵ -amino group of the proposed serine-lysine dyad of Lon (41). It was hypothesized that if the serine-lysine dyad of Lon was indeed analogous to the catalytic dyad of the proteasome, epoxomicin inhibition of Lon would provide further insight into the orientation of these residues.

Unfortunately, epoxomicin was unable to inhibit peptide hydrolysis by the *S. Typhimurium* protease (Table 3.3). Thus, the orientation of the active site residues of Lon and the proteasome are different. This result also further reinforces the unique specificity of epoxomicin for the proteasome.

Peptidyl aldehydes and boronates were designed to function as transition state analog inhibitors of proteolytic enzymes, with an active site thiol or hydroxyl, via formation of a tetrahedral adduct (Figure 3.11) (85, 93-96). Peptidyl aldehydes inhibit cysteine, serine, and threonine proteases effectively, with some preference for cysteine due to the higher nucleophilicity of the thiol. Peptidyl boronates, on the other hand, are much more potent against serine and threonine proteases due to the weakness of the boron-sulfur bond in the covalent adduct with cysteine (85). MG132, a peptidyl aldehyde, and MG262, a peptidyl boronate, both inhibit peptide hydrolysis by *S. Typhimurium* Lon, with IC_{50} values of $4.1 \pm 0.3 \mu\text{M}$ and $122 \pm 9 \text{ nM}$, respectively (Table 3.3, Figure 3.4). The K_i value for each can be estimated from the IC_{50} value ($2 \mu\text{M}$ for MG132, 60 nM for MG262) as described under Materials and Methods (84). Although these are some of the best inhibitors of Lon known to date, both are ~2000-fold more potent against the 20S proteasome (85). This weaker reactivity of MG132 and MG262 towards Lon may imply the local environment of the active site renders the hydroxyl less nucleophilic than in the proteasome and/or the peptide sequence is not optimal for binding to Lon. It is clear that transition state analogs will be useful in developing more potent inhibitors of Lon activity.

As no potent inhibitors of human Lon have been described, the ability of MG262 to inhibit peptide hydrolysis of this homolog was investigated as well. Like the *S.*

S. Typhimurium Lon enzyme, the inhibition was potent ($IC_{50} = 160 \pm 10 \mu\text{M}$) and displayed time-dependent or biphasic kinetics (Figure 3.8). Time-dependent kinetics are observed when the inhibition occurs on the timescale of enzymatic turnover, leading to a change in the rate of the reaction over time. Further studies, described in detail in Chapter 4, will be required to understand the mechanism behind these unique kinetics.

Clasto-lactacystin β -lactone is formed spontaneously at neutral pH from lactacystin, a *Streptomyces* metabolite (Figure 3.12) (97, 98). It has been shown to inhibit threonine and some serine proteases through formation of a covalent adduct; however the adduct is susceptible to hydrolysis (Figure 3.13) (80). *Clasto*-lactacystin β -lactone inhibits peptide hydrolysis by *S. Typhimurium* Lon with an IC_{50} value of $1.6 \pm 0.2 \mu\text{M}$ (Table 3.3, Figure 3.4). Estimation of the K_i from the IC_{50} results in a value of $0.8 \mu\text{M}$ which is 10-fold stronger than that observed in the proteasome (80). It is interesting to note that the inhibition by *clasto*-lactacystin β -lactone is time-dependent (Figure 3.5). Typical time-dependent inhibitors display an initial rate which is faster than the final steady-state rate, but inhibition by *clasto*-lactacystin β -lactone has a slower initial rate followed by a faster final steady-state rate. This may indicate that inhibition by the β -lactone is quite strong, but is subject to slow hydrolysis (Figure 3.13). This suggests the final inhibition observed is actually due to the dihydroxy acid; however confirmation of this mechanism will require further experiments with the pure dihydroxy acid.

MG262, the most potent inhibitor identified, has a peptidyl and a boronic acid moiety, both of which are important for inhibition of the 20S proteasome (85). To determine the importance of each of these moieties in inhibition of *S. Typhimurium* Lon,

the IC_{50} values for compounds representing each moiety separately were determined. To model the boronate moiety alone, both ethyl- and isopropylboronic acid were evaluated. The IC_{50} of ethylboronic acid was greater than 10 mM, however the IC_{50} for isopropylboronic was $810 \pm 50 \mu\text{M}$ (Table 3.4, Figure 3.6). The observed difference in IC_{50} for the two compounds is unknown, however it suggests the larger alkyl group may help anchor the boronic acid in the active site, thereby facilitating inhibition. The peptide $ZL_3\text{OH}$ was synthesized as a mimic of the peptidyl moiety of MG262 and it was found to have an IC_{50} of $740 \pm 29 \mu\text{M}$ (Table 3.4, Figure 3.7). Neither the boronate nor peptide alone could achieve the nanomolar potency found for MG262. The K_i value for each moiety can again be estimated from the IC_{50} value, as described under Materials and Methods (5 mM for ethylboronic acid, 400 μM for $ZL_3\text{OH}$) (84). If MG262 approximates a bivalent inhibitor made up of a boronic acid and peptidyl moiety, at best, an IC_{50} of $\sim 4 \mu\text{M}$ is expected (84). In reality, MG262 is 30-fold more potent (Table 3.3), indicating the inhibition is more complicated than simply increased affinity and will require further investigation.

Based upon the data obtained in this study, the following mechanism is proposed to account for MG262 inhibition of Lon (Figure 3.14). First, Lon binds to its substrates (MG262 and ATP) resulting in a ternary complex. It has previously been shown that ATP binding induces a conformational change in both *E. coli* Lon and HslUV and that in HslUV, this conformational change results in the productive alignment of the substrate with the active site threonine (54, 55, 99). Based on these observations, it is suggested the ternary complex next undergoes a conformational change. This conformational change correctly aligns the boronate moiety of MG262 for nucleophilic attack by the

active site serine of Lon. Finally, a tetrahedral intermediate is formed between MG262 and active site serine. The covalent modification would be reversible; however the equilibrium lies towards the covalently modified species, described in detail in Chapter 4, and is consistent with MG262 inhibition of the 20S proteasome (80). Alternately, the final step may simply be a tightening of the enzyme around the inhibitor. The first two steps appear to be fast, as inhibition by ZL₃OH occurs immediately upon addition (i.e., it is a classical inhibitor). The last step is believed to be slow, due to the observation of biphasic time courses (Figure 3.5). Further studies, described in detail in Chapter 4, will provide insight into the details of the proposed mechanism.

In this study, *S. Typhimurium* Lon was used as a model to quantitatively evaluate a series of peptide product inhibitors and commercially available proteasome inhibitors. The peptidyl boronate, MG262, was identified as a potent inhibitor of peptide hydrolysis by both the human and bacterial enzymes. As the bacterial and human proteases display differences in peptide substrate specificity, as discussed in Chapter 2, modifications to the peptidyl moiety should allow discrimination between them and reduce side-effects due to cross-reactivity. It should be noted that proteasome inhibitors, such as MG132, are able to diffuse into the mitochondria and inhibit the degradation of the steroidogenic acute regulatory protein (StAR), a physiological substrate of mammalian Lon (57, 100). Thus, detailed kinetic analysis of the mechanism by which these inhibitors affect Lon activity are necessary to minimize cross-reactivity with other proteases.

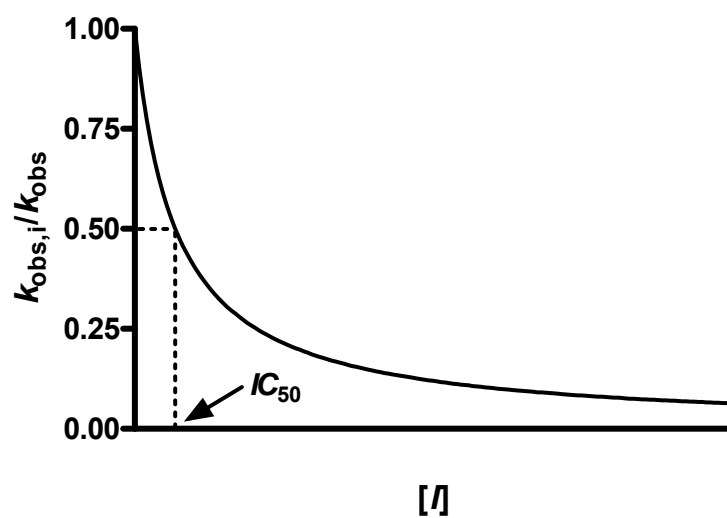
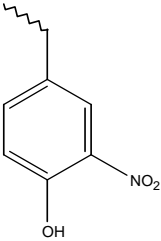
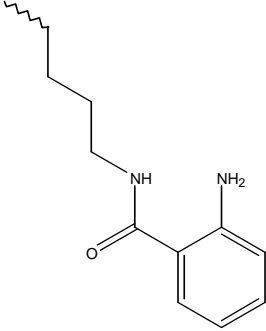
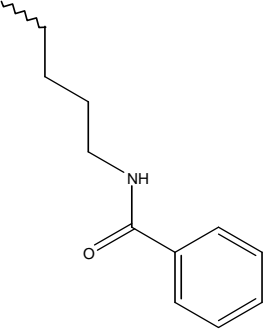
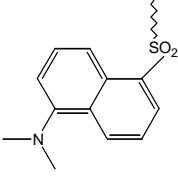
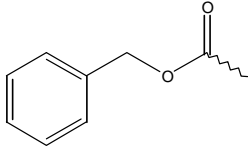


Figure 3.1 **Determination of the IC_{50} value of an inhibitor.** Representative plot of the values for k_{obs} in the presence of inhibitor / k_{obs} in the absence of inhibitor ($k_{\text{obs},i}/k_{\text{obs}}$) plotted against the corresponding inhibitor concentration. The IC_{50} value is equal to the $[I]$ in which $k_{\text{obs},i}/k_{\text{obs}} = 0.5$.

Table 3.1 Summary of Peptide-Based Substrates and Products

1	fluorescent non-fluorescent	Y(3-NO ₂)RGITCSGRQK(Abz) YRGITCSGRQK(Bz)		
2	fluorescent non-fluorescent	Y(3-NO ₂)RGIT-Abu-SGRQK(Abz) YRGIT-Abu-SGRQK(Bz)		
3	fluorescent	dansyl-YRGIT-Abu		
7	non-fluorescent	YRGIT-Abu		
9	non-fluorescent	YRGITC		
10	non-fluorescent	YRGITL		
11	non-fluorescent	YRGITC-NH ₂		
12	non-fluorescent	Z-YRGIT-Abu		
Y(3-NO ₂)	K(Abz)	K(Bz)	Abu	dansyl
				
Z				
				

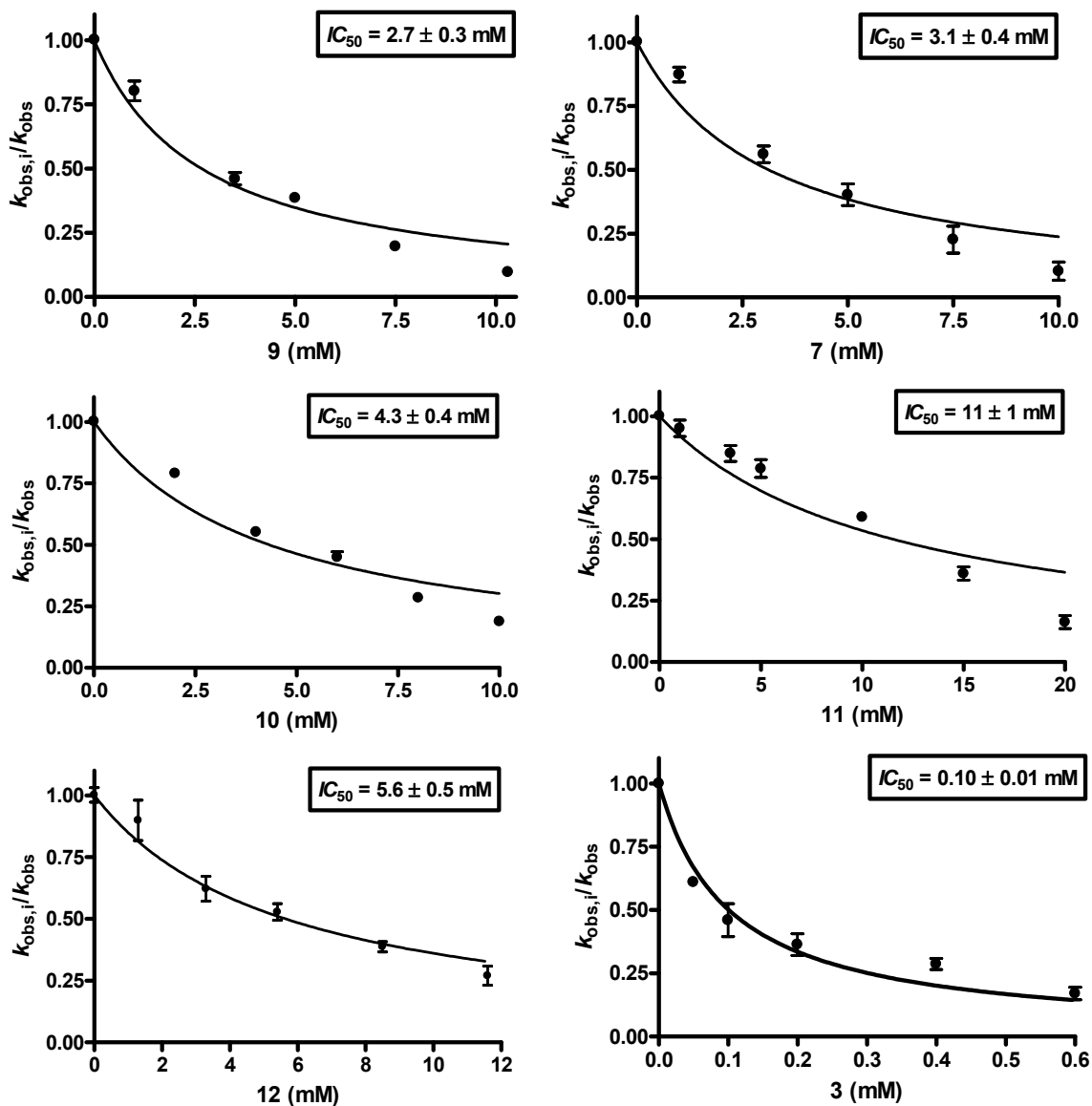


Figure 3.2 **Inhibition of *S. Typhimurium* Lon peptide cleavage by peptide hydrolysis products.** Reactions containing 300 nM *S. Typhimurium* Lon and 300 μ M **2** were preincubated in the presence and absence of varying concentrations of the peptide product inhibitor prior to the addition of 1 mM ATP. All experiments were performed in triplicate and the k_{obs} values determined as described in Materials and Methods. The averaged k_{obs} in the presence of inhibitor / k_{obs} in the absence of inhibitor ($k_{obs,i}/k_{obs}$, ± 1 SD) were plotted against the corresponding inhibitor concentration. The IC_{50} were determined by fitting the data with eq 2 as described in Materials and Methods.

Table 3.2 Summary of IC_{50} Values for Peptide Product Inhibitors

	IC_{50} (mM)	
	<i>S. Typhimurium</i>	human
9	2.7 ± 0.3	
7	3.1 ± 0.4	4 ± 1^a
10	4.3 ± 0.4	
11	11 ± 1	
12	5.6 ± 0.5	
3	0.10 ± 0.01	> 0.6

^a determined from a single data set

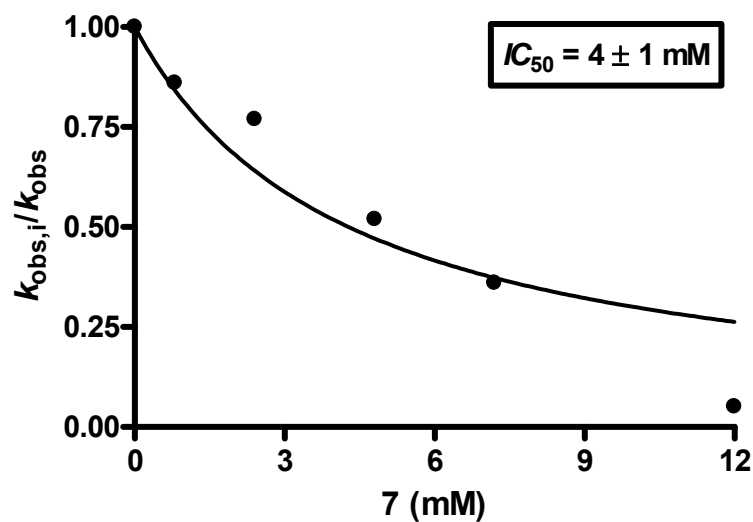


Figure 3.3 **Inhibition of human Lon peptide hydrolysis by 7.** Reactions containing 1 μ M human Lon and 1 mM **1** were preincubated in the presence and absence of varying concentrations of **7** prior to the addition of 1 mM ATP. The k_{obs} values were determined as described in Materials and Methods and the k_{obs} in the presence of inhibitor / k_{obs} in the absence of inhibitor ($k_{obs,i}/k_{obs}$) were plotted against the corresponding inhibitor concentration. The IC_{50} value was determined by fitting the data with eq 2 as described in Materials and Methods.

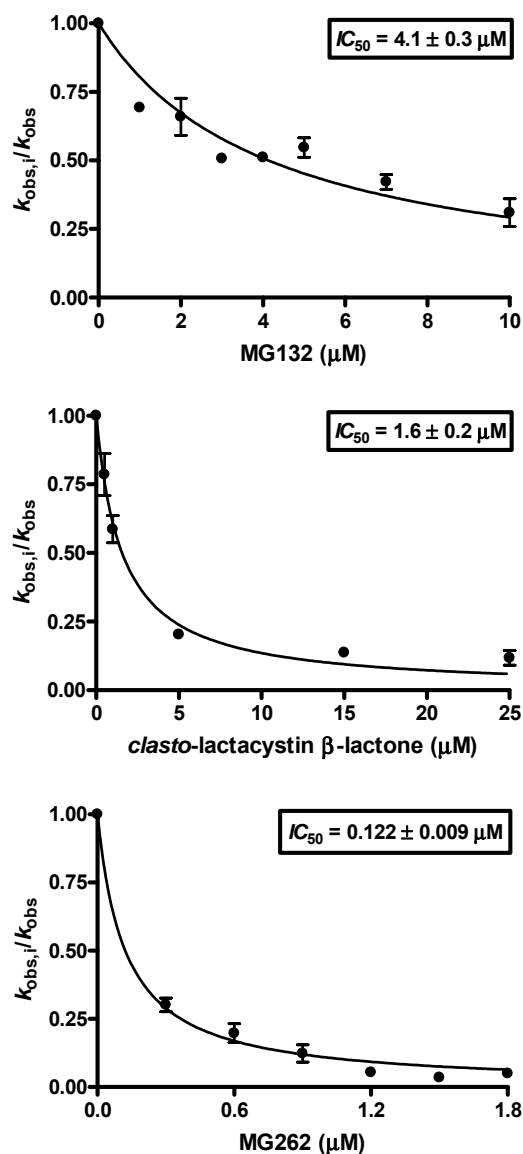
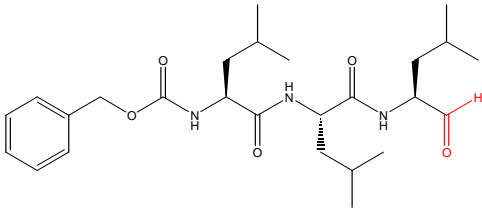
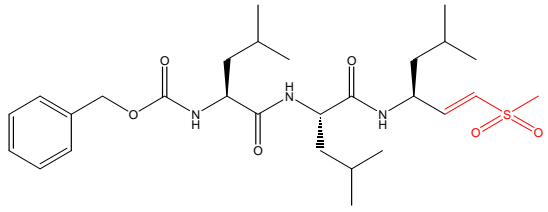
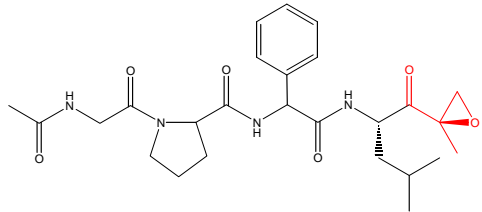
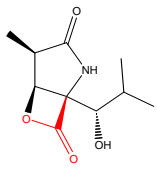
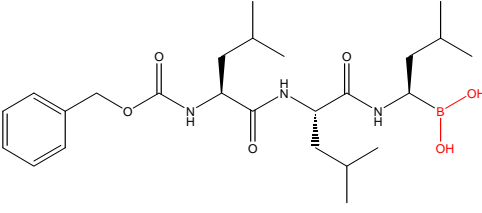


Figure 3.4 **Inhibition of *S. Typhimurium* Lon peptide hydrolysis by proteasome inhibitors.** Reactions containing 300 nM *S. Typhimurium* Lon were preincubated with 300 μM **2** prior to the addition of 1 mM ATP. After 50 s, varying concentrations of the inhibitor (in DMSO) were added and peptide cleavage monitored over 10 min. All experiments were performed in triplicate and the k_{obs} values determined as described in Materials and Methods. The averaged k_{obs} in the presence of inhibitor / k_{obs} in the absence of inhibitor ($k_{obs,i}/k_{obs}$, ± 1 SD) were plotted against the corresponding inhibitor concentration. The IC_{50} value was determined by fitting the data with eq 2 as described in Materials and Methods.

Table 3.3 Summary of IC_{50} Values for Proteasome Inhibitors

	structure	IC_{50} (μM)	
		<i>S.</i> Typhimurium	human
MG132	<p>aldehyde</p> 	4.1 ± 0.3	
ZL ₃ VS	<p>vinyl sulfone</p> 	> 167	
epoxomicin	<p>epoxyketone</p> 	> 200	
<i>clasto-</i> lactacystin β -lactone	<p>β-lactone</p> 	1.6 ± 0.2	
MG262	<p>boronate</p> 	0.122 ± 0.009	0.16 ± 0.01

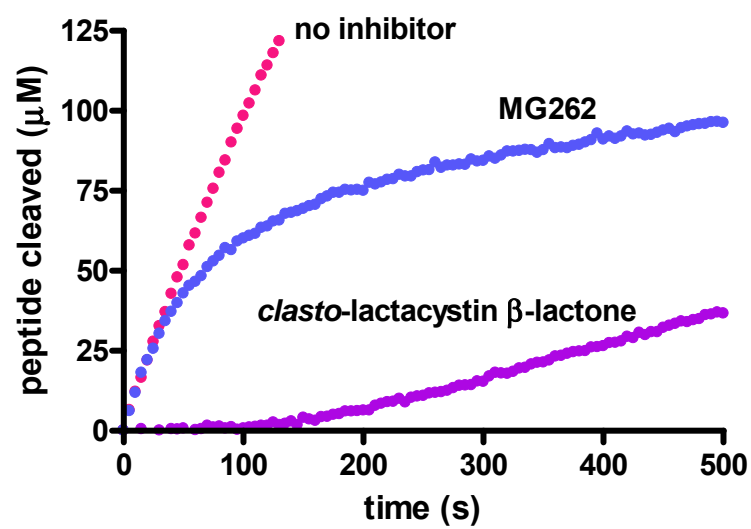
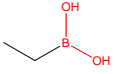
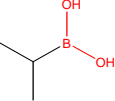
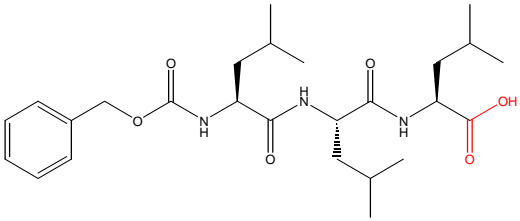


Figure 3.5 **Time-dependent inhibition by MG262 and *clasto*-lactacystin β -lactone.** Representative time courses for 300 nM *S. Typhimurium* Lon degradation of 300 μM **2** in the absence and presence of 0.9 μM MG262 or 5 μM *clasto*-lactacystin β -lactone.

Table 3.4 Summary of IC_{50} Values for Peptidyl and Boronic Acid Moieties

	structure	IC_{50} (μM)
ethylboronic acid		> 10000
isopropylboronic acid		810 ± 50
ZL ₃ OH		740 ± 29

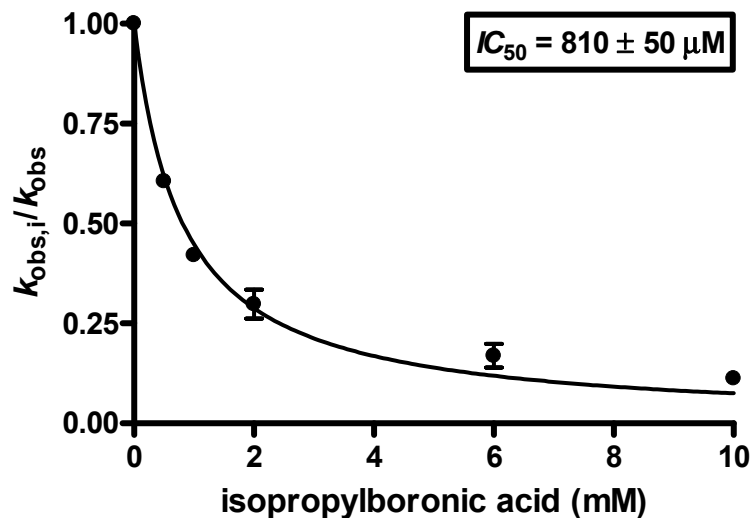


Figure 3.6 **Inhibition of *S. Typhimurium* Lon peptide hydrolysis by isopropylboronic acid.** Reactions containing 300 nM *S. Typhimurium* Lon were preincubated with 300 μ M **2** prior to the addition of 1 mM ATP. After 50 s, varying concentrations of isopropylboronic acid (in DMSO) were added and peptide cleavage monitored over 10 min. All experiments were performed in triplicate and the k_{obs} values determined as described in Materials and Methods. The averaged k_{obs} in the presence of inhibitor / k_{obs} in the absence of inhibitor ($k_{obs,i}/k_{obs}$, ± 1 SD) were plotted against the corresponding inhibitor concentration. The IC_{50} value was determined by fitting the data with eq 2 as described in Materials and Methods.

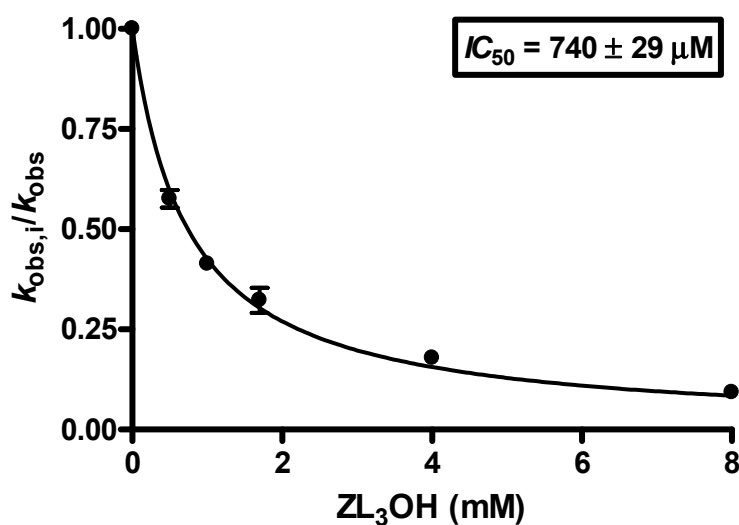


Figure 3.7 **Inhibition of *S. Typhimurium* Lon peptide hydrolysis by ZL_3OH .** Reactions containing 300 nM *S. Typhimurium* Lon were preincubated with 300 μM **2** prior to the addition of 1 mM ATP. After 50 s, varying concentrations of ZL_3OH (in DMSO) were added and peptide cleavage monitored over 10 min. All experiments were performed in triplicate and the k_{obs} values determined as described in Materials and Methods. The averaged k_{obs} in the presence of inhibitor / k_{obs} in the absence of inhibitor ($k_{obs,i}/k_{obs}$, ± 1 SD) were plotted against the corresponding inhibitor concentration. The IC_{50} value was determined by fitting the data with eq 2 as described in Materials and Methods.

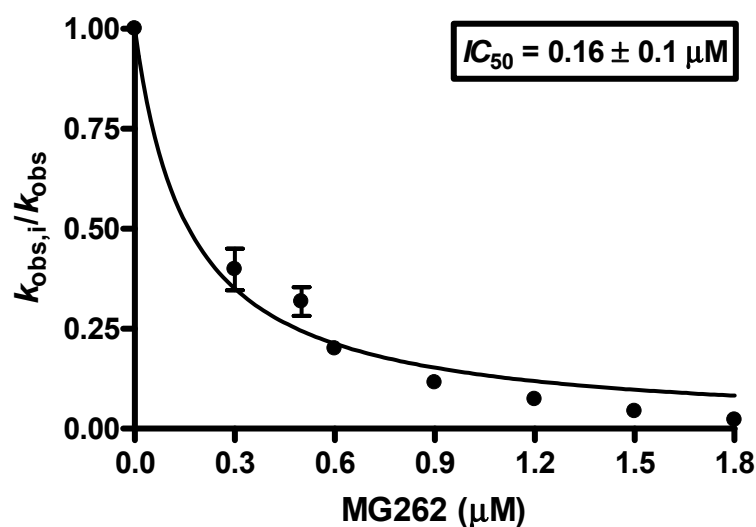


Figure 3.8 **Inhibition of human Lon peptide hydrolysis by MG262.** Reactions containing human Lon were preincubated with 1 mM **1** prior to the addition of 1 mM ATP. After 90 s, varying concentrations of MG262 (in DMSO) were added and peptide cleavage monitored over 10 min. All experiments were performed in triplicate and the k_{obs} values determined as described in Materials and Methods. The averaged k_{obs} in the presence of inhibitor / k_{obs} in the absence of inhibitor ($k_{obs,i}/k_{obs}$, ± 1 SD) were plotted against the corresponding inhibitor concentration. The IC_{50} value was determined by fitting the data with eq 2 as described in Materials and Methods.

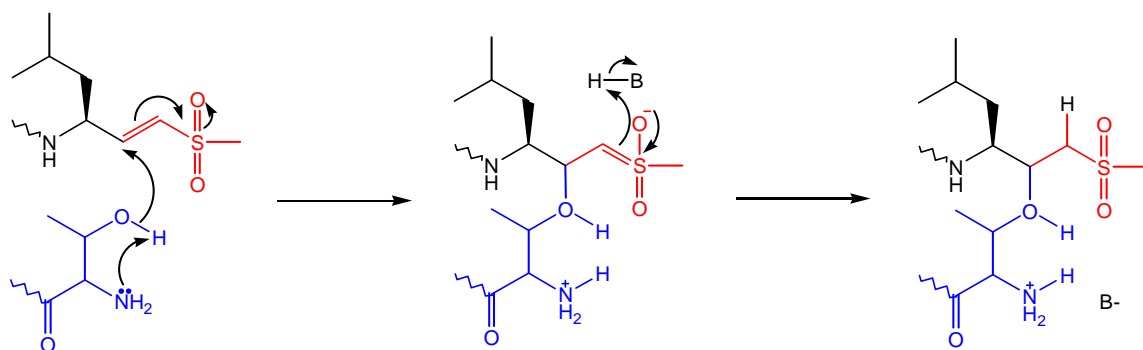


Figure 3.9 **General mechanism for inhibition by vinyl sulfones.** Representative mechanism for inhibition of the proteasome, a threonine protease, by a vinyl sulfone (red). The active site threonine of the proteasome, containing the N-terminal amino group, is shown in blue. Vinyl sulfones inhibit serine and cysteine proteases via a similar mechanism.

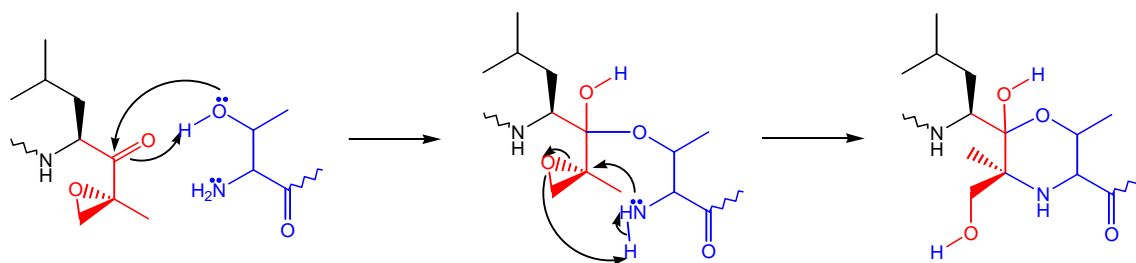


Figure 3.10 **General mechanism for inhibition of the proteasome by epoxomicin.** The epoxyketone is shown in red and active site threonine of the proteasome, containing the N-terminal amino group, is shown in blue.

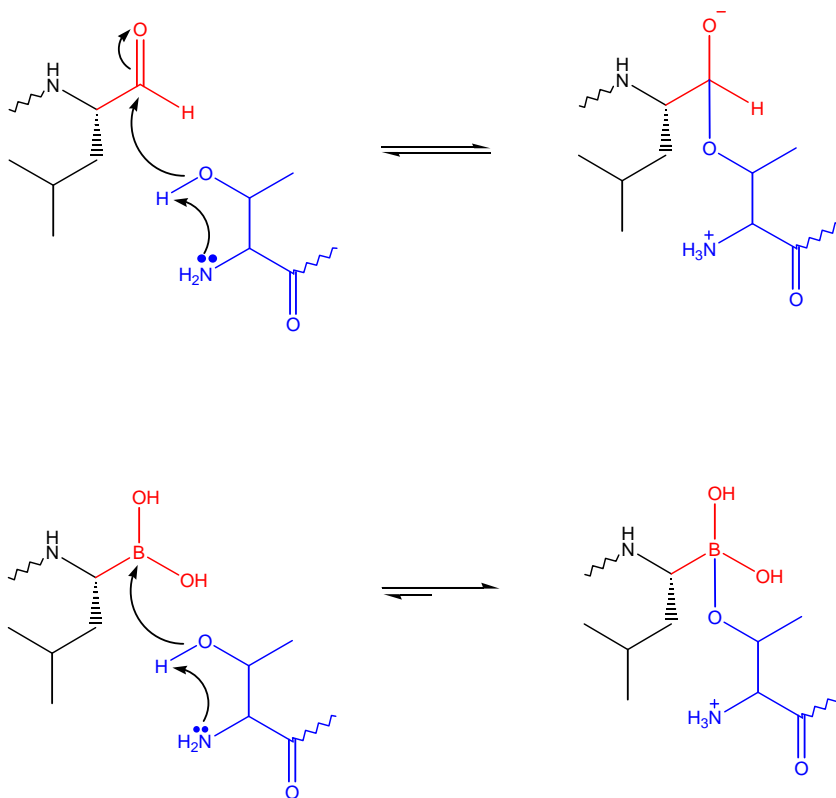


Figure 3.11 General mechanism for inhibition by peptidyl aldehydes and boronates. Representative mechanism for inhibition of the proteasome, a threonine protease, by a peptidyl aldehyde (top) and peptidyl boronate (bottom). The active site threonine of the proteasome, containing the N-terminal amino group, is shown in blue. The aldehyde and boronate moieties are shown in red. Peptidyl aldehydes inhibit serine and cysteine proteases via a similar mechanism. Peptidyl boronates inhibit serine proteases through an analogous mechanism.

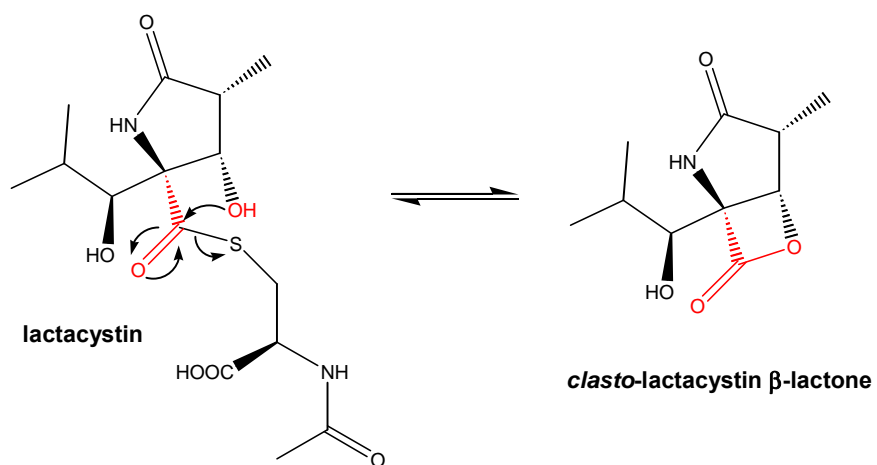


Figure 3.12 Spontaneous formation of *clasto*-lactacystin β -lactone from lactacystin at neutral pH.

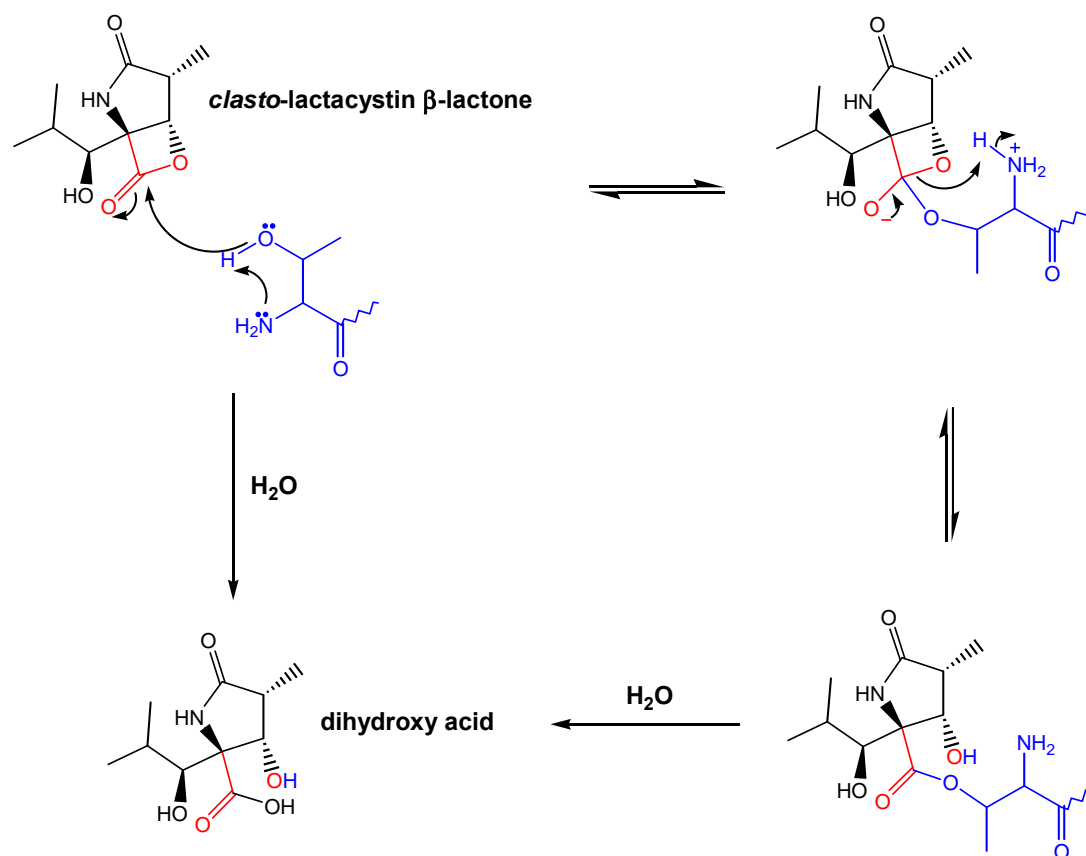


Figure 3.13 **General mechanism for inhibition by *clasto-lactacystin* β -lactone.** Representative mechanism for inhibition of the proteasome, a threonine protease, by *clasto-lactacystin* β -lactone. The active site threonine of the proteasome, containing the N-terminal amino group, is shown in blue. The β -lactone ring is shown in red. In general, β -lactones inhibit serine proteases through an analogous mechanism.

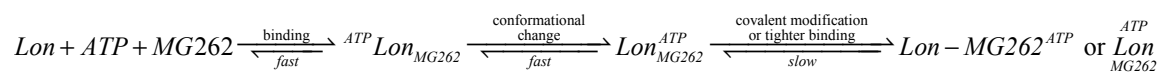


Figure 3.14 **Proposed mechanism for inhibition of Lon by MG262.** Lon binds to its substrates (MG262 and ATP) resulting in a ternary complex $\left(\textit{ATP Lon}_{\text{MG262}} \right)$. This is followed by a conformational change which aligns the active site for catalysis $\left(\textit{Lon}_{\text{MG262}}^{\textit{ATP}} \right)$. Finally, either a tetrahedral intermediate is formed between MG262 and active site serine $\left(\textit{Lon} - \textit{MG262}^{\textit{ATP}} \right)$ or the enzyme tightens down on the inhibitor $\left(\textit{Lon}_{\text{MG262}}^{\textit{ATP}} \right)$.

CHAPTER 4

Insight into the Mechanism for Time-Dependent Inhibition of the Peptide Hydrolysis
Activity of Lon Protease by Peptidyl Boronates^{‡‡}

Abstract

This study explores the mechanism by which the proteasome inhibitor MG262, a peptidyl boronate, inhibits the peptide hydrolysis activity of Lon. It also evaluates a novel fluorescent peptidyl boronate inhibitor based upon the amino acid sequence of a product of peptide hydrolysis by the enzyme. Steady-state kinetic techniques demonstrate that both peptidyl boronates are competitive inhibitors of the peptide hydrolysis activity of Lon and follow the same two-step, time-dependent inhibition mechanism. The first step is rapid and appears to involve binding of the inhibitor and formation of a covalent adduct with the active site serine. Next, a second slow step occurs in which the protease undergoes a conformational change, or isomerization, to enhance the interaction with the bound inhibitor with the proteolytic active site, to yield an overall inhibition constant of around 20 nM for both inhibitors. Although inhibition of serine and threonine proteases by peptidyl boronates has been detected previously, Lon is the first protease which has required the binding of ATP in order to observe inhibition.

^{‡‡} The bulk of this work was submitted for publication in *Biochemistry* on February 8, 2007.

Introduction

The emergence of new strains of antibiotic resistant bacteria requires the development of novel therapeutics to treat them. Studies aimed at identifying proteins necessary for bacterial virulence have implicated the importance of Lon protease (21, 23). Pathogenic *Salmonella enterica* are responsible for causing a range of human diseases from mild gastroenteritis (serovar Typhimurium and serovar Enteritidis) to typhoid fever (serovar Typhi). It has been shown that *Salmonella enterica* serovar Typhimurium (*S. Typhimurium*) Lon protease activity is required for systemic infection in mice, a common study model for *S. Typhi* infection in humans (23). In fact, Lon-deficient *S. Typhimurium*, when administered as an oral vaccine to mice, conferred subsequent protection against infection by virulent *S. Typhimurium* (24). Taken together, these studies highlight Lon as an important target in the development of novel therapeutic agents.

Lon, also known as the protease La, is a member of the AAA⁺ superfamily (ATPases Associated with different cellular Activities) along with other ATP-dependent proteases such as ClpXP, HslUV, and the proteasome (47, 79). It is a homo-oligomeric ATP-dependent serine protease which functions in the degradation of damaged and certain short-lived regulatory proteins (1-10). The ATP hydrolysis activities of the bacterial and human homologs are kinetically indistinguishable, however they display marked differences in their substrate specificity (82). The mechanism by which this protease recognizes a protein substrate or utilizes the energy from ATP hydrolysis to catalyze protein degradation is not well understood. *Escherichia coli* (*E. coli*) Lon has

long been used as a model for elucidating the molecular details of these processes. Crystallographic studies of a truncated mutant have suggested that it utilizes a serine-lysine dyad to catalyze peptide bond hydrolysis (45, 81). It has also been shown that the *E. coli* homolog requires only the binding, but not hydrolysis, of ATP in order to cleave a peptide substrate albeit at a reduced rate (64). Upon ATP binding, the enzyme undergoes a conformational change, which has been suggested to result in the productive alignment of the active site residues for peptide bond hydrolysis (54, 82).

Lon is unique, in that, although it is a serine protease, it is susceptible to inhibition by both serine and cysteine protease inhibitors (27, 60, 62, 80). The proteasome inhibitor, MG262 (Table 4.1), was identified as a potent inhibitor of the proteolytic activity of both *S. Typhimurium* and human Lon, described in detail in Chapter 3 (82). Inhibition of the enzyme by MG262 displayed time-dependent or slow-binding kinetics. Time-dependent inhibition is observed when inhibition occurs on the same timescale as enzymatic turnover. The rate of the reaction changes over time and the overall time course is biphasic. The rate at which the initial (v_i) and final steady-state (v_{ss}) rates interconvert is described by the rate constant k_{inter} (Figure 4.1). Time-dependent inhibitors are usually competitive with respect to their analogous substrate, with the value for k_{inter} decreasing with increasing substrate concentration (83, 84, 101). The mechanism for inhibition can be described by either a one-step or two-step process; however the two-step inhibition mechanism is considered the more general form. One-step time-dependent inhibition is characterized by a linear dependence of k_{inter} on the concentration of inhibitor (Figure 4.2) and v_i is independent of inhibitor concentration. On the other hand, two-step time-dependent inhibition displays a hyperbolic dependence

of k_{inter} on the concentration of inhibitor (Figure 4.3) and both v_i and v_{ss} vary with inhibitor concentration. Peptidyl boronates have previously been shown to inhibit other proteases via a two-step time-dependent inhibition mechanism (102).

This study employs steady-state enzyme kinetic techniques to investigate the mechanism by which peptidyl boronates inhibit the peptide hydrolysis activity of both the human and *S. Typhimurium* Lon proteases. In addition to MG262, a fluorescent peptidyl boronate inhibitor, **4** (Table 4.1), which was designed based upon the amino acid sequence of a product of peptide hydrolysis by the enzyme, is evaluated. Both MG262 and **4** inhibit peptide hydrolysis via the same two-step time-dependent inhibition mechanism and with comparable potency. The inhibition is competitive and results in an overall inhibition constant of around 20 nM for both inhibitors. Peptidyl boronate inhibition is unique in that, unlike other proteases, Lon requires the binding of ATP to be susceptible to peptidyl boronate inhibition. The fluorescent dansyl moiety of **4** has allowed monitoring of the interaction of **4** with the enzyme by fluorescence spectroscopy in the absence of a peptide or protein substrate. This has confirmed the involvement of the active site serine during inhibition.

Materials and Methods

Materials

All oligonucleotide primers were purchased from Integrated DNA Technologies, Inc. (Coralville, IA). All cloning reagents were purchased from Promega (Madison, WI), New England BioLabs, Inc. (Ipswich, MA), Invitrogen (Carlsbad, CA) and USB Corporation (Cleveland, OH). Fmoc-protected amino acids, Boc-2-Abz-OH, Fmoc-Lys(Aloc)-Wang resin, Fmoc-Abu-Wang resin, and HBTU were purchased from Advanced ChemTech and NovaBiochem. MG262 and ZL₃AMC were purchased from Biomol International, LP. Tris buffer, cell culture media, IPTG, chromatography media, DTT, Mg(OAc)₂, trypsin, kanamycin, ATP, ADP, AMPPNP, dansyl chloride, AMC, DMSO, EDTA, Tween 20, and all other materials were purchased from Fisher, Sigma, and Amresco (Solon, OH).

Plasmid Construction

S680A *S. Typhimurium* Lon

A *S. Typhimurium* Lon mutant containing an alanine residue in place of the active site serine (S680A) was created using the QuikChange Site-Directed Mutagenesis Kit (Stratagene) according to the manufacturer's instructions. The plasmid pHF020 (Appendix B) (82), described in Chapter 2, was used as a template and the oligonucleotides oHF071 (Appendix A) and oHF072 were used as primers. The new

plasmid, pHF031, was verified by DNA sequencing using the oligonucleotides oHF005, oHF006, oHF029, oHF30, oHF031, and oHF093.

Purification of Recombinant Lon

S. Typhimurium Lon

Recombinant wild type and S680A *S. Typhimurium* Lon were overexpressed in BL21 (DE3) (Novagen), using the plasmids pHF020 and pHF031, respectively. Cells were grown and the purified proteins isolated as described in Chapter 2 (82). The concentration of purified Lon monomer was determined by Bradford assay (73) using BSA as a standard, and the protein stored at -80°C.

Human Lon

Recombinant human Lon was overexpressed in Rosetta (DE3) (Novagen), using the plasmid pHF002, described in Chapter 2 (82). Cells were grown and the purified protein isolated as described in Chapter 2 (82). The concentration of purified human Lon monomer was determined by Bradford assay (73) using BSA as a standard, and the protein stored at -80°C.

Peptide Synthesis

The peptide substrate **1**, **2**, and their non-fluorescent analogs (Table 4.1) were synthesized using standard Fmoc solid-phase synthesis techniques (74). The peptide

inhibitor **3** (Table 4.1), was synthesized using standard Fmoc solid-phase synthesis techniques (74) and contains the amino acid sequence of the N-terminal cleavage product of **2** by Lon. The peptidyl boronate **4** was synthesized by Dr. Irene Lee in the Department of Chemistry at Case Western Reserve University. All peptides were purified by reverse phase HPLC (Appendix D) and their identities verified by mass spectrometry (Appendix E).

Steady-State Peptide Hydrolysis Assay

ZL₃AMC Hydrolysis Assay

Reactions contained 50 mM Tris (pH 8.1), 10 mM Mg(OAc)₂, 50 mM DTT, 1 mM EDTA (human 20S proteasome only), 0.03% SDS (human 20S proteasome only), and 100 μM ZL₃AMC in the absence and presence of 1 mM ATP (*S. Typhimurium* Lon only). After equilibration at 37°C for 1 min, the reaction was initiated by the addition of 1 μM *S. Typhimurium* Lon monomer or 33 nM human 20S proteasome. The fluorescent signal was monitored at 438 nm (slit 1) using a Fluoromax 3 spectrophotometer (Horiba Group) after excitation at 343 nm (slit 1) for 20 min. The amount of AMC liberated was calibrated by determining the change in fluorescence associated with varying concentrations of AMC under identical reaction conditions. All experiments were performed in triplicate.

Substrate Assays

Steady-state velocity data were collected on a Fluoromax 3 spectrophotometer (Horiba Group) as described in Chapter 2 with minor modifications (64). Reactions contained 50 mM Tris (pH 8.1), 10 mM Mg(OAc)₂, 2 mM DTT, 200 nM wild type or S680A *S. Typhimurium* Lon monomer, and 1 mM **2**. After equilibration at 37°C for 1 min, the reaction was initiated by the addition of 1 mM ATP. All experiments were performed at least in triplicate.

Inhibition Assays for Determination of IC_{50} Values

Steady-state velocity data were collected on a Fluoromax 3 spectrophotometer (Horiba Group) as described in Chapter 2 with minor modifications (82). Due to the fluorescence of the dansyl moiety of **3**, the amount of peptide cleaved was calibrated by determining the change in fluorescence/ μ M peptide cleaved in the presence of each concentration of **3** evaluated.

Inhibition Assays for Determination of K_i and K_i^* Values

Reactions contained 50 mM Tris (pH 8.1), 10 mM Mg(OAc)₂, 2 mM DTT, 150 mM NaCl (human Lon reactions only), 30 nM *S. Typhimurium* Lon monomer or 500 nM human Lon monomer, and varying concentrations of the peptide substrate (**1** or **2**). At peptide concentrations between 25 μ M and 1 mM, a mixture containing 10% fluorescent peptide and 90% of the corresponding non-fluorescent analog were used to avoid the inner filter effect. Likewise, at peptide concentrations greater than 1 mM, a mixture containing 1% fluorescent peptide and 99% of the corresponding non-fluorescent analog were used

to avoid the inner filter effect. After equilibration at 37°C for 1 min, the reaction was initiated by the addition of 1 mM ATP. Varying concentrations of the inhibitor (MG262, **3**, or **4**) were added once the enzyme reached steady-state turnover (50 s for *S. Typhimurium* Lon reactions or 90 s for human Lon reactions) and was considered time zero for the inhibition reaction. The fluorescent signal resulting from excitation at 320 nm (slit 2) was monitored over 40 min at 420 nm (slit 1) using a Fluoromax 3 spectrophotometer (Horiba Group). The amount of peptide cleaved was calibrated by determining the change in fluorescence/ μ M peptide cleaved after complete trypsin digestion under identical reaction conditions.

Steady-State ATP Hydrolysis Assay

Steady-state velocity data was collected as described in Chapter 2 with minor modifications (68). Reactions containing 50 mM Tris (pH 8.1), 10 mM Mg(OAc)₂, 2 mM DTT, and 200 nM S680A *S. Typhimurium* Lon monomer in the presence and absence of 1 mM **2** ($\sim 5x K_m$), were initiated by the addition of varying concentrations of [α -³²P] ATP (0 - 1 mM) and incubated at 37°C. At different time points (from 0 - 20 min), aliquots were quenched in 0.5 N formic acid. A 3 μ L aliquot of each quenched reaction time point was spotted onto a PEI-cellulose TLC plate (10 cm x 20 cm) and the plate developed in 0.3 M KP_i (pH 3.4). The amount of [α -³²P] ATP (ICN or Perkin-Elmer) and [α -³²P] ADP was quantified using a Packard Cyclone storage phosphor screen Phosphor imager (Perkin-Elmer Life Science). All experiments were performed in triplicate.

ATP-Dependence of Time-Dependent Inhibition

Reactions containing 50 mM Tris (pH 8.1), 10 mM Mg(OAc)₂, 2 mM DTT, 150 mM NaCl (human Lon reactions only), and 300 nM *S. Typhimurium* or 900 nM human Lon monomer were equilibrated for 1 min at 37°C prior to the addition of inhibitor (MG262 or **4**). At the times indicated 1 mM ATP or AMPPNP and K_m level of the peptide substrate (10% fluorescent, 90% non-fluorescent) were added. Upon addition of the peptide substrate, the fluorescent signal resulting from excitation at 320 nm (slit 2) was monitored over 40 min at 420 nm (slit 1) using a Fluoromax 3 spectrophotometer (Horiba Group).

Detecting the Interaction of **4** with Lon by Fluorescence Spectroscopy

Nucleotide Assays

Reactions containing 50 mM Tris (pH 8.1), 10 mM Mg(OAc)₂, 2 mM DTT, 1 μM **3** or **4**, and 1 mM of the indicated nucleotide were initiated by the addition of 100 nM – 1 μM *S. Typhimurium* Lon monomer. After incubation at 37°C for 10 min, the emission spectrum (excitation polarizer = 0°, emission polarizer = 55°) from 500 – 600 nm (slit 5) was monitored using a Fluoromax 3 spectrophotometer (Horiba Group) after excitation at 335 nm (slit 5). All reactions were performed in triplicate.

Reversibility Assay

Reactions containing 50 mM Tris (pH 8.1), 10 mM Mg(OAc)₂, 2 mM DTT, 1 μM **4**, and 1 mM ATP or AMPPNP were equilibrated at 37°C in the absence and presence of 100 nM *S. Typhimurium* Lon monomer prior to the addition of 0 or 10 μM MG262 (in DMSO). After further equilibration at 37°C for 3h, the emission spectrum (excitation polarizer = 0°, emission polarizer = 55°) from 500 – 600 nm (slit 5) was monitored using a Fluoromax 3 spectrophotometer (Horiba Group) after excitation at 335 nm (slit 5). All reactions were performed in triplicate.

Assay to Detect Covalent Adduct Using Separation by SDS-PAGE

Reactions containing 50 mM Tris (pH 8.1), 10 mM Mg(OAc)₂, 50 mM DTT, 30 μM **4**, and 1 mM of the indicated nucleotide were initiated by the addition of 57 μM *S. Typhimurium* Lon and incubated at 37°C. At different time points (from 0 – 3 h), aliquots were quenched in Lamelli sample buffer. The reactions were fractionated on a 10% Tris SDS-PAGE gel and visualized by both UV light and Coomassie stain.

Assay to Detect Covalent Adduct Using Separation by Gel Filtration

Reactions containing 50 mM Tris (pH 8.1), 10 mM Mg(OAc)₂, 50 mM DTT, 1 μM **4**, and 1 mM of the indicated nucleotide were initiated by the addition of 1 μM *S. Typhimurium* Lon and incubated at 37°C for 10 min. The emission spectrum (excitation polarizer = 0°, emission polarizer = 55°) from 500 – 600 nm (slit 5) was monitored using a Fluoromax 3 spectrophotometer (Horiba Group) after excitation at 335 nm (slit 5) using half the reaction mixture. The remainder of the reaction mixture was fractionated on a

Centri•Spin 10 column (Princeton Separations, Inc.) equilibrated in 50 mM Tris (pH 8.1), 10 mM Mg(OAc)₂, 0.01% Tween 20, and 6 M guanidium-HCl to remove any unbound **4**. The emission spectrum of the flow-through was recorded under the same conditions.

Data Analysis

Experimental Time Courses

For classical inhibitors, the steady-state velocities were determined from the linear phase of the reaction time courses using KaleidaGraph (Synergy, Inc.). For time-dependent inhibitors, the initial and steady-state velocities were determined by fitting the experimental time courses with eq 1 (83, 84, 101) using the nonlinear regression program Prism 4 (GraphPad Software, Inc.). All experiments were performed in triplicate.

$$P = v_{ss}t + \frac{v_i - v_{ss}}{k_{inter}}(1 - e^{-k_{inter}t}) \quad (1)$$

In eq 1, P is the amount of peptide cleaved or fluorescent signal, v_{ss} is the final steady-state rate, t is time, v_i is the initial rate, and k_{inter} is the rate constant for the interconversion of v_{ss} and v_i (Figure 4.1). Use of eq 1 is allowed with tight-binding inhibitors when the following condition is satisfied: $2[\text{Lon}] \leq [\text{inhibitor}] \geq K_i^{*app}$ (defined below) (101). All inhibitor concentrations evaluated satisfied this condition.

Determination of k_{obs} Values

The steady-state velocities were determined from the final linear phase of the reaction time courses using KaleidaGraph (Synergy, Inc.). These values were converted to k_{obs} using eq 2.

$$k_{obs} = \frac{v}{[E]} \quad (2)$$

In eq 2, k_{obs} is the observed rate constant, v is the steady-state velocity, and E is Lon monomer.

Determination of k_{cat} and K_m Values

The concentration of ADP generated was calculated from the phosphor imaging signal, in density light units (dlu), using eq 3. The steady-state velocities were then determined from the linear phase of a plot of the amount of ADP generated versus time using KaleidaGraph (Synergy, Inc.). The steady-state kinetic parameters associated with ATP hydrolysis were determined by fitting the k_{obs} data with eq 4 using the nonlinear regression program Prism 4 (GraphPad Software, Inc.). All experiments were performed in triplicate.

$$[ADP] = \left(\frac{ADP_{dlu}}{ATP_{dlu} + ADP_{dlu}} \right) [ATP] \quad (3)$$

$$k_{obs} = \frac{k_{cat} [ATP]}{K_m + [ATP]} \quad (4)$$

In eq 4, k_{obs} is the observed rate constant, k_{cat} is the maximal k_{obs} , and K_m is the Michaelis-Menton constant.

Determination of IC_{50} Values

The k_{obs} data in the presence of 1 mM ATP, K_m level of the peptide substrate, and varying concentrations of **3** were fit with eq 5 to obtain an IC_{50} value for the inhibitor (83).

$$\frac{k_{obs,i}}{k_{obs}} = \frac{1}{1 + \frac{[\mathbf{3}]}{IC_{50}}} \quad (5)$$

In eq 5, $k_{obs,i}$ is the observed rate constant in the presence of **3**, k_{obs} is the observed rate constant in the absence of **3**, and IC_{50} is the $[I]$ under which $k_{obs,i}/k_{obs} = 0.5$.

Mode of Inhibition

The mode of inhibition was determined fitting the k_{inter} data, at a single concentration of inhibitor (MG262 or **4**) and varying concentrations of peptide substrate (**1** or **2**), with eq 6 for competitive time-dependent inhibition (83, 84, 101) using the nonlinear regression program Prism 4 (GraphPad Software, Inc.).

$$k_{inter} = \frac{k_{inter,max}}{1 + \frac{[S]}{K_m}} \quad (6)$$

In eq 6, k_{inter} is as defined in eq 1, $k_{inter,max}$ is the maximal value for k_{inter} , S is the peptide substrate, and K_m is the Michaelis-Menton constant for the peptide substrate.

Estimation of Inhibition Constants from Initial and Steady-State Rate Data

The value of the inhibition constants K_i and K_i^* were estimated by fitting the v_i and v_{ss} data, at saturating peptide substrate and varying concentrations of inhibitor (MG262 or **4**), with eq 7 or 8 (83, 84) using the nonlinear regression program Prism 4 (GraphPad Software, Inc.). The use of eq 7 or 8 with tight-binding inhibitors is necessary to avoid errors due to significant changes in the concentration of free enzyme during the inhibition assay (83).

$$\frac{v_i}{v_0} = 1 - \frac{([E] + [I] + K_i^{app}) - \sqrt{([E] + [I] + K_i^{app})^2 - 4[E][I]}}{2[E]} \quad (7)$$

$$\frac{v_{ss}}{v_0} = 1 - \frac{([E] + [I] + K_i^{*app}) - \sqrt{([E] + [I] + K_i^{*app})^2 - 4[E][I]}}{2[E]} \quad (8)$$

In eqs 7 - 8, v_i and v_{ss} are as defined in eq 1, I is the inhibitor, E is Lon monomer, v_0 is the steady-state rate in the absence of inhibitor, K_i^{app} is the apparent dissociation constant for the initial Lon-inhibitor complex, and K_i^{*app} is the apparent dissociation constant for the final Lon-inhibitor complex. The apparent dissociation constants were then converted to the true dissociation constants using eq 9 or 10 for competitive inhibition (83, 84).

$$K_i^{app} = K_i \left(1 + \frac{[S]}{K_m} \right) \quad (9)$$

$$K_i^{*app} = K_i^* \left(1 + \frac{[S]}{K_m} \right) \quad (10)$$

In eqs 9 - 10, K_i is the true dissociation constant for the initial Lon-inhibitor complex, K_i^* is the true dissociation constant for the final Lon-inhibitor complex, and S and K_m are as defined in eq 6.

Determination of K_i and K_i^* Values

The true values for K_i and K_i^* were determined by fitting the k_{inter} data, at saturating peptide substrate and varying concentrations of inhibitor (MG262 or **4**), with eq 11 for two-step time-dependent inhibition (83, 84, 101) using the nonlinear regression program Prism 4 (GraphPad Software, Inc.).

$$k_{inter} = k_6 + \left(\frac{k_5[I]}{K_i^{app} + [I]} \right) = k_6 \left(\frac{1 + \frac{[I]}{K_i^{*app}}}{1 + \frac{[I]}{K_i^{app}}} \right) \quad (11)$$

In eq 11, k_{inter} is as defined in eq 1, k_6 and k_5 are as defined in Figure 4.3, I is the inhibitor, and K_i^{app} and K_i^{*app} are as defined in eq 7 and 8, respectively. The apparent dissociation constants were converted to the true dissociation constant using eq 9 or 10 for competitive inhibition (83, 84, 101). Alternately, the dissociation constant K_i^* can be determined using eq 12 (83, 84, 101).

$$K_i^* = \frac{k_6 K_i}{k_5 + k_6} \quad (12)$$

Global Nonlinear Fitting of Experimental Time Courses

Global nonlinear fitting of the averaged experimental time courses at saturating peptide substrate and varying concentrations of **4** was performed using DynaFit (BioKin Ltd) (103). Differential equations were written for each species in the mechanisms described in Figures 4.2 and 4.3, as well as the uninhibited reaction (Figure 4.4), and the reaction time courses fit directly. The values for K_m , K_i and K_i^* were then determined using the resultant rate constants and eq 13, 14, and 12, respectively, and summarized in Table 4.3.

$$K_m = \frac{k_2 + k_{cat}}{k_1} \quad (13)$$

$$K_i = \frac{k_4}{k_3} \quad (14)$$

In eqs 13 – 14, K_m is as defined in eq 6, K_i and K_i^* are as defined in eq 9 and 10, respectively, and k_1 , k_2 , k_{cat} , k_3 , and k_4 are as defined in Figures 4.3 and 4.4.

Determination of the Half-Life for Reversal of Inhibition

The half-life for reversal of 4 inhibition was determined using eq 15 (83, 84).

$$t_{1/2} = \frac{\ln 2}{k_6} \quad (15)$$

In eq 15, $t_{1/2}$ is the half-life for reversal of inhibition and k_6 is as defined in Figure 4.3.

Results

Lon Inhibition Assays

Studies described in Chapter 2 demonstrate that MG262 (Table 4.1) is a potent time-dependent inhibitor of the peptide hydrolysis activity of *S. Typhimurium* and human Lon (82). Analysis of time-dependent kinetics requires monitoring the inhibition reaction using a continuous assay (101). A continuous fluorescent peptide hydrolysis assay suitable for studying the inhibition of Lon by time-dependent inhibitors was described in detail in Chapter 1 (65).

Time-dependent inhibition reactions are typically initiated by the addition of enzyme or substrate(s) (101). Due to the presence of an initial lag phase in the time course for peptide hydrolysis (64, 82), the inhibitor was not added to the reaction until after the completion of the lag phase in order to assess the effect of the inhibitor on the steady-state rate of peptide hydrolysis (Figure 4.5). As such, the inhibition time courses were defined by the addition of the inhibitor.

To accurately define both the initial and final phases of inhibition (Figure 4.1), the timeframe over which the inhibition reaction is monitored must be linear to avoid complications in data analyses due to substrate depletion (101). To accomplish this, the concentration of Lon monomer used in the inhibition assays was reduced up to 10-fold that used in non-time-dependent inhibition assays. In addition, saturating concentrations of ATP were included in all inhibition reactions to prevent the production of significant concentrations of ADP, which has been shown to inhibit the peptide hydrolysis activity of

Lon (64, 104). Even under these reaction conditions, there are limitations in the range of inhibitor concentrations which could be evaluated. At high concentrations of the inhibitor, the lack of a significant fluorescent signal from peptide hydrolysis prevented an accurate determination of the initial rate. At low concentrations of the inhibitor, the final steady-state rate was not reached prior to the end of the linear phase. Therefore the usable concentration range for inhibitors evaluated in the following studies were experimentally determined.

Detection of ZL₃AMC Hydrolysis by Lon

Most peptidyl boronate inhibitors form a covalent adduct with their target enzyme by forming a stable B-O bond with the active site serine or threonine (105, 106). Therefore, the peptidyl moiety may serve to “deliver” the boronic acid moiety to the proteolytic site of the enzyme, where nucleophilic attack by active site residues occurs. As such, it was hypothesized the tripeptide ZL₃AMC, which replaces the boronic acid moiety with an amide bond and a fluorogenic AMC (7-amino-4-methylcoumarin) leaving group, would be a substrate analog of MG262. ZL₃AMC has only a weak fluorescent signal at 438 nm ($\lambda_{\text{max,excitation}} = 343$ nm); however its hydrolysis by Lon would liberate the strongly fluorescent free AMC (Figure 4.6). As shown in Figure 4.7, no ATP-dependent liberation of AMC, from ZL₃AMC, by the *S. Typhimurium* homolog was detected within 20 min, even with a 30-fold excess of the protease compared to a control reaction with the human 20S proteasome.

The Peptidyl Boronate Dansyl-YRGIT-Abu-B(OH)₂ (**4**)

MG262 is composed of a peptidyl moiety and a boronate moiety. Modifications to the peptidyl moiety have previously been used to improve the potency of peptidyl boronate inhibitors (85, 107). To further evaluate the structure-activity relationship between the amino acid sequence of the peptidyl moiety and efficacy of inhibition by peptidyl boronates, **4** was evaluated as an alternative peptidyl boronate inhibitor (Table 4.1). This compound contains the amino acid sequence of a hydrolysis product of **2** and a boronic acid moiety at the carboxyl terminal. In addition, the amino terminal was derivatized with a dansyl group to facilitate fluorescent detection of **4** interacting with the enzyme (see below). The peptidyl moiety of **4** (dansyl-YRGIT-Abu, **3**) has a much greater affinity for *S. Typhimurium* Lon than the peptidyl moiety of MG262 (ZL₃OH), as the *IC*₅₀ value for inhibiting peptide hydrolysis of **2** is 101 ± 9 μM (Figure 4.8), which is 8-fold greater than that obtained for ZL₃OH (*IC*₅₀ = 740 ± 29 μM) (82). As with ZL₃OH, inhibition by **3** was not time-dependent, indicating that binding was rapid (82).

Time-Dependent Inhibition of *S. Typhimurium* Lon Peptide Hydrolysis

As with MG262, inhibition of *S. Typhimurium* Lon peptide hydrolysis by **4** is time-dependent (Figure 4.9 and 4.10). Most time-dependent enzyme inhibitors interact competitively with the analogous substrate (101), therefore the mode of inhibition for MG262 and **4** was evaluated. This was done by determining the rate constant associated with the interconversion of the initial (*v*_i) and final steady-state (*v*_{ss}) rates, *k*_{inter}, at a fixed

concentration of the inhibitor (MG262 or **4**) and varying concentrations of **2**. The concentration of inhibitor was chosen such that both v_i and v_{ss} could be defined at all concentrations of **2** evaluated. As shown in Figure 4.11, the value for k_{inter} decreases with increasing substrate concentration, indicating that both MG262 and **4** act as competitive inhibitors of the peptide substrate.

In Chapter 3, it was proposed that MG262 inhibits via a two-step process (Figure 4.3) (82). As the detection of a dependency of v_i and v_{ss} on the inhibitor concentration will provide support for this proposal (83, 84, 101), the values for v_i , v_{ss} , and k_{inter} were determined for *S. Typhimurium* Lon hydrolysis of a fixed concentration of **2** and varying concentrations of inhibitor (MG262 and **4**). As shown in Figure 4.12, both v_i and v_{ss} vary with increasing concentration of MG262 or **4**, supporting the existence of a two-step mechanism. This data also provides estimates for the dissociation constants of the initial (K_i) and final (K_i^*) Lon-inhibitor complexes as outlined in Table 4.2. Figure 4.13 also reveals that the k_{inter} data associated with MG262 inhibition of the *S. Typhimurium* homolog varies hyperbolically with the concentration of MG262, further supporting a two-step inhibition mechanism (83, 84, 101). Interestingly, the k_{inter} data associated with **4** inhibition varies linearly with the concentration of **4** (Figure 4.13). A linear dependence of k_{inter} on the concentration of inhibitor is consistent with either a one-step inhibition mechanism (Figure 4.2) or a two-step inhibition mechanism in which $K_i \gg K_i^*$ (83, 84, 101). As the estimates for K_i and K_i^* for **4** vary by more than 30-fold (Table 4.2), it is plausible that the observed linear dependence represents the latter case. The value of the reverse rate constant, k_6 (Figure 4.3), was estimated by extrapolation of the data to zero inhibitor, which is the y-intercept shown in the insets of Figure 4.13. Data at higher

concentrations of **4** could not be obtained due to lack of a significant fluorescent signal from peptide hydrolysis. Data at lower concentrations of **4** could not be obtained as v_{ss} was not reached prior to the end of the linear phase of the uninhibited reaction.

To further evaluate whether **4** inhibits *S. Typhimurium* Lon by either a one-step or two-step mechanism, the averaged experimental time courses at saturating **2** and varying concentrations of **4** were globally fitted to both mechanisms using the nonlinear fitting program Dynafit (103). The data were best described by a two-step mechanism (Table 4.3, Figure 4.14) and the kinetic parameters obtained from conversion of the resultant rate constants to K_i , K_i^* and K_m , show close agreement with those obtained by other methods (Table 4.2 and 4.3). A value of $2.9 \times 10^{-4} \text{ s}^{-1}$ was obtained for the reverse rate constant k_6 , further supporting that inhibition by **4** is reversible.

ATP-Dependence of Peptidyl Boronate Inhibition of *S. Typhimurium* Lon

Previous work with *E. coli* Lon has shown that peptidyl chloromethyl ketones require ATP to inhibit Lon activity (4, 60). To further evaluate whether inhibition by MG262 and **4** also required ATP, *S. Typhimurium* Lon was preincubated with MG262 or **4** for 0 – 8 min. After the preincubation period, 1 mM ATP and 300 μM **2** were added and peptide cleavage monitored over 10 min. No differences in the time courses were observed (Figure 4.15), indicating that inhibition by MG262 and **4** did not begin until the addition of ATP and **2**. *S. Typhimurium* Lon was then preincubated with MG262 or **4** and 1 mM ATP for 0 – 8 min. After the preincubation period, **2** was added and peptide cleavage again monitored over 10 min. As the length of the preincubation period was

increased, time dependency was lost (Figure 4.15). In fact, preincubation with MG262 for 8 min resulted in a total loss of time dependency. Control reactions were performed in which MG262 (DMSO only) or **4** was omitted (Figure 4.16). The presence of ATP alone during the preincubation period did not affect the rate of peptide hydrolysis, thus the loss of time dependency was the direct result of inhibition by MG262 or **4** and not ATP depletion or ADP inhibition. Regardless of the length of the preincubation period, the final steady-state rates were comparable.

It has previously been shown that *E. coli* Lon requires the binding, but not hydrolysis, of ATP in order to cleave a peptide substrate albeit at a reduced rate (64). To determine whether inhibition by MG262 and **4** required both binding and hydrolysis of ATP, we repeated the latter experiment (preincubation with MG262 or **4** and nucleotide) with 1 mM AMPPNP. The same trend was observed with AMPPNP as with ATP (Figure 4.15). Time dependency was lost as the preincubation period was increased, and the steady-state rates were comparable regardless of the preincubation time. Control reactions were again performed without MG262 (DMSO only) or **4** and peptide hydrolysis was not affected by the presence of AMPPNP during the preincubation period (Figure 4.16), thus the observed trend was the direct result of inhibition by MG262 or **4**. Similar results were obtained for both MG262 and **4**, therefore only data for MG262 is shown.

Fluorescent Detection of the Interaction of *S. Typhimurium* Lon with **4**

A fluorescent signal is often influenced by its environment (108). The dansyl moiety has been shown to undergo an increase in fluorescence upon binding to the more hydrophobic interior of a protein, as well as a shift in the λ_{max} of the emission spectrum (108). To evaluate whether the fluorescent signal from **4** is altered upon binding to Lon, the emission spectrum ($\lambda_{\text{excitation}} = 335 \text{ nm}$) from $1 \mu\text{M}$ **4** and 1 mM ATP was monitored in the presence and absence of 100 nM and $1 \mu\text{M}$ of the *S. Typhimurium* enzyme. In the presence of Lon, **4** undergoes a concentration dependent increase in fluorescence and a shift in the λ_{max} of the emission spectrum from 555 to 545 nm (Figure 4.17). The emission spectrum of control reactions containing buffer alone or buffer with enzyme showed no fluorescence between 475 and 600 nm . All emission spectra were collected under so-called “magic angle” conditions (excitation polarizer = 0° , emission polarizer = 55°) to avoid interference due to scattered light.

In order to examine whether the active site serine is required for the interaction of **4** with Lon, a *S. Typhimurium* Lon mutant in which the active site serine was replaced by an alanine residue (S680A *S. Typhimurium* Lon) was generated. This mutant displayed both intrinsic and peptide-stimulated ATP hydrolysis activity comparable to the wild type enzyme, but was unable to catalyze peptide bond hydrolysis (Figure 4.18). This property is also observed in the analogous *E. coli* mutant (4). The emission spectrum from $1 \mu\text{M}$ **4** and 1 mM ATP was monitored in the absence and presence of 100 nM wild-type or S680A enzyme (Figure 4.17). No increase in fluorescence was observed, indicating the active site serine is required for interaction of **4** with Lon.

Inhibition of *S. Typhimurium* Lon by **4** requires the binding, but not hydrolysis of ATP (see above). Therefore it was predicted that the altered fluorescent signal from **4** interacting with the protease would still be observed in the presence of AMPPNP, a non-hydrolyzable analog of ATP, but not in the absence of nucleotide. The emission spectrum from 1 μ M **4** and 1 μ M wild type enzyme was monitored in the presence of 1 mM ATP, 1 mM AMPPNP or no nucleotide. Indeed, the increase in fluorescence and shift of the λ_{max} to 545 nm was observed only in the presence of 1 mM ATP or AMPPNP (Figure 4.17). Interestingly, an increase in fluorescence was not observed in the presence of 1 mM ADP (Figure 4.17), implying that, although hydrolysis of ATP is not necessary for inhibition, the presence of the gamma phosphate is required.

The value of the reverse rate constant, k_6 , is non-zero for both MG262 and **4** (Table 4.2), indicating that inhibition of *S. Typhimurium* Lon by peptidyl boronates is reversible. To further evaluate the reversibility of **4** inhibition, 100 nM of the *S. Typhimurium* protease was preincubated with 1 μ M **4** and 1 mM ATP or AMPPNP for 30 min prior to the addition of 10 μ M MG262. If inhibition by **4** is reversible, after 4 half-lives for reversal of inhibition (~ 3 h), the excess MG262 will replace **4** in the active site, leading to a loss of the altered fluorescent signal associated with Lon interacting with **4**. As shown in Figure 4.19, in the presence of ATP and MG262, the increase in fluorescence associated with *S. Typhimurium* Lon interaction with **4** is lost. The magnitude of the altered fluorescent signal is less after 3.5 h (Figure 4.19) than 10 min (Figure 4.17), presumably due to the production of high concentrations of ADP, which does not support the interaction between Lon and **4** (Figure 4.17). As a control, the experiment was also performed in the absence of MG262 (DMSO only) and the increase

in fluorescence was maintained. Similar results were also obtained with 1 mM AMPPNP.

Detection of the Putative Covalent Adduct

Detection of the putative covalent adduct between the active site serine and **4** proved unsuccessful. Upon separation of *S. Typhimurium* Lon and **4** by SDS-PAGE, no fluorescent band, corresponding to the modified enzyme, was detected under UV light. To ensure this was not due to instability of the covalent adduct over time, a rapid separation of the enzyme and **4** by gel filtration under denaturing conditions (6 M guanidium-HCl) was attempted. The column should trap unbound **4** while allowing the protease to pass through. The presence of a covalent adduct would yield a fluorescent signal in the flow-through. The emission spectrum, after equilibration at 37°C for 10 min, from 1 μ M **4** and 1 mM ATP in the absence and presence of 1 μ M *S. Typhimurium* Lon was monitored before and after gel filtration. No fluorescent signal was detected in the flow-through (Figure 4.20). Control reactions containing 1 μ M **4** in the column equilibration buffer were performed and a fluorescent signal was detected, thus the lack of signal is not due to the reaction conditions. Similar results were also obtained with 1 mM AMPPNP.

Time-Dependent Inhibition of Human Lon Peptide Hydrolysis

In Chapter 3, it was shown that MG262 also inhibits human Lon and with comparable potency to the *S. Typhimurium* homolog. Although the *S. Typhimurium* protease has a higher affinity for the peptidyl moiety of **4** than MG262, the values for K_i^* for both inhibitors are comparable (Table 4.2). As such, it is proposed that the binding interaction between the peptidyl moiety and Lon is not strong enough to dictate the specificity of peptidyl boronate inhibition. To test this hypothesis, the inhibition profile of **4** towards human Lon was determined. It has been shown the human and bacterial homologs display marked differences in their substrate specificity, as described in Chapter 2 (82). In fact, **3** was unable to inhibit peptide hydrolysis the by human enzyme at concentrations up to 600 μM . However, if the peptidyl moiety does not dictate potency, **4** will still inhibit the human protease with a similar potency as *S. Typhimurium* Lon.

Inhibition of human Lon peptide hydrolysis by **4** is time-dependent (Figure 4.21). The values for k_{inter} , at a fixed concentration of **4**, decrease with increasing concentration of **1**, indicating that **4** also inhibits the human enzyme in a competitive manner with respect to the peptide substrate (Figure 4.22). The concentration of inhibitor was again chosen such that both v_i and v_{ss} could be defined at all concentrations of **1** evaluated. The values for v_i , v_{ss} , and k_{inter} for hydrolysis of a fixed concentration of **1** and varying concentrations of **4** were also determined. As shown in Figure 4.23, both v_i and v_{ss} vary with increasing concentration of **4**, supporting a two-step inhibition mechanism. This data provides estimates for the dissociation constants of the initial (K_i) and final (K_i^*)

Lon-inhibitor complexes as outlined in Table 4.4. Figure 4.24 reveals that the k_{inter} data associated with **4** inhibition of the human protease also varies linearly with the concentration of **4**. Again, a linear dependence of k_{inter} on the concentration of inhibitor is consistent with either a one-step inhibition mechanism (Figure 4.2) or a two-step inhibition mechanism in which $K_i \gg K_i^*$ (83, 84, 101). As the estimates for K_i and K_i^* for **4** with respect to the human enzyme vary by more than 150-fold (Table 4.4), it is likely the observed linear dependence again represents the latter case. The value of the reverse rate constant, k_6 (Figure 4.3), was estimated by extrapolation of the data to zero inhibitor, which is the y-intercept shown in the inset of Figure 4.24. Data at higher concentrations of **4** could not be obtained due to lack of a significant fluorescent signal from peptide hydrolysis. Data at lower concentrations of **4** could not be obtained as v_{ss} was not reached prior to the end of the linear phase of the uninhibited reaction.

Discussion

Lon, also known as the protease La, belongs to the AAA⁺ superfamily (ATPases Associated with different cellular Activities) along with other ATP-dependent proteases such as ClpXP, HslUV, and the proteasome (47, 79). Despite the presence of a serine-lysine dyad in the proteolytic active site, Lon is relatively unreactive towards small serine protease inhibitors such as PMSF or DIFP (27, 45, 60, 62). The peptide hydrolysis activity of the *S. Typhimurium* and human proteases is readily inhibited by the peptidyl boronate, MG262 ($IC_{50} = 122 \pm 9$ nM and 160 ± 10 nM, respectively), as described in Chapter 3 (82). As *S. Typhimurium* Lon activity has been shown to be important for virulence in a study model for typhoid fever in humans (23), an understanding of the mechanism by which MG262 inhibits both homologs will provide insight which will benefit the design of novel therapeutic agents which target only the bacterial pathogen.

This study employs steady-state kinetic techniques to investigate the mechanism by which peptidyl boronates inhibit the peptide hydrolysis activity of Lon protease. In addition to MG262, a fluorescent peptidyl boronate inhibitor **4** is also evaluated (Table 4.1). Both MG262 and **4** inhibit the peptide hydrolysis activity of the *S. Typhimurium* enzyme via the same two-step, time-dependent mechanism, and with comparable potency (Table 4.2). The inhibition is competitive and requires the binding, but not hydrolysis, of ATP. Furthermore, the fluorescent dansyl moiety of **4** has allowed monitoring of the interaction of **4** with the active site serine of *S. Typhimurium* Lon, confirming the involvement of this residue in inhibition. Inhibition of the human protease by **4** is also competitive and proceeds through a two-step mechanism. Comparison of the inhibition

constants obtained with both inhibitors and Lon homologs suggests that the affinity of the peptidyl moiety does not dictate the potency of inhibition.

Analysis of the time courses for time-dependent inhibition of the peptide hydrolysis of Lon by MG262 and **4** has allowed the construction of a minimal kinetic model for their mechanism of inhibition. Examination of the dependence of the initial (v_i) and final steady-state (v_{ss}) rates for peptide hydrolysis in the presence of MG262 or **4** reveal that both are inversely dependent on the concentration of inhibitor (Figure 4.12 and 4.23). This relationship, in conjunction with the detection of k_{inter} (the rate constant for the interconversion of v_i and v_{ss}) values displaying a hyperbolic dependence on the concentration of inhibitor, fulfills the diagnostic requirement of a two-step time-dependent inhibition mechanism (Figure 4.3) (83, 84, 101). The k_{inter} data associated with MG262 inhibition of the *S. Typhimurium* protease varies hyperbolically, whereas the k_{inter} data associated with **4** appears to vary linearly with both the human and *S. Typhimurium* enzymes (Figure 4.13 and 4.24). Due to the detection limit of the peptide hydrolysis assay, k_{inter} values at higher inhibitor concentrations could not be evaluated. Therefore, the nonlinear fitting program Dynafit was used to globally fit the *S. Typhimurium* Lon peptide hydrolysis time courses to both a one-step (Figure 4.2) and two-step inhibition mechanism. The time courses were best described by a two-step mechanism (Table 4.3). The observation of a linear dependence of k_{inter} on the concentration of **4**, despite being a two-step mechanism, is supported by the estimated differences in the magnitudes of K_i and K_i^* for **4** (Table 4.2 and 4.4). To detect the hyperbolic dependence, the inhibitor must be varied in the range of 0.1 – 10 times both K_i^{app} and K_i^{*app} which was not possible due to the technical limitations of the assay.

The mode of inhibition for both MG262 and **4** is competitive with respect to the peptide substrate (Figure 4.11 and 4.22) and the presence of the peptidyl moiety has been shown to be required for inhibition by MG262, as described in Chapter 3 (82). Furthermore, fluorescence spectroscopic studies have implicated the active site serine as involved in the interaction of Lon with **4** (Figure 4.17). Taken together, these results suggest the binding interaction between the peptidyl moiety of MG262 and **4** serves to direct the boronate moiety to the proteolytic active site. The K_i value for the inhibitor represents the affinity of the inhibitor for the initial EI complex (Figure 4.3). If the first step represents simple binding of the peptidyl boronate to the enzyme, the difference in the K_i values of MG262 and **4** should reflect the difference in the binding affinity of the cognate peptidyl moieties (ZL₃OH and **3**, respectively). Based on the IC_{50} values, **4** would be predicted to have an 8-fold higher affinity for *S. Typhimurium* Lon, however estimation of the K_i values from the v_i data reveals that **4** has a 10-fold weaker affinity (Table 4.2). This suggests the K_i value does not reflect binding alone. X-ray crystallographic studies have confirmed the formation of a tetrahedral intermediate between peptidyl boronate inhibitors and the active site hydroxyl group of other serine and threonine proteases (Figure 4.25) (105, 106). The formation of a similar covalent adduct, during inhibition of Lon by MG262 and **4**, may imply the K_i values represent both binding of the inhibitor and formation of a covalent adduct. The K_i value would thus reflect the energy barrier between the ground state binding interaction of *S. Typhimurium* Lon and **4** (described by the IC_{50} values) and the transition state for B-O bond formation (Figure 4.26). The higher affinity of **4** for the enzyme results in ground

state stabilization of the E•I complex, thereby increasing the amount of energy (ΔG^\ddagger) required to reach the transition state (EI^\ddagger) and the magnitude of K_i relative to MG262.

Attempts to detect the putative covalent adduct by exploiting the fluorescence of **4** were unsuccessful. No fluorescently modified *S. Typhimurium* Lon was detected by SDS-PAGE, indicating that either a covalent adduct is not formed or that it is not stable over the timeframe required to separate the unbound **4** from the enzyme. To explore the latter possibility in more detail, the unbound **4** was rapidly separated from the protease using a small gel filtration column under denaturing conditions. Although the column successfully removed the unbound **4**, no fluorescence was detected in the flow-through (Figure 4.20). The reaction of Lon with the boronic acid moiety is reversible (Figure 4.19). The difficulty in detecting the tetrahedral intermediate is presumed to be the high pK_a (> 10) of the trivalent boronate, a weak Lewis acid, which would require strong base to stabilize the B-O bond (109). Confirmation of the covalent adduct will therefore require x-ray crystallographic studies with the peptidyl boronate bound to the active site, as has been used for other proteases (105, 106).

ATP has not been required for inhibition of serine or threonine proteases by peptidyl boronates, even those which are physiologically ATP-dependent (102, 105, 110). Therefore Lon is unique in its requirement for ATP binding during inhibition by peptidyl boronates. Preincubation of MG262 or **4** with the enzyme for varying lengths of time in the absence of any nucleotide did not affect the degradation of **2** (Figure 4.15). However, in the presence of ATP or AMPPNP, as the preincubation time was increased, time-dependency was lost (Figure 4.15). The binding, not hydrolysis, ATP during the preincubation period allows for the formation of the final Lon-inhibitor complex (EI^*).

Time-dependency only appears to be lost because less active protease is available upon the addition of **2**. The dependence of peptidyl boronate inhibition of Lon on ATP binding is of mechanistic importance, as it implies they are true mechanism-based inhibitors and cannot simply diffuse into the active site. This hypothesis is further supported by fluorescence spectroscopic studies which show no interaction between **4** and *S. Typhimurium* Lon in the absence of ATP or AMPPNP (Figure 4.17). Interestingly, these studies also revealed that ADP does not support the interaction of the enzyme with **4**, implying the gamma phosphate is also required for inhibition (Figure 4.17). Taken together, these results suggest that a residue(s) within the proteolytic active site of Lon may require allosteric activation induced by ATP binding. It also implies that the first-step (inhibitor binding and formation of the covalent adduct) must require the binding of ATP. Previous studies have confirmed the existence of a conformational change in the *E. coli* homolog upon binding of ATP, AMPPNP, and ADP (54). However, this work provides the first evidence that the conformational change detected in the presence of ATP and AMPPNP is different from that in the presence of ADP. Understanding the role of ATP in facilitating inhibition of Lon peptide hydrolysis will require further investigation and will provide insight useful in the design of future inhibitors as well as a deeper understanding of the kinetic mechanism of this protease.

The observation of a two-step time-dependent inhibition mechanism has previously been observed in peptidyl boronate inhibition of classical serine proteases (102). The first step is binding of the inhibitor and formation of a tetrahedral adduct, as we have proposed above, followed by a reversible second step in which the enzyme undergoes rearrangement of active site residues to strengthen the interaction between the

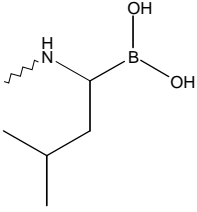
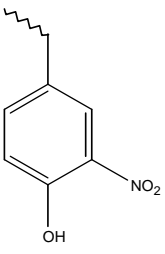
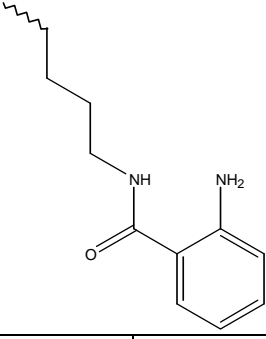
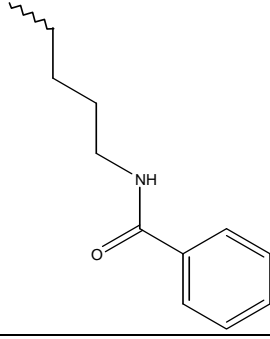
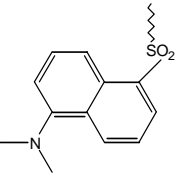
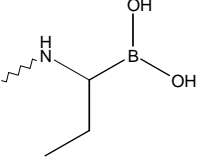
enzyme and inhibitor (102). Therefore, it is proposed that a similar conformational change or isomerization event would constitute the second, slow step of inhibition of Lon by peptidyl boronates. As the values for K_i^* , which represents the affinity of the inhibitor for the final EI^* complex (Figure 4.3), are comparable for both MG262 and **4**, the enhanced interaction between the enzyme and inhibitor does not appear to be dependent on the sequence of the peptidyl moiety. This hypothesis is further supported by detection of a similar K_i^* for the human homolog with **4** (Table 4.4). The detection of a non-zero value for the reverse rate constant k_6 for MG262 and **4** with both homologs supports the reversibility of the inhibition (Table 4.3 and 4.4). This was further confirmed by the loss of the altered fluorescent signal resulting from the interaction of **4** with the *S. Typhimurium* protease when excess MG262 was introduced into the reaction (Figure 4.19). The excess MG262 sequesters the free Lon upon dissociation of **4** from the active site.

This study has demonstrated that **4** inhibits both *S. Typhimurium* and human Lon peptide hydrolysis activity via the same two-step, time-dependent mechanism, and with comparable potency, as MG262. The overall mechanism for inhibition is proposed to involve three steps (Scheme 4.1). First, the peptidyl boronate binds to Lon to form an initial complex ($E \cdot I$). This is followed by rapid nucleophilic attack of the boronate by the active site serine to form a tetrahedral intermediate (EI). Finally, the enzyme undergoes an isomerization or conformational change which enhances the interaction between the peptidyl boronate and Lon (EI^*). The first two steps occur rapidly and are represented by the inhibitor dissociation constant K_i (Table 4.2 and 4.4). After slow formation of the EI^* complex, the overall inhibition constant, representing all three steps,

is given by K_i^* . Although ATP binding is required to detect the EI complex, it is unclear whether the first, second, or both steps are dependent on ATP binding and future investigation will be required.

The peptidyl boronate **4** will be useful as a mechanistic probe in future studies of Lon and other serine and threonine proteases, as it contains a fluorescent dansyl moiety with which to monitor the interaction of the enzyme and inhibitor in the absence of a peptide or protein substrate. Previous studies have demonstrated that peptidyl boronates are able to diffuse into the cell and even the mitochondria (107, 111). In fact the proteasome inhibitor bortezomib, a peptidyl boronate currently used in the treatment of multiple myeloma, causes mitochondrial damage by an unknown mechanism (111, 112). As modifications to the peptidyl moiety have previously been used to improve the potency of peptidyl boronate inhibitors (85, 107), this approach may be useful in developing future inhibitors which discriminate between various proteases. Studies with the ATP-dependent proteases ClpXP and the 20S proteasome are currently underway. Thus, **4** will serve as a lead compound in the development of enzyme-specific peptidyl boronates which will minimize cross-reactivity with other proteases, and allow each protease to be studied independently *in vivo*. The solubility of **4** in water will also provide the possibility to study how peptidyl boronates affect the ATP hydrolysis activity of Lon in the absence of DMSO, which has previously been shown to affect ATP hydrolysis (5).

Table 4.1 Summary of Peptide-Based Substrates and Inhibitors

MG262	non-fluorescent	Z-LL-L[B(OH) ₂]	
1	fluorescent	Y(3-NO ₂)RGITCSGRQK(Abz)	
	non-fluorescent	YRGITCSGRQK(Bz)	
2	fluorescent	Y(3-NO ₂)RGIT-Abu-SGRQK(Abz)	
	non-fluorescent	YRGIT-Abu-SGRQK(Bz)	
3	fluorescent	dansyl-YRGIT-Abu	
4	fluorescent	dansyl-YRGIT-Abu[B(OH) ₂]	
L[B(OH) ₂]	Y(3-NO ₂)	K(Abz)	K(Bz)
			
Abu	dansyl		Abu[B(OH) ₂]
			

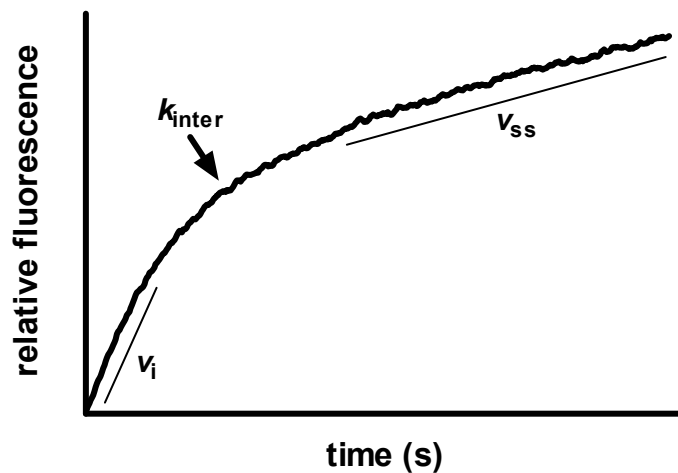


Figure 4.1 **Representative time course for time-dependent inhibition.** The initial (v_i) and steady-state (v_{ss}) rates are indicated, as well is the rate constant for their interconversion, k_{inter} .

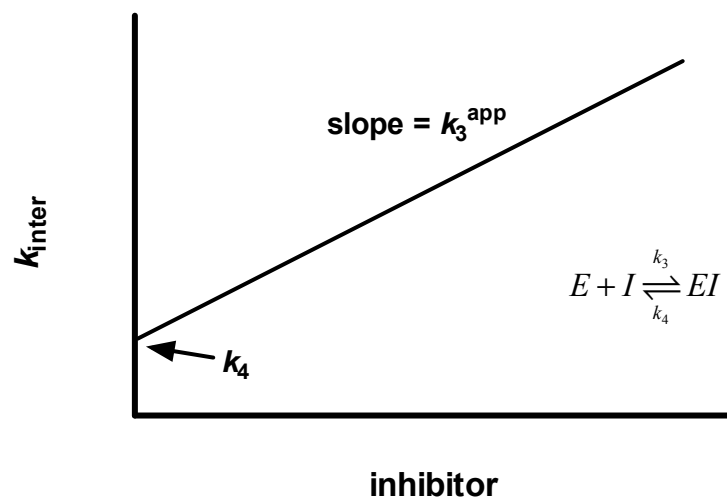


Figure 4.2 **One-step time-dependent inhibition.** Representative plot of k_{inter} against inhibitor concentration, where the y-intercept is equal to k_4 and the slope is equal to the apparent value of k_3 . The dissociation constant for the EI complex is given by $K_i = k_4/k_3$.

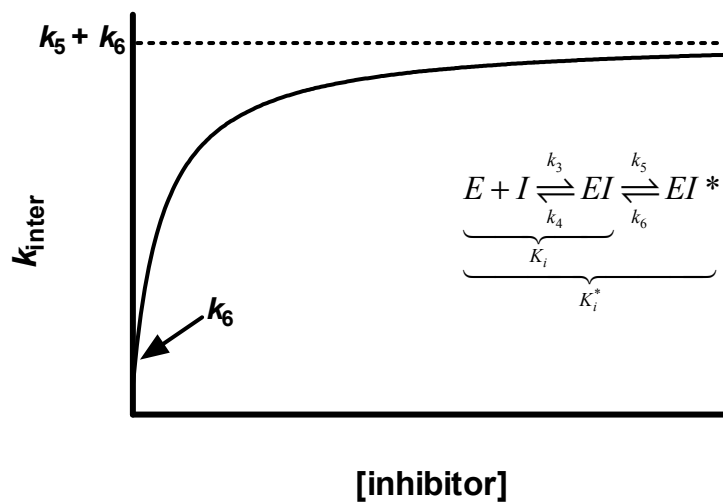


Figure 4.3 **Two-step time-dependent inhibition.** Representative plot of k_{inter} against inhibitor concentration, where the y-intercept is equal to k_6 and the maximal value for k_{inter} approaches $k_5 + k_6$. The dissociation constant for the initial (EI) and final (EI^*) complex are given by $K_i = k_4/k_3$ and $K_i^* = (k_6 K_i)/(k_5 + k_6)$, respectively.

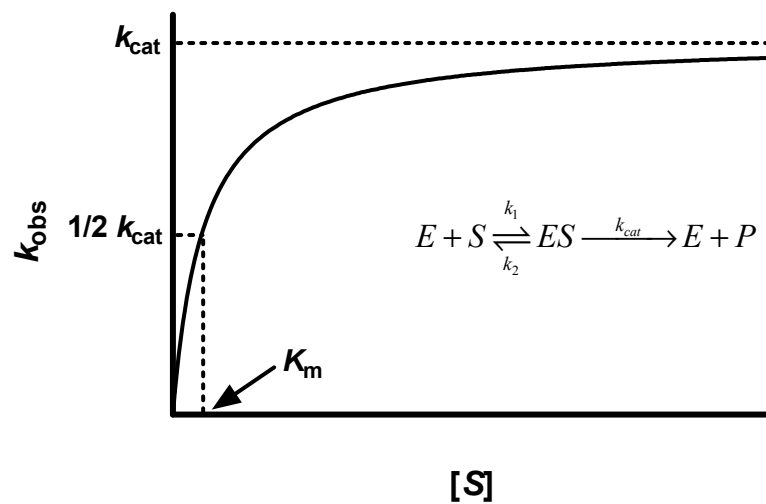


Figure 4.4 **Uninhibited enzymatic reaction.** Representative plot of k_{obs} against substrate concentration where the maximal value for k_{obs} approaches k_{cat} and K_m is equal to the $[S]$ in which $k_{\text{obs}} = \frac{1}{2} k_{\text{cat}}$.

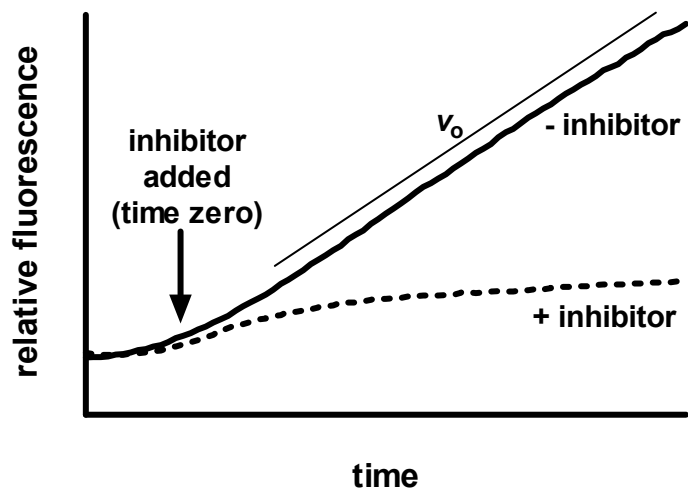


Figure 4.5 **Experimental setup for measuring time-dependent inhibition of Lon peptide hydrolysis.** Representative time courses for peptide hydrolysis in the absence (—) and presence (---) of a time-dependent inhibitor. In the absence of any inhibitor, time courses for Lon peptide hydrolysis display a lag prior to attaining steady-state turnover. When performing inhibition assays, the inhibitor was not added until steady-state turnover was reached and was considered time zero. The steady-state rate in the absence of inhibitor (v_0) is indicated.

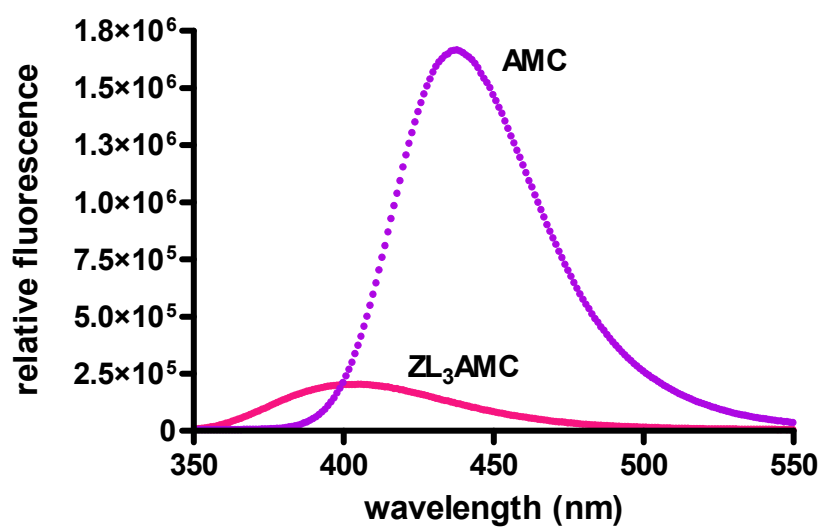


Figure 4.6 **Representative emission spectra of ZL₃OH and AMC.** Emission spectra from 100 μ M ZL₃AMC and free AMC upon excitation at 343 nm.

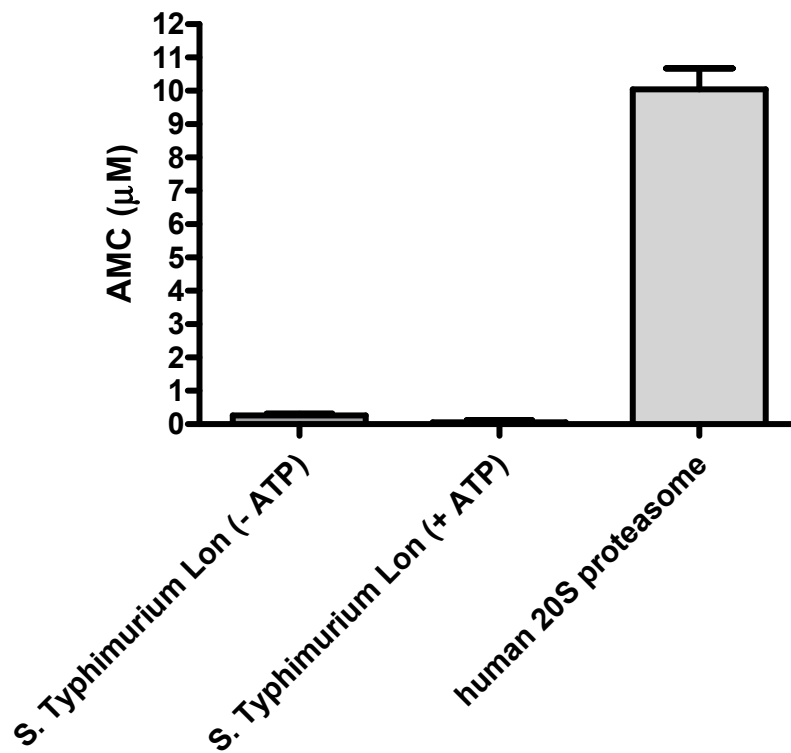


Figure 4.7 **Hydrolysis of ZL₃AMC by *S. Typhimurium* Lon.** Reactions containing 1 μM *S. Typhimurium* Lon or 33 nM human 20S proteasome and 100 μM ZL₃AMC were incubated at 37°C for 20 min in the absence and presence of 1 mM ATP (*S. Typhimurium* Lon reaction only). The amount of AMC generated was determined by measuring the fluorescence at 438 nm after excitation at 343 nm as described in Materials and Methods.

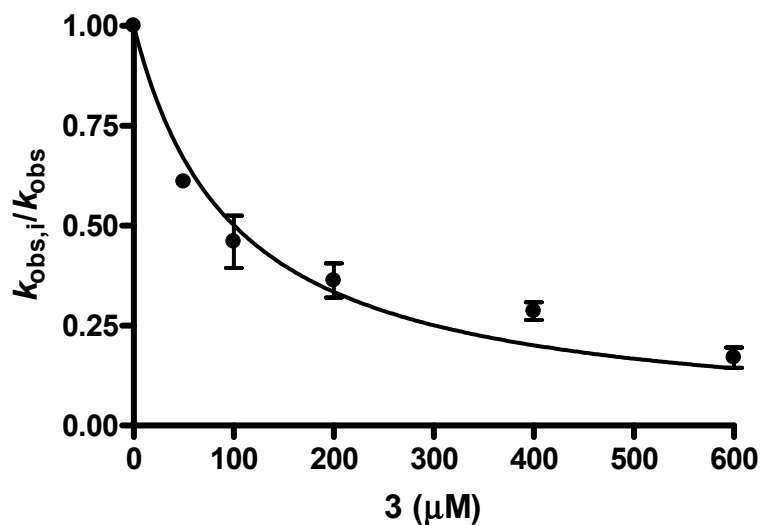


Figure 4.8 **Inhibition of *S. Typhimurium* Lon peptide hydrolysis by 3.** Reactions containing 300 nM *S. Typhimurium* Lon were preincubated with 300 μM **2** (K_m level) prior to the addition of 1 mM ATP. After 50 s, varying concentrations of **3** were added and peptide hydrolysis monitored over 10 min. All experiments were performed in triplicate and the k_{obs} values determined as described in Materials and Methods. The averaged k_{obs} in the presence of **3** / k_{obs} in the absence of **3** ($k_{obs,i}/k_{obs}$, ± 1 SD) were plotted against the corresponding inhibitor concentration. The IC_{50} (101 ± 9 μM) was determined by fitting the data with eq 5 as described in Materials and Methods.

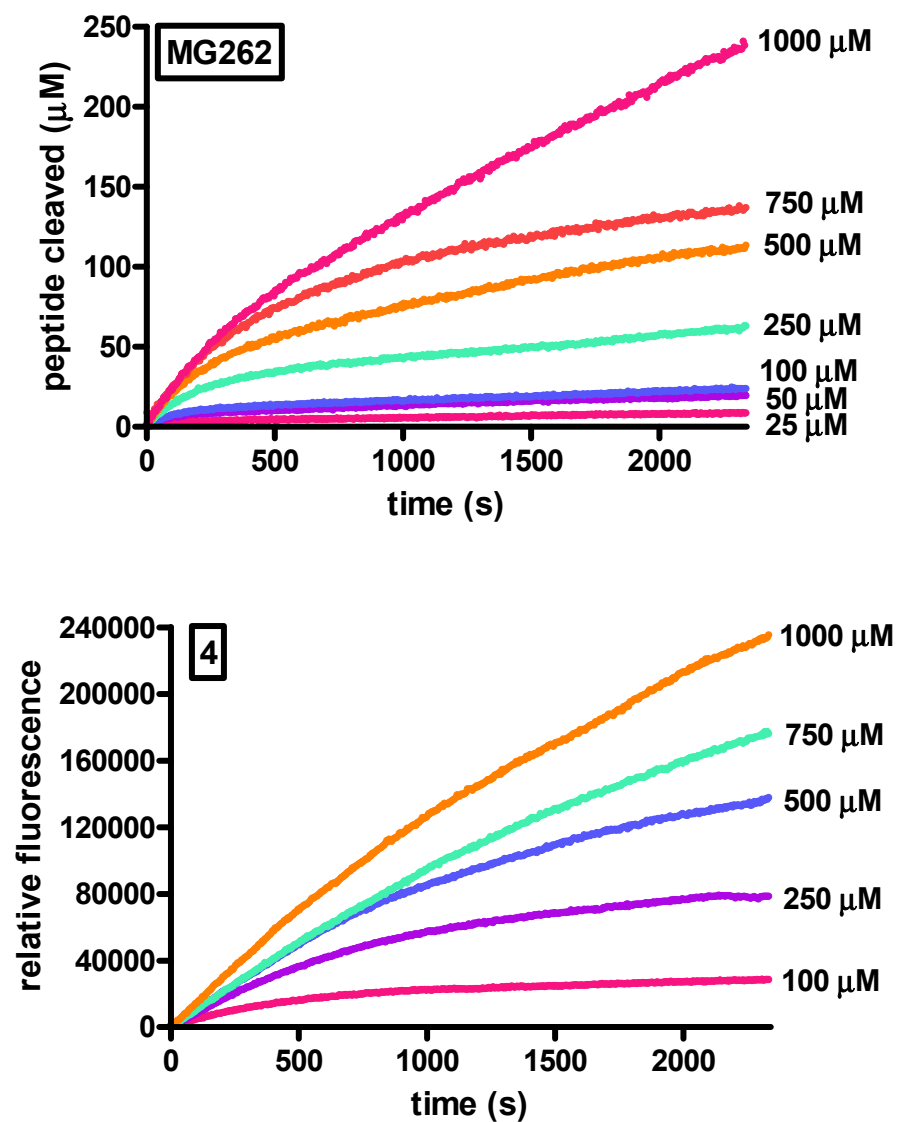


Figure 4.9 Time-dependent inhibition of *S. Typhimurium* Lon peptide hydrolysis by peptidyl boronates in the presence of varying concentrations of peptide substrate. Representative time courses for *S. Typhimurium* Lon (30 nM) degradation of varying concentrations of **2** in the presence of 1 mM ATP and 300 nM MG262 (top) or 267 nM **4** (bottom).

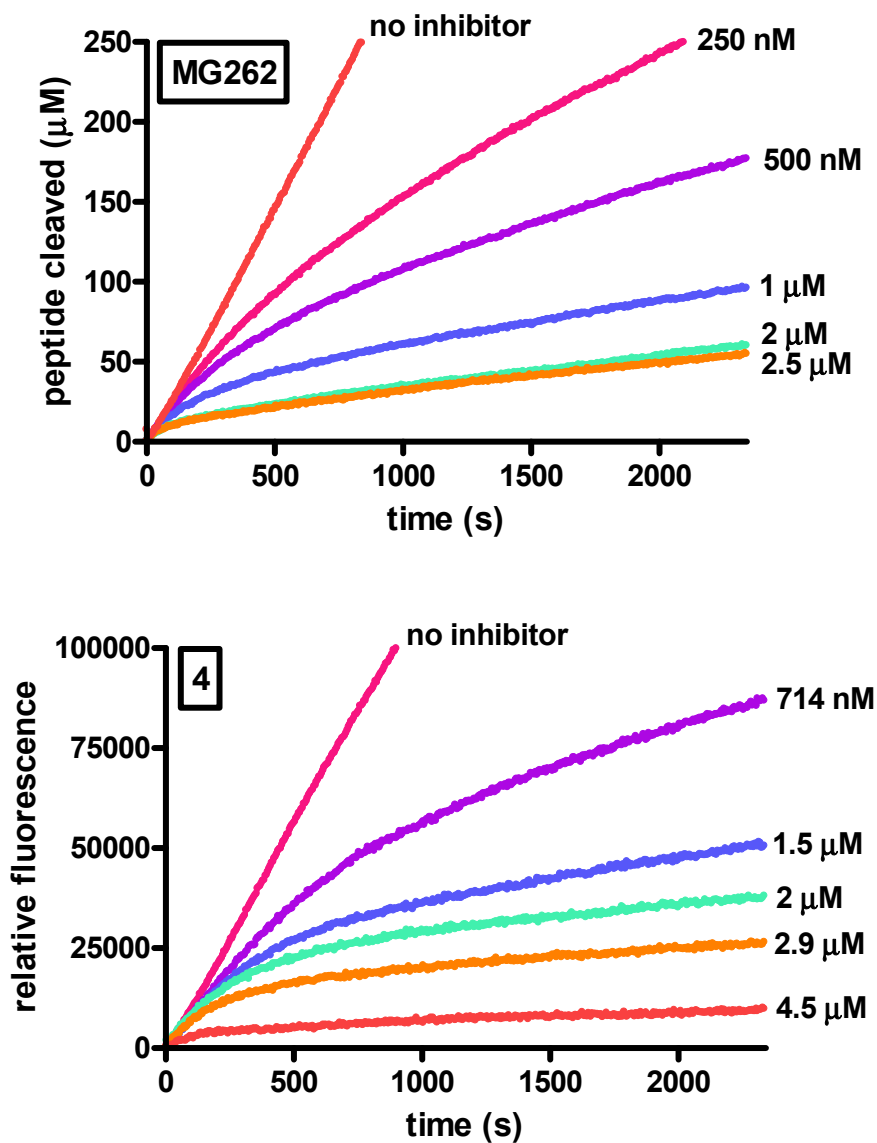


Figure 4.10 Time-dependent inhibition of *S. Typhimurium* Lon peptide hydrolysis by peptidyl boronates in the presence of varying concentrations of inhibitor. Representative time courses for *S. Typhimurium* Lon (30 nM) degradation of varying concentrations of MG262 (top) or 4 (bottom) in the presence of 1 mM ATP and 1 mM 2.

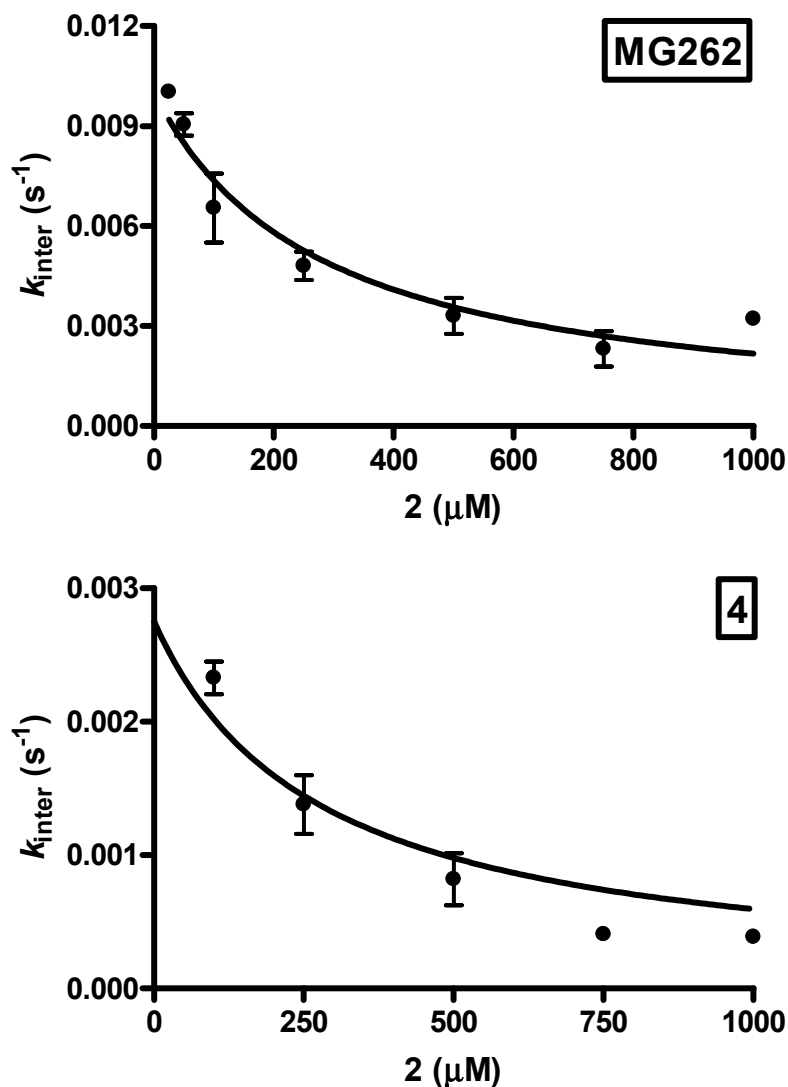


Figure 4.11 **Peptidyl boronates are competitive inhibitors of *S. Typhimurium* Lon peptide hydrolysis.** Reactions containing 30 nM *S. Typhimurium* Lon were preincubated with varying concentrations of **2** prior to the addition of 1 mM ATP. After 50 s, 300 nM MG262 (top) or 267 nM **4** (bottom) was added and peptide hydrolysis monitored over 40 min. All experiments were performed in triplicate and the k_{inter} values determined by fitting the time courses with eq 1 as described in Materials and Methods. The averaged k_{inter} (± 1 SD) were plotted against the corresponding peptide substrate concentration. The solid line represents the best fit of eq 6 for competitive time-dependent inhibition.

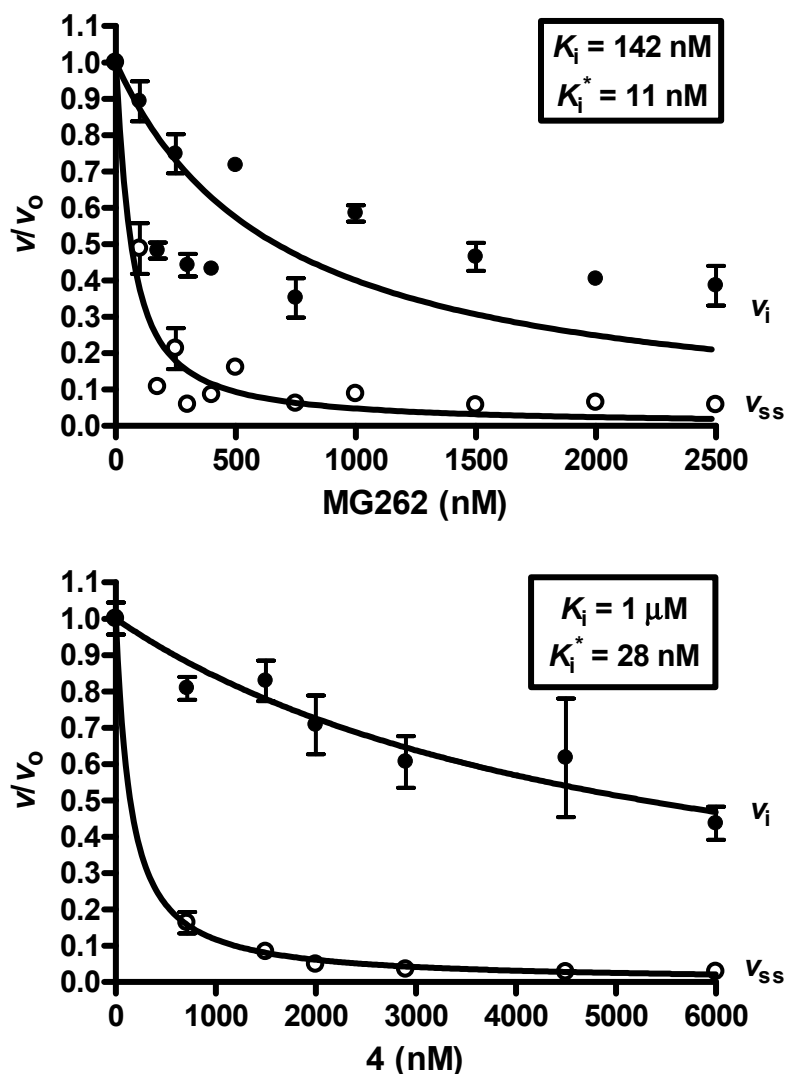


Figure 4.12 **The initial and final steady-state rates for *S. Typhimurium* Lon peptide hydrolysis vary during inhibition by peptidyl boronates.** Reactions containing 30 nM *S. Typhimurium* Lon were preincubated with 1 mM **2** prior to the addition of 1 mM ATP. After 50 s, varying concentrations of MG262 or **4** were added and peptide hydrolysis monitored over 40 min. All experiments were performed in triplicate and the v_i and v_{ss} values determined by fitting the time courses with eq 1 as described in Materials and Methods. The averaged v_i (●) or v_{ss} (○) in the presence of inhibitor / v_{ss} in the absence of the inhibitor (v/v_0 , ± 1 SD) were plotted against the corresponding inhibitor concentration. These data were fit with eq 7 or 8 to yield estimates for the values of K_i^{app} and $K_i^{*\text{app}}$. These were then converted, using eq 9 or 10, to yield estimates for the true values of K_i and K_i^* as described in Materials and Methods.

Table 4.2 Parameters for Peptidyl Boronate Inhibition of *S. Typhimurium* Lon

	MG262		4		
	estimate ^a	experimental ^b	estimate	experimental	global fitting ^c
K_i^{app} (nM)		3000 ± 1000			
K_i (nM)	142	647	1000		219
K_i^{*app} (nM)		51 ± 7		200 ± 8	
K_i^* (nM)	11	11	28	43	19
k_5 (s ⁻¹)		0.017 ± 0.003		$> 0.008^d$	
k_6 (s ⁻¹)		$3 \times 10^{-4}^e$		$3 \times 10^{-4}^e$	2.9×10^{-4}

^a values derived from the v_i and v_{ss} data in Figure 4.12

^b values derived from the k_{inter} data in Figure 4.13

^c values derived from nonlinear global fitting of the experimental time courses to a two-step time-dependent inhibition mechanism (Figure 4.3)

^d value cannot be determined from experimental data, but must be greater than the maximal value for k_{inter} detected in Figure 4.13

^e values are estimated from extrapolation of the k_{inter} data in Figure 4.13 to zero inhibitor

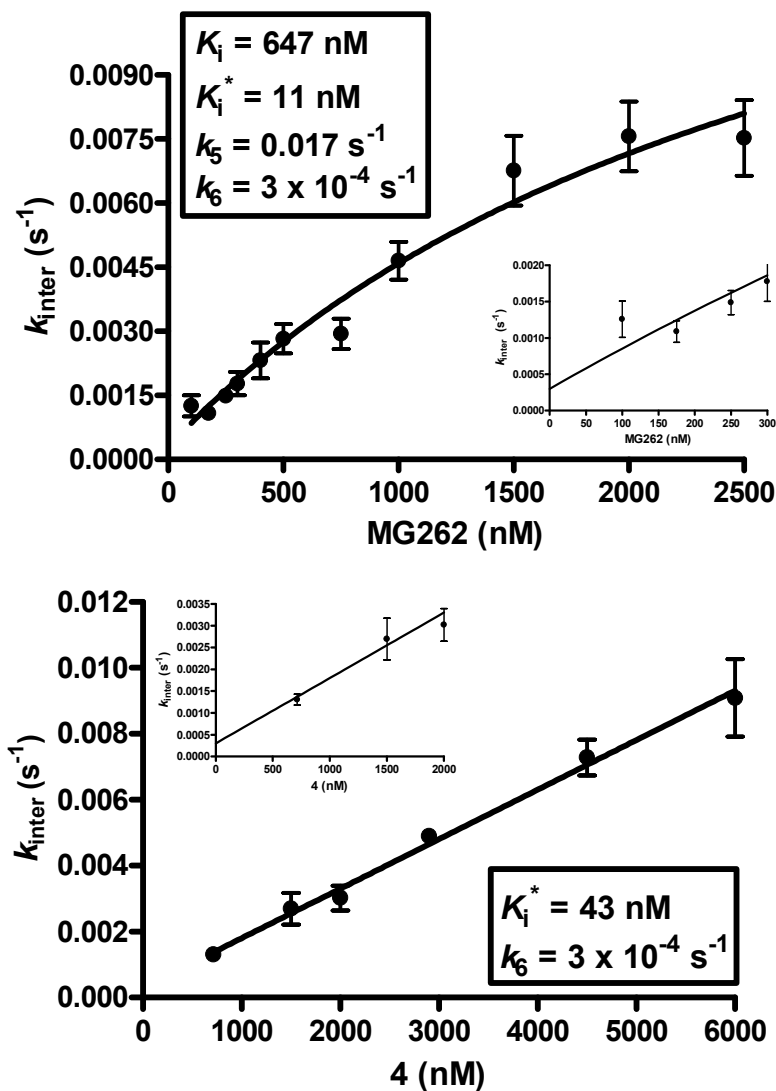


Figure 4.13 **Peptidyl boronates inhibit *S. Typhimurium* Lon peptide hydrolysis via a two-step mechanism.** Reactions containing 30 nM *S. Typhimurium* Lon were preincubated with 1 mM **2** prior to the addition of 1 mM ATP. After 50 s, varying concentrations of MG262 (top) or **4** (bottom) were added and peptide hydrolysis monitored over 40 min. All experiments were performed in triplicate and the k_{inter} values determined by fitting the time courses with eq 1 as described in Materials and Methods. The averaged k_{inter} (± 1 SD) data were plotted against the corresponding inhibitor concentration. The data were fit with eq 11 to yield the values of K_i , K_i^* , and/or k_5 as described in Materials and Methods.

Table 4.3 Parameters for Inhibition of *S. Typhimurium* Lon Derived from Global Fitting

	known ^a	one-step (Figure 4.2)	two-step (Figure 4.3)
k_1 ($\mu\text{M}^{-1} \text{s}^{-1}$)		0.029 ± 0.008	0.047 ± 0.003
k_2 (s^{-1})		1 ± 3^b	0.6 ± 0.4
k_{cat} (s^{-1})	11 ± 1	11^c	11^c
K_m (μM)	276 ± 38	433	248
k_3 ($\mu\text{M}^{-1} \text{s}^{-1}$)		0.010 ± 0.001	0.07 ± 0.01
k_4 (s^{-1})		0.00054 ± 0.00001	0.016 ± 0.004
K_i (nM)		54	219
k_5 (s^{-1})		ND ^d	0.0031 ± 0.0003
k_6 (s^{-1})		ND	0.00029 ± 0.00003
K_i^* (nM)		ND	19
residuals		29.5	22.8

^a from (82)

^b parameters have an error larger than the fitted value

^c parameter was not fitted and was held constant at the known value

^d not defined

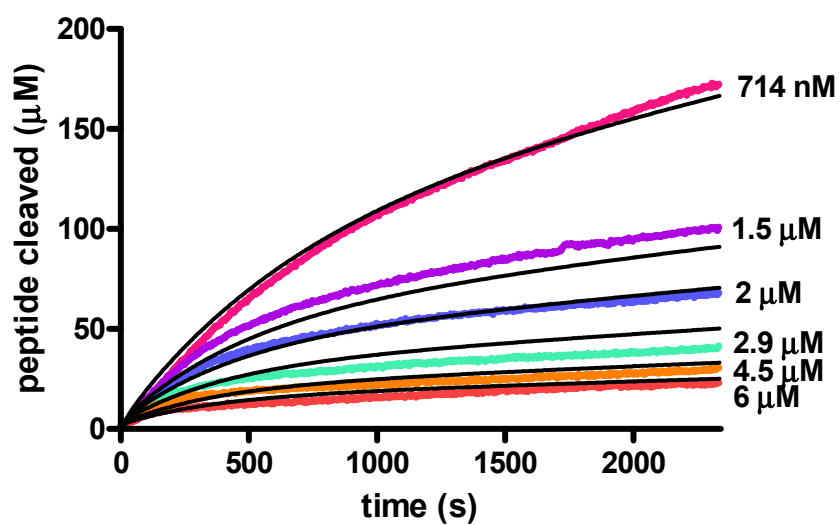


Figure 4.14 **Global nonlinear fitting of inhibition of *S. Typhimurium* Lon peptide hydrolysis by 4.** The colored lines represent the averaged experimental time courses at saturating 2 and varying concentrations of 4. The solid lines are the best fit resulting from global nonlinear fitting of the experimental time courses to a two-step time-dependent inhibition mechanism (Figure 4.3) using DynaFit (BioKin Ltd).

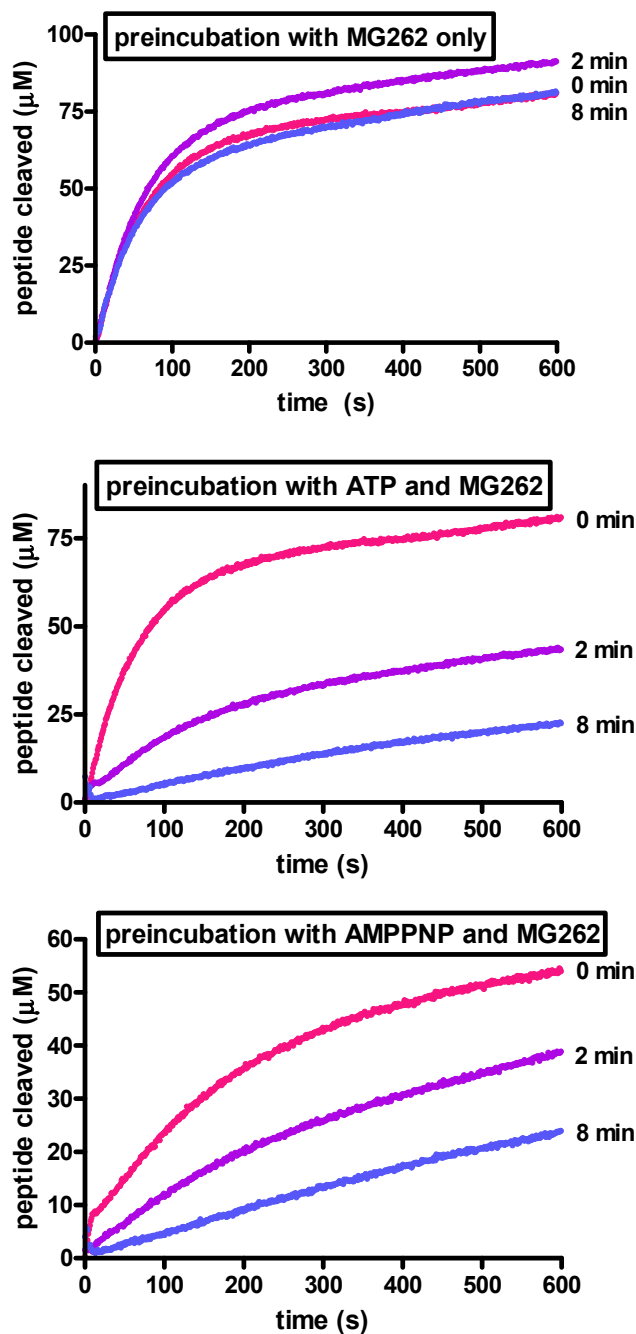


Figure 4.15 **Inhibition of *S. Typhimurium* Lon by **4** requires the binding of ATP.** Reactions containing 300 nM *S. Typhimurium* Lon were preincubated with 1.2 μM MG262 (top), 1.2 μM MG262 and 1 mM ATP (middle), or 1.2 μM MG262 and 1 mM AMPPNP (bottom) prior to the addition of 300 μM **2** and 1 mM ATP (top only) after the indicated time. Peptide cleavage was monitored over 10 min. All experiments were performed in triplicate and the averaged fluorescent signal plotted against time. Similar results are obtained with **4**.

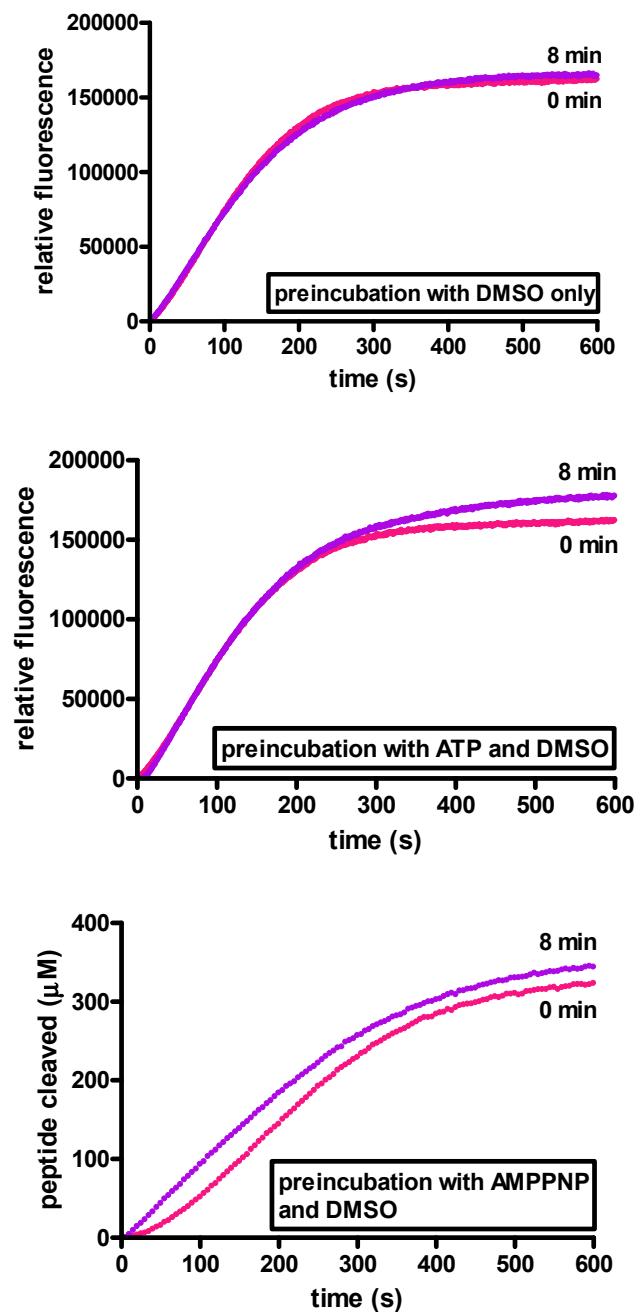


Figure 4.16 **The presence of DMSO during the preincubation period does not affect peptide hydrolysis by *S. Typhimurium* Lon.** Reactions containing 300 nM *S. Typhimurium* Lon were preincubated with 3.3% DMSO final (top), 3.3% DMSO final and 1 mM ATP (middle), or 3.3% DMSO final and 1 mM AMPPNP (bottom) prior to the addition of 300 μM **2** and 1 mM ATP (top only) after the indicated time. Peptide cleavage was monitored over 10 min. All experiments were performed in triplicate and the averaged fluorescent signal plotted against time. Similar results are obtained with the human homolog.

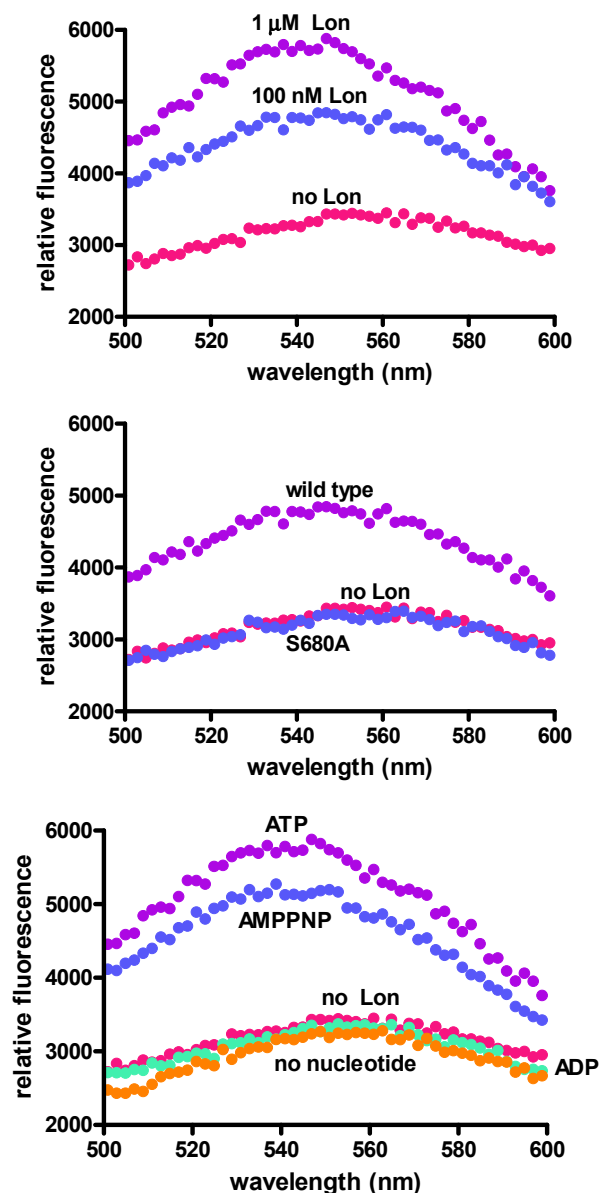


Figure 4.17 **Fluorescent detection of the interaction between *S. Typhimurium* Lon and 4.** Representative emission spectra ($\lambda_{\text{excitation}} = 335 \text{ nm}$) from reactions containing $1 \mu\text{M}$ 4, 1 mM of the indicated nucleotide, and varying concentrations of *S. Typhimurium* Lon were equilibrated at 37°C for 10 min. All reactions were performed in triplicate. (top) Emission spectra in the presence of 0 nM, 100 nM, or $1 \mu\text{M}$ *S. Typhimurium* Lon and 1 mM ATP. (middle) Emission spectra in the absence and presence of 100 nM wild type or S680A *S. Typhimurium* Lon and 1 mM ATP. (bottom) Emission spectra in the absence of *S. Typhimurium* Lon or presence of $1 \mu\text{M}$ *S. Typhimurium* Lon and 1 mM ATP, 1 mM AMPPNP, 1 mM ADP, or no nucleotide.

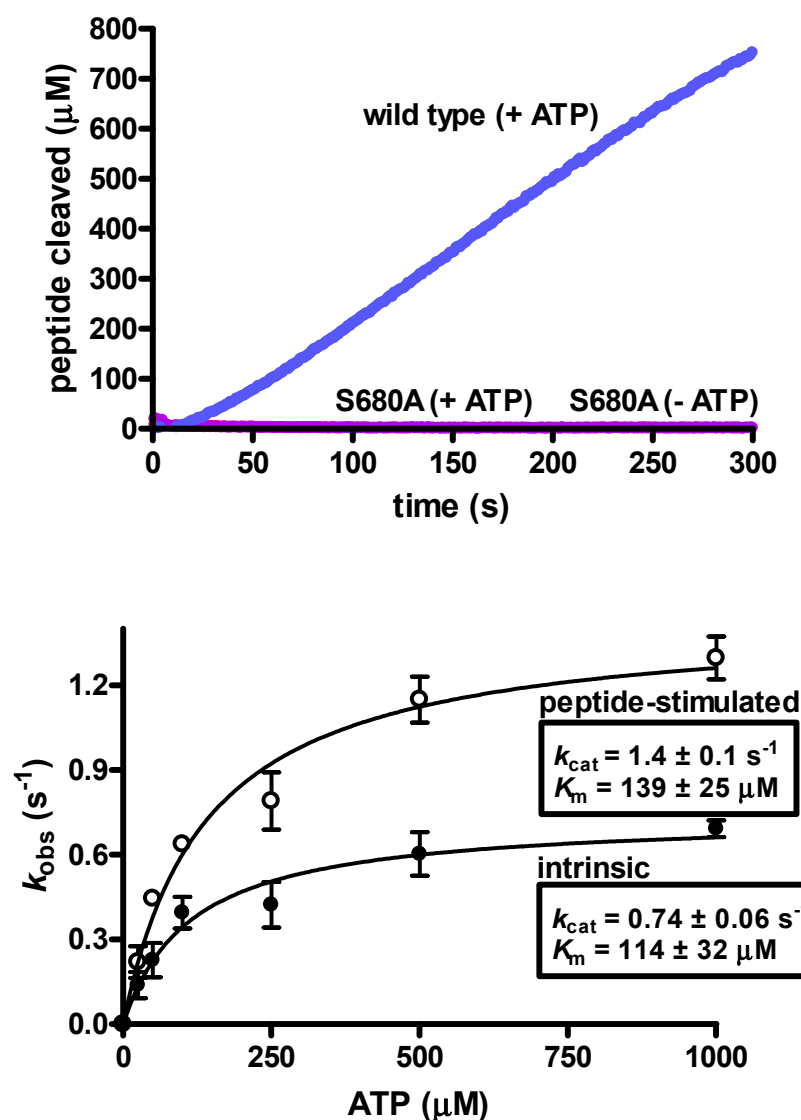


Figure 4.18 **Steady-state kinetic characterization of the S680A *S. Typhimurium* Lon mutant.** (top) Representative time courses for wild type and S680A *S. Typhimurium* Lon (200 nM) degradation of 1 mM **2** in the presence and absence of 1 mM ATP. (bottom) Reactions containing 200 nM *S. Typhimurium* Lon were preincubated in the absence (●) and presence of saturating ($\sim 5x K_m$) **2** (○) prior to the addition of varying concentrations of ATP. All experiments were performed at least in triplicate and the averaged k_{obs} values (± 1 SD) were plotted against the corresponding ATP concentration. The data were fit with eq 4 as described in Materials and Methods.

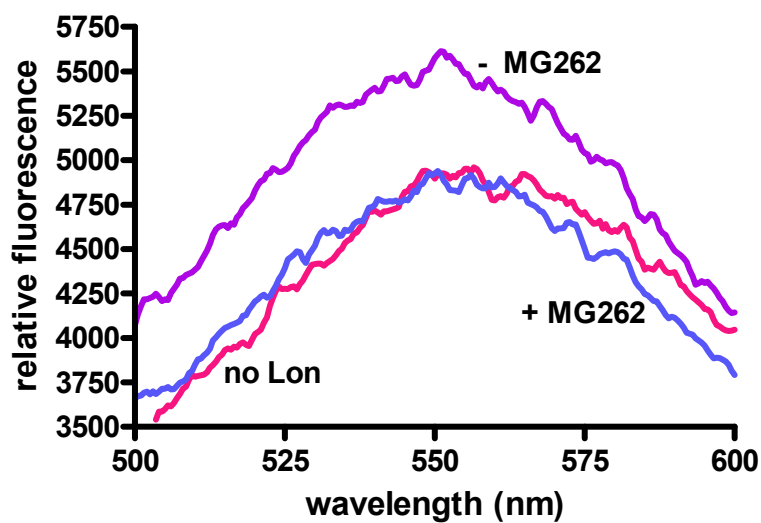


Figure 4.19. **Compound 4 is a reversible inhibitor of *S. Typhimurium* Lon.** Reactions containing 0 or 100 nM *S. Typhimurium* Lon and 1 mM ATP were preincubated with 1 μ M **4** for 30 min at 37°C prior to the addition of 0 or 10 μ M MG262 (in DMSO). Representative emission spectra ($\lambda_{\text{excitation}} = 335$ nm) of reactions after further equilibration at 37°C for 3h. All reactions were performed in triplicate.

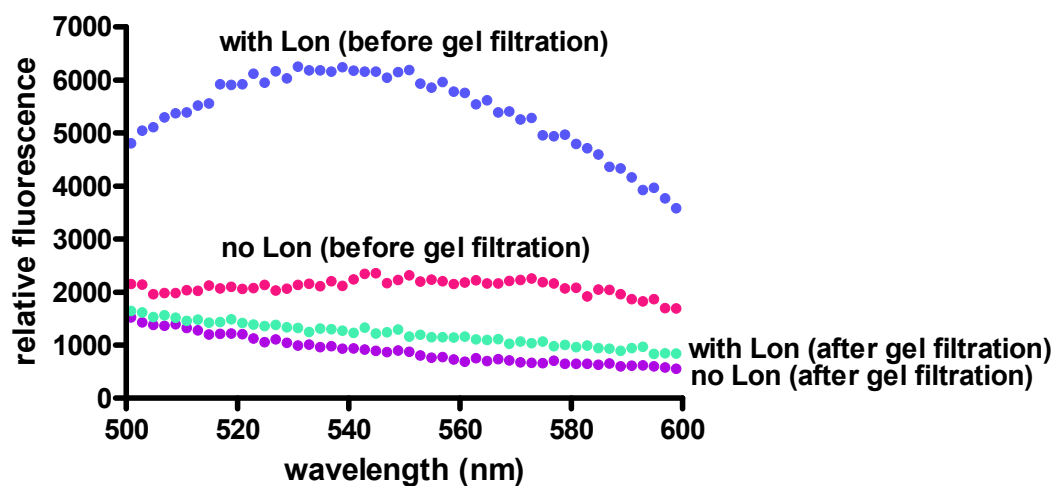


Figure 4.20 **Detection of the putative covalent adduct.** Reactions containing 1 μM **4** and 1 mM ATP in the presence and absence of 1 μM *S. Typhimurium* Lon were equilibrated at 37°C for 10 min. Representative emission spectra ($\lambda_{\text{excitation}} = 335$ nm) of the reaction mixture before and after separation of the unbound **4** from Lon by gel filtration.

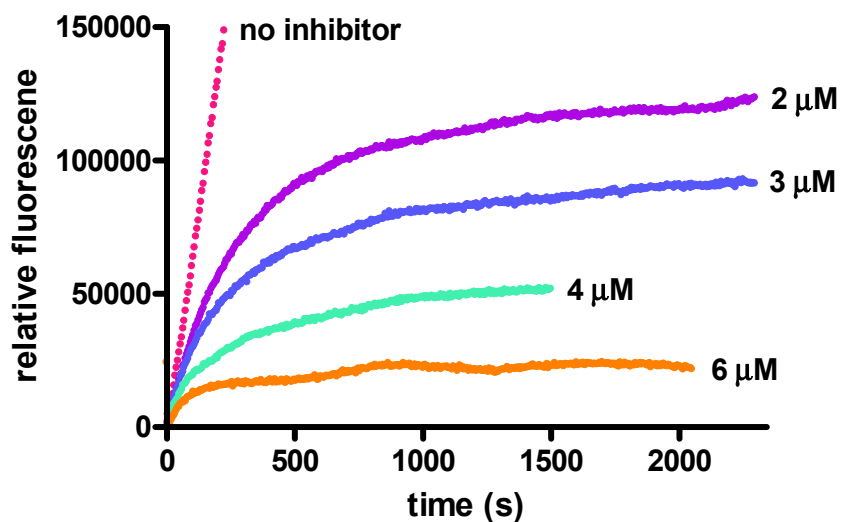


Figure 4.21 **Time-dependent inhibition of human Lon peptide hydrolysis by the peptidyl boronate 4 in the presence of varying concentrations of inhibitor.** Representative time courses for human Lon (500 nM) degradation of varying concentrations of 4 in the presence of 1 mM ATP and 1 mM 1.

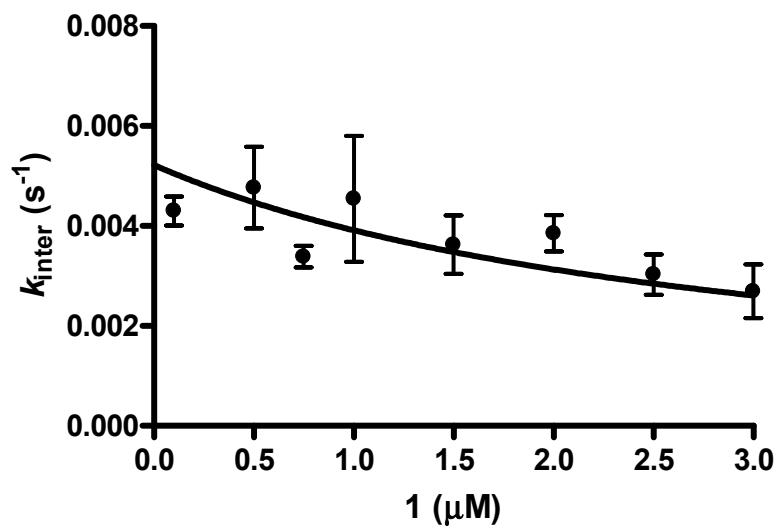


Figure 4.22 **The peptidyl boronate 4 is a competitive inhibitor of human Lon peptide hydrolysis.** Reactions containing 500 nM human Lon were preincubated with varying concentrations of **1** prior to the addition of 1 mM ATP. After 90 s, 2.5 μM **4** was added and peptide hydrolysis monitored over 40 min. All experiments were performed in triplicate and the k_{inter} values determined by fitting the time courses with eq 1 as described in Materials and Methods. The averaged k_{inter} (± 1 SD) were plotted against the corresponding peptide substrate concentration. The solid line represents the best fit of eq 5 for competitive time-dependent inhibition.

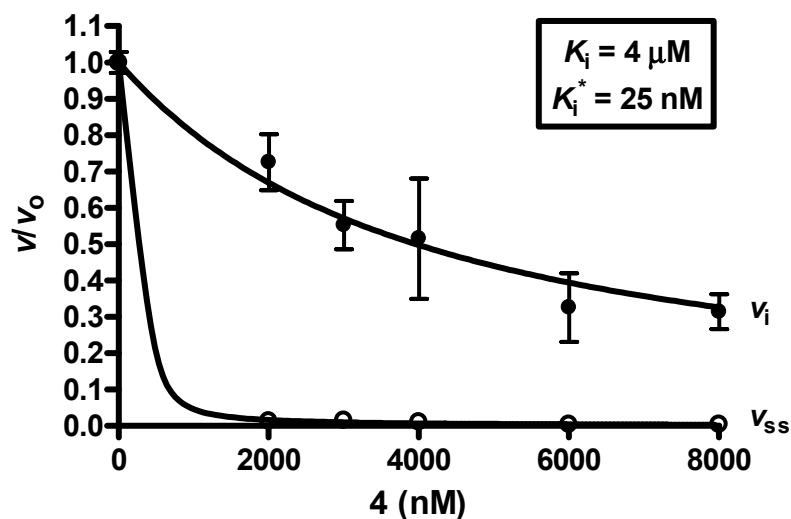


Figure 4.23 **The initial and final steady-state rates for human Lon peptide hydrolysis vary during inhibition by 4.** Reactions containing 500 nM human Lon were preincubated with 1 mM **1** prior to the addition of 1 mM ATP. After 90 s, varying concentrations of **4** were added and peptide hydrolysis monitored over 40 min. All experiments were performed in triplicate and the v_i and v_{ss} values determined by fitting the time courses with eq 1 as described in Materials and Methods. The averaged v_i (●) or v_{ss} (○) in the presence of inhibitor / v_{ss} in the absence of the inhibitor (v/v_0 , ± 1 SD) were plotted against the corresponding inhibitor concentration. These data were fit with eq 7 or 8 to yield estimates for the values of K_i^{app} and K_i^{*app} . These were then converted, using eq 9 or 10, to yield estimates for the true values of K_i and K_i^* as described in Materials and Methods.

Table 4.4 Parameters for Inhibition of Human Lon by **4**.

	4	
	estimate ^a	experimental ^b
K_i^{app} (nM)	4000	
K_i (nM)		
K_i^{*app} (nM)	25	47 ± 5
K_i^* (nM)		27
k_5 (s ⁻¹)		$> 0.02^c$
k_6 (s ⁻¹)		$1 \times 10^{-4}^d$

^a values derived from the v_i and v_{ss} data in Figure 4.22

^b values derived from the k_{inter} data in Figure 4.23

^c value cannot be determined from experimental data, but must be greater than the maximal value for k_{inter} detected in Figure 4.23

^d values are estimated from extrapolation of the k_{inter} data in Figure 4.23 to zero inhibitor

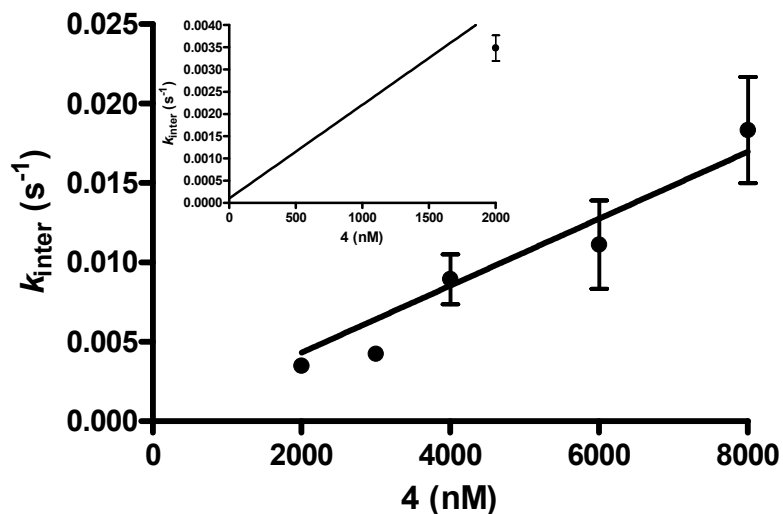


Figure 4.24 **The peptidyl boronate 4 inhibits human Lon peptide hydrolysis via a two-step mechanism.** Reactions containing 500 nM human Lon were preincubated with 1 mM **1** prior to the addition of 1 mM ATP. After 90 s, varying concentrations of **4** (bottom) were added and peptide hydrolysis monitored over 40 min. All experiments were performed in triplicate and the k_{inter} values determined by fitting the time courses with eq 1 as described in Materials and Methods. The averaged k_{inter} (± 1 SD) data were plotted against the corresponding inhibitor concentration. The data were fit with eq 11 to yield the values of K_i , K_i^* , and/or k_5 as described in Materials and Methods.

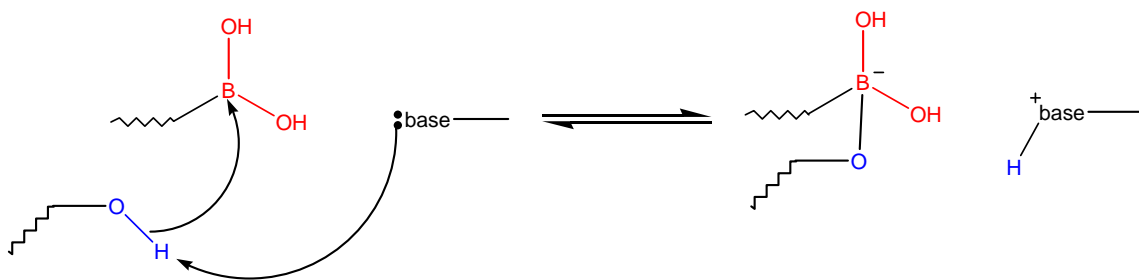


Figure 4.25 **Proposed mechanism for peptidyl boronate inhibition of serine and threonine proteases.** A general base abstracts a proton from the hydroxyl group of the active site serine or threonine resulting in nucleophilic attack on the boron to create a tetrahedral intermediate. The negative charge is formally drawn on the boron, but is actually distributed over the three oxygen atoms.

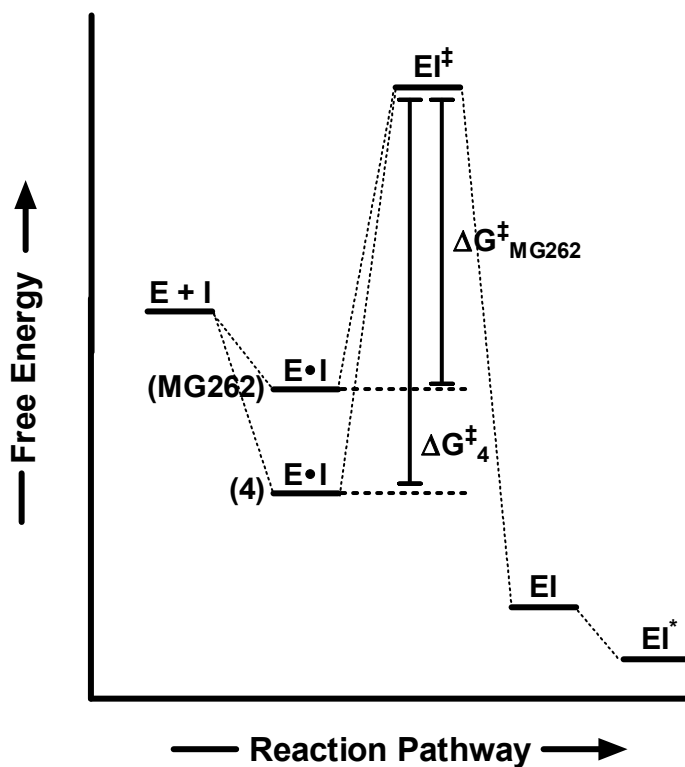
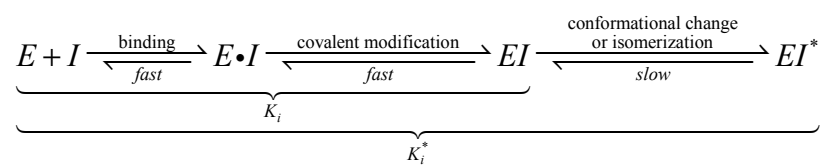


Figure 4.26 **Reaction pathway for inhibition of Lon by peptidyl boronates.** In the presence of ATP, Lon (E) binds the peptidyl boronate (I) to form an initial complex (E•I). The higher affinity of Lon for the peptidyl moiety of **4** stabilizes this complex, leading to a higher ΔG^\ddagger to reach the transition state (EI[‡]) for formation of the covalent adduct (EI). This is followed by a conformational change or isomerization to give the final inhibited complex (EI^{*}).

Scheme 4.1 Proposed mechanism for peptidyl boronate inhibition of Lon protease.



CHAPTER 5

Towards Developing a Peptide Substrate for the Human Lon Protease: The Steroidogenic
Acute Regulatory (StAR) Protein

Abstract

The steroidogenic acute regulatory protein (StAR) is a monomeric phosphoprotein responsible for the rate limiting step in steroidogenesis. In this study, the cloning and purification of the mature form of human StAR is described. Fluorescence spectroscopy is used to monitor the binding of cholesterol to the recombinant protein, allowing the determination of a $K_d = 22 \pm 3$ nM. Immunoblot analysis with an anti-phosphoserine antibody reveals the purified protein shows no phosphorylation, however it can subsequently be phosphorylated *in vitro* using protein kinase A. Finally, the first evidence that human StAR is a true substrate of the human Lon protease is presented. This work provides a starting point for the development of a physiologically relevant peptide substrate for this enzyme and for understanding the effect of mutations on the turnover of StAR in patients suffering from congenital lipoid adrenal hyperplasia.

Introduction

Lon is an ATP-dependent serine protease, which functions in the degradation of damaged and certain short-lived regulatory proteins (1-10). Steady-state kinetic characterization has demonstrated that the bacterial and human homologs display differences in their substrate specificity, as described in Chapter 2 (82). Few studies of the human enzyme have been completed as a result of a low yield in protein production and the lack of a suitable physiologically relevant substrate. A purification procedure has been described in Chapter 2 which yields as much as 1.2 mg of the recombinant human Lon protein per liter of culture (82). However, a substrate with a low micromolar K_m which is both physiologically relevant and mimics a protein substrate has yet to be described.

StAR facilitates the rate limiting step in steroidogenesis, transport of cholesterol from the cytosol to the inner mitochondrial membrane (113-115). Phosphorylation by protein kinase A stimulates this activity *in vivo* (116) (Figure 5.1). The protein is encoded in the nucleus as a preprotein and the N-terminal mitochondrial targeting sequence removed upon import into the mitochondria (117, 118) (Figure 5.1). StAR is no longer active upon import into the mitochondria and has been hypothesized to be degraded by Lon or Clp (100). Degradation of the murine homolog is inhibited by MG132 and *clasto*-lactacystin β -lactone, but not epoxomicin, which is consistent with the inhibition profile of Lon described in Chapter 4 (100, 119). In fact, human Lon was recently shown to degrade the murine StAR protein *in vitro* (57). Further studies will be required to demonstrate a similar degradation profile of the human homolog.

Mutations in the StAR gene are responsible for most forms of congenital lipoid adrenal hyperplasia (lipoid CAH), a severe form of CAH which causes insufficient production of glucocorticoids and mineralocorticoids (120). This results in impaired development of primary and secondary sex characteristics, sterility, and is often lethal in infants if not properly treated with hormone replacement therapy (121). As many as 35 distinct mutations in the StAR gene have been detected in patients with lipoid CAH (121, 122) (Figure 5.2). Many of these mutant proteins still localize to the mitochondria, but are improperly folded (123, 124). Furthermore, accumulation of StAR within the matrix leads to mitochondrial damage (121). To determine whether human Lon degrades both wild type and mutant StAR identically will provide novel insight into this disease and may present new approaches for its treatment.

This study describes the cloning and purification of the mature form of human StAR. The recombinant protein binds cholesterol with a dissociation constant comparable to the previously reported value (125) and can be phosphorylated *in vitro* using protein kinase A. Finally, evidence that human StAR is a true substrate of human Lon is presented. This work provides a starting point for developing a physiologically relevant peptide substrate for human Lon and understanding the effect of mutations on the turnover of StAR in patients suffering from lipoid CAH.

Materials and Methods

Materials

All oligonucleotide primers were purchased from Integrated DNA Technologies, Inc. (Coralville, IA). All cloning reagents were purchased from Promega (Madison, WI), New England BioLabs, Inc. (Ipswich, MA), Invitrogen (Carlsbad, CA) and USB Corporation (Cleveland, OH). NBD-cholesterol was purchased from Molecular Probes. The α -His antibody was purchased from Roche Applied Sciences. The α -phosphoserine antibody and goat α -mouse antibody conjugated to alkaline phosphatase were purchased from Sigma. Tris buffer, cell culture media, IPTG, chromatography media, DTT, NaCl, Mg(OAc)₂, imidazole, nitrocellulose, BCIP, NBT, kanamycin, EDTA, SDS, ATP, and all other reagents were purchased from Fisher, Sigma and Amresco (Solon, OH).

Plasmid Construction

D203A, F206L StAR

The StAR gene was amplified from human adrenal cDNA (Biochain Institute, Inc. Lot# A206095) using the oligonucleotides oHF015 (Appendix A) and oHF016. The resultant PCR product was used as a template to amplify the StAR gene with restriction sites using the oligonucleotides oHF012 and oHF011. This PCR product was cloned into the BamHI and HindIII sites of pCOLADuet-1 (Novagen) to create the plasmid pHF013 (Appendix B). The plasmid sequence was verified by DNA sequencing using the

oligonucleotides oHF017 and oHF005. The isolated StAR gene harbors both a D203A mutation, a known variant, and a novel F206L mutation. The expressed protein will contain an N-terminal 6x His tag followed by the consensus sequence for cleavage by enterokinase.

Wild Type StAR

The wild type StAR protein was created using the QuikChange Site-Directed Mutagenesis Kit (Stratagene) according to the manufacturer's instructions. The plasmid pHF013, described above, was used as a template and the oligonucleotides oHF021 and oHF022 were used as primers. The new plasmid, pHF014, was verified by DNA sequencing using the oligonucleotides oHF015, oHF017, and oHF005. The expressed protein will contain an N-terminal 6x His tag followed by the consensus sequence for cleavage by enterokinase.

Purification of Recombinant Proteins

StAR

Recombinant wild type StAR was overexpressed in Rosetta (DE3) (Novagen), using the plasmid pHF014. The cells were grown in superbrot (SB, per L: 5 g MOPS, 30 g tryptone, 20 g yeast extract, pH 7.5), containing 30 µg/mL kanamycin (Kan) and 34 µg/mL chloramphenicol (Cam), at 37°C and induced with 1 mM IPTG at OD₆₀₀ = 0.6 for 1 h. The cells were harvested at 2700 x g and resuspended in Buffer L (20 mM Tris, 50 mM NaH₂PO₄, 300 mM NaCl, 10 mM β-mercaptoethanol, 0.01% Tween 20, pH 7.4)

containing 0.5 mM PMSF. The cell paste was homogenized followed by sonication (5 min at 200 W in 5 s pulses) on ice. The homogenate was centrifuged at 12900 x g, 4°C for 30 min, to remove cell debris. The supernatant was incubated with Ni-NTA superflow resin (Qiagen), equilibrated in Buffer L, for 30 min at 4°C. The slurry was transferred to a column and StAR eluted using Buffer L containing 20 mM imidazole. The fractions containing StAR were pooled and dialyzed into Buffer S (20 mM Tris, 50 mM NaH₂PO₄, 300 mM NaCl, 0.01% Tween 20, pH 7.4) for native StAR or Buffer S containing 8 M urea for denatured StAR. The concentration of purified StAR was determined by its absorption at 280 nm or Bradford assay (73) using BSA as a standard and the protein stored at 4°C.

Human Lon

Recombinant human Lon was overexpressed in Rosetta (DE3) (Novagen), using the plasmid pHF002, described in Chapter 2 (82). Cells were grown and the purified protein isolated as described in Chapter 2 (82). The concentration of purified human Lon monomer was determined by Bradford assay (73) using BSA as a standard, and the protein stored at -80°C.

NBD-Cholesterol Binding Assay

The binding of StAR to cholesterol was monitored using a modified version of a fluorescence assay developed by Petrescu, A.D. *et al.* (125). A cuvette containing 2 mL 25 mM KP_i, pH 7.4 and 0 or 20-25 nM StAR was titrated with NBD-cholesterol in

acetonitrile. After equilibration at 37°C for 2 min, the emission spectrum from 500 – 600 nm (slit 5) after each addition of NBD-cholesterol was monitored using a Fluoromax 3 spectrophotometer (Horiba Group) after excitation at 473 nm (slit 5). All reactions were performed in triplicate.

Immunoblot Analysis

Protein samples were fractionated by 12.5% Tris SDS-PAGE and transferred to nitrocellulose at 100 V for 1 h. The nitrocellulose was blocked with 1% BSA /TBST (25 mM Tris, 150 mM NaCl, 0.05% Tween 20, pH 7.5) for 1 h at room temperature, followed by incubation with the primary monoclonal antibody (1: 2500 α -phosphoserine or 1:500 α -His in 1% BSA/TBST) for 2 h at room temperature. The excess antibody was removed by washing with TBST and the nitrocellulose incubated with the secondary antibody (1:3000 goat α -mouse conjugated to alkaline phosphatase in 1% BSA/TBST) for 1 h. The excess antibody was again removed by washing with TBST and protein bands visualized colorimetrically using BCIP/NBT.

Phosphorylation of StAR with ^{32}P

Reactions containing 40 mM Tris (pH 7.4), 20 mM Mg(OAc)₂, and 20 μM wild type StAR in the presence and absence of 1 unit protein kinase A (Sigma, Lot# 044K7400), were initiated by the addition of 0.3 mM [γ - ^{32}P] ATP (ICN or Perkin Elmer) and incubated at 37°C. At different time points (from 0 – 1.5 h), aliquots were quenched

in 0.5 N formic acid. A 3 μL aliquot of each quenched reaction time point was spotted onto nitrocellulose mounted on a Dot-Blot apparatus (BioRad) and the excess $[\gamma\text{-}^{32}\text{P}]$ ATP washed away with 0.5% H_3PO_4 /0.3% Tween 20. The amount of ^{32}P -labelled StAR was quantified using a Packard Cyclone storage phosphor screen Phosphor imager (Perkin-Elmer Life Science).

Degradation of StAR by Human Lon

Reactions containing 50 mM Tris (pH 8.1), 10 mM $\text{Mg}(\text{OAc})_2$, 150 mM NaCl, 2 mM DTT, 3 μM wild type StAR, and 1 μM human Lon monomer were initiated by the addition of 1 mM ATP and incubated at 37°C. At different time points (from 0 - 15 min), aliquots were quenched in 1x Lamelli sample buffer. The protein samples were subjected to immunoblot analysis.

Data Analysis

Determination of StAR Extinction Coefficient

The extinction coefficient at 280 nm for StAR was determined using eq 1 (126).

$$\epsilon_{280} = a(1280 \text{ cm}^{-1}\text{M}^{-1}) + b(5690 \text{ cm}^{-1}\text{M}^{-1}) + c(120 \text{ cm}^{-1}\text{M}^{-1}) \quad (1)$$

In eq 1, ϵ_{280} is the extinction coefficient at 280 nm, a is the number of tyrosine residues in the protein, b is the number of tryptophan residues in the protein, and c is the number of cysteine residues in the protein.

Determination of K_d Values

The fluorescence data was analyzed as previously described (125). Briefly, the emission spectra in the absence of StAR (background) were subtracted from the emission spectra in the presence of StAR to yield the emission spectra resulting from StAR binding to NBD-cholesterol. These normalized emission spectra were integrated and the integrated area at varying concentrations of NBD-cholesterol fit with eq 2 to give the value for K_d .

$$A = \frac{A_{\max}[\text{NBD-cholesterol}]^n}{K_d^n + [\text{NBD-cholesterol}]^n} \quad (2)$$

In eq 2, A is the integrated area, A_{\max} is the maximum value for A , K_d is the dissociation constant for NBD-cholesterol, and n is the Hill coefficient and is set equal to 2 as previously determined (125).

Results

Cloning and Purification of Recombinant StAR

The gene for StAR was amplified by PCR from human adrenal cDNA and cloned into the pCOLADuet-1 vector (Novagen). This plasmid, pHF013, contains both a kanamycin resistance gene and the powerful *T7/lac* promoter. DNA sequencing revealed the gene contained mutations, which were subsequently removed by site-directed mutagenesis to yield the wild type enzyme in the plasmid pHF014. The wild type protein contains both an N-terminal 6x His tag and enterokinase cleavage site (Figure 5.3). The His tag allows for rapid purification by metal affinity chromatography and the enterokinase site allows for the generation of the mature protein, free of any exogenous tag, if desired.

StAR was overexpressed in Rosetta (DE3) after induction with 1 mM IPTG. The Rosetta strain harbors a plasmid expressing tRNAs for codons not commonly used in the bacterial host, enhancing expression of eukaryotic enzymes. After lysing the cells, the cellular debris was removed by centrifugation and StAR recovered from the cell lysate by fractionation on Ni-NTA resin (Qiagen). As much as 5.8 mg of the purified enzyme can be recovered from each liter of culture (Figure 5.4).

Fluorescent Detection of the Cholesterol Binding Activity of StAR

In vivo, StAR functions to transport cholesterol from the outer mitochondrial to the inner mitochondrial membrane, which is the rate limiting step in steroidogenesis (113-115). To evaluate whether the recombinant wild type StAR was active, its ability to bind cholesterol was determined using a fluorescence-based assay (125). As mentioned in Chapter 4, a fluorescent signal is often influenced by its environment (108). NBD-cholesterol (Figure 5.5) is a fluorescent analog of cholesterol in which the NBD moiety undergoes an increase in fluorescence upon binding to StAR (Figure 5.6). The protein is known to bind two molecules of NBD-cholesterol, each with a K_d of ~ 32 nM (125). Titration of the wild type recombinant enzyme with NBD-cholesterol results in a concentration dependent increase in fluorescence (Figure 5.7). The integrated fluorescent signal varies sigmoidally with the concentration of NBD-cholesterol, which is not unexpected as the protein binds two molecules of the substrate (Figure 5.8). The resultant K_d is 22 ± 3 nM, which agrees with the previously reported value.

Phosphorylation of StAR

StAR contains two conserved consensus sequences for phosphorylation by protein kinase A (PKA), although only one of these sites occurs within the mature protein (Figure 5.1). Both sites are phosphorylated *in vivo*, however the cholesterol transfer activity of StAR is stimulated only by the phosphorylation of serine 195 (116). Immunoblot analysis of the purified protein, using an anti-phosphoserine antibody,

reveals no phosphorylation of the recombinant enzyme by the *E. coli* host. However, the purified StAR can be phosphorylated *in vitro* using PKA (Figure 5.9).

Degradation of Human StAR by Human Lon

The murine StAR has previously been shown to be a substrate of human Lon (57); however the human and mouse StAR homologs share only 87% sequence identity (13). In Chapter 2, it was shown that a single amino acid substitution can prevent recognition of substrate by Lon, therefore it is imperative to confirm that human StAR is a substrate of human Lon and determine its cleavage profile. Degradation of recombinant human StAR was monitored by immunoblot analysis with an α -His antibody in both the presence and absence of saturating ATP. Degradation of human StAR was observed only the presence of ATP (Figure 5.10).

Discussion

Kinetic studies of the human Lon protease are hindered by the lack of a physiologically relevant peptide substrate which mimics the degradation of a protein substrate and, more importantly, has a high affinity for the enzyme. Towards this goal, the mature form of human StAR has been cloned and the protein purified in high yield (Figure 5.4). The recombinant protein binds NBD-cholesterol with a $K_d = 22 \pm 3$ nM which is comparable to the previously reported value (Figure 5.8) (125). Upon purification, StAR displays no phosphorylation, however it can be phosphorylated *in vitro* using PKA (Figure 5.9). In the presence of ATP, human StAR is rapidly degraded by human Lon (Figure 5.10), demonstrating it is a true physiologically relevant substrate of the enzyme. This work provides the basis for the following studies.

Until recently, it had been assumed the human and bacterial Lon homologs function in a similar manner, however the studies described in Chapter 2 have highlighted differences in their substrate specificity (82). This is not surprising, as the two enzymes would be required to degrade a vastly different set of proteins. However, it does suggest that the two enzymes may function differently *in vivo*. In fact, the *E. coli* protease can only partially complement the function of the yeast homolog, a study model for the eukaryotic enzyme (20). The proteolytic activity of the human enzyme may be modulated differently within the mitochondrial matrix than the bacterial enzyme within the cytosol. The discovery and isolation of human StAR as a substrate of human Lon provides a new tool with which to approach these questions.

The model peptide substrate for *E. coli* Lon, described in Chapter 1, was developed based on the degradation profile of the λ N protein, a substrate of the enzyme. The five amino acids flanking a single cleavage site were used to create the model peptide. Determination of the degradation profile of human StAR, will allow a similar approach to be used in developing a model substrate for the human Lon homolog, which mimics a protein substrate and has a high affinity for the enzyme. This substrate will allow detailed mechanistic characterization of human Lon which was previously not possible, both on the steady-state and pre-steady-state timescale. It will simplify data analysis, as the substrate will contain only one cleavage site. The higher affinity will minimize the amount of substrate required, both reducing the cost of the assay and alleviating limitations due to solubility. Basic kinetic characterization of both the ATP and peptide hydrolysis activities of the enzyme can be fully explored as well as the effect of products and inhibitors on these activities. These parameters will be used to construct a model for the activity of the human homolog, which may differ from the bacterial system.

StAR will also serve as a model protein substrate for human Lon. The first kinetic studies of the human enzyme with a physiologically relevant substrate can be completed. Comparison of the degradation rates and profiles of the phosphorylated and unphosphorylated or native and denatured states of StAR can also be made. The generation of mutant forms of StAR, found in patients with lipoid CAH by site directed mutagenesis, will allow insight into the role Lon plays in this serious disease. Degradation in the presence of cholesterol will reveal whether substrate binding can

protect StAR from proteolysis. Together, these studies will suggest new mechanisms by which the proteolytic activity of Lon may be modulated.

The structure of a protein similar to StAR, MLN64, is known and is often used as a model for StAR (Figure 5.11) (127). If StAR is a substrate of both the human and bacterial Lon proteases, the degradation profiles of both can be compared with respect to both the secondary and tertiary structure to understand how each homolog degrades a structured substrate. Previous studies have focused on unstructured substrates, such as λ N and casein. Furthermore, the primary amino acid sequence can be compared to highlight differences in cleavage site selection by the two enzymes. These differences can then be exploited in generating novel inhibitors which specifically target either the human or bacterial Lon homologs.

1 MLLATFKLCAGSSYRHMNRNMKGLRQQAVMAISQELNRRALGGPTPSTWINQVR**RRSS**LLGSRLEETL
68 YSDQELAYLQQGEEAMQKALGILSNQEGWKKESQQDNGDKVMSKVVPDVGKVFRLLEVVDQPMERLY
135 EELVERMEAMGEWNPVKEIKVLQKIGKDTFITHELAAEAAGNLVGPRDFVSVRCAK**RRGS**TCVLAG
202 MATDFGNMPEQKGVIRAEHGPTCMVLHPLAGSPSKTKLTWLLSIDLKGWLPKSIINQVLSQTQVDFA
269 NHLRKRLESHPASEARC

Figure 5.1 **Amino acid sequence of human StAR.** The protein kinase A phosphorylation sites are highlighted in pink and the phosphorylated residues shown in white. The mitochondrial targeting sequence is underlined.

nucleotide change	amino acid change
C898T	Q258X
G671T	R182L
A632G	E169G
593delTT	frameshift
940del3bp	ΔR272
947insA	frameshift
548insTT	frameshift
C703T	R193X
T→A@-11 _{14/E5}	frameshift
C779T	A218V
T950C	L275P
G631A	E169K
246insG	frameshift
DNA insertion	frameshift
261delT	frameshift
838delA	frameshift
189delG	frameshift
T800C	M225T
C759T	Q212X
364del31bp	frameshift
650delC	frameshift
Tins@-3bp _{sds/E2}	frameshift
564del113bp	frameshift
238delA	frameshift
840delA	frameshift
G→A _{E7}	W250X
251insG	frameshift
163insA	frameshift
643insCT	frameshift
677insA	frameshift
G776C	R217T
A733C	D203A

Figure 5.2 **Summary of the majority of known StAR mutations found in patients with lipoid CAH.** The abbreviations used are as follows: del, deletion; ins, insertion; bp, base pairs; E, exon; sds, splice donor site.



Figure 5.3 **N-terminal of recombinant StAR.** The first 25 residues of the recombinant StAR from pHF014. The 6x His tag (red), enterokinase site (blue), and the sequence of the StAR protein (green) are shown. The protein enterokinase will cleave another enzyme after the consensus sequence DDDDL (as shown by the arrow). The beginning of the StAR protein (L²⁰) corresponds to the mature enzyme which lacks the N-terminal 62 amino acids after import into the mitochondria (128).

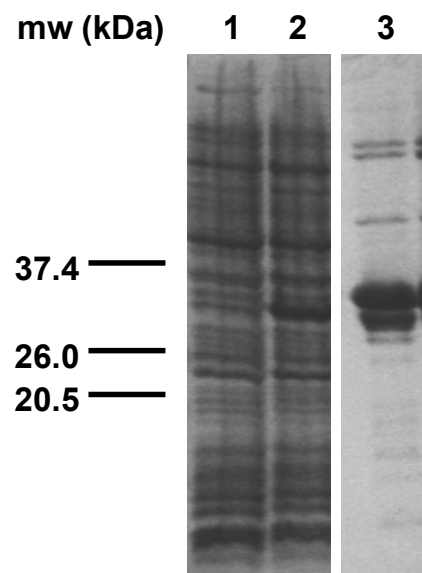


Figure 5.4 **Coomassie stain of purified recombinant human StAR.** SDS-PAGE of cell lysate before (lane 1) and after (lane 2) induction with 1 mM IPTG and the purified recombinant human StAR (27 kDa, lane 3) visualized by coomassie. Some truncated StAR is also observed.

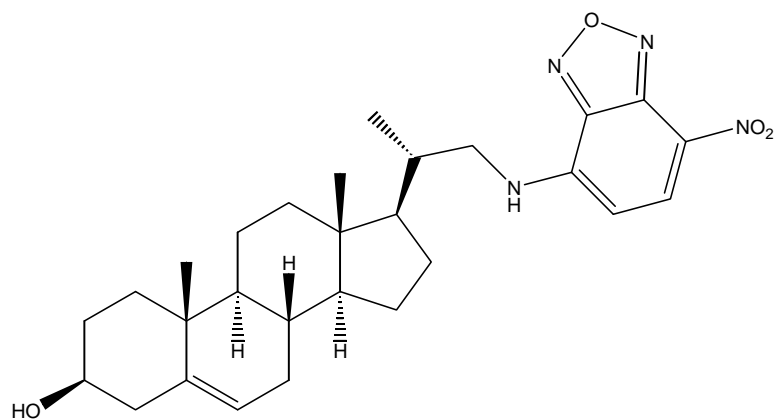


Figure 5.5 **Structure of NBD-cholesterol.** 22-(N-(7-nitrobenz-2-oxa-1,3-diazol-4-yl)amino)-23,24-bisnor-5-cholesterol-3 β -ol.

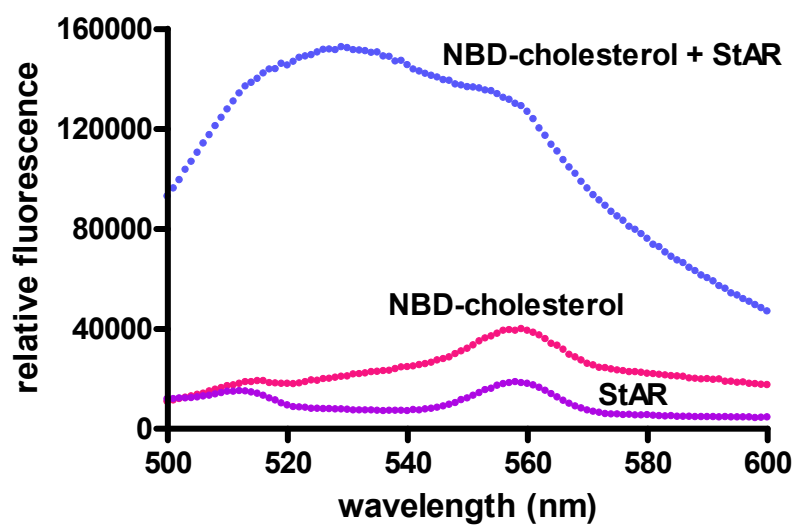


Figure 5.6 **Fluorescent detection of StAR binding to NBD-cholesterol.** Representative emission spectra ($\lambda_{\text{excitation}} = 469 \text{ nm}$) from reactions containing $1.5 \mu\text{M}$ wild type StAR and/or $1 \mu\text{M}$ NBD-cholesterol.

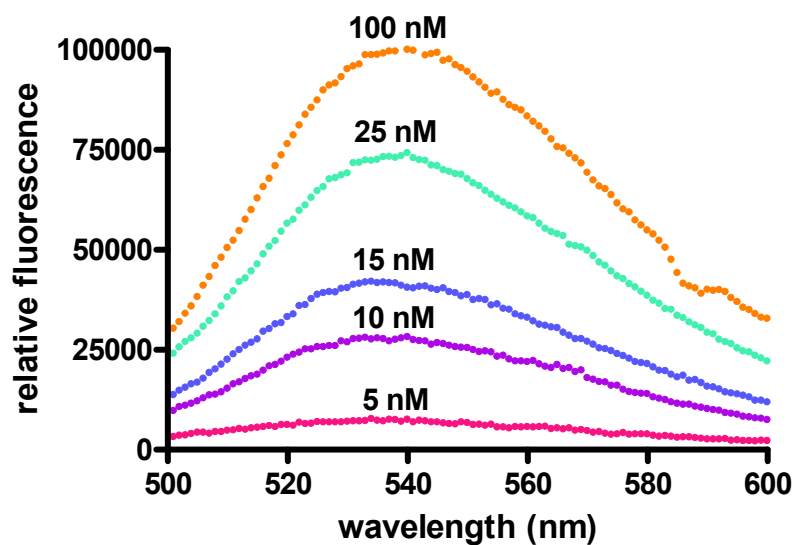


Figure 5.7 **Increased fluorescent signal from StAR binding to NBD-cholesterol is concentration dependent.** Representative normalized emission spectra ($\lambda_{\text{excitation}} = 473$ nm) from reactions containing 20 nM wild type StAR and varying concentrations of NBD-cholesterol.

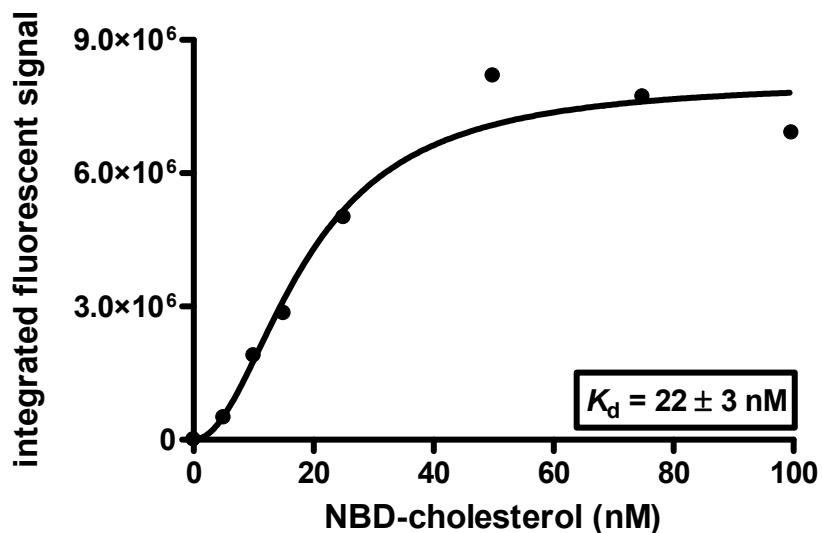


Figure 5.8 **Representative binding isotherm for StAR binding to NBD-cholesterol.** Reactions containing 0 or 20 nM human StAR were incubated with varying concentrations of NBD-cholesterol and the emission spectrum ($\lambda_{\text{excitation}} = 473 \text{ nm}$) monitored from 500 to 600 nm. All experiments were performed in triplicate and the integrated area determined as described in Materials and Methods. The integrated areas were plotted against the corresponding NBD-cholesterol concentration. The K_d ($22 \pm 3 \text{ nM}$) was determined by fitting the data with eq 2 as described in Materials and Methods.

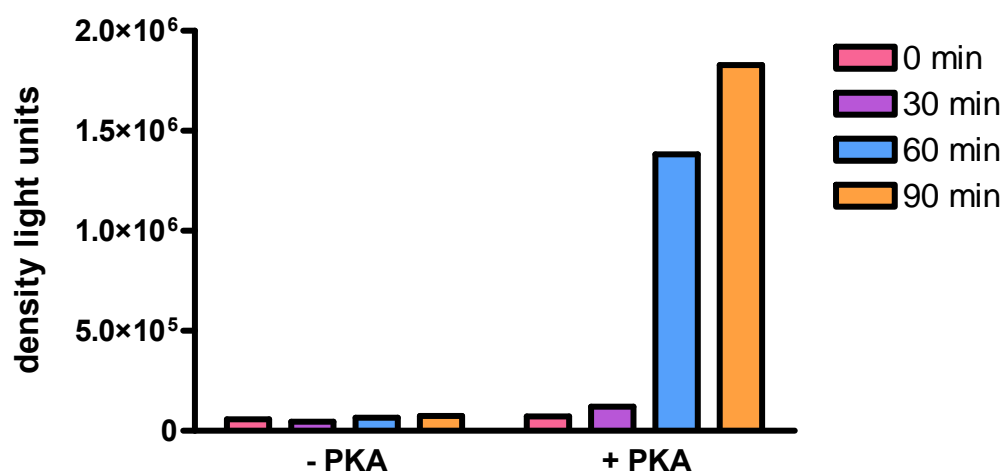


Figure 5.9 *In vitro* phosphorylation of human StAR by protein kinase A. Reactions contained 20 μ M wild type StAR and 0.3 mM [γ - 32 P] ATP in the presence and absence of 1 unit protein kinase A (PKA). The extent of phosphorylation, in density light units, was determined as described in Materials and Methods.

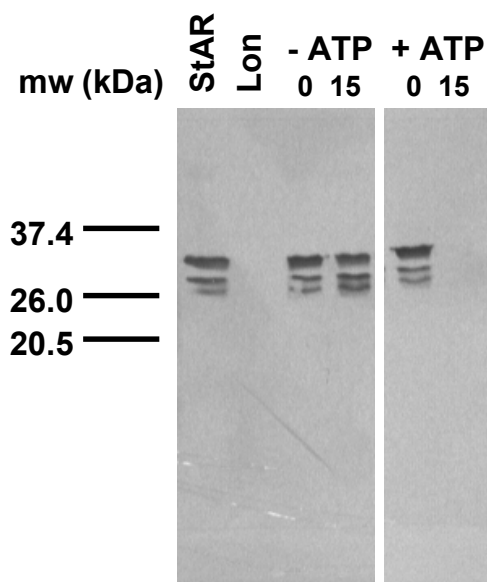


Figure 5.10 **Immunoblot analysis of human Lon degradation of human StAR.** Reactions contained 3 μ M wild type StAR and 1 μ M human Lon monomer in the presence and absence of 1 mM ATP. The reaction at 0 and 15 min was fractionated by 12.5% Tris SDS-PAGE and visualized by immunoblot analysis with an α -His antibody as described in Materials and Methods.



Figure 5.11 **Structure of MLN64.** Structure of MLN64, a protein closely related to StAR. The most common mutations found in lipoid CAH are shown in red. From (127).

Appendix A: Oligonucleotides

Table A.1 Oligonucleotides Used for Cloning and Site-Directed Mutagenesis.

	sequence (5' – 3')	molecular weight (g/mol)	melting temperature (°C)	µg/OD₂₆₀
oHF005	GCTAGTTATTGCTCAGCGG	5834.7	60.1	32.7
oHF006	AATACGACTCACTATAG	5162.3	39.9	29.6
oHF011	AGCTAAGCTTTGGTCTTCAACAC CTGGCT	8843.8	63.4	33.3
oHF012	ATCGGATCCAGATGACGATGACA AACTGGAAGAGACTCTCTAC	13253.7	65.4	30.7
oHF015	CTGGAAGAGACTCTCTAC	5483.6	47.9	31.8
oHF016	TCAACACCTGGCTTCAG	5130.4	52.0	33.0
oHF017	GGATCTCGACGCTCTCCCT	5715.7	58.5	34.6
oHF018	TAATACCCATGGGGAATCCTGAG CGTTCTGAA	9848.4	63.4	31.4
oHF019	AAACCCAAGCTTCTACTATTTTG CGTTACAACCT	10625.0	62.5	32.4
oHF021	GCTGGCATGGACACAGACTTCGG GAACATGCC	9859.4	68.1	32.2
oHF022	GGCATGTTCCCGAAGTCTGTGTC CATGCCAGC	9792.4	68.1	33.3
oHF029	CGACCCTGCACGTCTGG	5147.4	58.8	34.2
oHF030	CTTTCGGCGTTGCGCC	4840.2	58.4	36.3
oHF031	CCTGCGTCAGGCGCAG	4883.2	60.1	33.7
oHF037	GCAAGAAGGAGGCGGAGGACG	6619.3	62.6	29.8
oHF038	CGGCCCTGCTGTCCCTGG	5443.5	64.2	36.4
oHF045	CCAGGGACAGCAGGGCCG	5559.6	64.2	31.8
oHF046	CCTCGGAGTTCAATGTCACC	6053.0	55.5	32.8
oHF049	GCAGGCTGGCCAGCG	4619.0	61.1	33.3
oHF050	CGGTGTCACGTCATAC	4857.2	49.7	32.2
oHF071	CCGAAAGACGGTCCAGCCCGCGG TATCGCGATG	10149.6	71.1	32.3
oHF072	CATCGGATACCGGCGGCTGGAC CGTCTTTCGG	10122.6	71.1	33.8
oHF093	CGGACATCTCCAGTACG	5155.4	51.9	31.9

Appendix B: Plasmids

Table B.1 Plasmids Generated for the Expression of Recombinant Proteins

plasmid	protein	mutations	antibiotic resistance
pHF002	human Lon	wild type	30 µg/mL Kan
pHF013	human StAR	N-terminal 6x His tag N-terminal enterokinase site D203A F206L	30 µg/mL Kan
pHF014	human StAR	N-terminal 6x His tag N-terminal enterokinase site	30 µg/mL Kan
pHF020	<i>S. Typhimurium</i> Lon	V378I	30 µg/mL Kan
pHF031	<i>S. Typhimurium</i> Lon	V378I S680A	30 µg/mL Kan

Appendix C: Peptide Substrates, Hydrolysis Products, and Inhibitors

Table C.1 Structures of Non-Natural Amino Acids Used in Synthetic Peptides

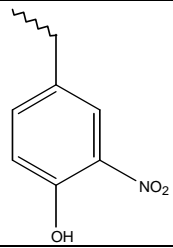
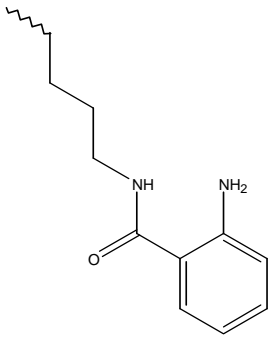
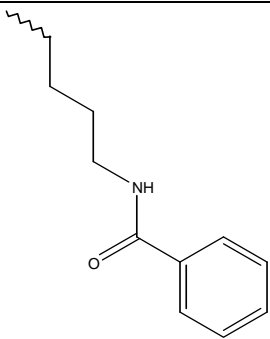
non-natural amino acid	abbreviation	side chain structure
3-nitrotyrosine	Y(3-NO ₂)	
lysine anthranilamide	K(Abz)	
lysine benzoic acid	K(Bz)	
2-aminobutyric	Abu	

Table C.2 Structures of N-terminal Protecting Groups Used in Synthetic Peptides

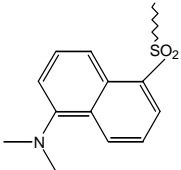
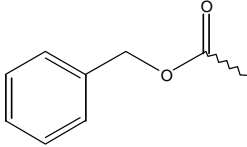
protecting group	abbreviation	structure
5-dimethylamino-1-naphthalenesulfonyl	dansyl	
benzyloxycarbonyl	Z	

Table C.3 Peptide Substrates

substrate	sequence	fluorescent?	extinction coefficient at 280 nm (M⁻¹ cm⁻¹)	molecular weight (Da)
1	Y(3-NO ₂)-RGITCSGRQ-K(Abz)	yes	5650	1432
	YRGITCSGRQ-K(Bz)	no	1321	1372
2	Y(3-NO ₂)-RGIT-Abu-SGRQ-K(Abz)	yes	5650	1414
	YRGIT-Abu-SGRQ-K(Bz)	no	1280	1354
5	Y(3-NO ₂)-RGITSSGRQ-K(Abz)	yes	5650	1416
6	Y(3-NO ₂)-RGITGSGRQ-K(Abz)	yes	5650	1386

Table C.4 Peptide Hydrolysis Products

product	sequence	fluorescent?	extinction coefficient at 280 nm (M⁻¹ cm⁻¹)	molecular weight (Da)
3	dansyl-YRGIT-Abu	yes	2718 ^a	927
7	YRGIT-Abu	no	1280	694
8	SGRQK(Bz)	no	n/a ^b	679
9	YRGITC	no	1280	712
10	YRGITL	no	1280	722
11	YRGITC-CONH ₂	no	1280	711
12	Z-YRGIT-Abu	no	1280	828

^a extinction coefficient at 350 nm

^b must use TNBSA assay to determine peptide concentration (Appendix G)

Table C.5 Peptide Inhibitors

product	sequence	fluorescent?	extinction coefficient at 350 nm ($M^{-1} \text{ cm}^{-1}$)	molecular weight (Da)
ZL₃OH	Z-LLL	no	n/a ^a	492
4	dansyl-YRGIT-Abu-B(OH) ₂	yes	2718	927

^a peptide concentration determined by mass only

Appendix D: HPLC Data for Synthetic Peptides

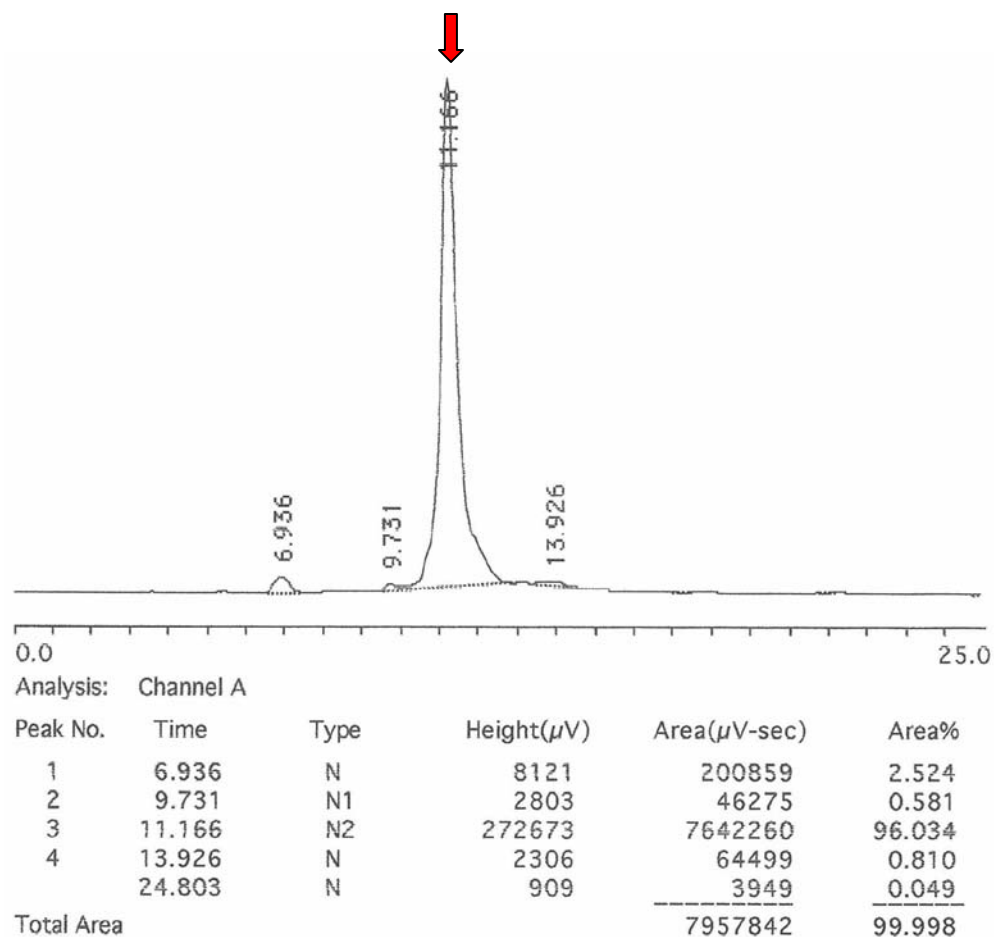


Figure D.1 **HPLC trace of the fluorescent analog of compound 1.** Analytical HPLC trace of the fluorescent analog of **1** fractionated on a Vydac C18 column (#218MS54) at 1 mL/min using a linear gradient from 5 – 25% acetonitrile/0.05% TFA over 20 min (detection at 220 nm). The peak corresponding to the fluorescent analog of **1** is marked with an arrow.

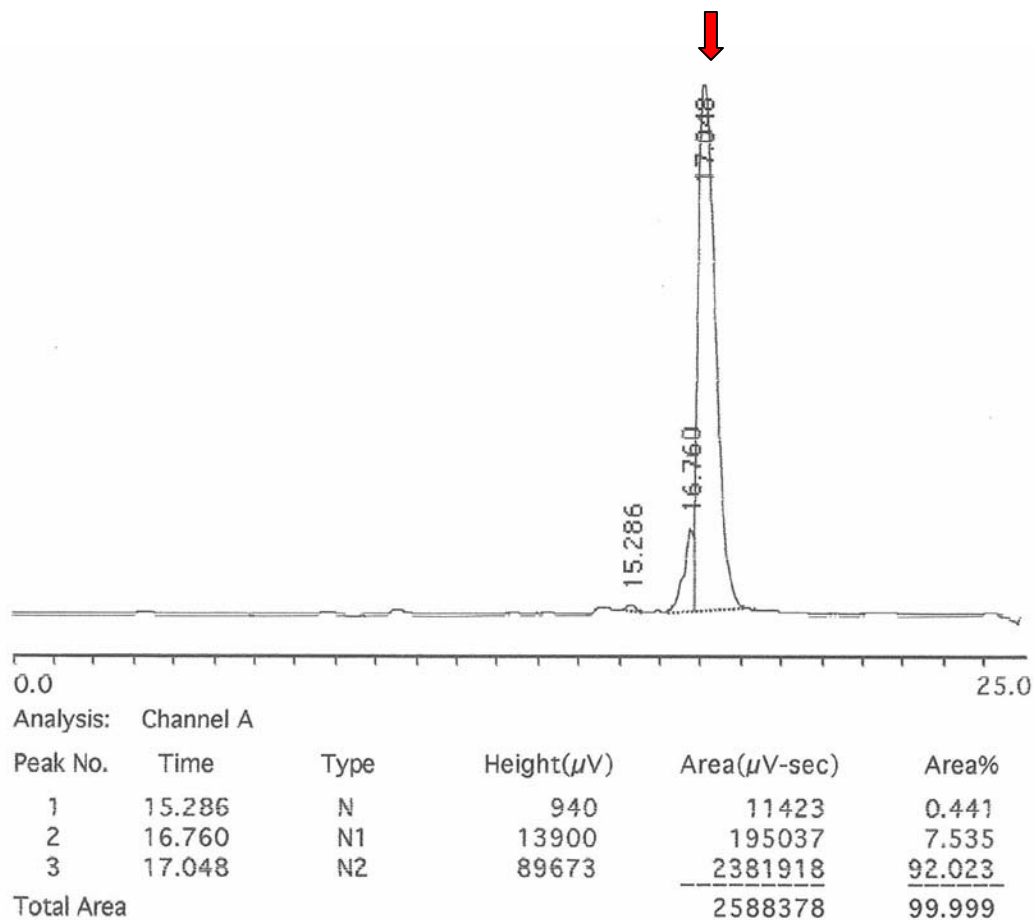


Figure D.2 **HPLC trace of the non-fluorescent analog of compound 1.** Analytical HPLC trace of the non-fluorescent analog of **1** fractionated on a Vydac C18 column (#218MS54) at 1 mL/min using a linear gradient from 5 – 25% acetonitrile/0.05% TFA over 20 min (detection at 220 nm). The peak corresponding to the non-fluorescent analog of **1** is marked with an arrow.

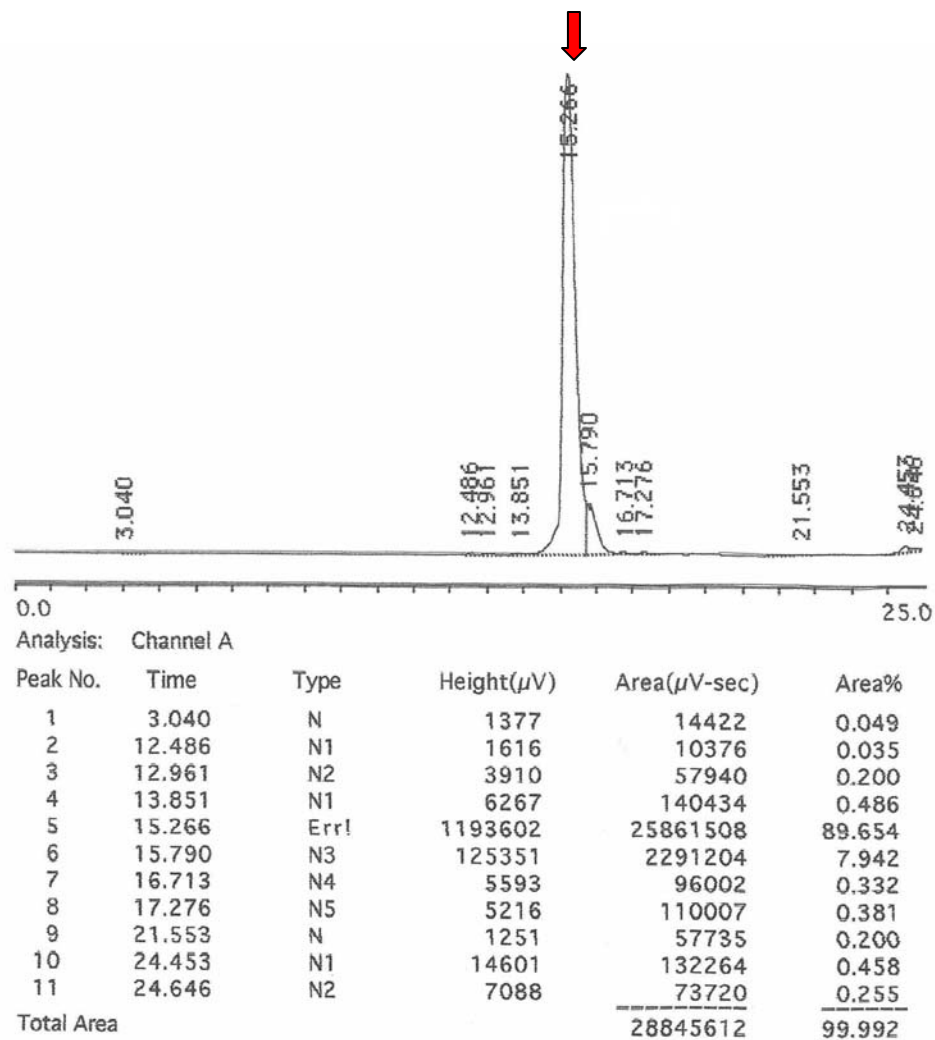


Figure D.3 **HPLC trace of the fluorescent analog of compound 2.** Analytical HPLC trace of the fluorescent analog of **2** fractionated on a Vydac C18 column (#218MS54) at 1 mL/min using a linear gradient from 5 – 25% acetonitrile/0.05% TFA over 20 min (detection at 220 nm). The peak corresponding to the fluorescent analog of **2** is marked with an arrow.

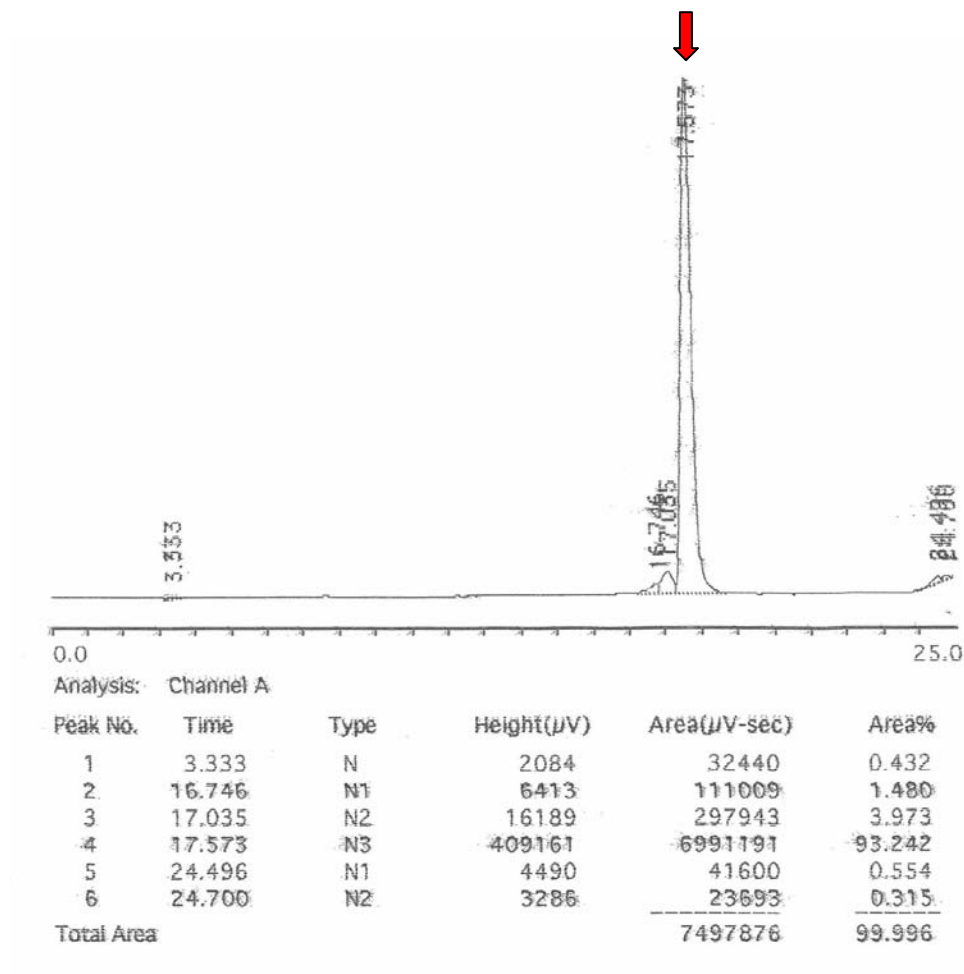


Figure D.4 **HPLC trace of the non-fluorescent analog of compound 2.** Analytical HPLC trace of the non-fluorescent analog of **2** fractionated on a Vydac C18 column (#218MS54) at 1 mL/min using a linear gradient from 5 – 25% acetonitrile/0.05% TFA over 20 min (detection at 220 nm). The peak corresponding to the non-fluorescent analog of **2** is marked with an arrow.

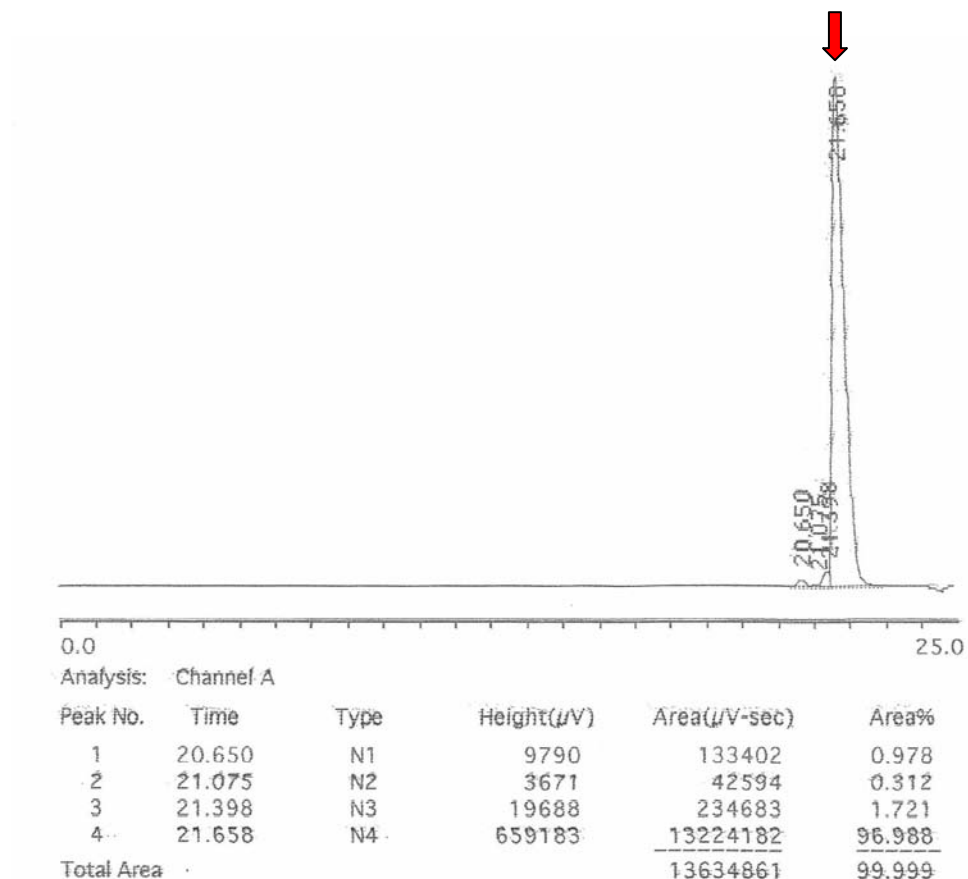


Figure D.5 **HPLC trace of compound 3.** Analytical HPLC trace of **3** fractionated on a Vydac C18 column (#218MS54) at 1 mL/min using a linear gradient from 5 – 25% acetonitrile/0.05% TFA over 20 min (detection at 280 nm). The peak corresponding to **3** is marked with an arrow.

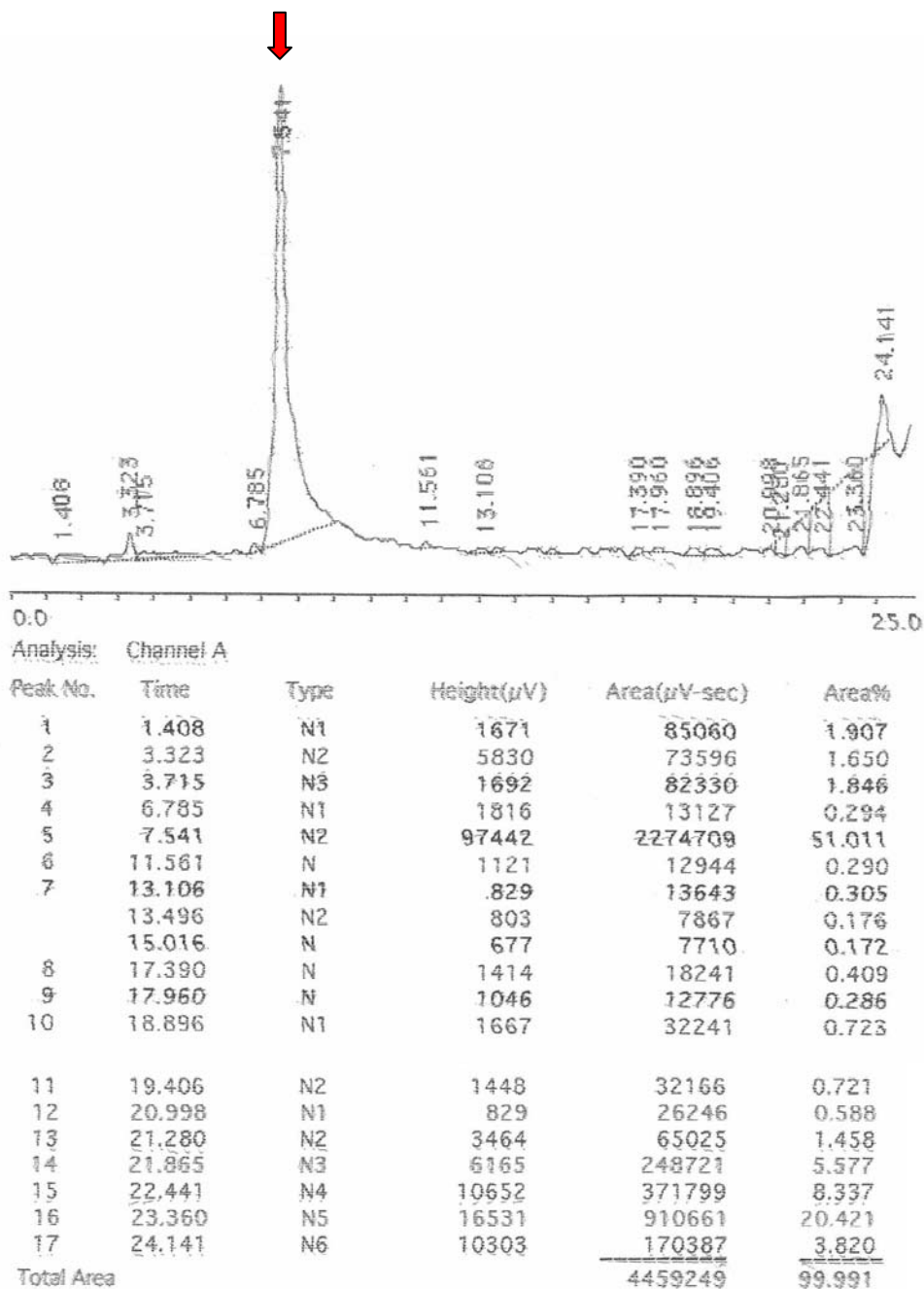


Figure D.6 **HPLC trace of compound 4.** Analytical HPLC trace of **4** fractionated on a Vydac C18 column (#218MS54) at 1 mL/min using a linear gradient from 5 – 25% acetonitrile/0.05% TFA over 20 min (detection at 220 nm). The peak corresponding to **4** is marked with an arrow.

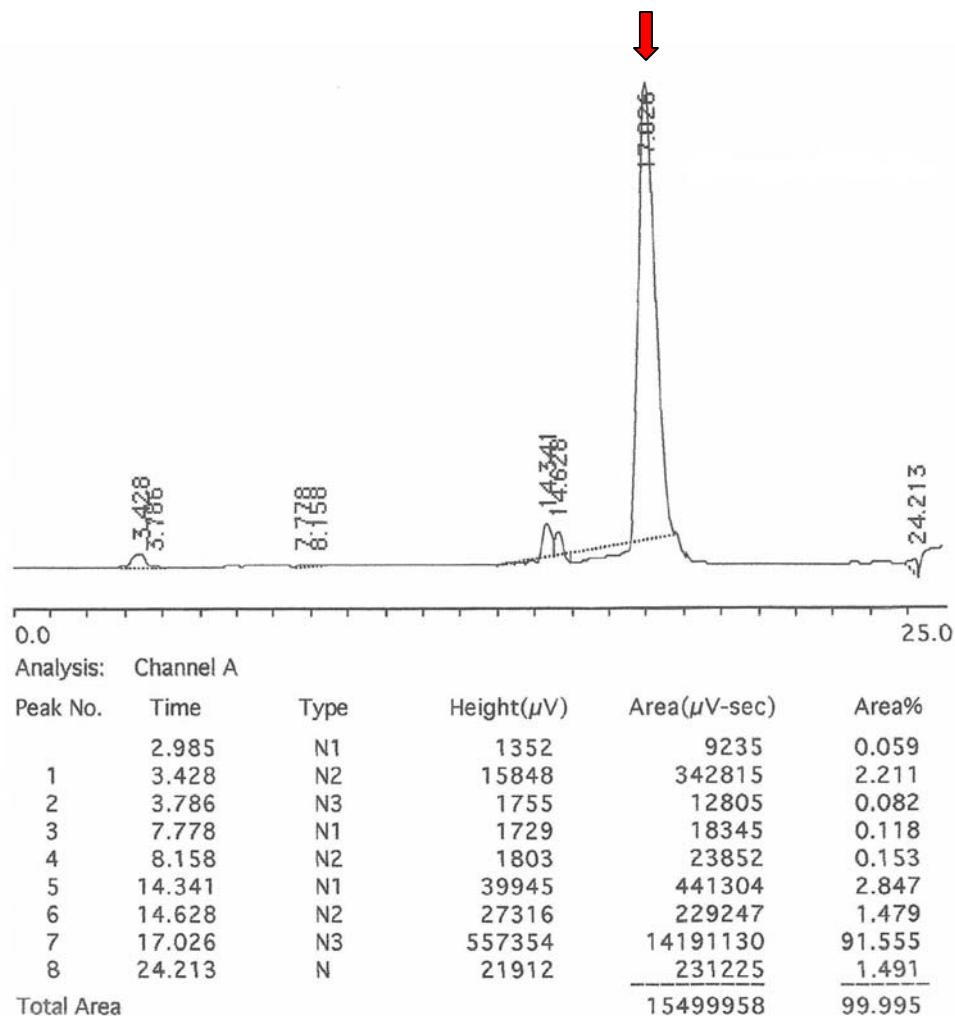


Figure D.7 **HPLC trace of compound 5**. Analytical HPLC trace of **5** fractionated on a Vydac C18 column (#218MS54) at 1 mL/min using a linear gradient from 5 – 25% acetonitrile/0.05% TFA over 20 min (detection at 220 nm). The peak corresponding to **5** is marked with an arrow.

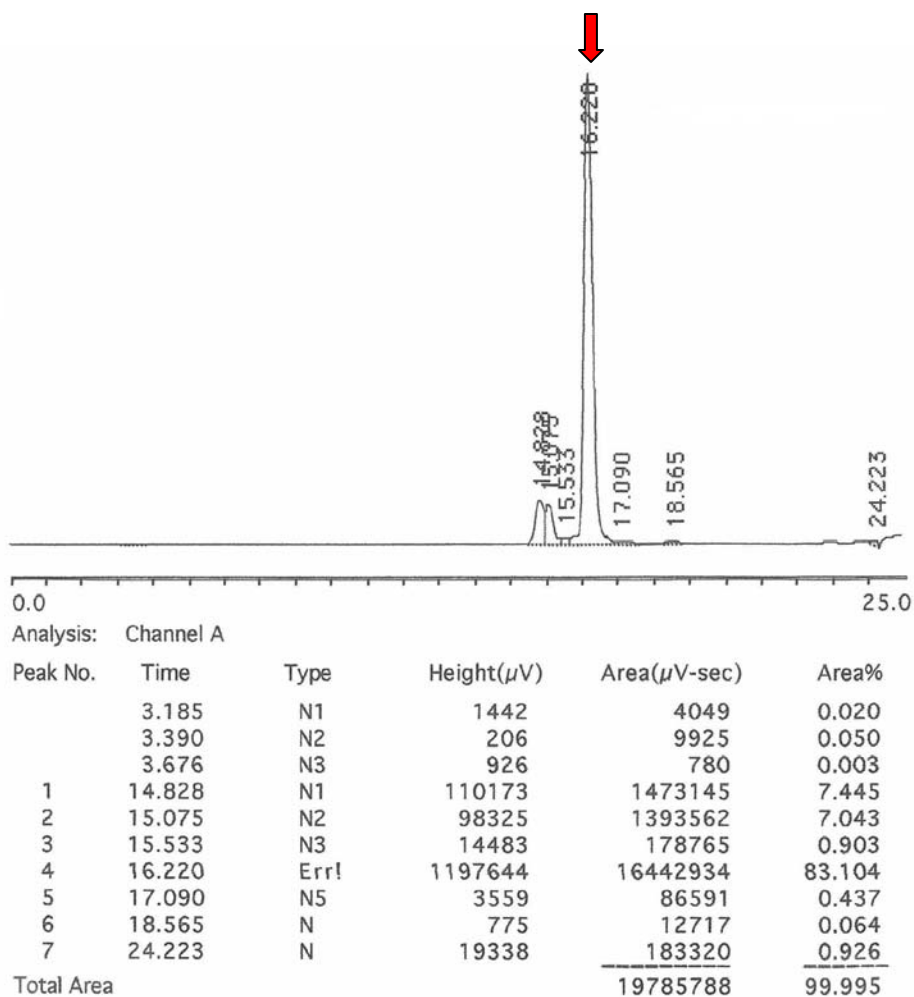


Figure D.8 **HPLC trace of compound 6.** Analytical HPLC trace of **6** fractionated on a Vydac C18 column (#218MS54) at 1 mL/min using a linear gradient from 5 – 25% acetonitrile/0.05% TFA over 20 min (detection at 220 nm). The peak corresponding to **6** is marked with an arrow.

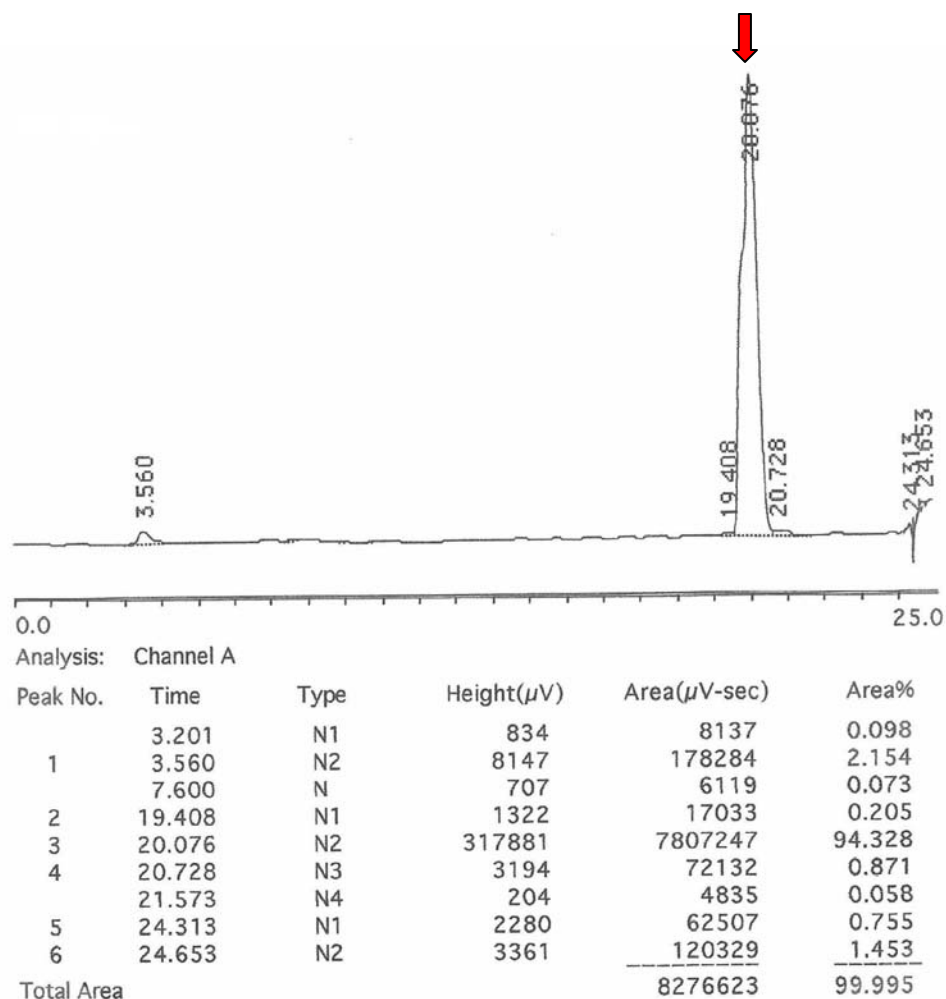


Figure D.9 **HPLC trace of compound 7**. Analytical HPLC trace of **7** fractionated on a Vydac C18 column (#218MS54) at 1 mL/min using a linear gradient from 5 – 25% acetonitrile/0.05% TFA over 20 min (detection at 220 nm). The peak corresponding to **7** is marked with an arrow.

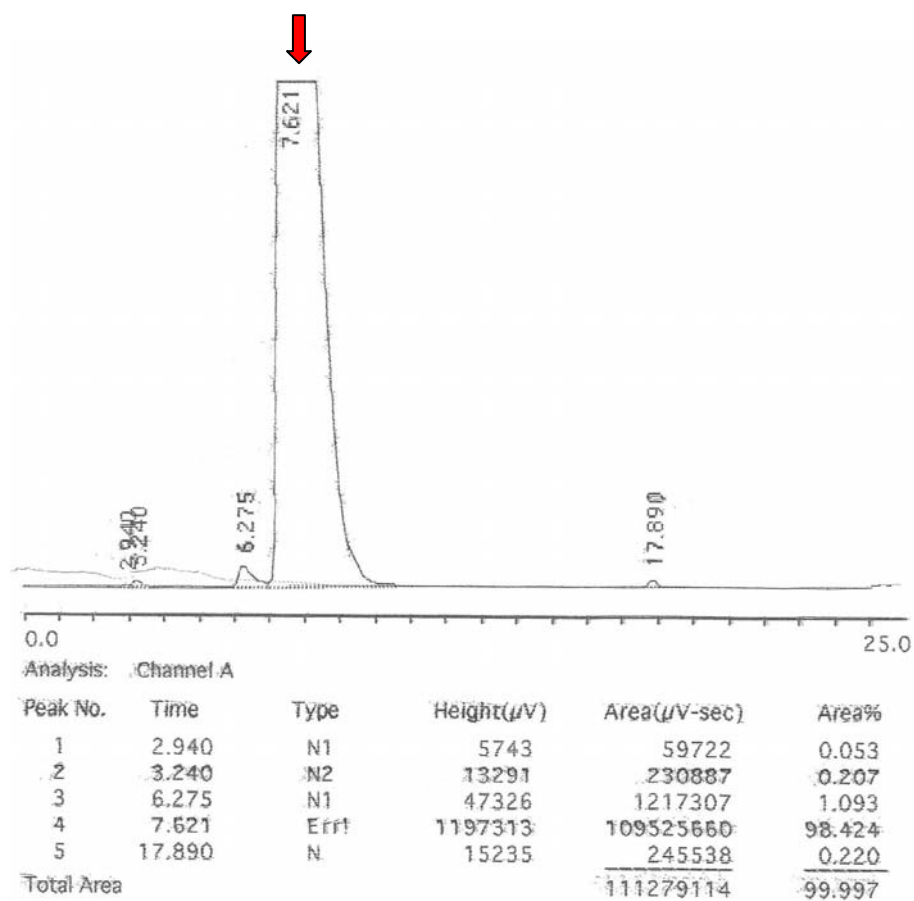


Figure D.10 **HPLC trace of compound 8**. Analytical HPLC trace of **8** fractionated on a Vydac C18 column (#218MS54) at 1 mL/min using a linear gradient from 5 – 25% acetonitrile/0.05% TFA over 20 min (detection at 220 nm). The peak corresponding to **8** is marked with an arrow.

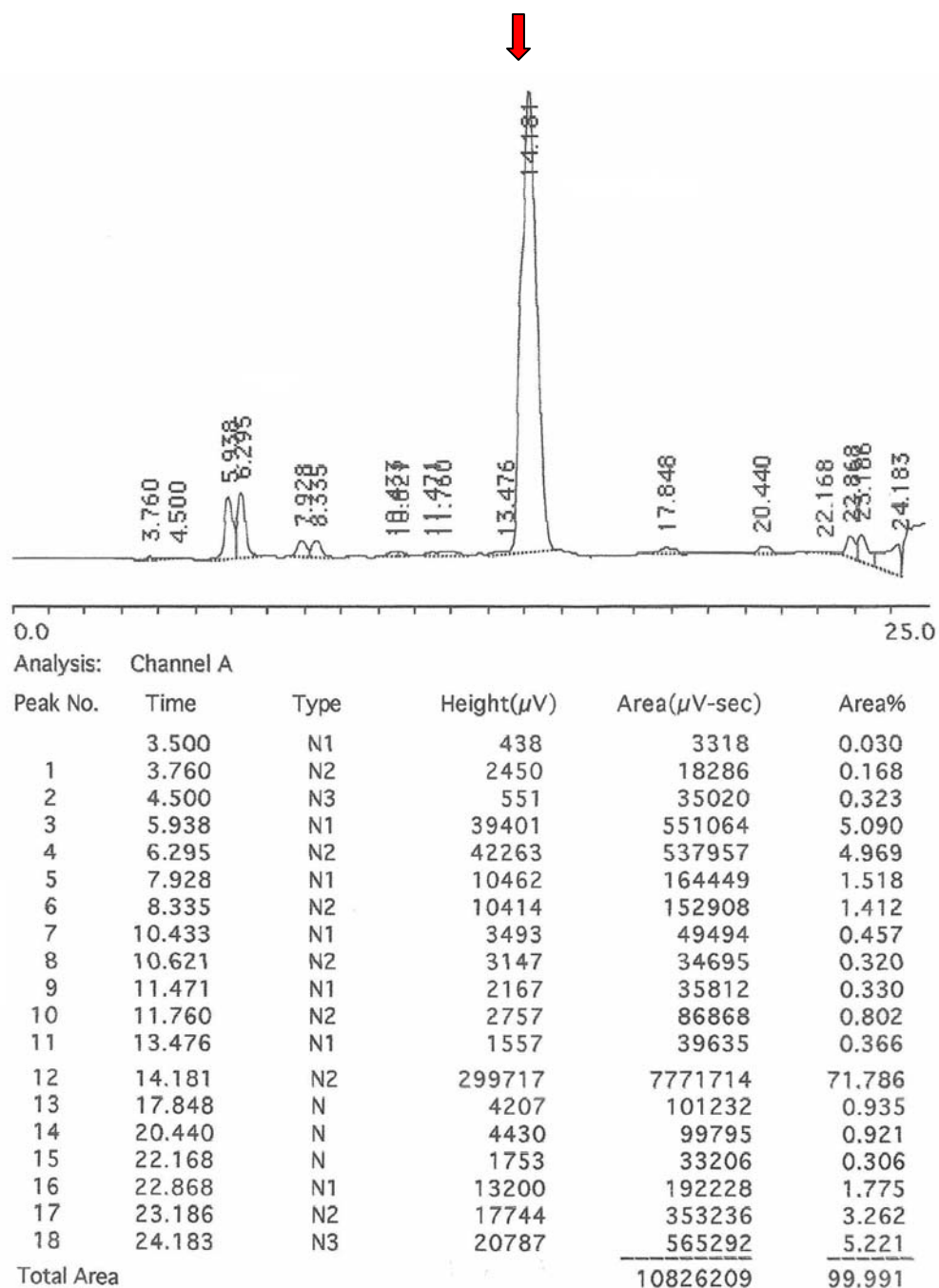


Figure D.11 **HPLC trace of compound 9**. Analytical HPLC trace of **9** fractionated on a Vydac C18 column (#218MS54) at 1 mL/min using a linear gradient from 5 – 25% acetonitrile/0.05% TFA over 20 min (detection at 220 nm). The peak corresponding to **9** is marked with an arrow.

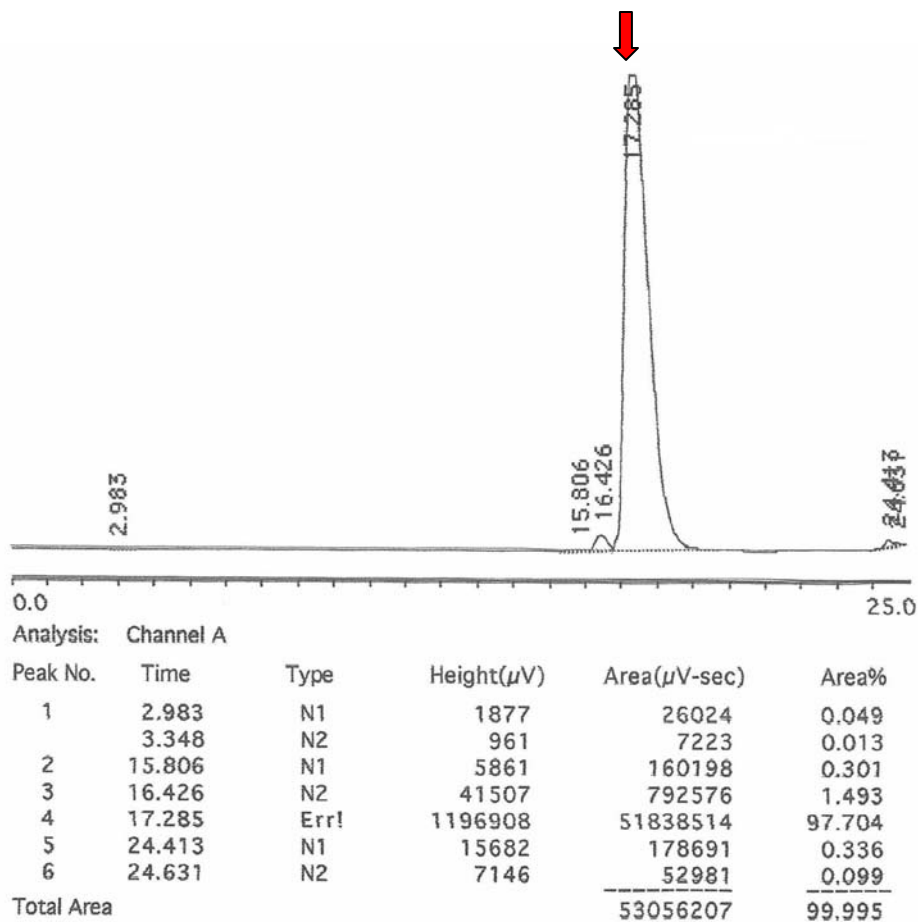


Figure D.12 **HPLC trace of compound 10.** Analytical HPLC trace of **10** fractionated on a Vydac C18 column (#218MS54) at 1 mL/min using a linear gradient from 5 – 25% acetonitrile/0.05% TFA over 20 min (detection at 220 nm). The peak corresponding to **10** is marked with an arrow.

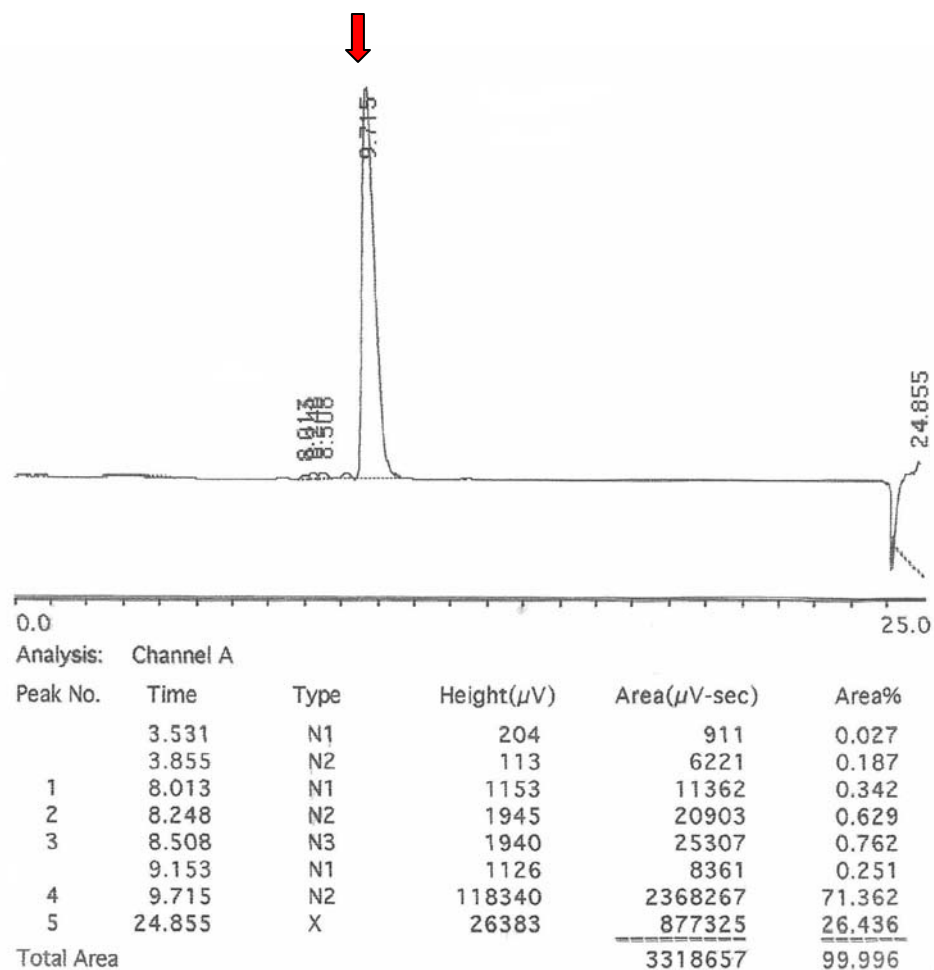


Figure D.13 **HPLC trace of compound 11.** Analytical HPLC trace of **11** fractionated on a Vydac C18 column (#218MS54) at 1 mL/min using a linear gradient from 5 – 25% acetonitrile/0.05% TFA over 20 min (detection at 280 nm). The peak corresponding to **11** is marked with an arrow.

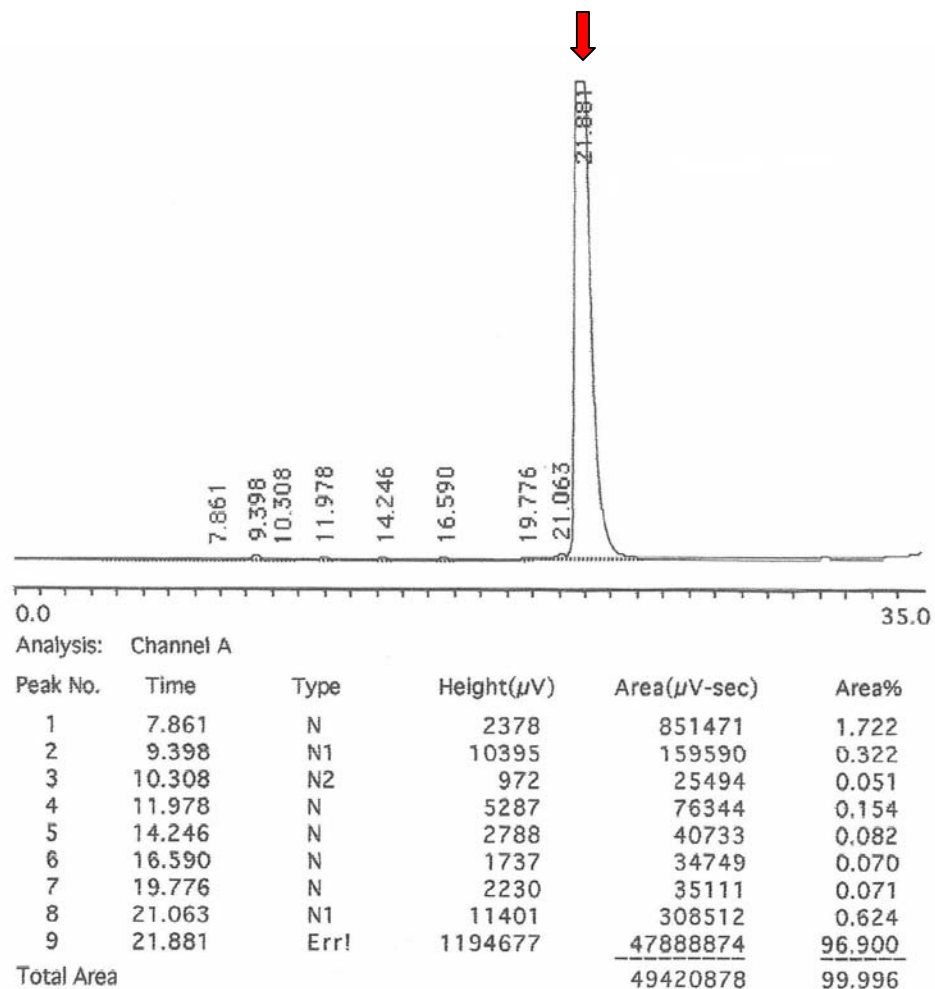


Figure D.14 **HPLC trace of compound 12.** Analytical HPLC trace of **12** fractionated on a Vydac C18 column (#218MS54) at 1 mL/min using a linear gradient from 5 – 35% acetonitrile/0.05% TFA over 30 min (detection at 220 nm). The peak corresponding to **12** is marked with an arrow.

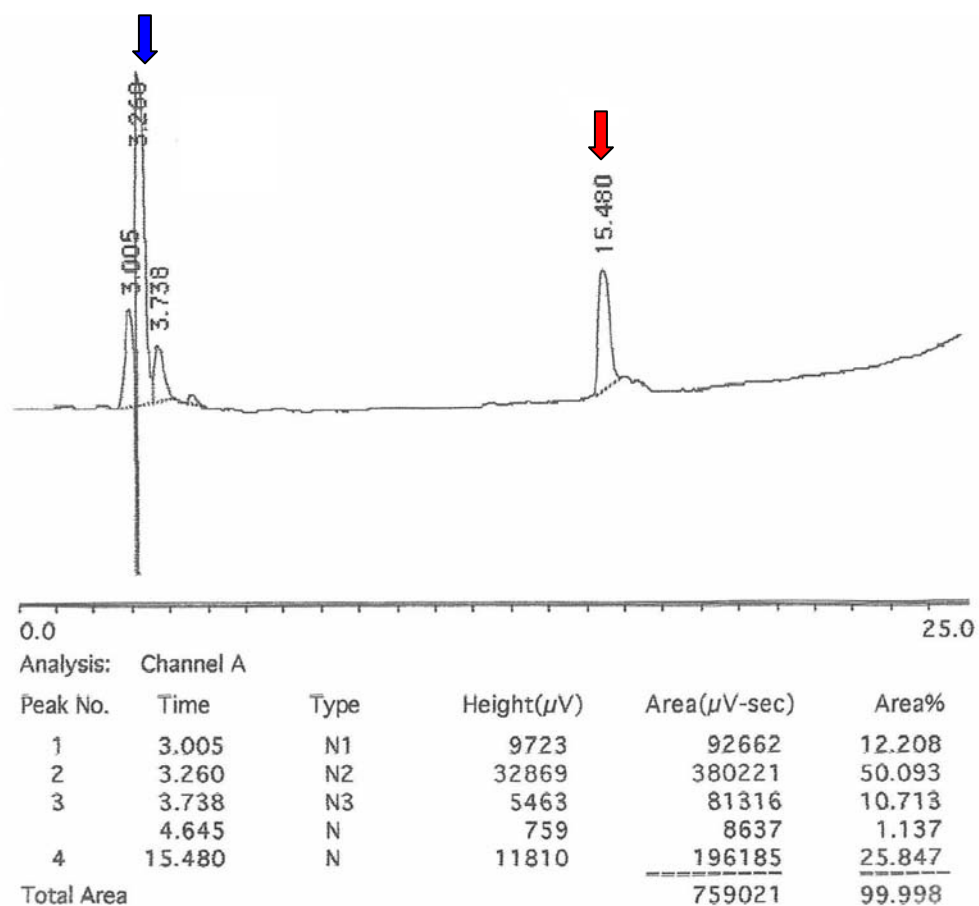


Figure D.15 **HPLC trace of ZL₃OH**. Analytical HPLC trace of ZL₃OH fractionated on a Vydac C18 column (#218MS54) at 1 mL/min using a linear gradient from 20 – 80% acetonitrile/0.05% TFA over 20 min (detection at 250 nm). The peak corresponding to ZL₃OH (red) and its solvent, DMSO, are marked with an arrow.

Appendix E: Mass Spectrometry Data for Synthetic Peptides

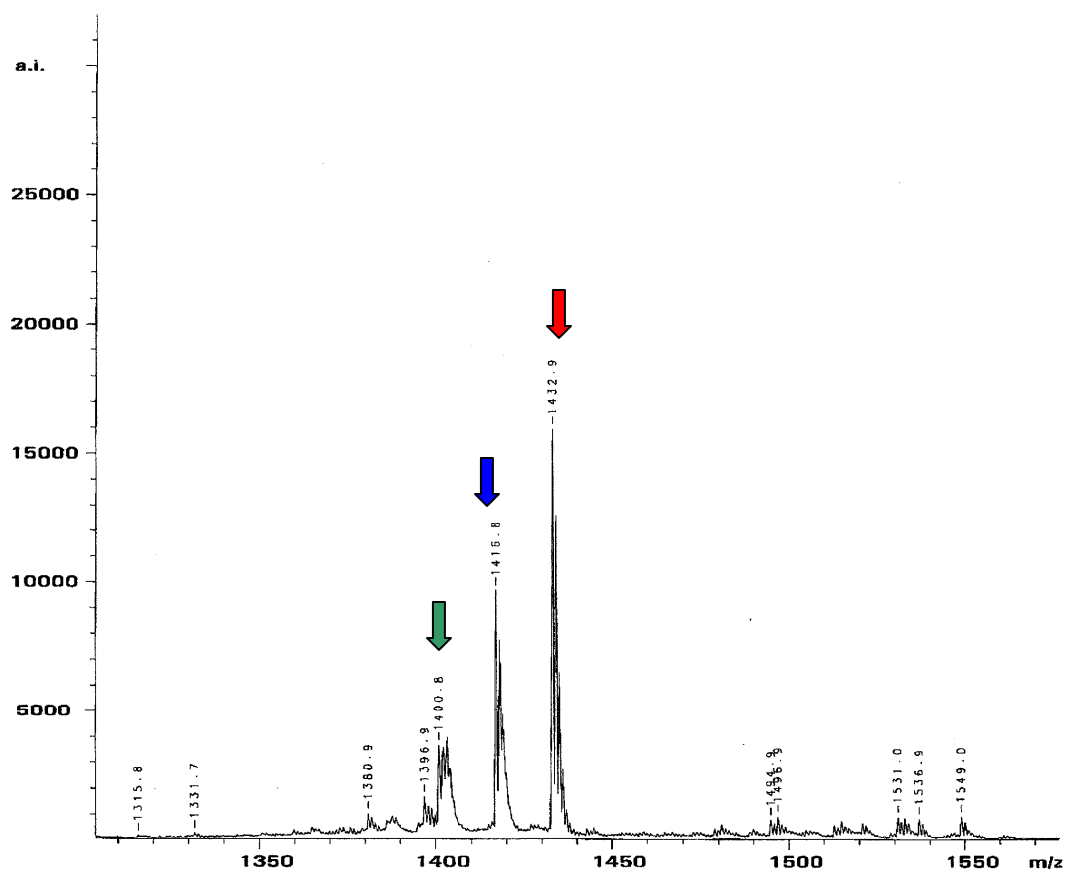


Figure E.1 MALDI mass spectrum of the fluorescent analog of compound 1. The $[M+H]^+$ (red), $[M+H-16]^+$ (blue), and $[M+H-32]^+$ (green) are indicated with arrows.

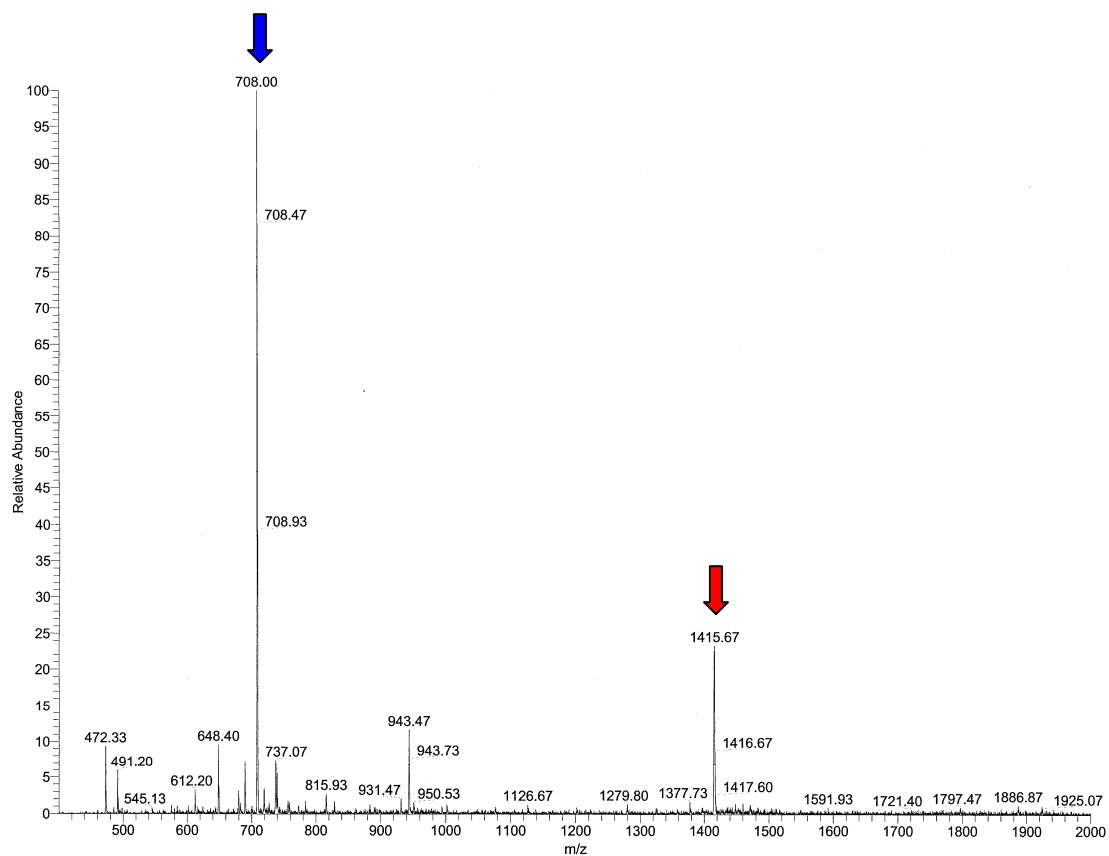


Figure E.2 **Positive mode electrospray ionization mass spectrum of the fluorescent analog of compound 2.** The $[M+H]^+$ (red) and $[M+H]^{2+}$ (blue) ions are indicated with an arrow.

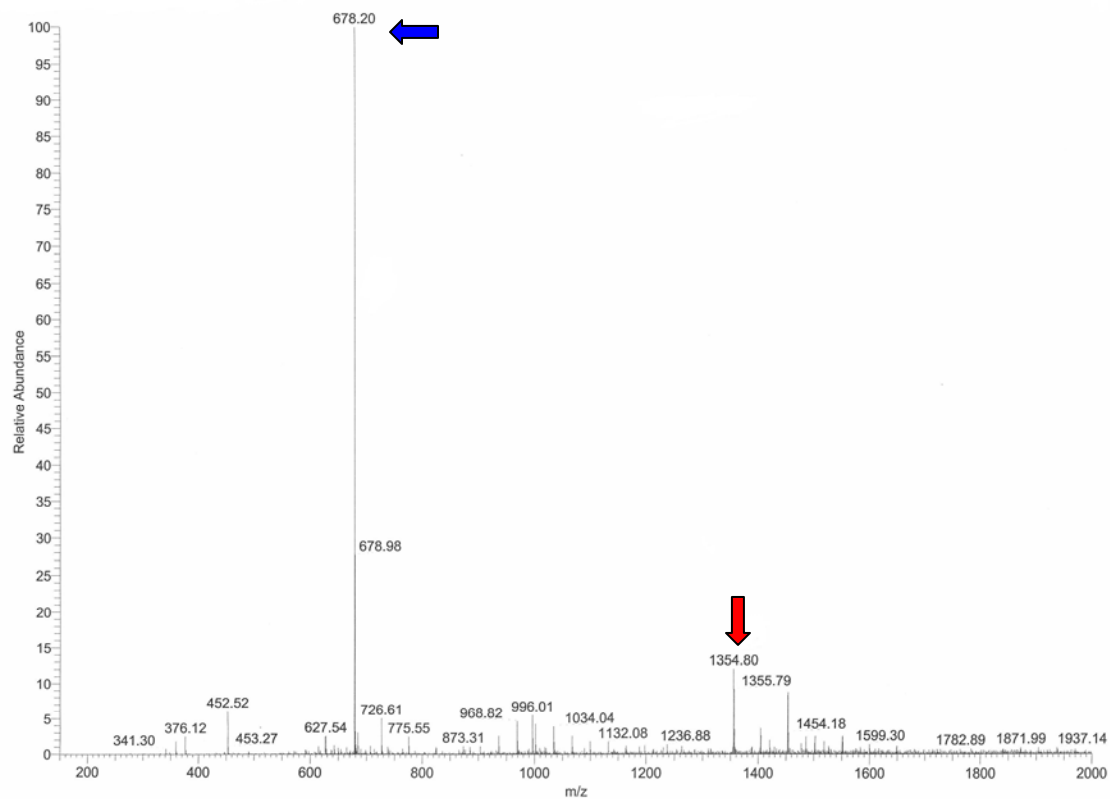


Figure E.3 Positive mode electrospray ionization mass spectrum of the non-fluorescent analog of compound 2. The $[M+H]^+$ (red) and $[M+H]^{2+}$ (blue) ions are indicated with an arrow.

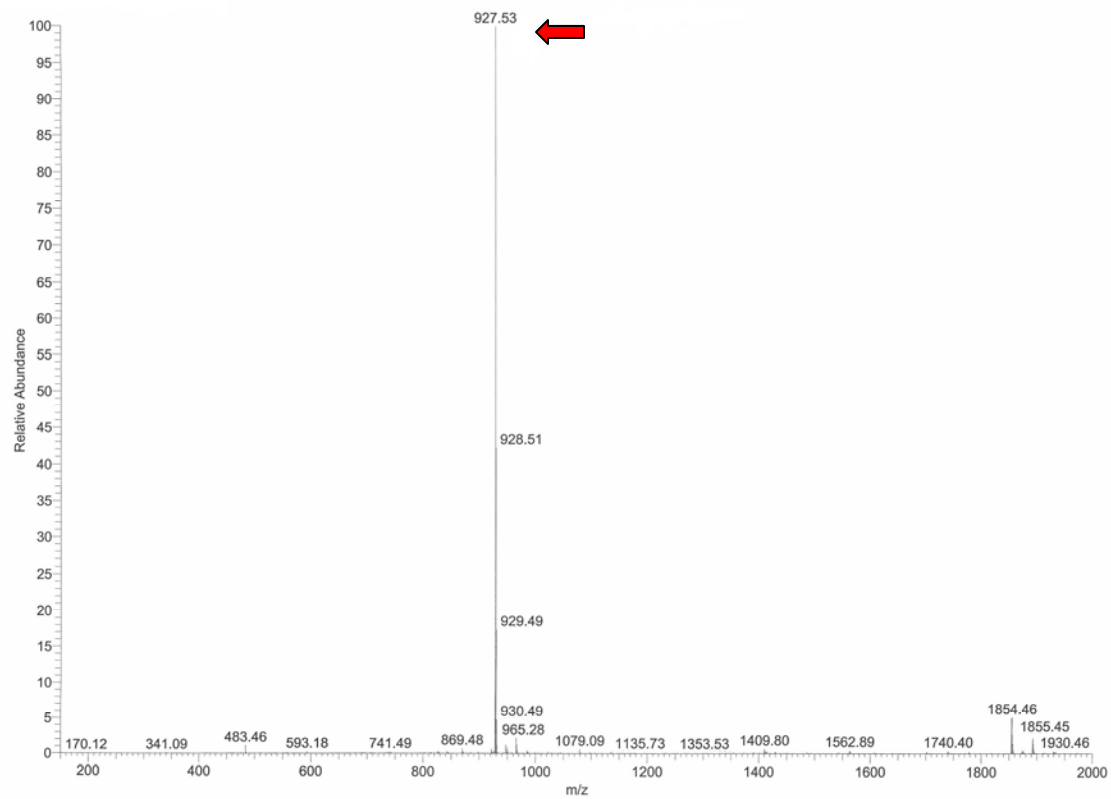


Figure E.4 **Positive mode electrospray ionization mass spectrum of compound 3.** The $[M+H]^+$ ion is indicated with an arrow.

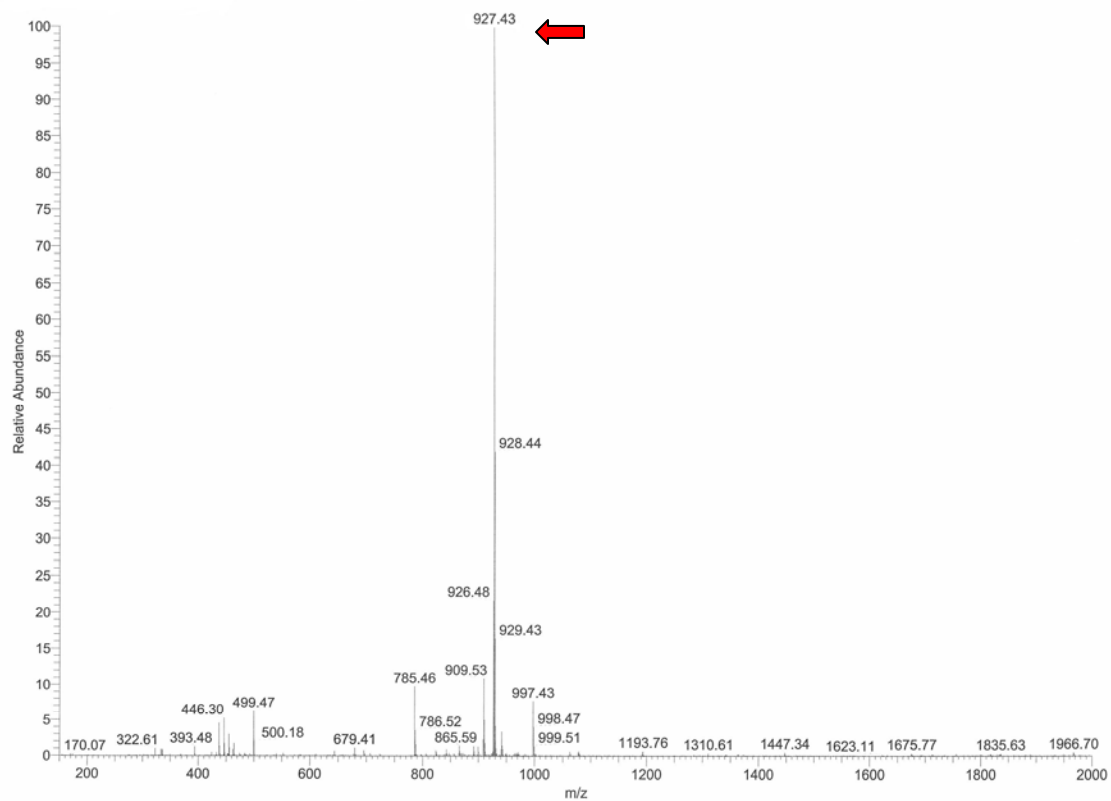


Figure E.5 Positive mode electrospray ionization mass spectrum of compound 4. The $[M+H]^+$ ion is indicated with an arrow.

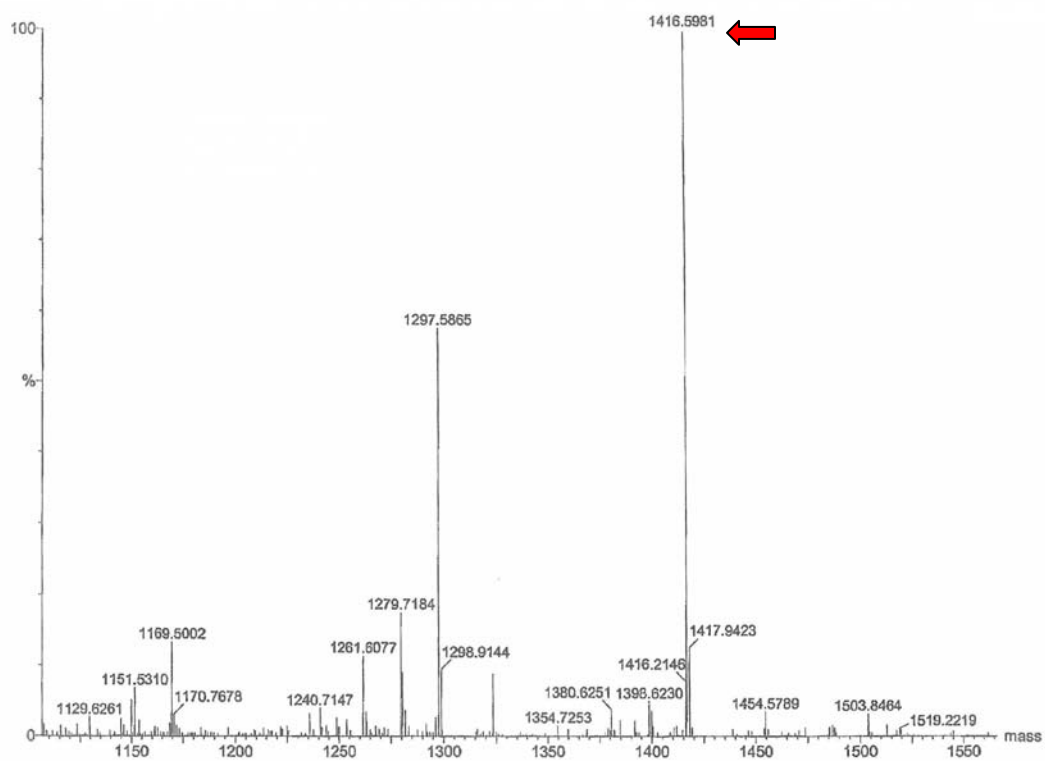


Figure E.6 **Positive mode electrospray ionization mass spectrum of compound 5.** The $[M+H]^+$ ion is indicated with an arrow.

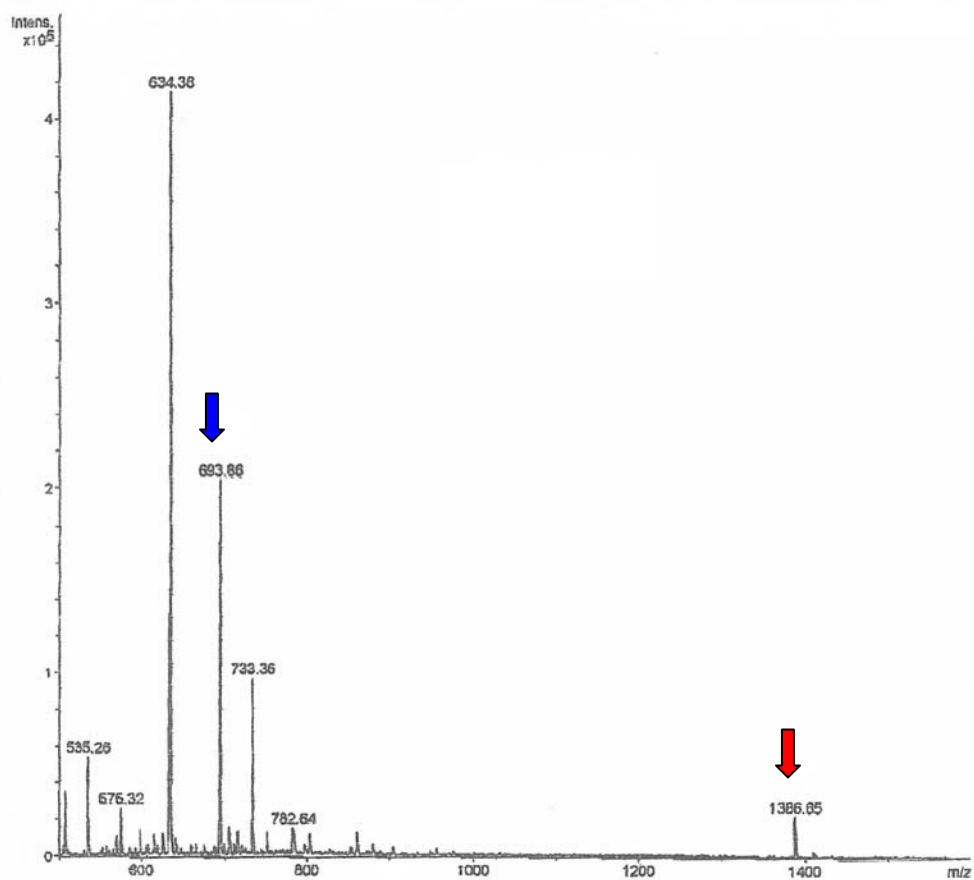


Figure E.7 **Positive mode electrospray ionization mass spectrum of compound 6.** The $[M+H]^+$ (red) and $[M+H]^{2+}$ (blue) ions are indicated with an arrow.

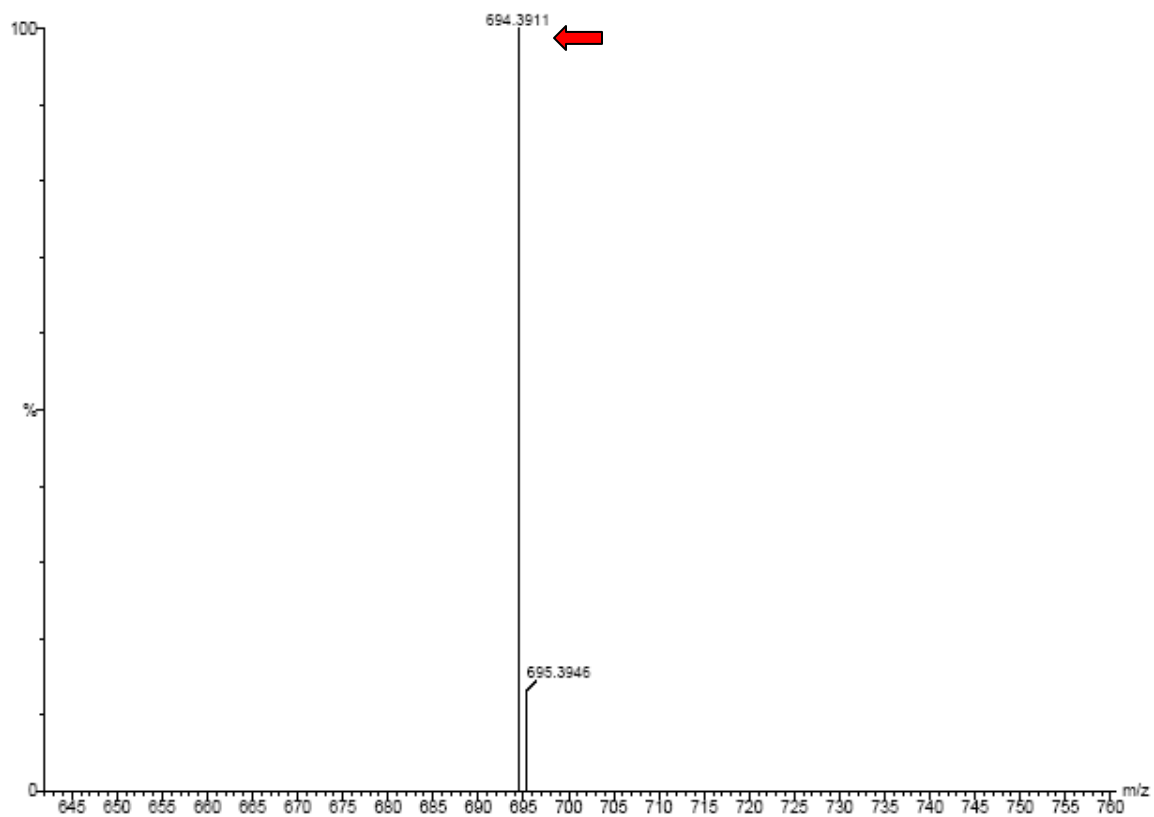


Figure E.8 **Positive mode electrospray ionization mass spectrum of compound 7.** The $[M+H]^+$ ion is indicated with an arrow.

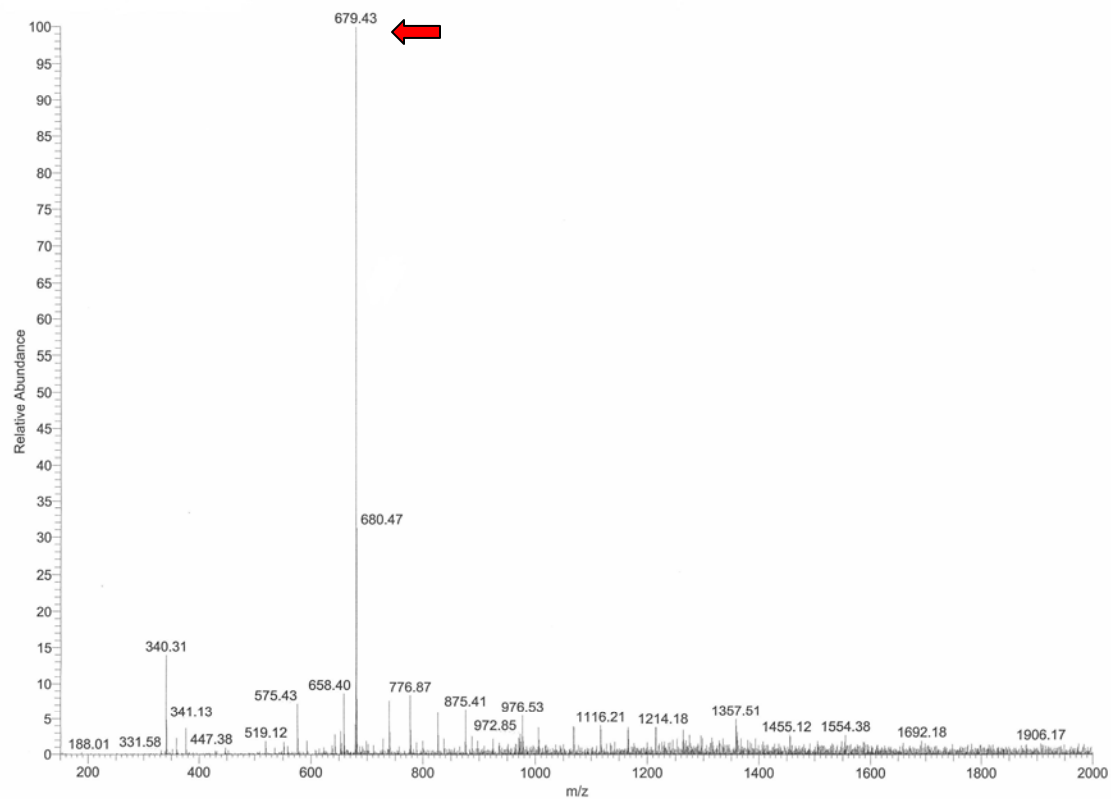


Figure E.9 Positive mode electrospray ionization mass spectrum of compound 8. The $[M+H]^+$ ion is indicated with an arrow.

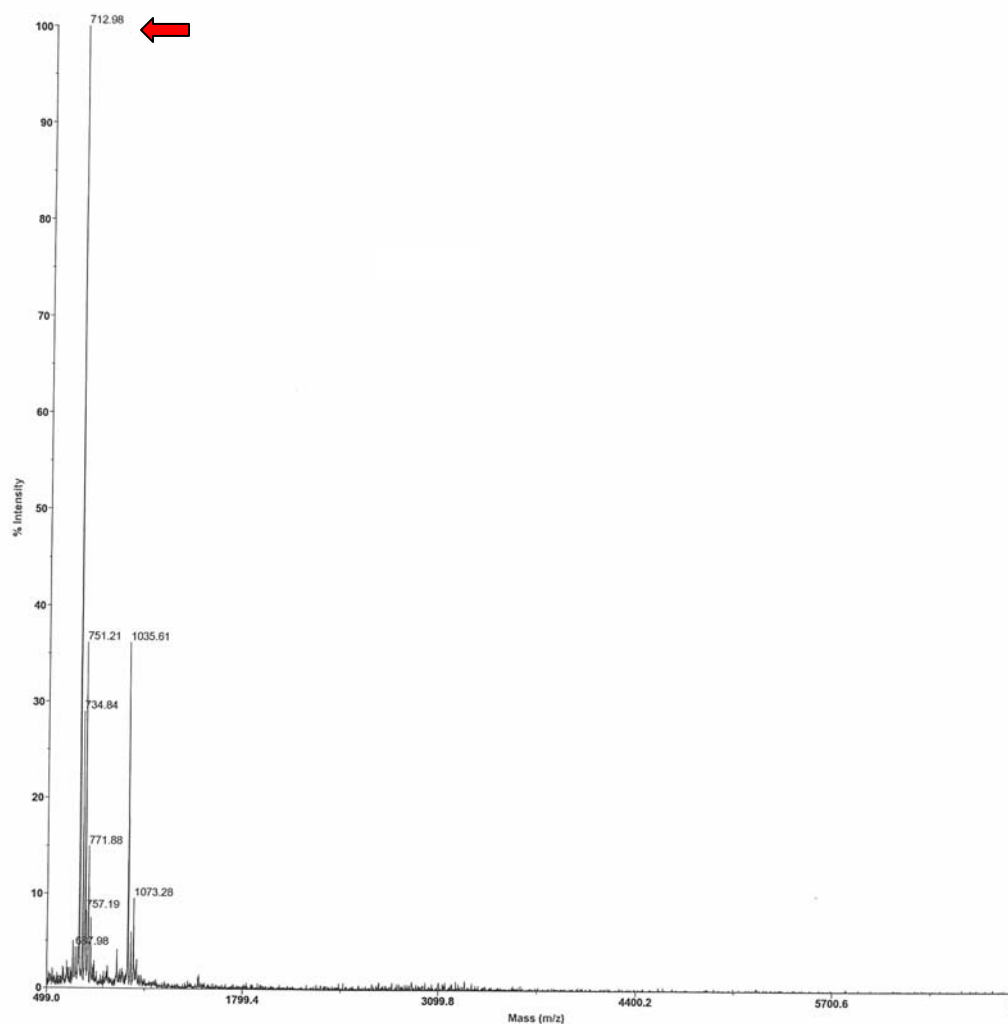


Figure E.10 **Positive mode electrospray ionization mass spectrum of compound 9.**
The $[M+H]^+$ ion is indicated with an arrow.

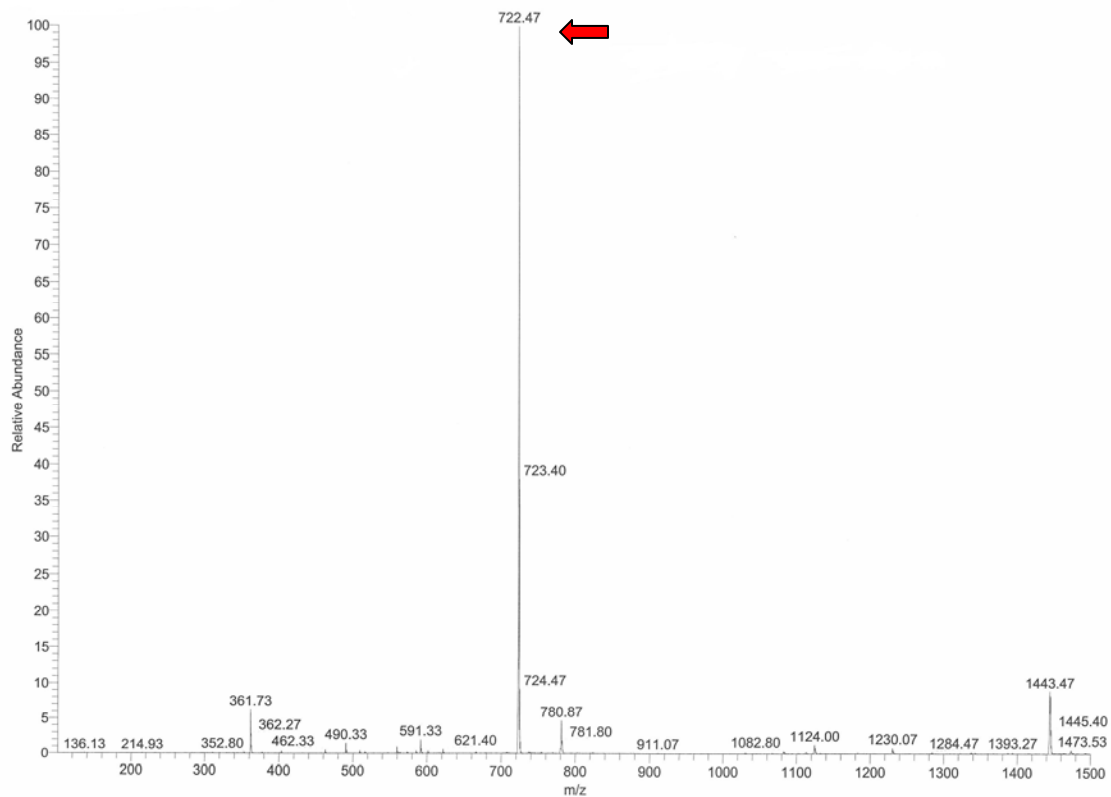


Figure E.11 **Positive mode electrospray ionization mass spectrum of compound 10.** The $[M+H]^+$ ion is indicated with an arrow.

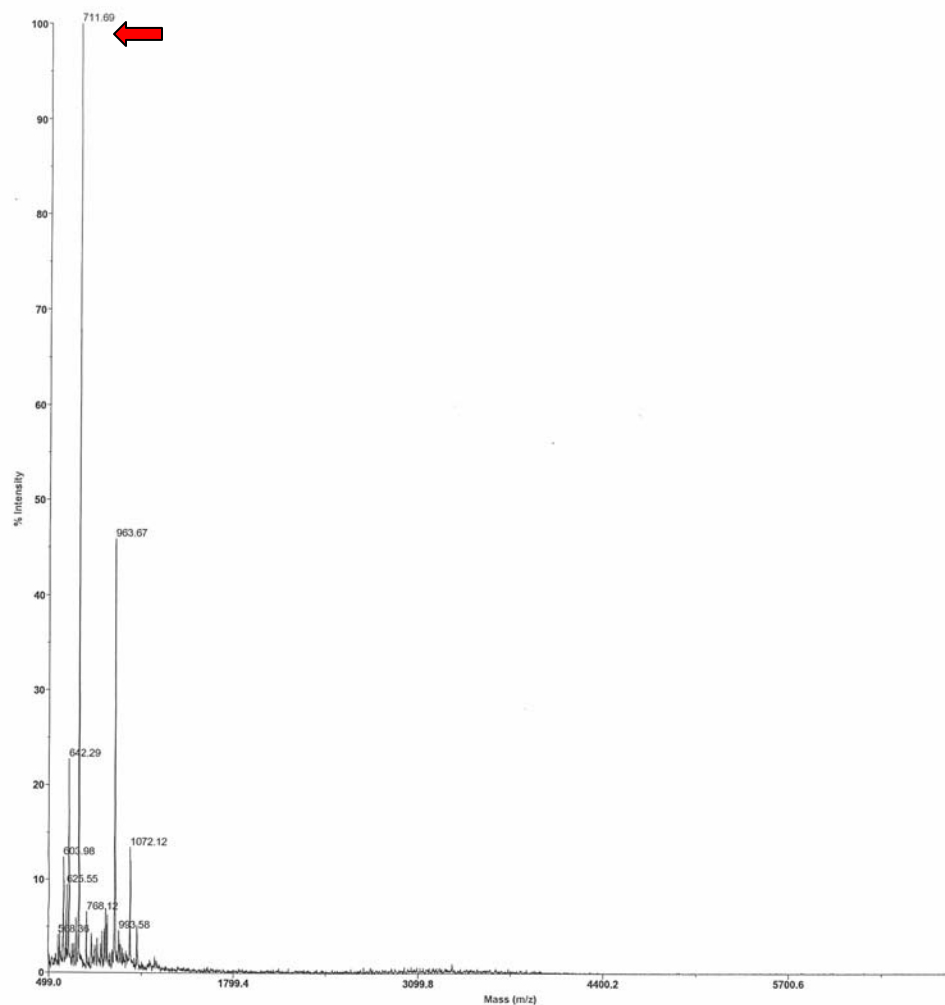


Figure E.12 **Positive mode electrospray ionization mass spectrum of compound 11.** The $[M+H]^+$ ion is indicated with an arrow.

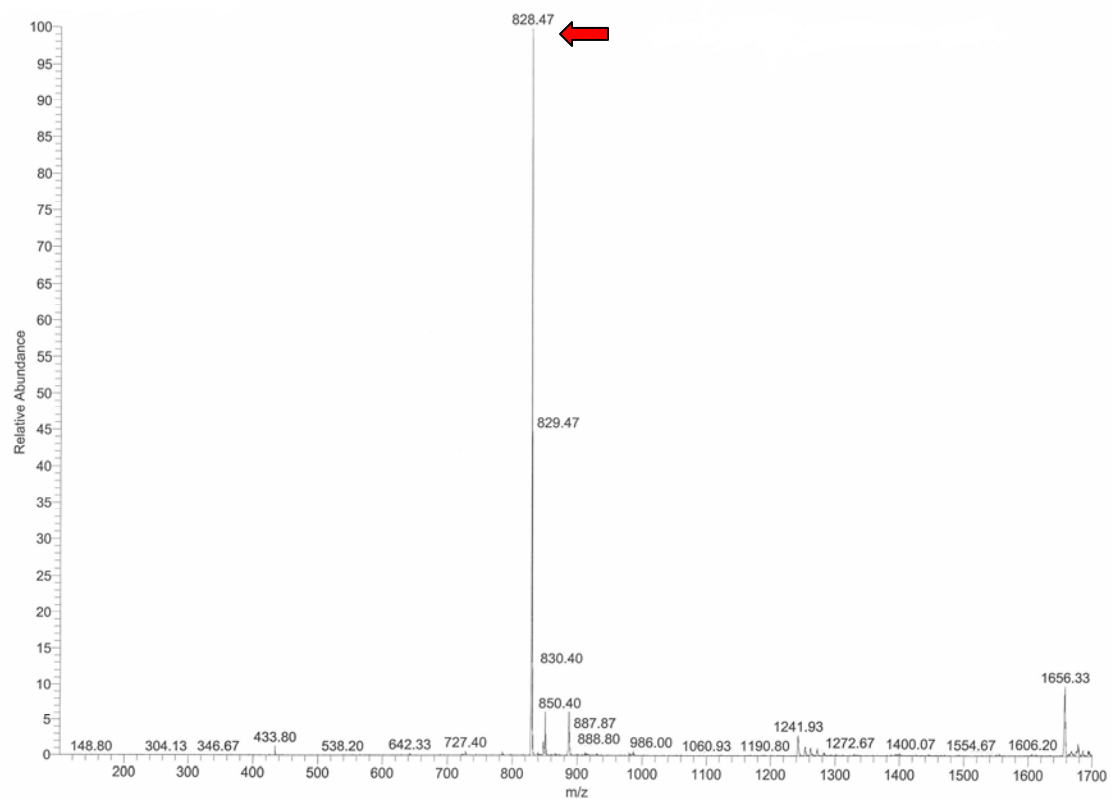


Figure E.13 **Positive mode electrospray ionization mass spectrum of compound 12.** The $[M+H]^+$ ion is indicated with an arrow.

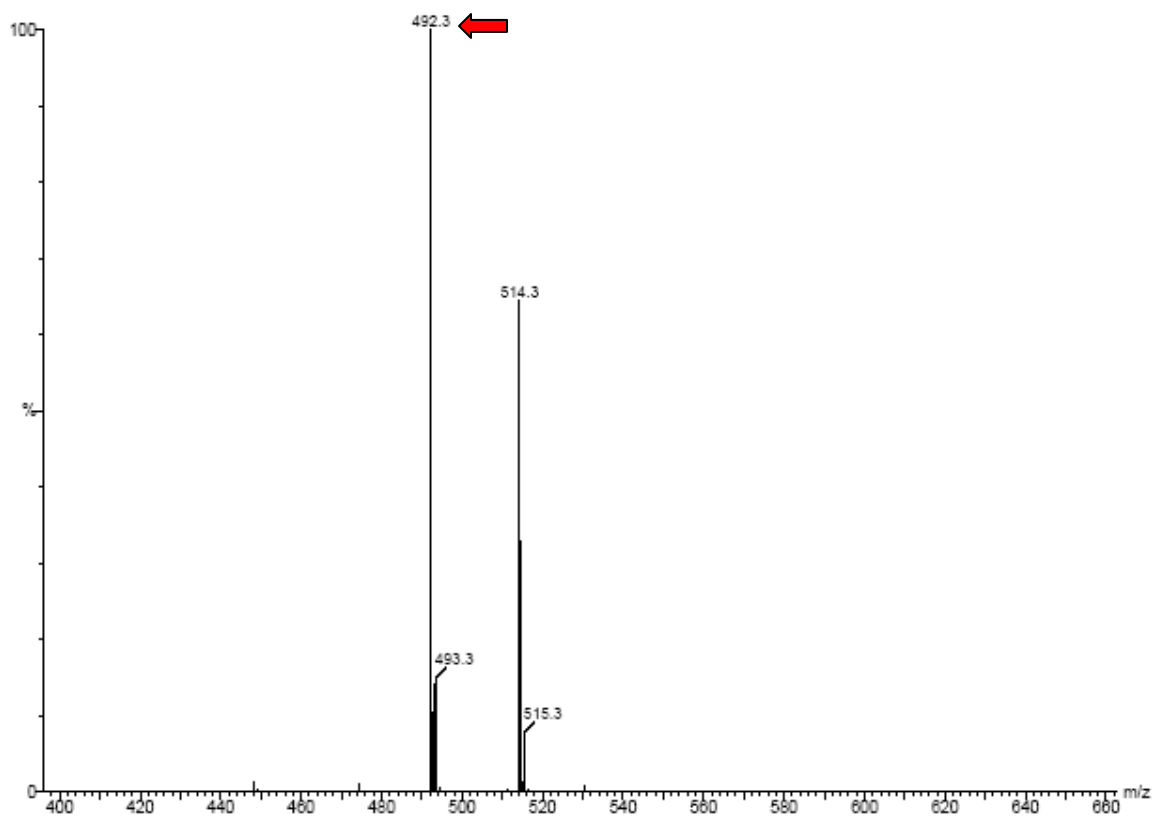


Figure E.14 **Positive mode electrospray ionization mass spectrum of ZL₃OH.** The $[M+H]^+$ ion is indicated with an arrow.

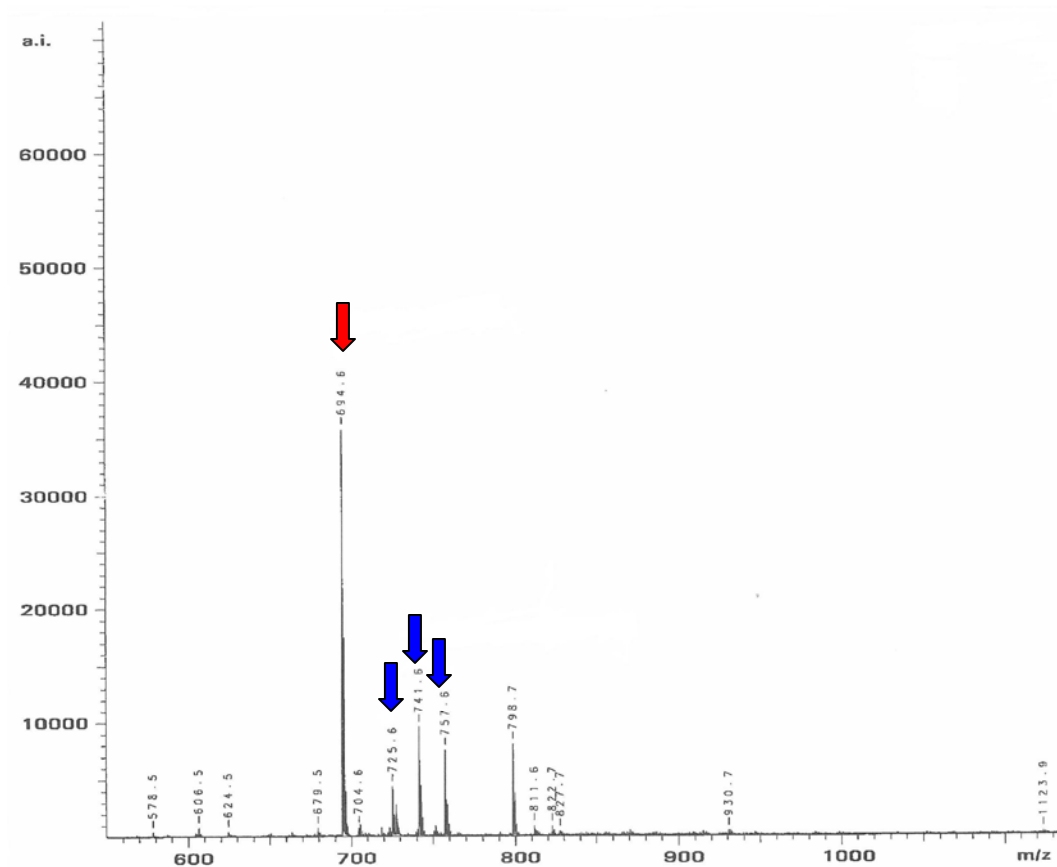
Appendix F: Mass Spectrometry Data for Peptide Degradation by Lon

Figure F.1 *S. Typhimurium* Lon degradation of the fluorescent analog of **1**. MALDI mass spectrum of 200 nM *S. Typhimurium* Lon degradation of 100 μ M **1** (fluorescent analog) in the presence of 1 mM ATP. The $[M+H]^+$, $[M+H-16]^+$, and $[M+H-32]^+$ ions of the N-terminal product (blue) and $[M+H]^+$ ion of the C-terminal product (red) are indicated with arrows.

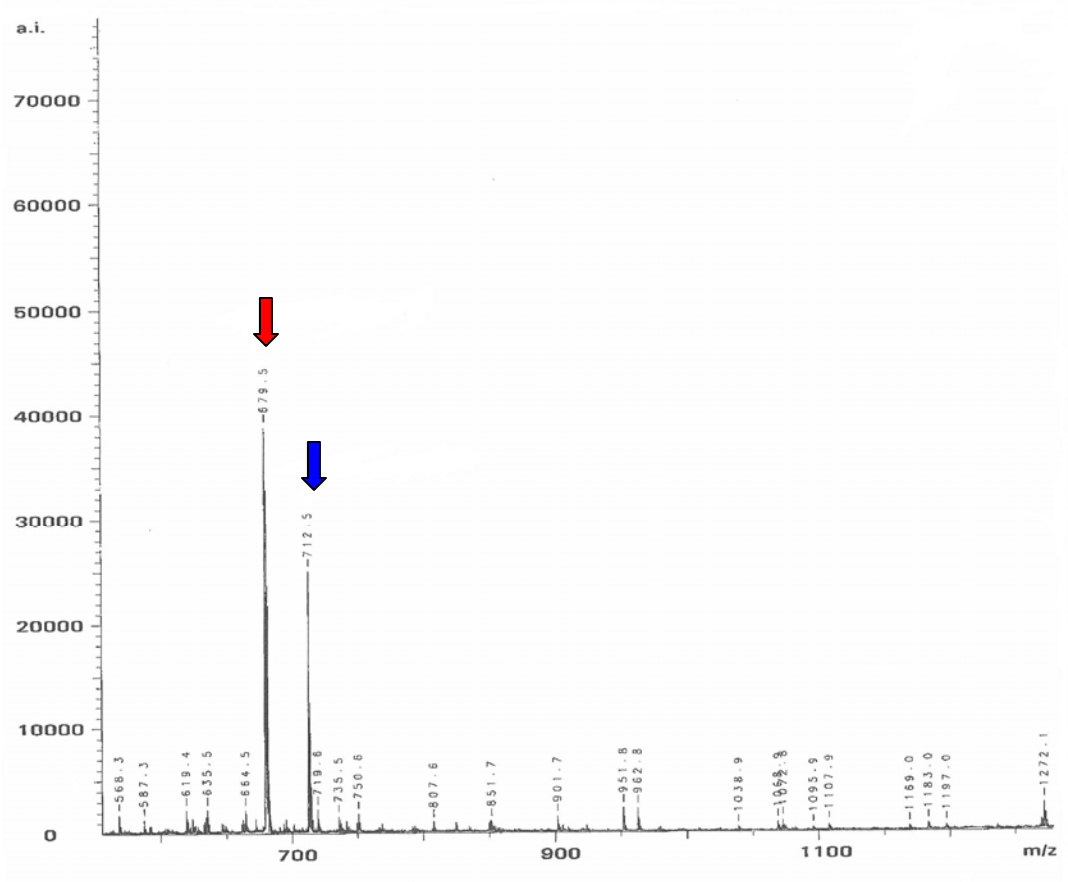


Figure F.2 *S. Typhimurium* Lon degradation of the non-fluorescent analog of **1**. MALDI mass spectrum of 200 nM *S. Typhimurium* Lon degradation of 100 μM **1** (non-fluorescent analog) in the presence of 1 mM ATP. The $[\text{M}+\text{H}]^+$ ion of the N-terminal (blue) and C-terminal (red) products are indicated with arrows.

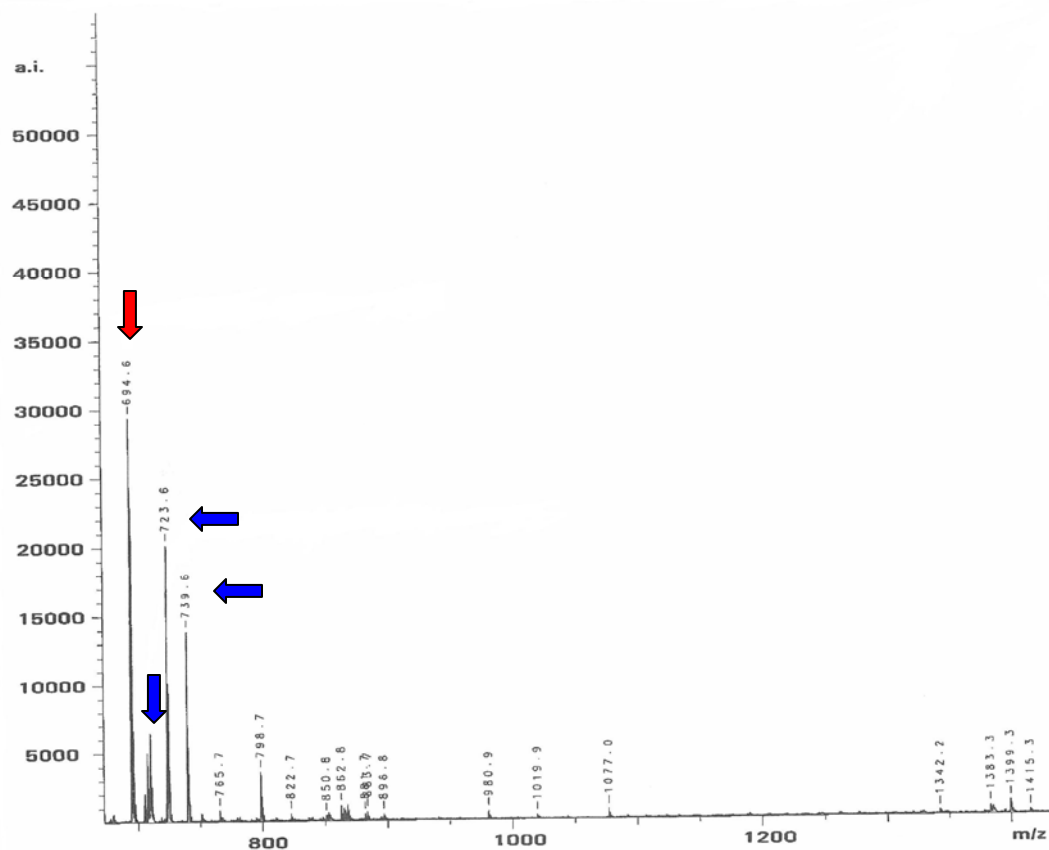


Figure F.3 *S. Typhimurium* Lon degradation of the fluorescent analog of **2**. MALDI mass spectrum of 200 nM *S. Typhimurium* Lon degradation of 100 μ M **2** (fluorescent analog) in the presence of 1 mM ATP. The $[M+H]^+$, $[M+H-16]^+$, and $[M+H-32]^+$ ions of the N-terminal product (blue) and $[M+H]^+$ ion of the C-terminal product (red) are indicated with arrows.

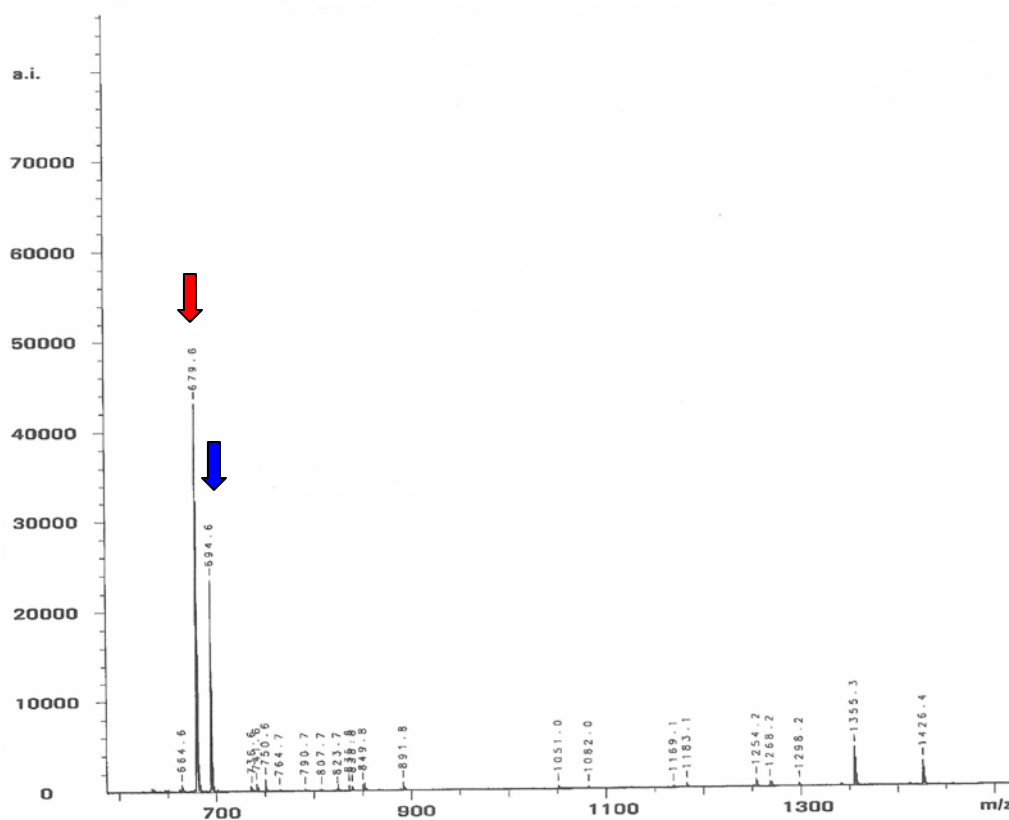


Figure F.4 *S. Typhimurium* Lon degradation of the non-fluorescent analog of **2**. MALDI mass spectrum of 200 nM *S. Typhimurium* Lon degradation of 100 μ M **2** (non-fluorescent analog) in the presence of 1 mM ATP. The $[M+H]^+$ ion of the N-terminal (blue) and C-terminal (red) products are indicated with arrows.

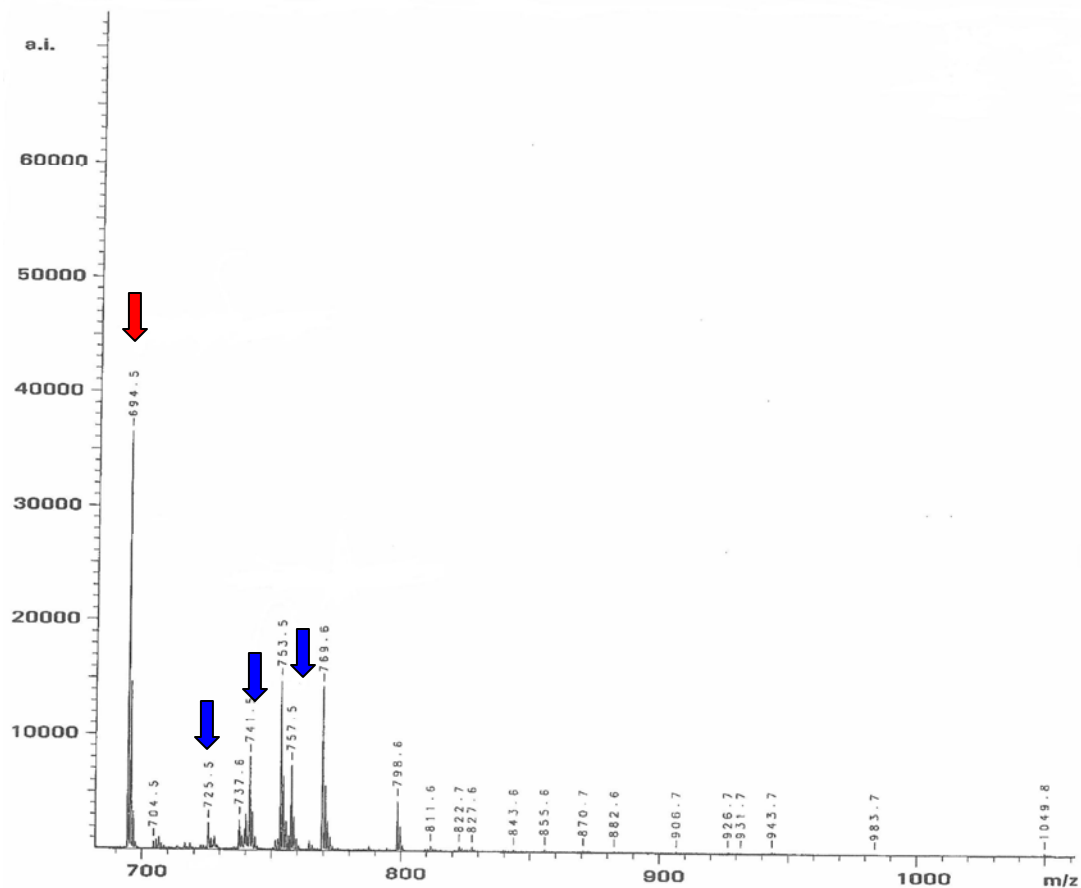


Figure F.5 **Human Lon degradation of the fluorescent analog of 1.** MALDI mass spectrum of 900 nM human Lon degradation of 100 μM **1** (fluorescent analog) in the presence of 1 mM ATP. The $[\text{M}+\text{H}]^+$, $[\text{M}+\text{H}-16]^+$, and $[\text{M}+\text{H}-32]^+$ ions of the N-terminal product (blue) and $[\text{M}+\text{H}]^+$ ion of the C-terminal product (red) are indicated with arrows.

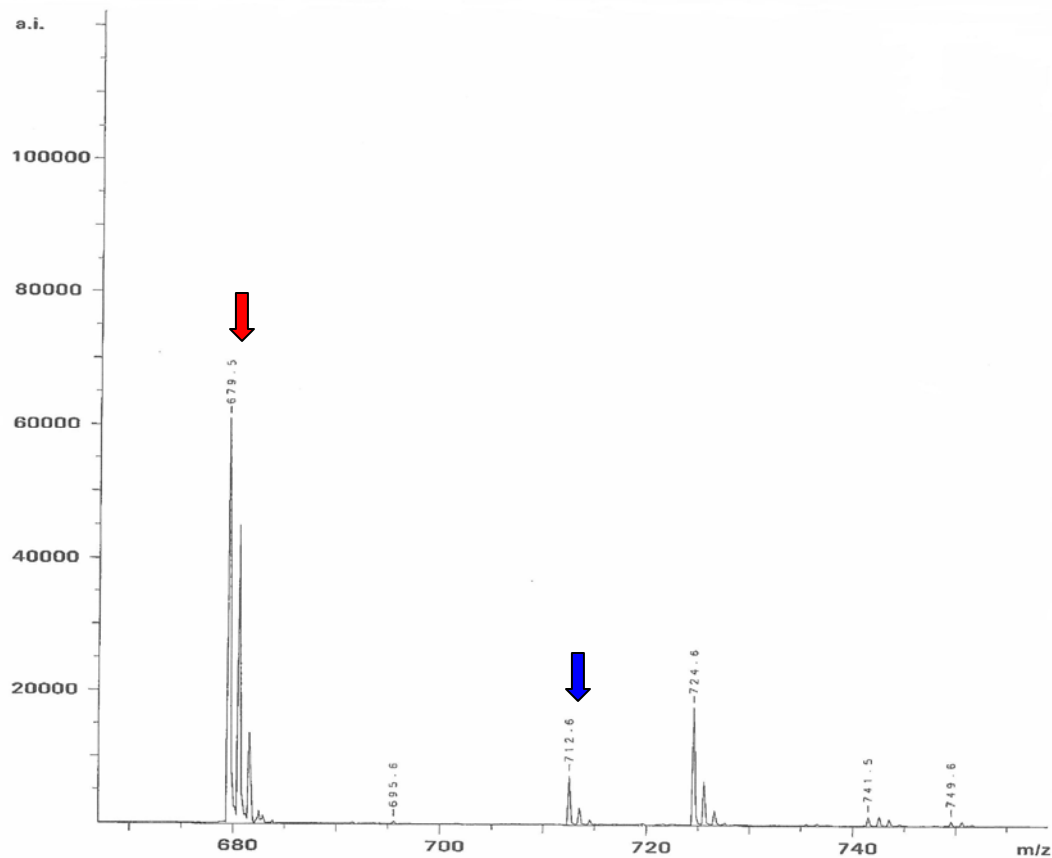


Figure F.6 **Human Lon degradation of the non-fluorescent analog of 1.** MALDI mass spectrum of 900 nM human Lon degradation of 100 μM **1** (non-fluorescent analog) in the presence of 1 mM ATP. The $[\text{M}+\text{H}]^+$ ion of the N-terminal (blue) and C-terminal (red) products are indicated with arrows.

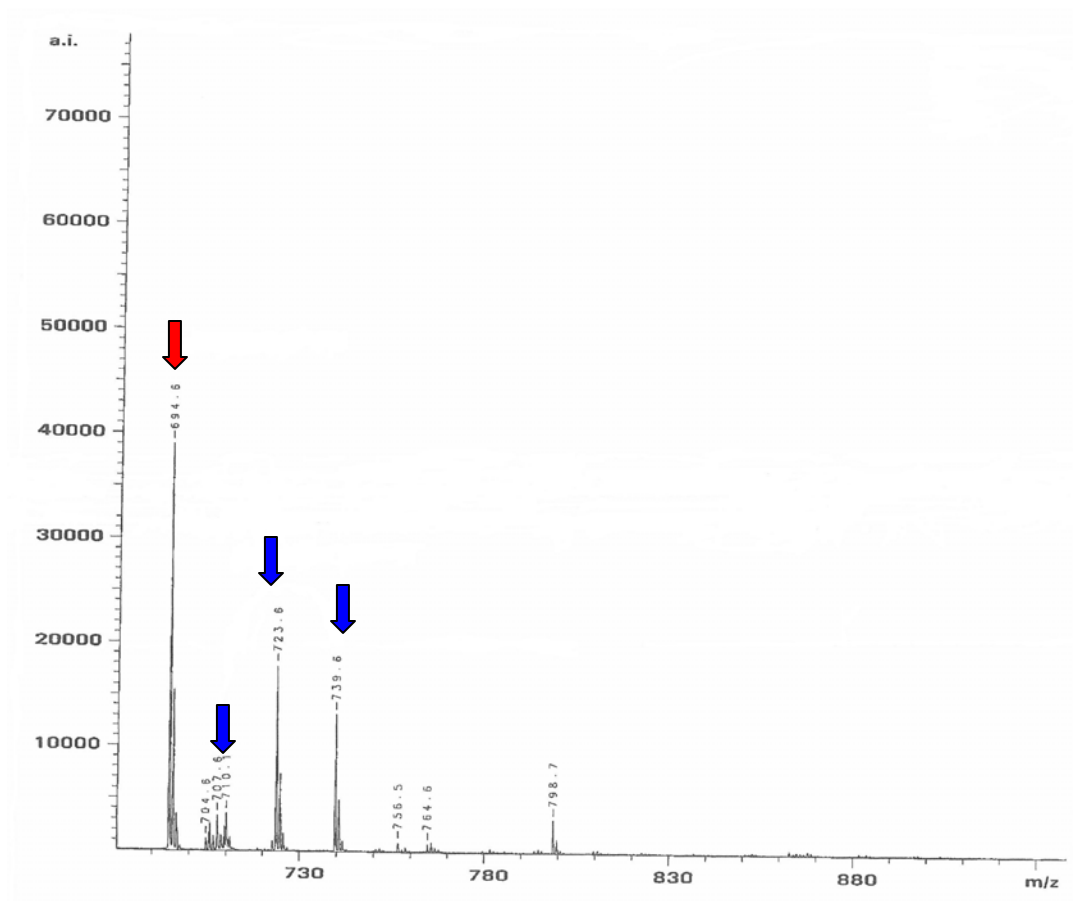


Figure F.7 **Human Lon degradation of the fluorescent analog of 2.** MALDI mass spectrum of 900 nM human Lon degradation of 100 μM **2** (fluorescent analog) in the presence of 1 mM ATP. The $[\text{M}+\text{H}]^+$, $[\text{M}+\text{H}-16]^+$, and $[\text{M}+\text{H}-32]^+$ ions of the N-terminal product (blue) and $[\text{M}+\text{H}]^+$ ion of the C-terminal product (red) are indicated with arrows.

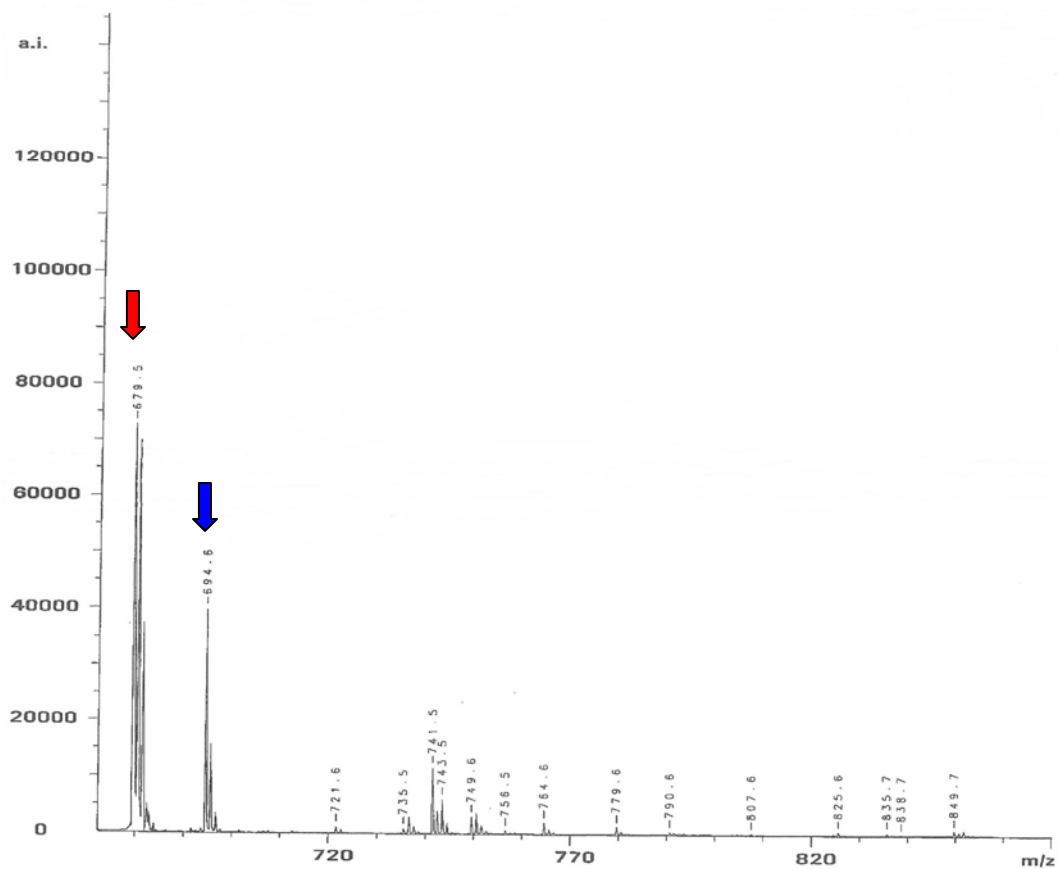


Figure F.8 **Human Lon degradation of the non-fluorescent analog of 2.** MALDI mass spectrum of 900 nM human Lon degradation of 100 μM **2** (non-fluorescent analog) in the presence of 1 mM ATP. The $[\text{M}+\text{H}]^+$ ion of the N-terminal (blue) and C-terminal (red) products are indicated with arrows.

Appendix G: TNBSA Assay

Peptides without tyrosine, tryptophan, or cysteine residues can be quantified using 2,4,6-trinitrobenzene sulfonic acid (TNBSA) to spectroscopically determine the concentration of free amines. This assay will not work correctly if the peptide contains lysine residues, as they may also react with TNBSA, in addition to the N-terminal amine. The amino acid L-phenylalanine ($\text{mw} = 165.19 \text{ g/mol}$, $\epsilon_{220} = 257 \text{ cm}^{-1} \text{ M}^{-1}$) is used as a standard as its concentration can be determined by its absorption at 220 nm. Reactions containing 500 μL L-phenylalanine standard (12, 24, 48, 72, 96, and 120 μM) or unknown and 250 μL TNBSA solution (0.01% TNBSA, 100 mM NaHCO_3 , pH 8.5) are incubated at 37°C for 2 h. The reaction is then quenched with 250 μL 10% (w/v) SDS and 125 μL 1 N HCl. The absorption at 335 nm is measured and compared to the standards to determine the concentration of the unknown peptide.

Appendix H: Limited Tryptic Digest of Human Lon

Reactions containing 50 mM Tris (pH 8.1), 5 mM Mg(OAc)₂, 2 mM DTT, 150 mM NaCl, 2.1 μM mature human Lon with an N-terminal 6x His tag, and 1 mM of the indicated nucleotide were initiated by the addition of 4 μg/mL trypsin and incubated at 37°C. At different time points (0 – 60 min) aliquots were quenched in 175 μg/mL SBTI. The proteins were TCA precipitated (6% final) at 4°C for 1 h and the precipitate resuspended in Lamelli sample buffer. The reactions were fractionated by 7.5% Tris SDS-PAGE (Figure H.1) and transferred to a PVDF membrane in 10 mM CAPS, pH 11, containing 10% MeOH, at 100 V for 2 h. The membrane was rinsed with water and stained with Coomassie for 2 min. The excess stain was removed by washing with Buffer I (50% MeOH, 7% HOAc, 43% water), Buffer J (10% HOAc, 90% MeOH), and finally water. The membrane was allowed to air dry and the trypsin protected protein fragments cut out and submitted to the Lerner Research Institute Proteomics Laboratory at Cleveland Clinic for protein sequencing. The amino acids detected during sequencing are shown in Figure H.2. Fragment A corresponds to human Lon which has lost the N-terminal 139 amino acids and fragment B corresponds to the enzyme which has lost the N-terminal 311 amino acids (Figure H.1).

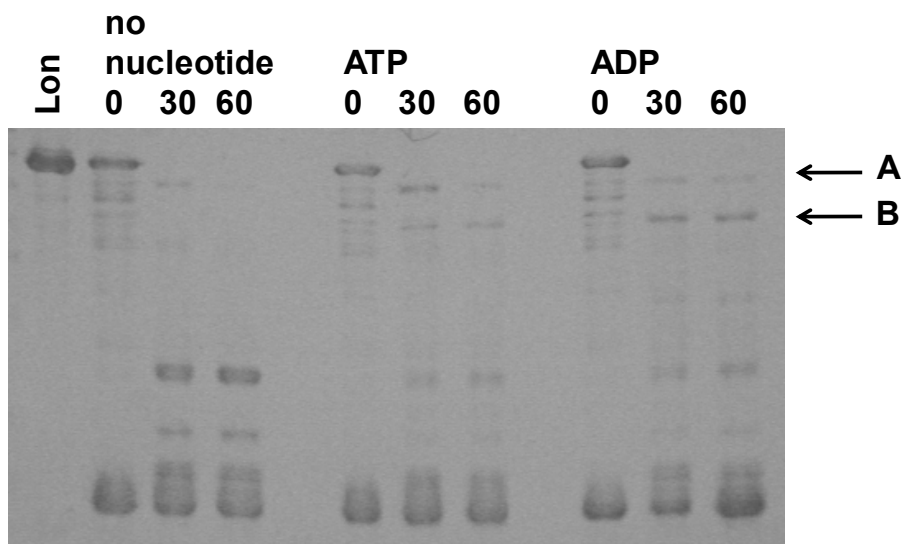


Figure H.1 **Limited tryptic digest of human Lon.** Reactions contained 2.1 μM mature human Lon with an N-terminal 6x His tag, 1 mM of the indicated nucleotide, and 4 $\mu\text{g}/\text{mL}$ trypsin. The reactions after 0, 30, and 60 min were fractionated by 7.5% Tris SDS-PAGE and visualized by Coomassie. The trypsin protected protein fragments (A and B) are indicated.

```

1   MGHHHHHHDY  DIPTTENLYF  QGAHMTIPDV  FPHLPLIAIT  RNPVFPRFIK
51  IIEVKNKKLV  ELLRRKVRLA  QPYVGVFLKR  DDSNESDVVE  SLDEIYHTGT
101 FAQIHEMQDL  GDKLRMIVMG  HRRVHISRQL  EVEPEEPEAE  NKHKPRRKS
151 RGKKEAEDEL  SAR↓HPAELAM  ETPPELPAEV  LMVEVENVH  EDFQVTEEVK
201 ALTAEIVKTI  RDIIALNPLY  RESVLQMMQA  GQRVVDNPIY  LSDMGAALTG
252 AESHELQDVL  EETNIPKRLY  KALSLLKKEF  ELSKLQORLG  REVEEKIKQT
301 HRKYLLQEQ  K↓IIKKELGLE  KDDKDAIEEK  FRERLKELVV  PKHVMDVVDE
352 ELSKLGLLDN  HSSEFNVTRN  YLDWLTSIPW  GKYSNENLDL  ARAQAVLEED
401 HYGMEDVKKR  ILEFIAVSQ  RGSTQ GKILC  FYGPPGVGKT  SIARSIARAL

```

Figure H.2 Protein sequencing of trypsin protected protein fragments. Partial amino acid sequence of mature human Lon containing an N-terminal 6x His tag. The amino acid residues identified by sequencing of the trypsin protected protein fragments, A (red) and B (green), are indicated as well as the predicted trypsin cleavage site (blue arrow).

List of References

1. Charette, M. F., Henderson, G. W., Doane, L. L., and Markovitz, A. (1984) DNA-stimulated ATPase activity on the lon (CapR) protein, *J Bacteriol* 158, 195-201.
2. Chung, C. H., and Goldberg, A. L. (1981) The product of the lon (capR) gene in Escherichia coli is the ATP-dependent protease, protease La, *Proc Natl Acad Sci USA* 78, 4931-4935.
3. Goff, S. A., and Goldberg, A. L. (1985) Production of abnormal proteins in E. coli stimulates transcription of lon and other heat shock genes, *Cell* 41, 587-595.
4. Goldberg, A. L., Moerschell, R. P., Chung, C. H., and Maurizi, M. R. (1994) ATP-dependent protease La (lon) from Escherichia coli, *Methods Enzymol* 244, 350-375.
5. Goldberg, A. L., and Waxman, L. (1985) The role of ATP hydrolysis in the breakdown of proteins and peptides by protease La from Escherichia coli, *J Biol Chem* 260, 12029-12034.
6. Gottesman, S. (1996) Proteases and their targets in Escherichia coli, *Annu Rev Genet* 30, 465-506.
7. Gottesman, S., Gottesman, M., Shaw, J. E., and Pearson, M. L. (1981) Protein degradation in E. coli: the lon mutation and bacteriophage lambda N and cII protein stability, *Cell* 24, 225-233.
8. Gottesman, S., and Maurizi, M. R. (1992) Regulation by proteolysis: energy-dependent proteases and their targets, *Microbiol Rev* 56, 592-621.

9. Maurizi, M. R. (1992) Proteases and protein degradation in *Escherichia coli*, *Experientia* 48, 178-201.
10. Schoemaker, J. M., Gayda, R. C., and Markovitz, A. (1984) Regulation of cell division in *Escherichia coli*: SOS induction and cellular location of the *sulA* protein, a key to *lon*-associated filamentation and death, *J Bacteriol* 158, 551-561.
11. Suzuki, C. K., Kutejova, E., and Suda, K. (1995) Analysis and purification of ATP-dependent mitochondrial *lon* protease of *Saccharomyces cerevisiae*, *Methods Enzymol* 260, 486-494.
12. Wang, N., Maurizi, M. R., Emmert-Buck, L., and Gottesman, M. M. (1994) Synthesis, processing, and localization of human *Lon* protease, *J Biol Chem* 269, 29308-29313.
13. <http://us.expasy.org/tools/sim-prot.html>. (2005).
14. Apte, B. N., Rhodes, H., and Zipser, D. (1975) Mutation blocking the specific degradation of reinitiation polypeptides in *E. coli*, *Nature* 257, 329-331.
15. Downs, D., Waxman, L., Goldberg, A. L., and Roth, J. (1986) Isolation and characterization of *lon* mutants in *Salmonella typhimurium*, *J Bacteriol* 165, 193-197.
16. Gottesman, S., and Zipser, D. (1978) Deg phenotype of *Escherichia coli lon* mutants, *J Bacteriol* 133, 844-851.
17. Grossman, A. D., Burgess, R. R., Walter, W., and Gross, C. A. (1983) Mutations in the *lon* gene of *E. coli* K12 phenotypically suppress a mutation in the sigma subunit of RNA polymerase, *Cell* 32, 151-159.

18. Howard-Flanders, P., Simson, E., and Theriot, L. (1964) A Locus That Controls Filament Formation And Sensitivity To Radiation In *Escherichia coli* K-12, *Genetics* 49, 237-246.
19. Mizusawa, S., and Gottesman, S. (1983) Protein degradation in *Escherichia coli*: the lon gene controls the stability of sulA protein, *Proc Natl Acad Sci U S A* 80, 358-362.
20. Teichmann, U., van Dyck, L., Guiard, B., Fischer, H., Glockshuber, R., Neupert, W., and Langer, T. (1996) Substitution of PIM1 protease in mitochondria by *Escherichia coli* Lon protease, *J Biol Chem* 271, 10137-10142.
21. Robertson, G. T., Kovach, M. E., Allen, C. A., Ficht, T. A., and Roop, R. M., 2nd. (2000) The *Brucella abortus* Lon functions as a generalized stress response protease and is required for wild-type virulence in BALB/c mice, *Mol Microbiol* 35, 577-588.
22. Takaya, A., Tomoyasu, T., Tokumitsu, A., Morioka, M., and Yamamoto, T. (2002) The ATP-dependent lon protease of *Salmonella enterica* serovar Typhimurium regulates invasion and expression of genes carried on *Salmonella* pathogenicity island 1, *J Bacteriol* 184, 224-232.
23. Takaya, A., Suzuki, M., Matsui, H., Tomoyasu, T., Sashinami, H., Nakane, A., and Yamamoto, T. (2003) Lon, a stress-induced ATP-dependent protease, is critically important for systemic *Salmonella enterica* serovar typhimurium infection of mice, *Infect Immun* 71, 690-696.
24. Matsui, H., Suzuki, M., Isshiki, Y., Kodama, C., Eguchi, M., Kikuchi, Y., Motokawa, K., Takaya, A., Tomoyasu, T., and Yamamoto, T. (2003) Oral

- immunization with ATP-dependent protease-deficient mutants protects mice against subsequent oral challenge with virulent *Salmonella enterica* serovar typhimurium, *Infect Immun* 71, 30-39.
25. Murphy, M. P., and Smith, R. A. (2000) Drug delivery to mitochondria: the key to mitochondrial medicine, *Adv Drug Deliv Rev* 41, 235-250.
 26. Van Dyck, L., and Langer, T. (1999) ATP-dependent proteases controlling mitochondrial function in the yeast *Saccharomyces cerevisiae*, *Cell Mol Life Sci* 56, 825-842.
 27. Bota, D. A., and Davies, K. J. (2002) Lon protease preferentially degrades oxidized mitochondrial aconitase by an ATP-stimulated mechanism, *Nat Cell Biol* 4, 674-680.
 28. Van Dyck, L., Pearce, D. A., and Sherman, F. (1994) PIM1 encodes a mitochondrial ATP-dependent protease that is required for mitochondrial function in the yeast *Saccharomyces cerevisiae*, *J Biol Chem* 269, 238-242.
 29. Suzuki, C. K., Suda, K., Wang, N., and Schatz, G. (1994) Requirement for the yeast gene LON in intramitochondrial proteolysis and maintenance of respiration, *Science* 264, 891.
 30. Bota, D. A., Ngo, J. K., and Davies, K. J. (2005) Downregulation of the human Lon protease impairs mitochondrial structure and function and causes cell death, *Free Radic Biol Med* 38, 665-677.
 31. Luciakova, K., Sokolikova, B., Chloupkova, M., and Nelson, B. D. (1999) Enhanced mitochondrial biogenesis is associated with increased expression of the mitochondrial ATP-dependent Lon protease, *FEBS Lett* 444, 186-188.

32. Wang, N., Gottesman, S., Willingham, M. C., Gottesman, M. M., and Maurizi, M. R. (1993) A human mitochondrial ATP-dependent protease that is highly homologous to bacterial Lon protease, *Proc Natl Acad Sci U S A* 90, 11247-11251.
33. Wagner, I., van Dyck, L., Savel'ev, A. S., Neupert, W., and Langer, T. (1997) Autocatalytic processing of the ATP-dependent PIM1 protease: crucial function of a pro-region for sorting to mitochondria, *Embo J* 16, 7317-7325.
34. Roudiak, S. G., and Shrader, T. E. (1998) Functional role of the N-terminal region of the Lon protease from *Mycobacterium smegmatis*, *Biochemistry* 37, 11255-11263.
35. Walker, J. E., Saraste, M., Runswick, M. J., and Gay, N. J. (1982) Distantly related sequences in the alpha- and beta-subunits of ATP synthase, myosin, kinases and other ATP-requiring enzymes and a common nucleotide binding fold, *Embo J* 1, 945-951.
36. Lenzen, C. U., Steinmann, D., Whiteheart, S. W., and Weis, W. I. (1998) Crystal structure of the hexamerization domain of N-ethylmaleimide-sensitive fusion protein, *Cell* 94, 525-536.
37. Hattendorf, D. A., and Lindquist, S. L. (2002) Cooperative kinetics of both Hsp104 ATPase domains and interdomain communication revealed by AAA sensor-1 mutants, *Embo J* 21, 12-21.
38. Karata, K., Inagawa, T., Wilkinson, A. J., Tatsuta, T., and Ogura, T. (1999) Dissecting the role of a conserved motif (the second region of homology) in the

- AAA family of ATPases. Site-directed mutagenesis of the ATP-dependent protease FtsH, *J Biol Chem* 274, 26225-26232.
39. Hattendorf, D. A., and Lindquist, S. L. (2002) Analysis of the AAA sensor-2 motif in the C-terminal ATPase domain of Hsp104 with a site-specific fluorescent probe of nucleotide binding, *Proc Natl Acad Sci U S A* 99, 2732-2737.
40. Smith, C. K., Baker, T. A., and Sauer, R. T. (1999) Lon and Clp family proteases and chaperones share homologous substrate-recognition domains, *Proc Natl Acad Sci U S A* 96, 6678-6682.
41. Botos, I., Melnikov, E. E., Cherry, S., Tropea, J. E., Khalatova, A. G., Rasulova, F., Dauter, Z., Maurizi, M. R., Rotanova, T. V., Wlodawer, A., and Gustchina, A. (2004) The catalytic domain of Escherichia coli Lon protease has a unique fold and a Ser-Lys dyad in the active site, *J Biol Chem* 279, 8140-8148.
42. Park, S. C., Jia, B., Yang, J. K., Van, D. L., Shao, Y. G., Han, S. W., Jeon, Y. J., Chung, C. H., and Cheong, G. W. (2006) Oligomeric structure of the ATP-dependent protease La (Lon) of Escherichia coli, *Mol Cells* 21, 129-134.
43. Rudyak, S. G., Brenowitz, M., and Shrader, T. E. (2001) Mg²⁺-linked oligomerization modulates the catalytic activity of the Lon (La) protease from Mycobacterium smegmatis, *Biochemistry* 40, 9317-9323.
44. Stahlberg, H., Kutejova, E., Suda, K., Wolpensinger, B., Lustig, A., Schatz, G., Engel, A., and Suzuki, C. K. (1999) Mitochondrial Lon of Saccharomyces cerevisiae is a ring-shaped protease with seven flexible subunits, *Proc Natl Acad Sci U S A* 96, 6787-6790.

45. Botos, I., Melnikov, E. E., Cherry, S., Khalatova, A. G., Rasulova, F. S., Tropea, J. E., Maurizi, M. R., Rotanova, T. V., Gustchina, A., and Wlodawer, A. (2004) Crystal structure of the AAA+ alpha domain of E. coli Lon protease at 1.9A resolution, *J Struct Biol* 146, 113-122.
46. Li, M., Rasulova, F., Melnikov, E. E., Rotanova, T. V., Gustchina, A., Maurizi, M. R., and Wlodawer, A. (2005) Crystal structure of the N-terminal domain of E. coli Lon protease, *Protein Sci* 14, 2895-2900.
47. Dougan, D. A., Mogk, A., Zeth, K., Turgay, K., and Bukau, B. (2002) AAA+ proteins and substrate recognition, it all depends on their partner in crime, *FEBS Lett* 529, 6-10.
48. Rohrwild, M., Coux, O., Huang, H. C., Moerschell, R. P., Yoo, S. J., Seol, J. H., Chung, C. H., and Goldberg, A. L. (1996) HslV-HslU: A novel ATP-dependent protease complex in Escherichia coli related to the eukaryotic proteasome, *Proc Natl Acad Sci U S A* 93, 5808-5813.
49. Bochtler, M., Ditzel, L., Groll, M., and Huber, R. (1997) Crystal structure of heat shock locus V (HslV) from Escherichia coli, *Proc Natl Acad Sci U S A* 94, 6070-6074.
50. Yoo, S. J., Seol, J. H., Seong, I. S., Kang, M. S., and Chung, C. H. (1997) ATP binding, but not its hydrolysis, is required for assembly and proteolytic activity of the HslVU protease in Escherichia coli, *Biochem Biophys Res Commun* 238, 581-585.

51. Sousa, M. C., Trame, C. B., Tsuruta, H., Wilbanks, S. M., Reddy, V. S., and McKay, D. B. (2000) Crystal and solution structures of an HslUV protease-chaperone complex, *Cell* 103, 633-643.
52. Bochtler, M., Hartmann, C., Song, H. K., Bourenkov, G. P., Bartunik, H. D., and Huber, R. (2000) The structures of HslU and the ATP-dependent protease HslU-HslIV, *Nature* 403, 800-805.
53. Wang, J., Song, J. J., Seong, I. S., Franklin, M. C., Kamtekar, S., Eom, S. H., and Chung, C. H. (2001) Nucleotide-dependent conformational changes in a protease-associated ATPase HslU, *Structure* 9, 1107-1116.
54. Patterson, J., Vineyard, D., Thomas-Wohlever, J., Behshad, R., Burke, M., and Lee, I. (2004) Correlation of an adenine-specific conformational change with the ATP-dependent peptidase activity of Escherichia coli Lon, *Biochemistry* 43, 7432-7442.
55. Sousa, M. C., Kessler, B. M., Overkleeft, H. S., and McKay, D. B. (2002) Crystal structure of HslUV complexed with a vinyl sulfone inhibitor: corroboration of a proposed mechanism of allosteric activation of HslV by HslU, *J Mol Biol* 318, 779-785.
56. Maurizi, M. R. (1987) Degradation in vitro of bacteriophage lambda N protein by Lon protease from Escherichia coli, *J Biol Chem* 262, 2696-2703.
57. Ondrovicova, G., Liu, T., Singh, K., Tian, B., Li, H., Gakh, O., Perecko, D., Janata, J., Granot, Z., Orly, J., Kutejova, E., and Suzuki, C. K. (2005) Cleavage site selection within a folded substrate by the ATP-dependent Lon protease, *J Biol Chem* 280, 25103-25110.

58. Van Melderer, L., Thi, M. H., Lecchi, P., Gottesman, S., Couturier, M., and Maurizi, M. R. (1996) ATP-dependent degradation of CcdA by Lon protease. Effects of secondary structure and heterologous subunit interactions, *J Biol Chem* 271, 27730-27738.
59. Nishii, W., Suzuki, T., Nakada, M., Kim, Y. T., Muramatsu, T., and Takahashi, K. (2005) Cleavage mechanism of ATP-dependent Lon protease toward ribosomal S2 protein, *FEBS Lett* 579, 6846-6850.
60. Waxman, L., and Goldberg, A. L. (1985) Protease La, the lon gene product, cleaves specific fluorogenic peptides in an ATP-dependent reaction, *J Biol Chem* 260, 12022-12028.
61. Kutejova, E., Durcova, G., Surovkova, E., and Kuzela, S. (1993) Yeast mitochondrial ATP-dependent protease: purification and comparison with the homologous rat enzyme and the bacterial ATP-dependent protease La, *FEBS Lett* 329, 47-50.
62. Waxman, L., and Goldberg, A. L. (1982) Protease La from Escherichia coli hydrolyzes ATP and proteins in a linked fashion, *Proc Natl Acad Sci U S A* 79, 4883-4887.
63. Larimore, F. S., Waxman, L., and Goldberg, A. L. (1982) Studies of the ATP-dependent proteolytic enzyme, protease La, from Escherichia coli, *J Biol Chem* 257, 4187-4195.
64. Thomas-Wohlever, J., and Lee, I. (2002) Kinetic characterization of the peptidase activity of Escherichia coli Lon reveals the mechanistic similarities in ATP-

- dependent hydrolysis of peptide and protein substrates, *Biochemistry* 41, 9418-9425.
65. Lee, I., and Berdis, A. J. (2001) Adenosine triphosphate-dependent degradation of a fluorescent lambda N substrate mimic by Lon protease, *Anal Biochem* 291, 74-83.
 66. Waxman, L., and Goldberg, A. L. (1986) Selectivity of intracellular proteolysis: protein substrates activate the ATP-dependent protease (La), *Science* 232, 500-503.
 67. Meldal, M., and Breddam, K. (1991) Anthranilamide and nitrotyrosine as a donor-acceptor pair in internally quenched fluorescent substrates for endopeptidases: multicolumn peptide synthesis of enzyme substrates for subtilisin Carlsberg and pepsin, *Anal Biochem* 195, 141-147.
 68. Gilbert, S. P., and Mackey, A. T. (2000) Kinetics: a tool to study molecular motors, *Methods* 22, 337-354.
 69. Vineyard, D., Patterson-Ward, J., Berdis, A. J., and Lee, I. (2005) Monitoring the Timing of ATP Hydrolysis with Activation of Peptide Cleavage in *Escherichia coli* Lon by Transient Kinetics, *Biochemistry* 44, 1671-1682.
 70. <http://www.ch.embnet.org/software/ClustalW.html>. (2005).
 71. Wang, J., Song, J. J., Seong, I. S., Franklin, M. C., Kamtekar, S., Eom, S. H., and Chung, C. H. (2001) Nucleotide-dependent conformational changes in a protease-associated ATPase HslU, *Structure (Camb)* 9, 1107-1116.

72. Fu, G. K., and Markovitz, D. M. (1998) The human LON protease binds to mitochondrial promoters in a single-stranded, site-specific, strand-specific manner, *Biochemistry* 37, 1905-1909.
73. Bradford, M. M. (1976) A rapid and sensitive method for the quantitation of microgram quantities of protein utilizing the principle of protein-dye binding, *Anal Biochem* 72, 248-254.
74. Wellings, D. A., and Atherton, E. (1997) Standard Fmoc protocols, *Methods Enzymol* 289, 44-67.
75. Petersson, A. S., Steen, H., Kalume, D. E., Caidahl, K., and Roepstorff, P. (2001) Investigation of tyrosine nitration in proteins by mass spectrometry, *J Mass Spectrom* 36, 616-625.
76. Huang, X., and Miller, W. (1991) A Time-Efficient, Linear-Space Local Similarity Algorithm, *Advances in Applied Mathematics* 12, 337-357.
77. Tossi, A., Sandri, L., and Giangaspero, A. (2002) New consensus hydrophobicity scale extended to non-proteinogenic amino acids, in *Peptides 2002, Proceedings of the 27th European Peptide Symposium* (Benedetti, E., and Pedone, C., Eds.), pp 416-417, Sorrento, Italy.
78. Monaghan, R. L., and Barrett, J. F. (2006) Antibacterial drug discovery--then, now and the genomics future, *Biochem Pharmacol* 71, 901-909.
79. Patel, S., and Latterich, M. (1998) The AAA team: related ATPases with diverse functions, *Trends Cell Biol* 8, 65-71.
80. Kisselev, A. F., and Goldberg, A. L. (2001) Proteasome inhibitors: from research tools to drug candidates, *Chem Biol* 8, 739-758.

81. Lowe, J., Stock, D., Jap, B., Zwickl, P., Baumeister, W., and Huber, R. (1995) Crystal structure of the 20S proteasome from the archaeon *T. acidophilum* at 3.4 Å resolution, *Science* 268, 533-539.
82. Frase, H., Hudak, J., and Lee, I. (2006) Identification of the proteasome inhibitor MG262 as a potent ATP-dependent inhibitor of the *Salmonella enterica* serovar Typhimurium Lon protease, *Biochemistry* 45, 8264-8274.
83. Copeland, R. A. (2000) *Enzymes: A Practical Introduction to Structure, Mechanism, and Data Analysis*, 2nd ed., John Wiley & Sons, Inc., New York.
84. Copeland, R. A. (2005) *Evaluation of Enzyme Inhibitors in Drug Discovery: A Guide for Medicinal Chemists and Pharmacologists*, John Wiley & Sons, Inc., Hoboken, NJ.
85. Adams, J., Behnke, M., Chen, S., Cruickshank, A. A., Dick, L. R., Grenier, L., Klunder, J. M., Ma, Y. T., Plamondon, L., and Stein, R. L. (1998) Potent and selective inhibitors of the proteasome: dipeptidyl boronic acids, *Bioorg Med Chem Lett* 8, 333-338.
86. Palmer, J. T., Rasnick, D., Klaus, J. L., and Bromme, D. (1995) Vinyl sulfones as mechanism-based cysteine protease inhibitors, *J Med Chem* 38, 3193-3196.
87. Bogyo, M., McMaster, J. S., Gaczynska, M., Tortorella, D., Goldberg, A. L., and Ploegh, H. (1997) Covalent modification of the active site threonine of proteasomal beta subunits and the *Escherichia coli* homolog HslV by a new class of inhibitors, *Proc Natl Acad Sci U S A* 94, 6629-6634.
88. Joyeau, R., Maoulida, C., Guillet, C., Frappier, F., Teixeira, A. R., Schrevel, J., Santana, J., and Grellier, P. (2000) Synthesis and activity of pyrrolidinyl- and

- thiazolidinyl-dipeptide derivatives as inhibitors of the Tc80 prolyl oligopeptidase from *Trypanosoma cruzi*, *Eur J Med Chem* 35, 257-266.
89. Bogyo, M., Shin, S., McMaster, J. S., and Ploegh, H. L. (1998) Substrate binding and sequence preference of the proteasome revealed by active-site-directed affinity probes, *Chem Biol* 5, 307-320.
 90. Meng, L., Mohan, R., Kwok, B. H., Elofsson, M., Sin, N., and Crews, C. M. (1999) Epoxomicin, a potent and selective proteasome inhibitor, exhibits in vivo antiinflammatory activity, *Proc Natl Acad Sci U S A* 96, 10403-10408.
 91. Hanada, M., Sugawara, K., Kaneta, K., Toda, S., Nishiyama, Y., Tomita, K., Yamamoto, H., Konishi, M., and Oki, T. (1992) Epoxomicin, a new antitumor agent of microbial origin, *J Antibiot (Tokyo)* 45, 1746-1752.
 92. Groll, M., Kim, K. B., Kairies, N., Huber, R., and Crews, C. M. (2000) Crystal structure of epoxomicin: 20S proteasome reveals a molecular basis for selectivity of a',b'-epoxyketone proteasome inhibitors, *J Am Chem Soc* 122, 1237-1238.
 93. Koehler, K. A., and Lienhard, G. E. (1971) 2-phenylethaneboronic acid, a possible transition-state analog for chymotrypsin, *Biochemistry* 10, 2477-2483.
 94. Thompson, R. C. (1973) Use of peptide aldehydes to generate transition-state analogs of elastase, *Biochemistry* 12, 47-51.
 95. Westerik, J. O., and Wolfenden, R. (1972) Aldehydes as inhibitors of papain, *J Biol Chem* 247, 8195-8197.
 96. Vinitsky, A., Michaud, C., Powers, J. C., and Orlowski, M. (1992) Inhibition of the chymotrypsin-like activity of the pituitary multicatalytic proteinase complex, *Biochemistry* 31, 9421-9428.

97. Omura, S., Fujimoto, T., Otaguro, K., Matsuzaki, K., Moriguchi, R., Tanaka, H., and Sasaki, Y. (1991) Lactacystin, a novel microbial metabolite, induces neuritogenesis of neuroblastoma cells, *J Antibiot (Tokyo)* 44, 113-116.
98. Dick, L. R., Cruikshank, A. A., Grenier, L., Melandri, F. D., Nunes, S. L., and Stein, R. L. (1996) Mechanistic studies on the inactivation of the proteasome by lactacystin: a central role for clasto-lactacystin beta-lactone, *J Biol Chem* 271, 7273-7276.
99. Yoo, S. J., Kim, H. H., Shin, D. H., Lee, C. S., Seong, I. S., Seol, J. H., Shimbara, N., Tanaka, K., and Chung, C. H. (1998) Effects of the cys mutations on structure and function of the ATP-dependent HslVU protease in Escherichia coli. The Cys287 to Val mutation in HslU uncouples the ATP-dependent proteolysis by HslVU from ATP hydrolysis, *J Biol Chem* 273, 22929-22935.
100. Granot, Z., Geiss-Friedlander, R., Melamed-Book, N., Eimerl, S., Timberg, R., Weiss, A. M., Hales, K. H., Hales, D. B., Stocco, D. M., and Orly, J. (2003) Proteolysis of normal and mutated steroidogenic acute regulatory proteins in the mitochondria: the fate of unwanted proteins, *Mol Endocrinol* 17, 2461-2476.
101. Morrison, J. F., and Walsh, C. T. (1988) The behavior and significance of slow-binding enzyme inhibitors, *Adv Enzymol Relat Areas Mol Biol* 61, 201-301.
102. Kettner, C. A., and Shenvi, A. B. (1984) Inhibition of the serine proteases leukocyte elastase, pancreatic elastase, cathepsin G, and chymotrypsin by peptide boronic acids, *J Biol Chem* 259, 15106-15114.
103. Kuzmic, P. (1996) Program DYNAFIT for the analysis of enzyme kinetic data: application to HIV proteinase, *Anal Biochem* 237, 260-273.

104. Menon, A. S., and Goldberg, A. L. (1987) Protein substrates activate the ATP-dependent protease La by promoting nucleotide binding and release of bound ADP, *J Biol Chem* 262, 14929-14934.
105. Groll, M., Berkers, C. R., Ploegh, H. L., and Ovaas, H. (2006) Crystal structure of the boronic acid-based proteasome inhibitor bortezomib in complex with the yeast 20S proteasome, *Structure* 14, 451-456.
106. Matthews, D. A., Alden, R. A., Birktoft, J. J., Freer, S. T., and Kraut, J. (1975) X-ray crystallographic study of boronic acid adducts with subtilisin BPN' (Novo). A model for the catalytic transition state, *J Biol Chem* 250, 7120-7126.
107. Adams, J., Palombella, V. J., Sausville, E. A., Johnson, J., Destree, A., Lazarus, D. D., Maas, J., Pien, C. S., Prakash, S., and Elliott, P. J. (1999) Proteasome inhibitors: a novel class of potent and effective antitumor agents, *Cancer Res* 59, 2615-2622.
108. Lakowicz, J. R. (1999) *Principles of Fluorescence Spectroscopy*, 2nd ed., Plenum, New York.
109. Hall, D. G. (2005) *Boronic Acids: Preparation and Applications in Organic Synthesis and Medicine*, 1st ed., Wiley-VCH.
110. Katz, B. A., Finer-Moore, J., Mortezaei, R., Rich, D. H., and Stroud, R. M. (1995) Episelection: novel Ki approximately nanomolar inhibitors of serine proteases selected by binding or chemistry on an enzyme surface, *Biochemistry* 34, 8264-8280.

111. Pei, X. Y., Dai, Y., and Grant, S. (2003) The proteasome inhibitor bortezomib promotes mitochondrial injury and apoptosis induced by the small molecule Bcl-2 inhibitor HA14-1 in multiple myeloma cells, *Leukemia* 17, 2036-2045.
112. Ling, Y. H., Liebes, L., Zou, Y., and Perez-Soler, R. (2003) Reactive oxygen species generation and mitochondrial dysfunction in the apoptotic response to Bortezomib, a novel proteasome inhibitor, in human H460 non-small cell lung cancer cells, *J Biol Chem* 278, 33714-33723.
113. Crivello, J. F., and Jefcoate, C. R. (1980) Intracellular movement of cholesterol in rat adrenal cells. Kinetics and effects of inhibitors, *J Biol Chem* 255, 8144-8151.
114. Tuckey, R. C., Headlam, M. J., Bose, H. S., and Miller, W. L. (2002) Transfer of cholesterol between phospholipid vesicles mediated by the steroidogenic acute regulatory protein (StAR), *J Biol Chem* 277, 47123-47128.
115. Kallen, C. B., Billheimer, J. T., Summers, S. A., Stayrook, S. E., Lewis, M., and Strauss, J. F., 3rd. (1998) Steroidogenic acute regulatory protein (StAR) is a sterol transfer protein, *J Biol Chem* 273, 26285-26288.
116. Arakane, F., King, S. R., Du, Y., Kallen, C. B., Walsh, L. P., Watari, H., Stocco, D. M., and Strauss, J. F., 3rd. (1997) Phosphorylation of steroidogenic acute regulatory protein (StAR) modulates its steroidogenic activity, *J Biol Chem* 272, 32656-32662.
117. Stocco, D. M., and Sodeman, T. C. (1991) The 30-kDa mitochondrial proteins induced by hormone stimulation in MA-10 mouse Leydig tumor cells are processed from larger precursors, *J Biol Chem* 266, 19731-19738.

118. Clark, B. J., Wells, J., King, S. R., and Stocco, D. M. (1994) The purification, cloning, and expression of a novel luteinizing hormone-induced mitochondrial protein in MA-10 mouse Leydig tumor cells. Characterization of the steroidogenic acute regulatory protein (StAR), *J Biol Chem* 269, 28314-28322.
119. Frase, H., and Lee, I. (2007) Peptidyl Boronates Inhibit *Salmonella enterica* serovar Typhimurium Lon Protease by a Competitive ATP-Dependent Mechanism, submitted to *Biochemistry*.
120. Bhangoo, A., Gu, W. X., Pavlakis, S., Anhalt, H., Heier, L., Ten, S., and Jameson, J. L. (2005) Phenotypic features associated with mutations in steroidogenic acute regulatory protein, *J Clin Endocrinol Metab* 90, 6303-6309.
121. Stocco, D. M. (2002) Clinical disorders associated with abnormal cholesterol transport: mutations in the steroidogenic acute regulatory protein, *Mol Cell Endocrinol* 191, 19-25.
122. Fluck, C. E., Maret, A., Mallet, D., Portrat-Doyen, S., Achermann, J. C., Leheup, B., Theintz, G. E., Mullis, P. E., and Morel, Y. (2005) A novel mutation L260P of the steroidogenic acute regulatory protein gene in three unrelated patients of Swiss ancestry with congenital lipoid adrenal hyperplasia, *J Clin Endocrinol Metab* 90, 5304-5308.
123. Katsumata, N., Horikawa, R., and Tanaka, T. (2006) Replacement of alanine with asparagic acid at position 203 in human steroidogenic acute regulatory protein impairs the ability to enhance steroidogenesis in vitro, *Endocr J* 53, 427-431.

124. Bose, H. S., Baldwin, M. A., and Miller, W. L. (1998) Incorrect folding of steroidogenic acute regulatory protein (StAR) in congenital lipid adrenal hyperplasia, *Biochemistry* 37, 9768-9775.
125. Petrescu, A. D., Gallegos, A. M., Okamura, Y., Strauss, J. F., 3rd, and Schroeder, F. (2001) Steroidogenic acute regulatory protein binds cholesterol and modulates mitochondrial membrane sterol domain dynamics, *J Biol Chem* 276, 36970-36982.
126. Gill, S. C., and von Hippel, P. H. (1989) Calculation of protein extinction coefficients from amino acid sequence data, *Anal Biochem* 182, 319-326.
127. Tsujishita, Y., and Hurley, J. H. (2000) Structure and lipid transport mechanism of a StAR-related domain, *Nat Struct Biol* 7, 408-414.
128. Arakane, F., Sugawara, T., Nishino, H., Liu, Z., Holt, J. A., Pain, D., Stocco, D. M., Miller, W. L., and Strauss, J. F., 3rd. (1996) Steroidogenic acute regulatory protein (StAR) retains activity in the absence of its mitochondrial import sequence: implications for the mechanism of StAR action, *Proc Natl Acad Sci U S A* 93, 13731-13736.